

**Spectral behavior of the coupled land-atmosphere  
system**

by

Pierre Gentine

Submitted to the Department of Civil and Environmental Engineering  
in partial fulfillment of the requirements for the degree of

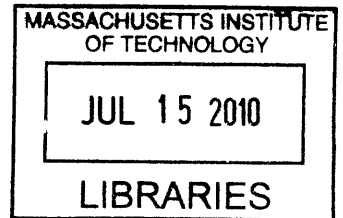
Doctor of Philosophy in the Field of Civil and Environmental  
Engineering

at the


MASSACHUSETTS INSTITUTE OF TECHNOLOGY


February 2010

**ARCHIVES**



©Massachusetts Institute of Technology 2009. All rights reserved.

Author ..... *Pi* .....   
Department of Civil and Environmental Engineering  
September 22, 2009

Certified by .....   
Dara Entekhabi  
Bacardi and Stockholm Water Foundation  
Professor of Civil and Environmental Engineering  
Thesis Supervisor

Accepted by .....   
Daniele Veneziano  
Chairman, Departmental Committee for Graduate Students



# Spectral behavior of the coupled land-atmosphere system

by

Pierre Gentine

Submitted to the Department of Civil and Environmental Engineering  
on September 22, 2009, in partial fulfillment of the  
requirements for the degree of  
Doctor of Philosophy in the Field of Civil and Environmental Engineering

## Abstract

The main objective of this thesis is to understand the daily cycle of the energy coupling between the land and the atmosphere in response to a forcing of incoming radiation at their common boundary, the land surface. This is of fundamental importance as that the initial/boundary conditions of the land-surface state variables (e.g. soil moisture, soil temperature) exert strong control at various temporal scales on hydrologic, climatic and weather related processes. Hence diagnosing these state variables is crucial for extreme hydrological forecasting (flood/drought), agronomic crop management as well as weather and climatic forecasts.

Consequently in this thesis, the daily behavior of a simple land-atmosphere model is examined. A conceptual and linearized land-atmosphere model is first introduced and its response to a daily input of incoming radiation at the land surface is investigated. The solution of the different state and fluxes in the Atmospheric Boundary Layer (ABL) and in the soil are expressed as temporal Fourier series with vertically dependent coefficients. These coefficients highlight the impact of both the surface parameters and the frequency of the radiation on the heat propagation in the ABL and in the soil. The simplified model is shown to compare well with field measurements thus accounting for the main emergent behaviors of the system.

The first chapter of the thesis describes the theoretical background of the equations governing the evolution of temperature and humidity in the ABL and in the soil.

In the second chapter, the pioneering work of Lettau (1951), which inspired our approach is summarized. In his work Lettau studied the response of a simplified linearized land-atmosphere model to a sinusoidal net radiation forcing at the land surface.

The third chapter of the thesis describes the SUDMED project, which took place in Morocco in 2003. During this project a wheat field was fully instrumented with continuous measurements of soil moisture, radiative fluxes, turbulent heat fluxes and soil heat flux. This site will be taken as a reference for model comparison.

The fourth chapter of the thesis presents the three studies with distinctive goals. In these studies our linearized land-atmosphere model is first introduced. Then the propagation of the land-surface diurnal heating is presented and the model is com-

pared to observations from the SUDMED project. Finally the repercussion of a land-surface energy budget error noise is investigated.

Finally in the last chapter of the thesis we discuss possible evolution and improvements of the analytical coupled model presented in this thesis. In particular, it is emphasized that the non-linearity of the the boundary-layer height is of great importance for the predictability of the ABL state.

Thesis Supervisor: Dara Entekhabi

Title: Bacardi and Stockholm Water Foundation

Professor of Civil and Environmental Engineering

## Acknowledgments

First, I would like to sincerely thank my thesis advisor, Professor Dara Entekhabi from both a personal and professional point of view. Few people can claim to have reached such scientific success, while staying as humble and natural as he is. Moreover, throughout my studies at MIT, Dara has been extremely understandable about personal issues. I am extremely grateful to him. He has clearly become a model for my academic career, as he has achieved the right balance between scientific excellence and human qualities.

Then I would like to express my gratitude to Jan Polcher for welcoming me in the Laboratoire de Météorologie Dynamique in Paris and for his advice throughout my PhD. I have enjoyed our scientific discussions and exchanges during this period. He has always been very enthusiastic and friendly, and he has respected my point of view and treated me as a peer.

I also wish to truly thank my family for their support, especially during these two years. They have been extremely encouraging and supportive.

Last but not least, I would like to deeply thank Marie, my wife, who has been a tremendous support during my MIT years and throughout my education. When I was sick and could not stand the pain, you were the very reason why I wanted to fight for. When I could not walk, you were the crutch that helped me stand. Thank you again. This work is also yours.

I would like to dedicate this thesis to the  
memory of my grandparents.  
You taught me the value of human beings  
and of the Earth.  
You lived and left together.

"Don't empty the water jar until the rain falls."

Ewé proverb from Togo, Africa.





# Contents

<b>1</b>	<b>Governing equations of state</b>	<b>17</b>
1.1	Soil . . . . .	18
1.1.1	Water movement . . . . .	18
1.1.2	Temperature evolution . . . . .	19
1.2	The Atmospheric Boundary Layer (ABL) . . . . .	20
1.2.1	Thermodynamics . . . . .	21
1.2.2	Daily evolution . . . . .	26
1.2.3	ABL dynamics equations . . . . .	28
1.2.4	Mean ABL dynamics equations . . . . .	29
1.2.5	André et al. 1978 . . . . .	32
1.3	Coupling . . . . .	37
<b>2</b>	<b>Lettau's 1951 publication</b>	<b>49</b>
<b>3</b>	<b>SUDMED project and main site of study</b>	<b>53</b>
3.1	Site description . . . . .	53
3.2	Experimental data set . . . . .	55
3.3	Calibration and validation of the SVAT model . . . . .	57
<b>4</b>	<b>Spectral behavior of a coupled land-surface and boundary-layer system</b>	<b>69</b>
<b>5</b>	<b>Harmonic Characteristics of Land Surface Evaporation in the Soil-Atmosphere Continuum</b>	<b>123</b>

<b>6</b>	<b>Impact of noise in the surface energy budget on screen-level and land-surface variables within a coupled land-atmosphere model</b>	<b>181</b>
<b>7</b>	<b>Future research</b>	<b>243</b>
7.1	Non-local closure: countergradient formulation . . . . .	244
7.2	Eddy-diffusivity and counter-gradient approximation: theoretical justification . . . . .	246
7.3	Solving the Unstable/stable ABL . . . . .	250
7.4	Radiative transfer . . . . .	252
7.5	Free atmosphere . . . . .	253
7.6	Comparisons with coupled soil-LES: advantages/disadvantages . . . . .	253
7.7	Time-dependent ABL height . . . . .	254
<b>A</b>	<b>Brownian Bridge</b>	<b>263</b>
A.1	Karhunen-Loève (K-L) expansion . . . . .	263
A.2	Fourier expansion . . . . .	264

# List of Figures

1-1	Daily course of the ABL structure taken from Stull (1988) . . . . .	39
1-2	Daily course of mean virtual potential temperature $\theta_v$ taken from Stull (1988) . . . . .	40
1-3	Typical profiles of temperatures and scalar during the day, with a well mixed boundary layer, taken from Stull (1988) . . . . .	41
1-4	Typical profiles of temperature, humidity and wind speed in the ABL, taken from Margulis' PhD Thesis (2002) . . . . .	42
1-5	Diurnal profiles of mean potential temperature $\theta$ from André et al. (1978) . . . . .	43
1-6	Nocturnal mean potential temperature profiles from André et al. (1978)	44
1-7	Diurnal profiles of specific humidity $q$ from André et al. (1978) . . . .	45
1-8	Diurnal profiles of the turbulent flux of potential temperature from André et al. (1978) . . . . .	46
1-9	Diurnal profiles of the turbulent flux of specific humidity from André et al. (1978) . . . . .	47
1-10	Daytime virtual potential temperature variance budget from André et al. (1978) . . . . .	48
3-1	Map of Morocco . . . . .	60
3-2	Solar incoming radiation measured over parcel R3-B123 in 2003 . . . .	61
3-3	Air temperature measured over parcel R3-B123 in 2003 . . . . .	62
3-4	Air specific humidity measured over parcel R3-B123 in 2003 . . . . .	63
3-5	Wind speed measured over parcel R3-B123 in 2003 . . . . .	64

3-6	Net radiation measured at 2m high over parcel R3-B123 in 2003 . . .	65
3-7	Sensible Heat Flux measured using eddy correlation over parcel R3-B123 in 2003 . . . . .	66
3-8	Latent Heat Flux measured using eddy correlation over parcel R3-B123 in 2003 . . . . .	67
3-9	Mean ground heat flux measured using 3 flux plates over parcel R3-B123 in 2003 . . . . .	68
7-1	Non-dimensional vertical turbulent velocity variance, giving the eddy-diffusivity coefficient of the K-theory(from Holtslag and Moeng 1991). Solid curve is parameterized to fit the AMTEX data (circles) and 96 LES experiment (shaded region) and convection tanks (squares) . . .	255
7-2	Profiles of the mean potential temperature (solid line) and sensible heat flux (dotted line) in steady state from Stevens (2000) . . . . .	256
7-3	Normalized creation/destruction terms of turbulent sensible heat flux equation (7.5) as function of relative height (from Holtslag and Moeng 1991). . . . .	257
7-4	Non-dimensional counter-gradient term a)HM91 b)D72 c)HM91 with parameterized $(\overline{w'^2})^{3/2}$ (from Holtslag and Moeng 1991). . . . .	258
7-5	Non-dimensional eddy-diffusivity coefficient for heat a) HM91 with parameterized counter-gradient, b) HM91 with parameterized counter-gradient and velocity variance c) parameterized $K_H$ (from Holtslag and Moeng 1991). . . . .	259

# Introduction

The atmosphere and the land are two complex systems that interact through the exchange of water, energy and carbon dioxide at their common interface. Historically, meteorologists have considered the atmosphere as their control volume, where the primary forcing comes from the land surface. Conversely, hydrologists have studied the responses of soil, vegetation, and surface water to atmospheric forcing. The "outputs" of one community were considered as the "inputs" of the other. Yet the land and atmosphere are coupled and together form a higher-order system, in which interactions and feedbacks modulate the variability of the weather and climate. Like many other non-linear coupled systems, the land-atmosphere system exhibits emergent behaviors that are different from the behavior of its constitutive systems taken alone. These emergent behaviors can be either simple or more complex (e.g. chaotic), thus introducing new spatial and time scales to the dynamics. A relatively simple periodic forcing (solar radiation) is translated to variability covering a wide range of scales from planetary and interdecadal to turbulence dissipation scales (centimeters and seconds).

Meteorological predictions require accurate representation of these feedback mechanisms. However, much remains to be understood about the role of solar radiation as the driving source for the dynamics and physics of the soil-atmosphere continuum. Few theoretical studies have been dedicated to the understanding of the effect of solar radiation forcing on the coupled land-atmosphere system. Specifically, a strong emphasis should be placed on the understanding of the diurnal cycle of heat fluxes and temperatures at the land surface. Virtually all major near-surface processes, such as phase changes of water, photosynthetic activity, and thermal mixing, receive their

primary forcing from the diurnal solar radiation cycle. Better comprehension of this diurnal cycle will guide the improvement of land-surface models for meteorological forecasting and the design of observing systems, which in turn will improve weather and climatic forecasts.

In this context, the goal of this PhD thesis is to introduce a tractable analytic model to investigate the harmonic response of the coupled land-atmosphere system to daily forcing of solar radiation at the land-surface. This analytical modeling captures the important aspects of the coupled system dynamics to directly reveal the main sources and consequences of the interactions without the use of complex numerical models. Moreover the problem is solved in the temporal frequency domain thus emphasizing the attenuation or increase (in amplitude) of high- versus low-frequency forcing in the system as well as the lag-lead of the system response through the study of the phase. This gives a new point of view on land-surface modeling through the strong frequency constraints imposed by the coupling between the soil and the Atmospheric Boundary Layer (ABL) .

In this thesis work, both deterministic and stochastic approaches are adopted. The objective of the deterministic approach is to analyze the propagation of heat flux and temperature waves induced by solar forcing at the land surface into the soil-ABL continuum. We especially focus on investigating the amplitude and phase of heat fluxes and temperatures, and highlight their dependence on land-surface parameters. In particular, this study can be used for the design of sampling schemes for satellites observing the land-surface temperature.

Finally, a stochastic approach is introduced to assess the repercussion of variability in the surface heat budget at the land surface. This study underscores the importance of accurate radiation modeling or measurement as the error strongly impacts the soil-ABL media, therefore reducing the predictability of meteorological forecasts. Moreover this study shows that the synergy of microwave brightness temperature and air temperature at screen level is optimal to reduce the influence of incoming radiation noise on the land-surface assimilation scheme, as well as to better estimate the land-surface state (e.g. soil moisture). In addition we demonstrate that the assimilation

of screen-level specific humidity is not reliable in order to determine the land-surface state.





# Chapter 1

## Governing equations of state

The land surface couples the exchange of energy and water through the energy partitioning. The land surface receives the energy from the sun and atmosphere in the form of respectively a shortwave  $S_{\downarrow}$  and longwave  $L_{\downarrow}$  radiation. This energy received is dissipated by the surface through different processes: i) radiative dissipation  $L_{\uparrow}$  in the longwave, because the surface acts as a grey body, which temperature and emissivity define the emitted radiation to the surrounding atmosphere. ii) Ground heat flux  $G_0$ , which diffuses part of the received energy into the soil. iii) Sensible heat flux  $H$ , which corresponds to the conductance of energy in the atmosphere through mechanical turbulence. This flux is due to land surface-air temperature differences. iv) Latent heat flux  $\lambda E$ , which corresponds to the evaporation of soil moisture in the atmosphere induced by turbulence and humidity gradients between the land surface and the surrounding air. Another dissipation of incoming radiation can occur in the form of thermal accumulation in the vegetation layer, yet this effect is assumed negligible in this study because the vegetation heat capacity considered is low.

Such energy partitioning at the land surface indicates that soil moisture and temperature are strongly coupled because the former controls the release of surface energy in the form of latent or ground heat flux, through the modification of the soil heat capacity which depends on the soil water content. This shows that soil moisture has a control on soil temperature because this latter results from land-surface equilibrium between the heat fluxes. Yet the change in soil temperature also controls the differ-

ent land-surface heat fluxes and in particular latent heat flux, consequently impacting soil moisture over the longer run. This behavior proves that soil moisture and temperature are two strongly coupled variables and that this coupling is fundamental to better predict the soil and atmospheric states.

In the rest of the study the horizontal variation of the state and fluxes are assumed to be negligible when compared to their vertical variations. Hence all partial differential equations will omit the addition of horizontal divergence.

## 1.1 Soil

### 1.1.1 Water movement

The movement of water in the unsaturated surface layer of the soil is usually described by the Richards' equation (1931) [27], which is a non-linear differential equation:

$$\frac{\partial w}{\partial t} = \frac{\partial}{\partial z} \left[ K(w) \left( \frac{\partial \psi}{\partial z} + 1 \right) \right] \quad (1.1)$$

where:  $w$  is the soil moisture content [ $\text{m}^3 \text{m}^{-3}$ ]

$z$  is the depth [m]

$K$  is the hydraulic conductivity [ $\text{m s}^{-1}$ ]

$\psi$  is the matric head [m]

In this thesis the soil water movement is assumed to be negligible as we are working at the daily timescale and in non rainy conditions. In these conditions the movement of water in the soil can be assumed to be negligible in particular when compared to other processes. This has important repercussions since the only control of soil moisture on the energy partitioning will be through the modification of evapotranspiration (evaporation plus transpiration), the daily changes in the soil heat capacity are assumed negligible. However because of the energy coupling at the land surface, the modification of the latent heat flux will induce changes in all other components of the land-surface energy balance. Moreover this approximation will

strongly simplify the problem since the Richard's equation is strongly non-linear and would have posed many issues during the linearization of the system.

### 1.1.2 Temperature evolution

In the soil, the temporal evolution of the temperature is described by a simple diffusion equation, where the soil heat flux is given by Fourier's law, which coefficient is dependent on the local soil temperature and moisture.

$$G(z, t) = k_T \frac{\partial T_s}{\partial z} \quad (1.2)$$

where  $G$  is the soil heat flux [ $\text{W m}^{-2}$ ]

$k_T$  is the soil thermal conductivity [ $\text{W K}^{-1} \text{m}^{-2}$ ]

$T_s$  is the soil temperature [K]

Then the conservation of soil heat leads to the following diffusion equation introduced by De Vries (1958) [7]:

$$c_s \frac{\partial T_s}{\partial t} = \frac{\partial G}{\partial z} \quad (1.3)$$

where  $c_s$  is the soil heat capacity [ $\text{J m}^{-3} \text{K}^{-1}$ ].

Throughout the rest of our study the soil heat capacity and thermal conductivity will be assumed to be constant and uniform throughout the soil profile. This represents one of the major assumptions of our work, yet it can be partly justified by several arguments. First of all since we are only interested in the daily variations of the soil and atmospheric coupling, the influence of the evolution of soil moisture in this diffusion equation can be neglected. Second, as will be emphasized in this thesis the diurnal solar heating only influences a very shallow layer of the soil of a few centimeters, in which soil moisture can reasonably be assumed to be uniform. However the temperature dependency of the upper soil heat capacity and thermal conductivity will be neglected for the sake of simplicity and to allow for analytical solutions.

## 1.2 The Atmospheric Boundary Layer (ABL)

The atmosphere can be decomposed in five main regions: i) the atmospheric boundary layer, which will be described with further detail in this section. This layer is located in the vicinity of the Earth's surface and is mostly dominated by turbulent motion. Moreover as will be shown in forthcoming sections, the ABL structure is controlled by the daily course of the energy fluxes at the land surface. The ABL is usually defined as the region of the atmosphere influenced by hourly changes of the land-surface heat fluxes. Its height is of the order of one km but depends on the latitude, meteorological conditions and land-surface radiation. ii) The troposphere, which includes the ABL, has a height of about 8 to 15 km depending on the latitude and season. Above the ABL the air temperature gradient is negative and of the order of  $6.4 \text{ K km}^{-1}$ . The tropospheric layer concentrates most of the meteorological phenomena, it is therefore in this layer that the water cycle is mostly located, leading to an important water quantity. iii) Above the troposphere, the stratosphere possesses a positive temperature gradient, which is due to the presence of ozone. This region has a height of about 12 to 50 km depending on the latitude and is the place of negligible turbulence. iv) On top of the stratosphere and below 80 km, the mesosphere possesses negative air temperature gradients. It is a transition region between the Earth and the space. v) Finally, farthest away from the surface the thermosphere has a height of about 500 km, in which the air composition is not uniform since the air blending is insufficient to maintain the distribution of the mixing as in the inferior layers.

The atmospheric boundary layer is consequently the region of the atmosphere responding to the daily turbulent heat exchange with the land surface. This turbulence is generated by either wind drag (forced convection) or surface air instability induced by solar heating of the surface (free convection). It is most often a combination of both. The atmospheric boundary layer height is highly varying, with values from 10 m in the case of strongly stabilized nighttime turbulence to several kilometers, for highly unstable turbulent motions during daylight hours. During daytime, the layer is usually characterized by an important vertical structure with three main subre-

gions, since in response to solar heating of the surface, the surface is warmer than the overlying air. i) The surface layer has a height of about one tenth of the total height, where the scalar (temperature, specific humidity) vertical gradients are strong and the changes in turbulent fluxes are small. ii) Above the surface layer, the convective layer, which is a place of intense turbulent motions, tends to mix scalar values, leading to relatively uniform scalar gradients. iii) The entrainment zone, which separates the boundary layer from the free troposphere, possesses a much smaller turbulent activity (see Figure 1-4).

### 1.2.1 Thermodynamics

#### Ideal gas law

To better comprehend the diurnal evolution of the ABL it is interesting to return to the basic definition of thermodynamics in a moist fluid. Indeed the region of validity of the hypotheses used in the ABL are often overlooked but are fundamental to comprehend the motion and evolution of a moist fluid parcel within the ABL.

First, the ideal gas law gives:

$$p\alpha = RT \tag{1.4}$$

Where:  $p$  is the fluid pressure [Pa]

$\alpha = 1/\rho$  is the specific volume [ $\text{m}^3 \text{kg}$ ] defined as the ratio between the parcel volume  $V$  and its mass  $M$ .

$\rho$  is the fluid density in [ $\text{kg m}^3$ ]

$R$  is the gas constant in [ $\text{J kg}^{-1} \text{K}^{-1}$ ]

$T$  is the temperature of the air parcel [K]

#### First law of thermodynamics

In a fluid the internal energy conservation (1st law of thermodynamics) can be rewritten (per unit mass):

$$du = \delta q + \delta w = \delta q - pd\alpha \tag{1.5}$$

where  $u$  is the internal energy per unit mass,  $q$  is the enthalpy per unit mass and  $\delta q$  represents the variation of this quantity.

$\delta w$  is the infinitesimal work on the parcel. If one introduces the specific heat at constant volume  $C_v = \left(\frac{\partial u}{\partial T}\right)_\alpha$ , so that equation (1.5) can be rewritten as:

$$\delta q = C_v dT + p d\alpha \quad (1.6)$$

Or another convenient form for meteorologists is obtained with the introduction of the specific heat at constant pressure:  $C_p = \left(\frac{\partial u}{\partial T}\right)_p = C_v + R$ , equation (1.5) can be rewritten as:

$$\delta q = C_p dT - \alpha dp \quad (1.7)$$

Thus several types of processes can be defined:

a) Isobaric process:  $dp = 0$

$$\delta q = C_p dT \quad (1.8)$$

b) Isothermal process:  $dT = 0$

$$\delta q = -\alpha dp = \delta w \quad (1.9)$$

c) Adiabatic process:  $\delta q = 0$

$$C_p dT = \alpha dp \quad (1.10)$$

Many of the temperature changes in the atmosphere can be approximated as adiabatic. In the case of a fluid (even moist) the equation of state can be reformulated using the ideal gas law:  $C_p dT = RT \frac{dp}{p}$ . Therefore we can introduce the (virtual) potential temperature  $\theta$  ( $\theta_v$ ) in a dry (moist) atmosphere. The potential temperature is defined as the temperature that the parcel would obtain if brought adiabatically to a standard reference pressure  $P_0$ , usually taken as 1000 mb:

$$\theta = T (P_0/P)^{R/C_p} \quad (1.11)$$

where:  $T$  is the temperature of the air parcel [ $K$ ],  $R$  is the gas constant of dry air. In the case of a moist fluid the virtual potential temperature is used instead of potential temperature and shares the same definition except that temperature is replaced by virtual temperature  $T_v$ . The virtual temperature  $T_v$  takes into account the humidity of the gas using the mixing ratio  $w$  (or specific humidity  $q$ ) of the fluid parcel, through  $R_{wet} = R_{dry}(1 + \epsilon w)$ , and with  $\epsilon = R_{dry}/R_{water} \approx 0.622$  and  $w$  being the mixing ratio (mass of water vapor per unit mass of dry air).  $T_v$  is given by:

$$T_v = T \frac{1 + w/\epsilon}{1 + w} \approx T \left( 1 + \frac{1 - \epsilon}{\epsilon} w \right) \quad (1.12)$$

$c_p$  is the specific heat capacity at constant pressure [ $J \text{ kg}^{-1} \text{ K}^{-1}$ ]

$\theta$  (resp.  $\theta_v$ ) is a conserved quantity in an adiabatic process of a dry (resp. wet) atmosphere.

## Second law of thermodynamics

The entropy, which is a state variable of the fluid, can be introduced through the second law of thermodynamics and related to the heat added to the fluid (per unit mass):

$$ds = \frac{\delta q}{T} \quad (1.13)$$

The entropy of the dry (resp. moist) gas can be related to the (resp. virtual) potential temperature of the fluid, using equation (1.10) in conjunction with (1.11):

$$s = C_p \ln(\theta) + cst \quad (1.14)$$

Therefore adiabatic processes in the atmosphere are also isentropic.

In the rest of our study, the cases of ABL with condensation of water vapor will be avoided so that pseudoadiabatic processes will not be studied further.

## Stability criteria

Virtual potential temperature has a second advantage: it can serve as an indicator of the stability/instability of the air.

In an atmosphere in hydrostatic equilibrium, vertical pressure gradient forces is in equilibrium with gravitational forces so that:

$$-\frac{1}{\rho} \frac{\partial p}{\partial z} = g \quad (1.15)$$

For an air parcel undergoing an adiabatic process:

$$C_p \frac{dT_v}{T_v} = R \frac{dp}{p} \quad (1.16)$$

where  $C_p$  is specific heat and  $R$  is perfect gas constant of the dry air, virtual temperature is introduced in the equation to take into account water vapor content. Thus for an ascending or descending motion of the air parcel:

$$\frac{dT_v}{dz} = \frac{R}{C_p} \frac{T_v}{p} \frac{dp}{dz} \quad (1.17)$$

But a fluid parcel pressure has to instantaneously adjust with the pressure of the surrounding air so that:

$$\frac{dp}{dz} = \frac{\partial p}{\partial z} = -\rho' g \quad (1.18)$$

Where  $\rho'$  is the ambient air density:  $\rho' = p/RT'_v$  and  $T'_v$  is ambient virtual temperature.

If we combine this equation we obtain (as  $T_v/T'_v \approx 1$ ):

$$\frac{dT_v}{dz} = -\frac{g}{C_p} = -\Gamma \approx 0.98K/100m \quad (1.19)$$

$\Gamma$  is the adiabatic lapse rate for moist (but unsaturated) air, which is identical to the dry adiabatic lapse rate except that the virtual temperature is considered instead of the actual air temperature.



If one considers a parcel of air, the buoyant force acting in this parcel is:

$$B = g \frac{\rho' - \rho}{\rho} = g \frac{T_v' - T_v}{T_v} \quad (1.20)$$

because the parcel pressure equals the environment pressure. Therefore when the parcel is warmer (in the meaning of virtual temperature i.e. taking into account the effect of water vapor) than the surrounding air, it will tend to rise and inversely it will sink when it is colder than the surrounding air.

Now assume that the ambient lapse rate is defined as:

$$-\frac{\partial T_v'}{\partial z} = \gamma \quad (1.21)$$

When a parcel with initial temperature  $T_v$  rises adiabatically by a distance  $\Delta z$ , its virtual temperature will decrease and become  $T_v - \Gamma \Delta z$ . Consequently the air is unstable if  $\gamma > \Gamma$  (increased velocity) the air is stable if  $\gamma < \Gamma$  (restoring force) and neutral for the special case  $\gamma = \Gamma$  (no buoyancy). This stability criteria can be rewritten in terms of the virtual potential temperature, indeed  $dT_v/T_v = d\theta_v/\theta_v + (R/C_p)dp/p$ , so that:

$$\frac{1}{\theta_v} \frac{\partial \theta_v}{\partial z} = \frac{1}{T_v} \frac{\partial \theta_v}{\partial z} - \frac{R}{C_p} \frac{1}{C_p} \frac{\partial p}{\partial z} = \frac{1}{T_v} (\Gamma - \gamma) \quad (1.22)$$

Thus the virtual potential temperature can be used to determine the stability of the atmosphere. In the case of a dry atmosphere, one would use the potential temperature in lieu the virtual potential temperature. The stability criteria can be summarized as:

- Subadiabatic

$$\frac{\partial \theta_v}{\partial z} > 0$$

- Adiabatic

$$\frac{\partial \theta_v}{\partial z} = 0$$

- Superadiabtic

$$\frac{\partial\theta_v}{\partial z} < 0$$

Very often meteorologists use the term stable for subadiabatic, neutral for adiabatic, and unstable for superadiabatic. In most cases the terms can be confounded yet there are a few situations where it does not hold. For instance the air can be adiabatic (no virtual potential temperature gradients) but unstable as is observed in the case of the mixed layer of the ABL. This paradox can be avoided if one also looks at the lapse rate of the air immediately below or above the adiabatic layer. If the lower air is superadiabatic, both the superadiabatic layer and the adiabatic upper layer are statistically unstable. The terms stable/neutral/unstable reflects an integrated view of the ABL even though locally the fluid can be sub/superadiabatic.

### 1.2.2 Daily evolution

The diurnal course of a typical ABL growth is depicted on Figure 1-1 taken from Stull (1988) [31]. The understanding of the daily cycle of the ABL is of great importance to better comprehend the coupling of the soil and the atmosphere throughout the day. Here our study focuses on fair weather conditions with no snow cover and weak advection.

The turbulent mixing in the ABL is performed by eddies of different sizes, ranging from a few millimeters to large thermals with a size of the order of the ABL height. After sunrise, the sun warms the land surface leading to an increase of the land-surface temperature and of the one in its vicinity. Since the air at the surface is warmer and thus lighter than the air above it, the air becomes unstable thus generating intense turbulence, which tends to mix the near-surface layer with the air above. Indeed the surface warming triggers a convective motion (vertical mechanical motion of air), which is accompanied by a descending motion of an overlying, colder, air volume. There is consequently a conversion of potential energy into kinetic energy. The convective process is associated with positive sensible heat flux and evapotranspiration. This convective process leads to the formation of a convective boundary layer, also

called **mixed layer**, in which scalars, such as momentum, potential temperature and specific humidity, are well mixed. This adiabatic layer is however in a constant unstably state with frequent updrafts of lighter, warmer, air from below and accompanied by downdrafts of colder, heavier, air from above. Near the soil there remains a layer with strong scalar gradients and relative small changes in momentum and heat fluxes: the **surface layer**.

Then before sunset, solar heating remains insufficient to keep the land temperature warmer than the overlying air leading to the stabilization of the air near the surface, accompanied by negative sensible heat flux. This stabilization effect will destroy the mixed layer that will collapse almost instantaneously since it is not anymore fed by the instability at the land surface. The surface stabilization creates a stable ABL in which turbulence is intermittent and acting at much smaller spatial scales than during daylight hours. The ABL over land is distinguished from that over the ocean through its large diurnal amplitude. Over oceans the ABL is nearly constant and uniform at around 500m because there is only small variations in the sea-surface temperature. The large diurnal amplitude of land-surface temperature leads to the large diurnal range of the ABL over land (of the order of 10m to up to 2 km). The lower part of this stable layer is still characterized by strong scalar gradients and remains named surface layer. Above the stable ABL, there remains a residual layer, mark of the preexisting convective boundary layer, with relative uniform scalar repartition. This adiabatic layer is statistically neutral.

The corresponding profiles of virtual potential temperature, i.e. an indicator of buoyancy, are shown on Figure 1-2. The different structure of the ABL throughout the day is easily described and corresponding to the sounding times of Figure 1-1. Moreover the typical diurnal shape of a well-mixed boundary layer is described on Figure 1-3. It is clear on this figure that most variables are almost uniform throughout the ABL. It is also interesting to note that there can be a gradient of scalars at the land surface, which corresponds to the surface layer.

### 1.2.3 ABL dynamics equations

#### Mass conservation

In the atmospheric boundary layer the fluid can be considered as incompressible:

$$\frac{\partial U_j}{\partial x_j} = 0 \quad (1.23)$$

Where  $U_j$  is the velocity component in the  $j^{\text{th}}$  cartesian direction in  $[\text{m s}^{-1}]$ .

#### Conservation of momentum

Since the air in the ABL acts as an incompressible Newtonian fluid, to a close approximation the velocity components in the referential perpendicular to gravity can be written:

$$\frac{\partial U_i}{\partial t} + U_j \frac{\partial U_i}{\partial x_j} = -\delta_{i3}g - 2\epsilon_{ijk}\Omega_j U_k + \nu \frac{\partial^2 U_i}{\partial x_j^2} \quad (1.24)$$

where:  $\Omega_j$  is the Earth's angular velocity vector in  $[\text{rad s}^{-1}]$  and the product term is the Coriolis acceleration,  $\nu$  is the molecular diffusion in  $[\text{m}^2\text{s}^{-1}]$

#### Conservation of moisture

The conservation of water vapor  $q$  reads:

$$\frac{\partial q}{\partial t} + U_j \frac{\partial q}{\partial x_j} = \frac{S_q}{\rho} + \frac{E}{\rho} + \nu_q \frac{\partial^2 q}{\partial x_j^2} \quad (1.25)$$

The conservation of water in liquid form  $q_L$  reads:

$$\frac{\partial q_L}{\partial t} + U_j \frac{\partial q_L}{\partial x_j} = \frac{S_{qL}}{\rho} - \frac{E}{\rho} \quad (1.26)$$

Where:  $\nu_q$  is the molecular diffusivity for water vapor in the air in  $[\text{m}^2 \text{s}^{-1}]$ .

$S_x$  is a net moisture source/sink term, per unit volume and unit time.

$E$  is the mass of water vapor per unit volume and unit time induced by phase change.

Molecular diffusion is assumed to be negligible on the liquid phase.

## Conservation of enthalpy

The first law of thermodynamics reads:

$$\frac{\partial \theta}{\partial t} + U_j \frac{\partial \theta}{\partial x_j} = -\frac{1}{\rho C_p} \frac{\partial Q_j}{\partial x_j} - \frac{L_p E}{\rho C_p} + \nu_\theta \frac{\partial^2 \theta}{\partial x_j^2} \quad (1.27)$$

where:  $\nu_\theta$  is the thermal diffusivity in  $[\text{m}^2 \text{s}^{-1}]$

$L_p$  is the latent heat associated with phase change.

$Q_j$  is the component of net radiation in the  $j^{\text{th}}$  direction.

$C_p$  is the specific heat for moist air, which can be rewritten as:  $C_p = C_{p,dry} (1 + 0.85q)$ .

Typical ABL values of specific humidity can play an important role on specific heat and therefore on potential temperature values.

### 1.2.4 Mean ABL dynamics equations

Any turbulent variable  $X$  can be decomposed as a Reynolds sum with its mean value  $\bar{X}$  and the turbulent fluctuation around this mean  $X'$  as  $X = \bar{X} + X'$ , with  $\bar{X}' = 0$ . Moreover because the typical values of the Reynolds number in the ABL are very large, of the order of  $10^6 - 10^7$ , viscosity forces will be negligible compared to other forces in this layer, except in the vicinity of the surface (of the order of a few cm) where diffusion remains an essential process. The dynamics equation can consequently be rewritten for the mean state.

#### Boussinesq approximation

When the fluid is turbulent and when we consider the fluid density  $\rho = \bar{\rho} + \rho'$ , the variations of the air density  $\rho'$  can be neglected in the inertia term but should be retained in the buoyancy term of the momentum equation. Finally, in practice in the turbulent equations of the fluid,  $\rho$  can be replaced by  $\bar{\rho}$  except in the buoyancy term where it should be taken into account and all occurrences of  $g$  should be replaced by  $g - \theta'_v / \bar{\theta}_v g$ . (See Stull (1988) [31] p84 for a reference).

## Mass conservation

The mean flow can be considered as incompressible:

$$\frac{\partial \bar{U}_j}{\partial x_j} = 0 \quad (1.28)$$

## Conservation of momentum

The Navier-Stokes equation for the mean flow becomes:

$$\frac{\partial \bar{U}_i}{\partial t} + \bar{U}_j \frac{\partial \bar{U}_i}{\partial x_j} = -\delta_{i3}g - 2\epsilon_{ijk}\Omega_j \bar{U}_k + \nu \frac{\partial^2 \bar{U}_i}{\partial x_j^2} - \frac{\partial (\overline{u'_i u'_j})}{\partial x_j} \quad (1.29)$$

The last term appearing in this equation is the Reynolds stress, or the effect of turbulence on the mean flow.

## Conservation of moisture

The conservation of mean water vapor  $\bar{q}$  reads:

$$\frac{\partial \bar{q}}{\partial t} + \bar{U}_j \frac{\partial \bar{q}}{\partial x_j} = \frac{\bar{S}_q}{\bar{\rho}} + \frac{\bar{E}}{\bar{\rho}} + \nu_q \frac{\partial^2 \bar{q}}{\partial x_j^2} - \frac{\partial (\overline{q' u'_j})}{\partial x_j} \quad (1.30)$$

The conservation of water in liquid form  $q_L$  reads:

$$\frac{\partial \bar{q}_L}{\partial t} + \bar{U}_j \frac{\partial \bar{q}_L}{\partial x_j} = \frac{\bar{S}_{qL}}{\bar{\rho}} - \frac{\bar{E}}{\bar{\rho}} - \frac{\partial (\overline{q'_L u'_j})}{\partial x_j} \quad (1.31)$$

## Conservation of enthalpy

The first law of thermodynamics reads:

$$\frac{\partial \bar{\theta}}{\partial t} + \bar{U}_j \frac{\partial \bar{\theta}}{\partial x_j} = -\frac{1}{\bar{\rho} \bar{C}_p} \frac{\partial \bar{Q}_j}{\partial x_j} - \frac{L_p \bar{E}}{\bar{\rho} \bar{C}_p} + \nu_\theta \frac{\partial^2 \bar{\theta}}{\partial x_j^2} - \frac{\partial (\overline{\theta' u'_j})}{\partial x_j} \quad (1.32)$$

Very similar equations hold for the first-order perturbations  $X'$  as a function of the second-order perturbations  $X''$ , ..., and  $X^{(n)}$  to  $X^{(n+1)}$ ... In fact it is fundamental to see that a closure is required at some order  $n$  in order to entirely solve these equa-

tions. One such approach is to relate the (short-term) turbulent fluctuation fluxes to the (long-term) mean values. Therefore the fluxes are parameterized as a function of the mean flow variables. There could be several possible approaches such as an eddy diffusivity approach (in which the scalar flux is parameterized as a diffusion with non-constant non-uniform diffusion term:  $\overline{w'c'} = K_c(z, t) \frac{\partial \bar{c}}{\partial z}$ ) or a counter-gradient approach as will be described later.

In most simple ABL models these parameterizations are deterministic but could also be stochastic. Some believe that deterministic parameterization cannot realistically represent reality and that probabilistic formulations are necessary. Indeed when a process is non-linear, such as turbulence in the atmosphere, there is no spectral separation in the energy spectrum that could thus justify the use of large (spatial or temporal) versus small scale. Instead one observes a continuous cascade of energy with a given spectral slope, so that the projection on some basis (be it a grid or a spectral basis) cannot solve the entire energy spectrum, and part of this spectrum has to be missing. To account for this energy cascade some authors have introduced a stochastic parameterization, corresponding to the inherent uncertainty associated with the truncation/bulk parameterization. One such example is the fundamental work of Selten (1995) [30]. Selten used the Lorenz 63 equations [23] projected on an EOF (Empirical Orthogonal Functions) basis: the two first component of the variance account for 95% of the total variance. Yet if we remove one dimension (third one for instance) and replace it by a deterministic parameterization as a function of the two first components, the chaos disappears as well as the continuous energy spectrum. Instead of the deterministic formula, Selten then introduced a stochastic parameterization. If the corresponding noise is strong enough (red enough) the Lorenz attractor reappears and the flow is again (pseudo-) chaotic! In fact this stochastic parameterization can be thought as the large scale flow (two first dimensions) coupled with the small scale flow (third dimension). This inherent stochastic behavior could explain why similarity theories, such as Monin-Obukhov's, are never extremely accurate and are prone to strong scattering around the mean curve.

### 1.2.5 André et al. 1978

The summary of the fundamental work of André et al. (1978) [3] gives very important insights on the 24-hour evolution of the ABL. In this study the authors investigated the evolution of the 24h ABL as well as the main factors influencing its evolution and aspect. In particular the authors give critical insight on the ABL structure, which has received little attention afterward, whereas this is of crucial importance to understand the development and collapse of the daily ABL.

The authors used a Large Eddy Simulation (LES), which is closed using a parameterization of the molecular dissipation. The equations are recalled here after.

- Zero-order equations (horizontally homogeneous and no advection):

$$\frac{\partial \bar{\theta}}{\partial t} = -\frac{\partial \overline{w'\theta'}}{\partial z} - \bar{R} \quad (1.33)$$

Where  $R$  is the cooling rate due to the divergence  $\partial \bar{F}/\partial z$  of the mean longwave radiative flux  $\bar{F} = \bar{F}_\uparrow - \bar{F}_\downarrow$ . André et al. used the formulation of Sasamori (1972) [29] to express the divergence of the vertical structure of the ABL:

$$\frac{\partial \bar{F}}{\partial z} = \int_0^z \frac{\partial A(z, z')}{\partial z} \frac{\partial B}{\partial z'} dz' + \int_z^{z_T} \frac{\partial A(z, z')}{\partial z} \frac{\partial B}{\partial z'} dz - \frac{\partial A(z, \infty)}{\partial z} B(z_T) \quad (1.34)$$

Where  $B(z)$  is the blackbody emission at the mean temperature  $\bar{T}(z)$  at altitude  $z$  and  $A(z, z')$  is the total absorptivity of water vapor between altitudes  $z$  and  $z'$ . The diurnal evolution of potential temperature is shown on Figure 1-5. The formation of the convective, well-mixed, boundary layer is clear before noon, when sensible heat flux is positive. It is accompanied by an increase in the ABL height, directly influenced by the input of sensible heat at the bottom of the ABL. The corresponding sensible heat is shown on Figure 1-8 and linearly decreases in most of the surface and convective layer. Near the top of the ABL the sensible heat flux vanishes quickly while the potential temperature profile tends to the free troposphere lapse rate. Sensible heat flux is maximum at the surface since this latter is the main source of heat for the system. The free troposphere also constitutes a source of heat for the system



because of the entering hotter air from the overlying free troposphere (as the lapse rate of potential temperature is positive in the free troposphere).

The nocturnal evolution of potential temperature in Figure 1-6 highlights the rapid collapse of the convective boundary layer, which is replaced by a stable layer capped by a residual layer.

The evolution of specific humidity is driven by the following equation:

$$\frac{\partial \bar{q}}{\partial t} = - \frac{\partial \overline{w'q'}}{\partial z} \quad (1.35)$$

The diurnal evolution of specific humidity is displayed on Figure 1-7. Again the convective ABL is clearly visible after 11AM. Moreover the top of the well-mixed humidity region tends to extend slightly lower than the region of well mixed potential temperature. This comment has some importance for the formation of clouds within the ABL: because of the negative slope of the specific humidity lapse rate in the free-atmosphere, the propagation of the region of well-mixed humidity is rendered more difficult than that of potential temperature and leads to an inflexion point at the connection between this region and the free troposphere. ABL clouds thus tends to form below the top of the ABL (when defined using potential temperature) corresponding to observations. Therefore the expression cloud-topped ABL is usually misleading since the top of the ABL will be located above the ABL cloud formation level.

The diurnal evolution of the latent heat profile is described on Figure 1-9. It should be noted that latent heat tends to vary linearly in the ABL like sensible heat flux. Even though the surface is an important source of moisture for the ABL the entrance of much drier air from the overlying free troposphere will create a strong latent heat near the top of the ABL. Thus the behavior is much different from the sensible heat case, where the free troposphere constituted a source of sensible heat entering the ABL top, whereas for humidity the free troposphere constitutes a sink of latent heat for the ABL. Moreover as the mean wind components are horizontally uniform the

mean equation of continuity reads:

$$\frac{\partial \bar{w}}{\partial z} = 0 \quad (1.36)$$

The vertical sensible heat flux equation can be written:

$$\frac{\partial \overline{w'\theta'}}{\partial z} = -\frac{\partial \overline{w'^2\theta'}}{\partial z} - \left( \overline{w'^2} \frac{\partial \bar{\theta}}{\partial z} + \overline{w'\theta'} \frac{\partial \bar{w}}{\partial z} \right) - \frac{1}{\rho_0} \overline{\theta'} \frac{\partial p'}{\partial z} \quad (1.37)$$

The variance of potential temperature can be rewritten:

$$\frac{\partial \overline{\theta'^2}}{\partial z} = -\frac{\partial \overline{w'\theta'^2}}{\partial z} - 2\overline{w'\theta'} \frac{\partial \bar{\theta}}{\partial z} - \epsilon_{\theta\theta} - \epsilon_R \quad (1.38)$$

with  $\epsilon_{\theta\theta}$  and  $\epsilon_R$  being the molecular and radiative destruction rates of potential temperature variance  $\overline{\theta'^2}$ .

Notice that equation (1.37) can be rewritten using the continuity of mean wind speed:

$$\begin{aligned} \frac{\partial \overline{w'\theta'}}{\partial z} = & \underbrace{-\frac{\partial \overline{w'^2\theta'}}{\partial z}}_{\text{Turbulent flux of sensible heat flux}} \\ & \underbrace{-\overline{w'^2} \frac{\partial \bar{\theta}}{\partial z}}_{\text{Eddy diffusivity of sensible heat flux}} \\ & + \alpha g \overline{\theta'^2} \underbrace{-\frac{1}{\rho_0} \overline{\theta'} \frac{\partial p'}{\partial z}}_{\text{Pressure covariance}} \end{aligned} \quad (1.39)$$

Similarly for the flux/covariances of specific humidity:

$$\begin{aligned} \frac{\partial \overline{w'q'}}{\partial z} = & \underbrace{-\frac{\partial \overline{w'^2q'}}{\partial z}}_{\text{Turbulent flux of latent heat flux}} \\ & \underbrace{-\overline{w'^2} \frac{\partial \bar{q}}{\partial z}}_{\text{Eddy diffusivity of latent heat flux}} \\ & + \alpha g \overline{\theta'q'} \underbrace{-\frac{1}{\rho_0} \overline{q'} \frac{\partial p'}{\partial z}}_{\text{Pressure covariance}} \end{aligned} \quad (1.40)$$

$$\frac{\partial \overline{q'^2}}{\partial z} = -\frac{\partial \overline{w'q'^2}}{\partial z} - 2\overline{w'q'}\frac{\partial \overline{q}}{\partial z} - \epsilon_{qq} \quad (1.41)$$

On the basis of dimensional arguments, the dissipative terms are parameterized as:  $\epsilon_{\theta\theta} = c_2\epsilon\bar{e}^{-1}\overline{\theta'^2}$ ,  $\epsilon_{qq} = c_2\epsilon\bar{e}^{-1}\overline{q'^2}$ , with  $c_2 = 2.5$  and  $\epsilon = c_1(l)\bar{e}^{-3/2}/l$ .

Moreover the pressure covariance terms is modeled by a return-to-isotropy as suggested by Rotta's (1951) [28]:

$$-\frac{1}{\rho_0}\overline{\theta'}\frac{\partial p'}{\partial z} = c_6\epsilon\bar{e}^{-1}\overline{w'\theta'} - c_7P_{z\theta} \quad (1.42)$$

$$-\frac{1}{\rho_0}\overline{q'}\frac{\partial p'}{\partial z} = c_6\epsilon\bar{e}^{-1}\overline{w'q'} - c_7P_{zq} \quad (1.43)$$

With  $c_6 = 4.85$ ,  $(1 - c_7)/c_6 = 0.125$ ,  $P_{z\theta} = \alpha g\overline{\theta'^2} - \overline{w'\theta'}\frac{\partial \overline{w}}{\partial z} = \alpha g\overline{\theta'^2}$  and  $P_{zq} = \alpha g\overline{\theta'q}$ . The radiative destruction rate  $\epsilon_R$  has to be included to account for the nocturnal behavior of the ABL. Following Townsend (1958) [33]:  $\epsilon_R = \beta\overline{\theta'^2}$ , with  $\beta = 0.1\bar{q}$  in  $[\text{s}^{-1}]$ . With these equations the production/destruction terms as well as the evolution of the ABL can be studied throughout the day.

Figure 1-10 displays the daytime budget of the production of variance of virtual potential temperature. Clearly, radiation is negligible in the adiabatic layer (and thus negligible when there is little potential temperature gradients) but is important near the top of the ABL and at the surface.

Finally the main results of the authors can be summarized as:

- "The convective development of the ABL is characterized by large buoyant production of turbulence near the ground and as this turbulence is transferred upward it leads to a strong mixing of potential temperature, momentum and humidity (mixed layer) [...] an accurate simulation of such a phenomenon requires a sophisticated treatment of turbulence (e.g. Hanna 1977 [17])".

During daytime:

- The divergence of radiative flux in the adiabatic layer (or mixed layer, during daytime) is negligible as compared to that of turbulent heat flux, that is why the turbulent

heat flux  $\overline{w'\theta'}$  is a linear function of elevation in this region.

- Humidity tends to be well mixed in the adiabatic layer but one can notice that there is a small but persistent decrease with altitude.
- During daytime, the effect of radiative transfer is small compared to that of turbulence.

At night:

- "The development of the nocturnal inversion is driven by both radiative transfer and turbulence. [...] both must be taken into account [...]"
- The radiative destruction rate  $\epsilon_R$  must be included for a good description of the nocturnal evolution of the ABL.
- The temperature budget shows that radiative effects are much more important than turbulent transport except close to the ground. The divergence of the longwave radiative flux is determined by the interplay between thermal stratification and humidity distribution. The radiative cooling decreases rapidly with height in the lower layers. Above this region and below the top of the ABL the near constancy of radiative cooling is due to a competitive effect of decreasing temperature and humidity with height. At the inversion level, the strong temperature jump explains the radiative cooling minimum. "This preponderance of radiative transfer over turbulence also characterizes the study of Yamada and Mellor (1975) [35] and casts serious doubts on studies where this effect is neglected."
- Radiative transfer and mesoscale pressure gradient are much more important than turbulence in driving the nocturnal ABL evolution, which is particularly true in most of the stable layer where turbulent transfer is negligible.
- The radiative term can be neglected in the equation for sensible heat flux conservation  $\overline{w'\theta'}$ . This is of importance since we can have an equation with radiative transfer in the potential temperature equations but it can be neglected in the sensible heat flux equation.

### 1.3 Coupling

Throughout the day there is strong coupling between the land and the atmosphere. Indeed the land surface serves as a boundary condition for the atmospheric boundary layer because the atmospheric state is conditioned by the temporal evolution of the land fluxes of momentum, heat and scalars. In land-atmosphere studies, this boundary condition is usually considered as a flux condition, or a Neumann condition for the ABL. The air scalar gradients near the land surface are high and the sources of heat and moisture are usually variably distributed at the surface because of the natural heterogeneity of natural vegetated surfaces. These strong gradients, whose boundaries are not well-defined lead to difficulties in the representation as a Dirichlet problem. In contrast, turbulent heat fluxes are only slightly varying in the surface layer overlying the vegetation, leading to a simplified representation as a Neumann problem.

Conversely the land state is conditioned by the atmospheric state as the thermodynamic equilibrium of the land surface temperature is closely related to the dissipation of heat at the surface through the release of sensible and latent heat as well as through radiation. This boundary condition can be thought as a mixed boundary condition where both the fluxes and state have to be combined.

Physically it is easy to appreciate how the two media are related: if the incoming radiation at the land surface increases there is a consequential increase of the land-surface temperature in order to dissipate the added energy through the release of heat by radiation, sensible and latent heat. There is consequently an increase of the surface temperature gradients between the land and the air, thus introducing a change in the aerodynamic resistance of the overlying air for dissipation. The sensible and latent heat fluxes at the surface thus increase leading to the rise of the potential temperature and scalar concentration in the ABL. Moreover through the release of heat at the surface the land-surface temperature decreases, thus leading to reduced gradients between the land-surface and air temperatures. This again changes the air resistance to temperature increase and scalar dissipation and both sensible and latent

heat fluxes are decreased. This process will go on until the system reaches a quasi-steady state (in terms of the mean values). In fact this corresponds to the turbulence convergence (or Monin-Obukhov length convergence).

This simple example shows how complex the coupling between the land and the atmosphere can be, as well as the many feedbacks, be they positive or negative, that can occur at very different time scales in response to a simple forcing.

Better understanding of the coupling between the land and the overlying atmosphere is required to improve weather and climatic forecasts as well as hydrological prediction. Indeed the atmosphere is a complex non-linear system, thus poor specification of its boundary and initial conditions leads to incorrect state estimate and thus incorrect prediction. As the land and the atmosphere are strongly coupled, full understanding of the diurnal surface energy partitioning cannot be thought after without the land coupling. Therefore the land and atmosphere systems have to be considered as one single system.

Finally there have been few studies focusing on the understanding of the daily coupling of the two media and of the frequency response of the coupled system to a daily forcing of incoming radiation. Yet the understanding of the coupling at the daily timescale is fundamental to improve the predictability of the atmospheric and soil state. One of the main theoretical work describing the coupling at the daily timescale is the pioneering work of Lettau (1951) [22].

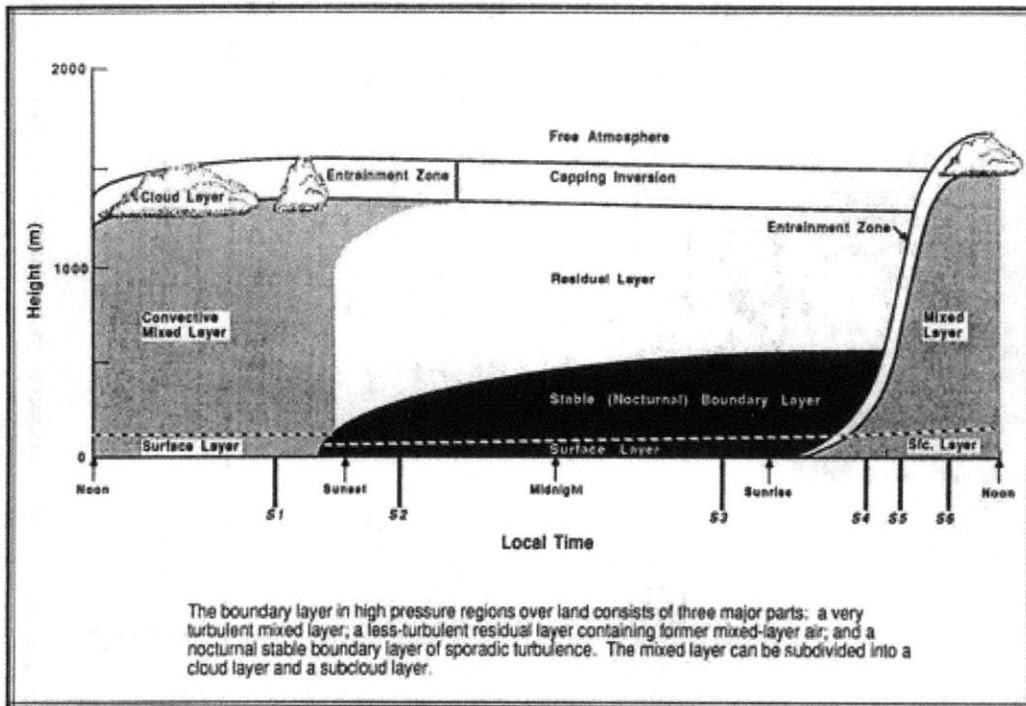


Figure 1-1: Daily course of the ABL structure taken from Stull (1988)

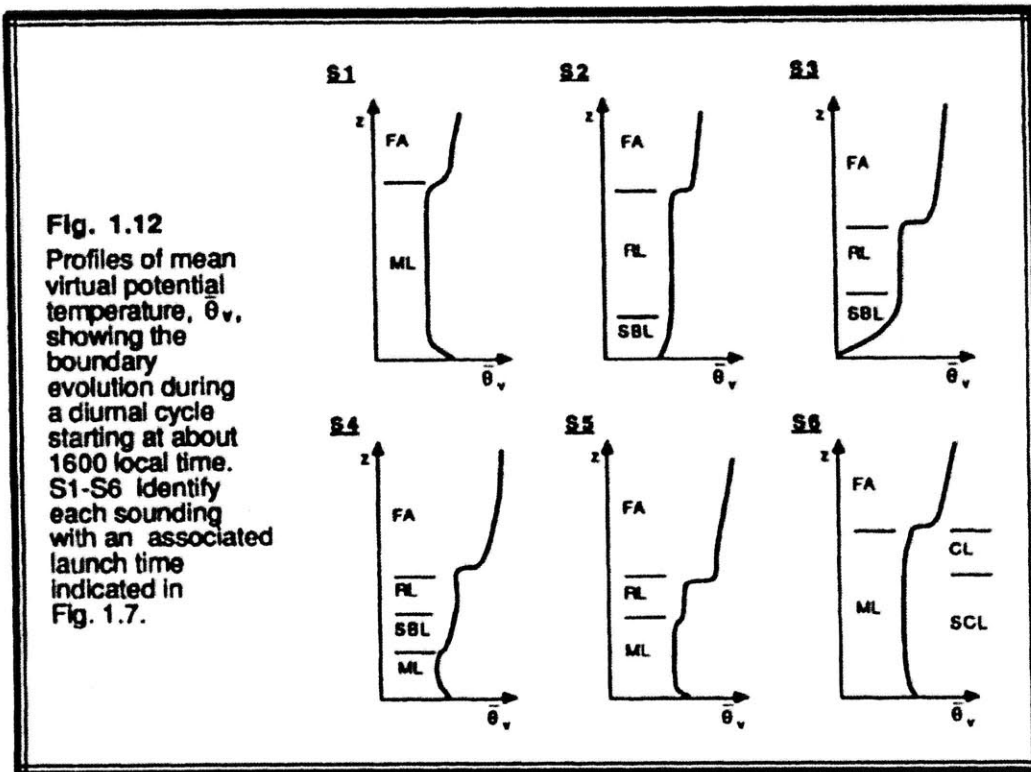


Figure 1-2: Daily course of mean virtual potential temperature  $\theta_v$  taken from Stull (1988)



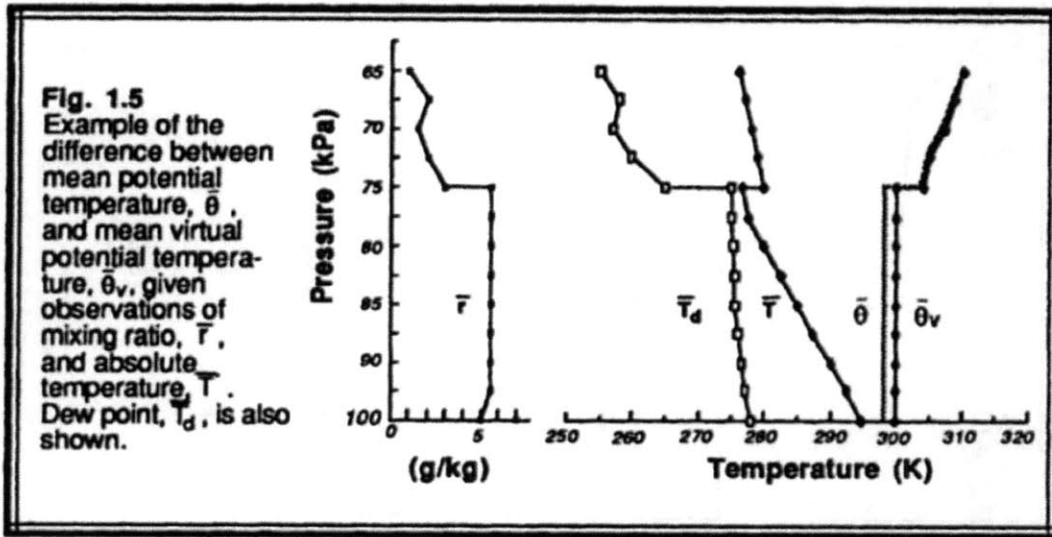


Figure 1-3: Typical profiles of temperatures and scalar during the day, with a well mixed boundary layer, taken from Stull (1988)

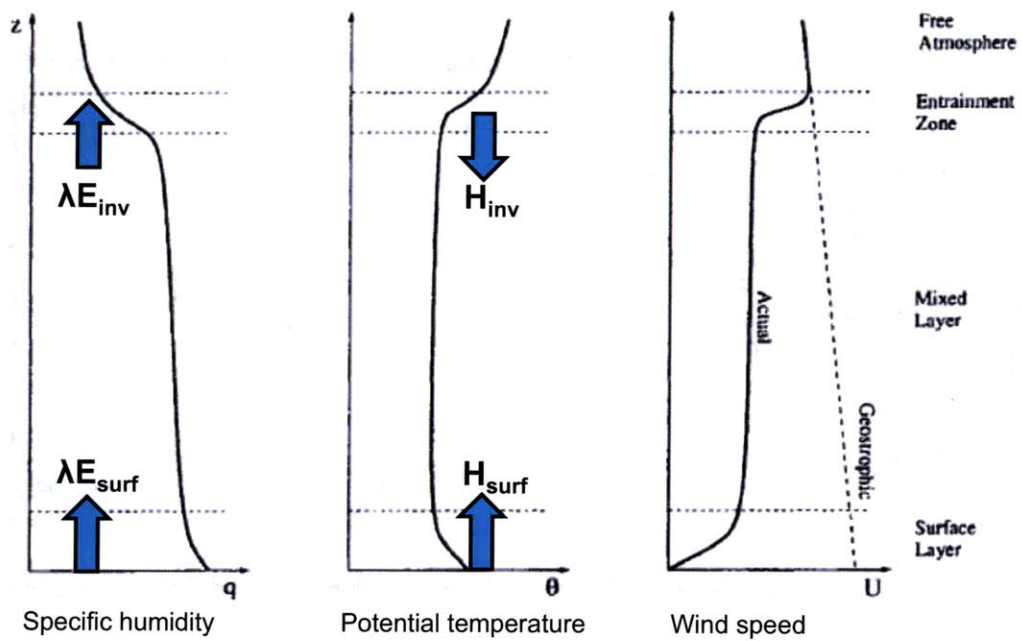


Figure 1-4: Typical profiles of temperature, humidity and wind speed in the ABL, taken from Margulis' PhD Thesis (2002)

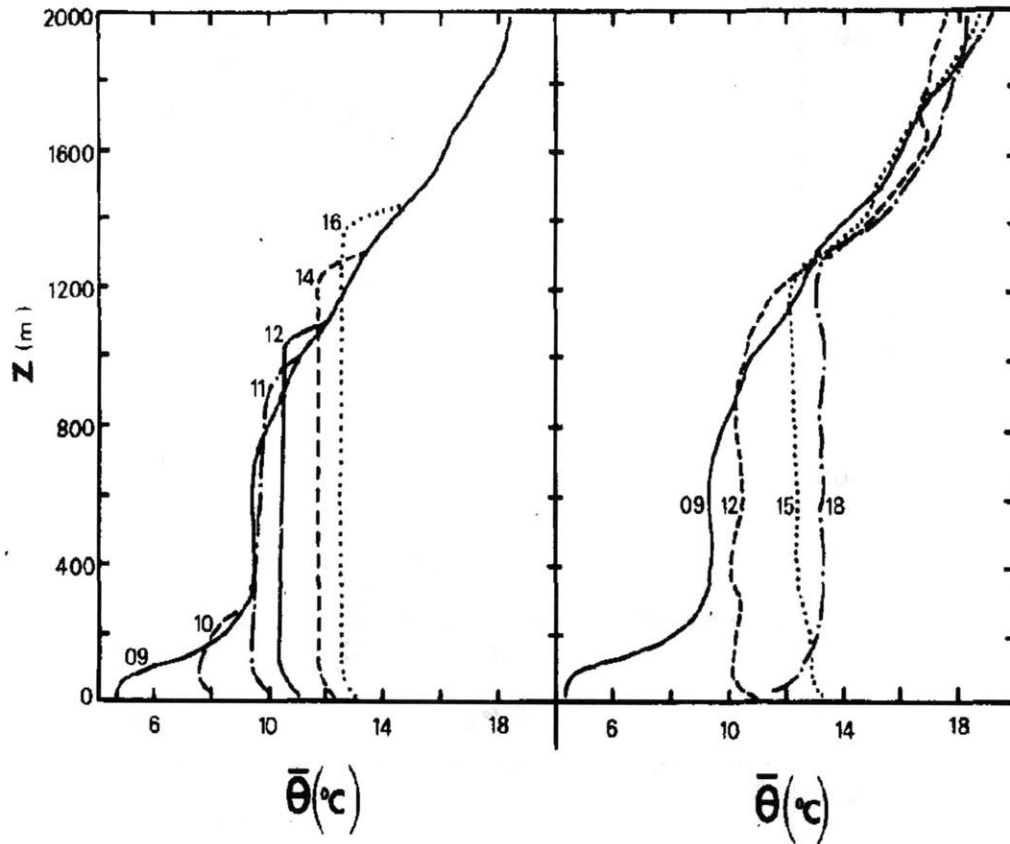


FIG. 2. Computed (left) and observed (right) profiles of mean virtual potential temperature during Day 33.

Figure 1-5: Diurnal profiles of mean potential temperature  $\theta$  from André et al. (1978)

In all figures,  $T$  denotes the turbulent transport term,  $M$  mechanical (shear) production (due to the mean-gradient),  $B$  the buoyant production,  $P$  the pressure covariance,  $D$  is the dissipation and  $R$  the radiative destruction.

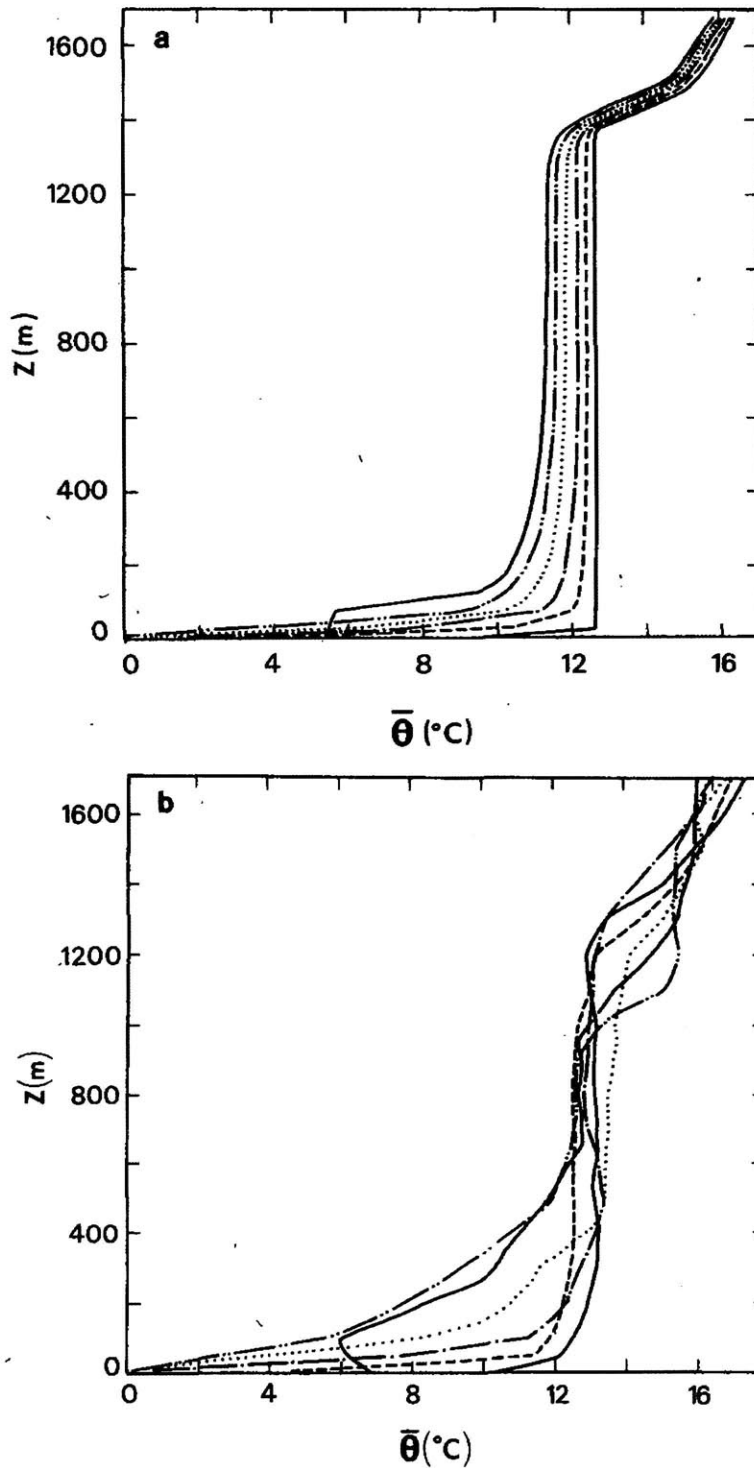


FIG. 15. Computed (a) and observed (b) profiles of mean virtual potential temperature during Night 33-34: —,  $t=18$  h; ---,  $t=21$  h; - · - · -,  $t=00$  h; · · · · ·,  $t=03$  h; - - - - -,  $t=06$  h; — · — · —,  $t=09$  h.

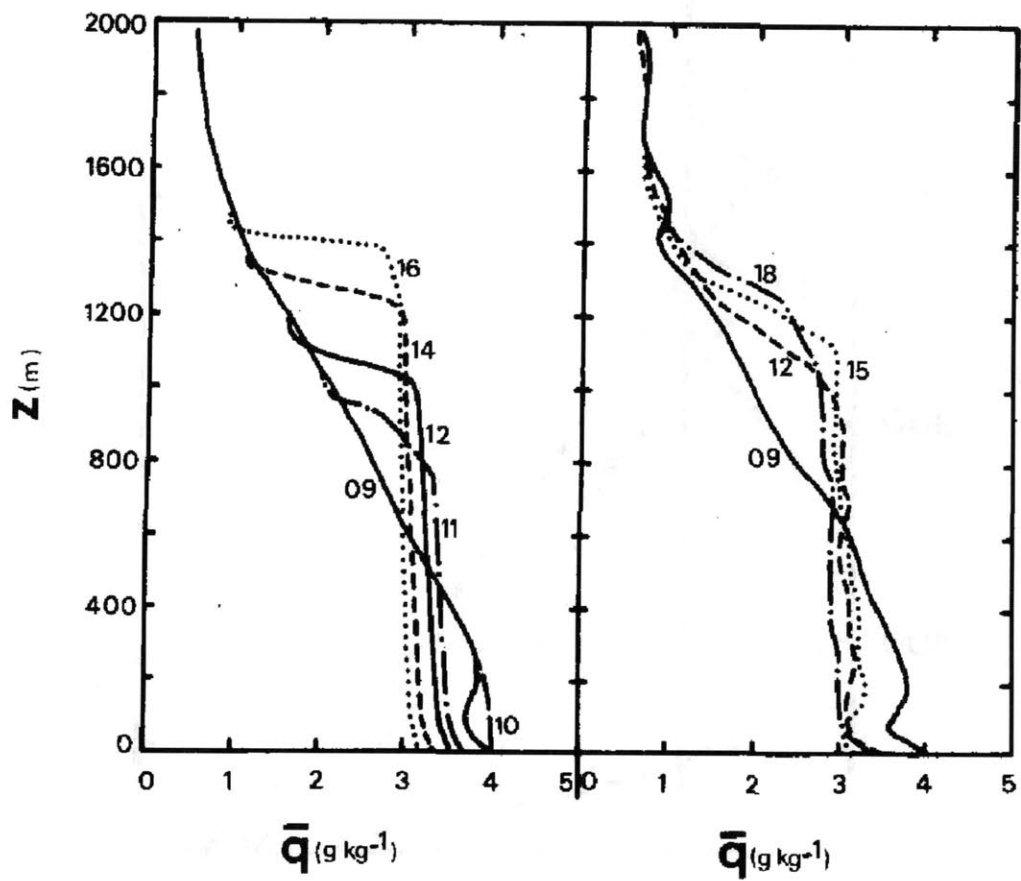


Figure 1-7: Diurnal profiles of specific humidity  $q$  from André et al. (1978)

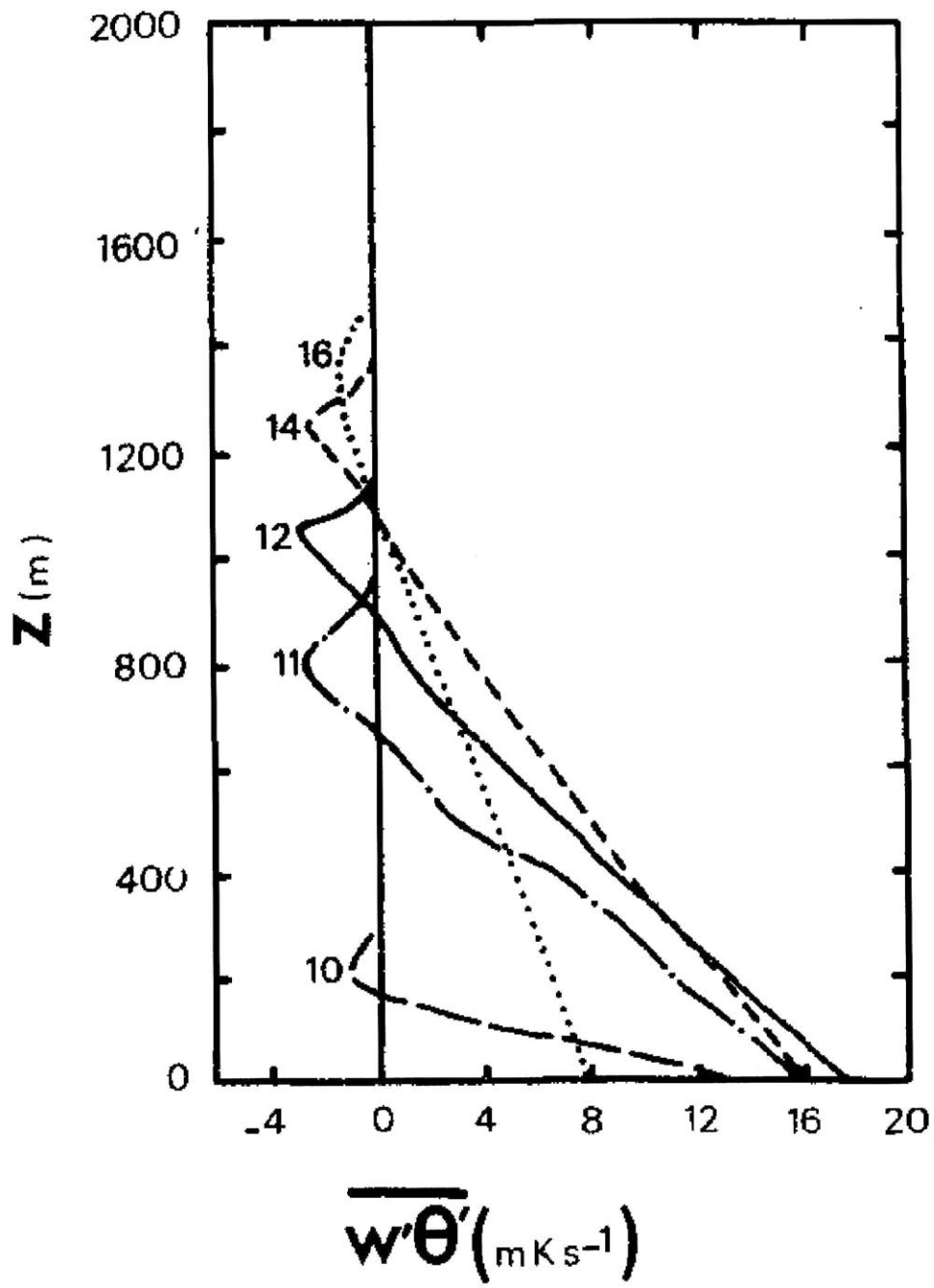


Figure 1-8: Diurnal profiles of the turbulent flux of potential temperature from André et al. (1978)

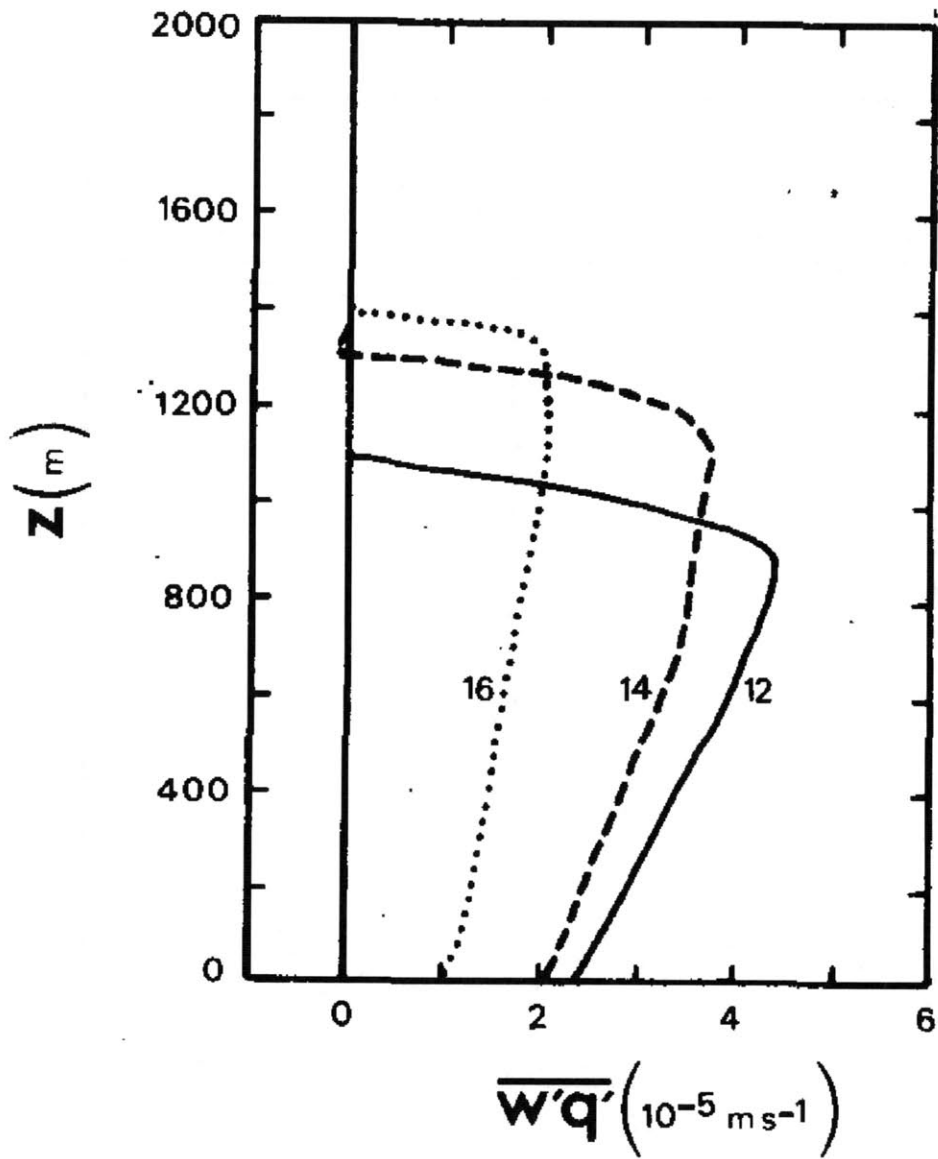


Figure 1-9: Diurnal profiles of the turbulent flux of specific humidity from André et al. (1978)

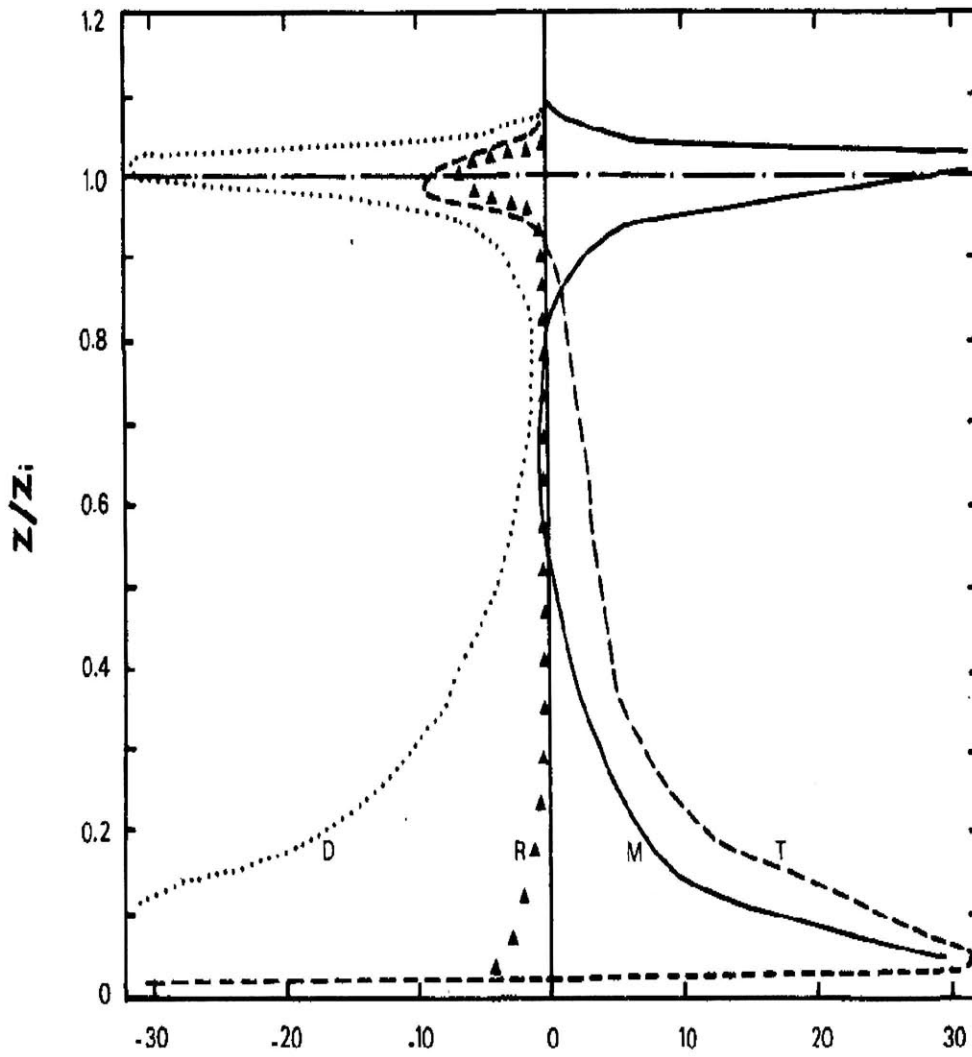


Figure 1-10: Daytime virtual potential temperature variance budget from André et al. (1978)



## Chapter 2

### Lettau's 1951 publication

This PhD thesis is mainly based on the work of Lettau (1951) [22]. In this fundamental publication, Heinz Lettau investigated the analytical response of the coupled soil-atmosphere system in response to a forcing of sinusoidal net radiation at the land-surface. The forcing at the land surface was prescribed as a sinusoid with periodicity  $T$  (of either a day or a year). The land-atmosphere partial differential equations were first linearized, in order to obtain a solution in the Fourier domain. The boundary conditions were assumed to be the following:

i) For large heights and depths, sensible and soil heat fluxes vanish:

$$\lim_{z \rightarrow \infty} H(z, t) = \lim_{z \rightarrow -\infty} G(z, t) = 0 \quad (2.1)$$

ii) At the land surface, i.e. at  $z = 0$ , both air and soil temperatures are continuous at any time:

$$T_0 = \lim_{z \rightarrow 0_-} T(z, t) = \lim_{z \rightarrow 0_+} \theta(z, t) = \theta_0 \quad (2.2)$$

iii) At the land surface, net radiation is given as a complex harmonic of time:

$$\widetilde{R}_n = \widetilde{R}_{n_0} + \widetilde{r}_{n,0} e^{-j\nu t} \quad (2.3)$$

iu) Latent heat at the land surface is considered to be independent of time:

$$\lambda E(t) = \lambda E_0 \quad (2.4)$$

u) At the surface the energy budget is closed in the sense that:

$$R_n(t) - G(t) = H(t) + \lambda E(t) \quad (2.5)$$

ui) The friction velocity at the land surface is assumed to remain constant throughout the period of interest  $T$ .

The solution was then assumed to be periodic, transitory regimes were not studied and assumed to be unimportant, the time derivative  $\frac{\partial}{\partial t}$  were transformed into a multiplicative factor depending on the frequency of the net radiation forcing:  $-j2\pi/T = -j\nu$ .

Lettau managed to obtain an analytical expression of the temperature and flux profiles in both the soil and in the ABL, as a continuous function of time and altitude.

This allowed him to obtain interesting conclusions on the nature and properties of this daily coupling. First of all, regardless of the frequency and amplitude, as well as land or meteorological properties, the land temperature was found to lag the soil heat flux wave by a phase of  $\pi/4 = 45^\circ$ , that is 3 hours for daily oscillations. This is in strong contrast with the phase of the sensible heat flux at the surface, which is dependent on the frequency of the forcing  $\nu$ , the surface roughness length  $z_0$ , and friction velocity  $u_*$ . The phase lag between the surface temperature and sensible heat flux will generally be much smaller, of the order of 30 minutes for typical values of the surface parameters and for a daily frequency.

Lettau also observed that the vertical atmospheric potential temperature gradient near the surface increases when roughness length increase. Moreover he emphasized that for a given soil type the tendency is toward a microclimate of greater extremes when the wind force and/or the roughness length decrease.

Finally Lettau discussed the response to a given amplitude of temperature forcing at the land surface. Soils with increasing heat capacity will tend to exhibit a stronger

diurnal cycle but the phase is unchanged and soil heat flux remains in phase delay of  $45^\circ$ , i.e. 3h for a daily forcing. Sensible heat flux will behave somewhat differently: its amplitude will increase when either friction velocity or roughness length increase (i.e. when drag increase). Yet there is a slight phase change with changing land or meteorological values but this difference remains of the order of 30 mn for most physical values.

Finally, we can add much physical insight to the conclusions of Lettau. Soil heat flux is always in large phase advance (of the order of 2 to 3 hours) over radiation forcing at the land surface, whereas sensible heat is slightly delayed. This result is due to the heat capacity and transfer capabilities of each medium. When solar radiation heats the land surface, surface temperature rises leading to strong surface soil gradient and thus to strong soil heat flux. Then the underneath part of the soil is heated by the thermal diffusion of heat through the soil (there is no global motion in the soil, only at the microscopic scale). The peak of soil heat flux takes consequently place much before that of solar radiation.

Sensible heat flux behaves differently: its strength is due to the warming of the surface, which increases as surface temperature rises and propagates heat to the air. Turbulent transfer is almost instantaneous, compared to soil diffusion, because of the global motion of the air parcels induced by turbulence. Yet little energy is absorbed by a unit of air compared to a soil unit because of the much lower heat capacity of this former. Thus the peak of sensible heat flux will take place near solar noon, with only a short lag induced by heat transfer and very small air heating inertia.

We build on the Lettau (1951) approach and extend it in several important directions:

- 1) Solution is obtained for all frequencies up to diurnal.
- 2) A vegetation layer is added to allow for discontinuity at the surface.
- 3) The ABL height is finite which allows steady-state solution as well.
- 4) Latent heat flux is variable and dependent on the new specific humidity state.
- 5) Stochasticity is introduced at the surface boundary energy balance.



## Chapter 3

# SUDMED project and main site of study

### 3.1 Site description

The SUDMED experiment is located in the region of Marrakech, Morocco (see Figure 3-1), which is a typical Mediterranean semi-arid region. In those regions the environmental conditions are extremely diverse. The air temperature, for instance, ranges from  $-2^{\circ}\text{C}$  at night in the winter, to  $50^{\circ}\text{C}$  during the hottest days of the summer. Moreover, those regions experience a wet period in the winter with intense rains leading to flash floods and a dry period in the summer. The study of semi-arid regions is suitable for understanding the main processes of the transfer of energy and water into the atmosphere because over a year diverse environmental and soil moisture conditions are observable. This permits a better understanding of the main parameters regulating the evapotranspiration over the land surface. Moreover, vegetation is generally sparse in these regions, therefore the soil evaporation and the transpiration of the plants are typically of the same order. Consequently, while studying the evapotranspiration in semi-arid regions, we can have an understanding of the factors influencing both evaporation and transpiration.

The field study is part of the SUDMED and IRRIMED projects. The SUDMED project is an applied study that deals with the characterization, modeling and fore-

casting of hydro-ecological resources of semi-arid Mediterranean regions, applied to the Tensift watershed around Marrakech. Its objective was to develop sustainable management tools integrating field information, models and satellite measurements. The associate partners participating in this project are CESBIO (Centre d'Etudes Spatial de la BIOSphère: French Center for Biosphere Studies), IRD (Institut de Recherche pour le Développement: French Research Institute for Development), Caddy Ayyad University in Marrakech, ORMVAH (Office de Mise en Valeur Agricole du Haouz: Moroccan Agricultural Improvement Agency), DREF (Direction Regionale des Eaux et Forets: Moroccan Water and Forest Regional Agency) and the Agence de Bassin du Tensift (Tensift Basin Agency). The follow-up of this project was called IRRIMED. The general scientific objective of this latter project is the assessment of the temporal and spatial variability of water consumption of an irrigated agriculture under limited water resources condition. Ground and satellite measurements are combined into models to determine evapotranspiration (ET) over large areas. This will ultimately allow an efficient and sustainable water management for irrigation. New participants were added to the previous project as this project had an international objective: Wageningen University (Netherland), UoJ, NCARTT and MWI (Jordan), ACSAD (Syria) and INRGREF (Tunisia).

During the SUDMED project, two wheat parcels and one olive tree orchard were instrumented. Biomass, vegetation height, meteorological conditions and energy fluxes were measured in 2002 and 2003. Our zone of interest is a wheat parcel. The site is composed of sparse, seasonal crop in which latent and sensible heat fluxes may be of the same size and may result from comparable contributions of bare soil and canopy. The R3 site is located in an irrigated area in the Haouz plain surrounding Marrakech, where wheat is mainly cultivated. Each parcel was assigned a number based on the counting of all parcels in this zone. Our parcel of interest is named R3-B123.

The entire site called R3 is a 2800-ha wheat irrigated area of 593 agricultural parcels, located at around 45 km East of Marrakech. In this perimeter, two fields were fully equipped, namely the 123rd (R3-B123) and 130th (R3-B130) parcels. Those

parcels are wheat cultivated; the sowing date is January 13 for parcel 123. The climate is characterized by a dry and warm period with little precipitation in the Summer and Fall, and almost 200 mm in the Winter and Spring. The observation period in which energy fluxes were continuously measured started on DOY 35 for B123 parcel and lasted for the entire wheat season until DOY 141 for both parcels. This covered all cycles of a wheat season: sowing, vegetation installation, vegetative growth, fully grown vegetation and the senescence. Vegetation appears on February 7: DOY 38 for B123, with a growth peak on April 20: DOY 110 (B123), followed by the senescence period until the end of May. Both sites are periodically irrigated by flooding the entire parcel with a network of water channels. B123 is irrigated on February 4 (DOY 35), March 20 (DOY 79), April 13 (DOY 103) and April 21 (DOY 111) with a mean 25 mm supply.

## 3.2 Experimental data set

All the fluxes and meteorological data was continuously measured and recorded every 30 minutes. Flux values derived from measurements which were spikes were replaced by time interpolated values, and when data was missing or erroneous for more than one consecutive day, the fluxes for this period were rejected. The missing meteorological data could easily be interpolated using surrounding meteorological stations measurements. Finally, a continuous meteorological data set was obtained.

Near-continuous heat flux measurements were recorded during the entire season. On parcel B123, sensible heat flux was measured with a 3D sonic anemometer (CSAT3, Campbell Scientific, Logan, UT) at 3 m high. A KH20 krypton hygrometer also measured the latent heat flux at this height. The soil heat flux is monitored by three heat flux plates at 1 cm below the surface, 2 plates at 10 cm and 1 plate located at 30 cm. The net radiation was monitored by a CNR1 located at 2 m above the surface. Moisture is monitored by TDR located at 5, 10, 20, 30, 40, 50 cm below the surface and soil temperatures are measured by thermistances located at the same depth. The air temperature was monitored at 6 m high by Vaisala HMP45C probes,

and the shortwave incoming radiation was recorded by a 3 m high CM5 pyranometer.

The solar incoming radiation measured from DOY 35 to DOY 145 is shown on Figure 3-2. Only few cloudy days are present during the whole period of measurements. Cloudy conditions lead to a drop in solar incoming radiation and are therefore easy to determine compared to sunny days. The daily maximum value of solar incoming radiation is generally high, even in the mid-Winter maximum values of  $700 \text{ [W m}^{-2}\text{]}$  are common. In the late April, the solar incoming radiation can generally reach 900 to  $1000 \text{ [W m}^{-2}\text{]}$  at solar noon. Air temperature was recorded for the same period. As seen on Figure 3-3, the range of air temperature is large, with minimum temperature of about  $2 \text{ [}^\circ\text{C]}$  at night in January, and maximum temperatures of about  $40 \text{ [}^\circ\text{C]}$  in late April. Air specific humidity is generally low, as seen on Figure 3-4. Indeed the humidity in the air is small in this semi-arid region. Even when air temperature rises to  $40 \text{ [}^\circ\text{C]}$  in late April, the specific humidity rarely exceeds  $10 \text{ [g}_{\text{H}_2\text{O}}/\text{kg}_{\text{air}}\text{]}$ . Wind speed was measured at 2m height. The wind speed cycle is shown on Figure 3-3. Wind speed fluctuates faster than the other environmental variables and was generally below  $5 \text{ [m s}^{-1}\text{]}$ . Net radiation was recorded at 2m above the ground, and usually reached a maximum of  $400 \text{ W m}^{-2}$  in February to almost  $750 \text{ [W m}^{-2}\text{]}$  in late April just before harvest. Some sensible and latent heat flux data was missing due to the sensor sensitivity to bad weather conditions, in particular after a strong rainfall event. Sensible heat flux was small at the beginning of the measurement period with a maximum value of about  $100 \text{ [W m}^{-2}\text{]}$ , and became high during the senescence period leading to daily maxima of the order of  $250 \text{ [W m}^{-2}\text{]}$ . Latent heat flux was also low at first, when the vegetation was growing and installing, but it became large just before the senescence period, reaching high values of the order of  $400 \text{ [W m}^{-2}\text{]}$ . The ground heat flux was calculated as the mean value of the 3 measuring plates. This mean value is seen on Figure 3-9. The maximum possible values reached  $150 \text{ [W m}^{-2}\text{]}$  just after sowing, when there was almost no vegetation shade. The smallest amplitude of the flux was obtained before senescence, when the vegetation cover and the greenness were high.



### 3.3 Calibration and validation of the SVAT model

The Soil-Vegetation-Atmospher-Transfer (SVAT) model used in this thesis is named ICARE SVAT and is described in Gentine et al. (2007) [16]. This model describes the evolution of the soil water content and temperature profiles using the energy budget over the soil and canopy. Because the SVAT model requires a significant number of parameters, we first performed a sensitivity analysis in order to identify the importance of each parameter for calibration. We first used a priori values taken from both literature review and field measurements. The parameters calculated using field measurements or empirical models related to the soil composition are: the soil hydraulic conductivity at saturation  $k_{sat}$ , the shape parameter of Brooks and Corey retention curve B, the soil water content at field capacity  $\theta_{fc}$ , the soil water content at wilting point  $\theta_{wilt}$ , and the water content at saturation  $\theta_{sat}$ . The parameters derived from literature review are the soil resistance parameters  $A_{rss}$ ,  $B_{rss}$ , and the stress parameters of the stomatal resistance  $D_p$ ,  $D_T$  and the minimum stomatal resistance  $r_{sc,min}$ . The calibration of the model was based on a manual iterative procedure, which compared the time series of estimated variables ( $Y_{est}$ ) and observed variables ( $Y_{obs}$ ) and minimized their difference by adjusting the chosen parameters. The optimization was obtained by minimizing the Root Mean Square Error (RMSE) between the two time series.

$$\min_{\alpha} \{ RMSE = \left[ \frac{1}{N-1} \sum_{n=1}^N |Y_{obs}(i) - Y_{est}(i)|^2 \right]^{1/2} \}$$

with  $N$ : number of observations. The initial values of the parameters are the a priori values. The minimization treated the parameters following their importance, found after the sensitivity test. The optimization iteratively used the simplex search method on Matlab (The Mathworks Inc.). A list of the parameters is provided at the end of the chapter.

Samples of the soil were analyzed to determine the fractions of clay and sand. On R3-B123, 47.5 [%] of the soil was clay and 15.8 [%] was sand. Then using gravimetry tests, Brooks and Corey (1964) [4] retention curves were fitted to the data. On R3-B123, we obtained for the potential at saturation  $\psi_{sat} = -0.3$  [m] and the shape

parameter of the curve  $B = 5.25$ . Then the following values were found: soil water content at saturation  $w_{sat} = 0.47$  [ $\text{m}^3 \text{ m}^{-3}$ ], soil water content at field capacity  $w_{fc} = 0.37$  [ $\text{m}^3 \text{ m}^{-3}$ ] and soil water content at wilting point  $w_{wilt} = 0.14$  [ $\text{m}^3 \text{ m}^{-3}$ ]. The soil hydraulic and thermal properties were also measured in situ. The following values were found on R3-B123: the soil dry density was  $1.55$  [ $\text{kg m}^{-3}$ ], the soil specific heat was  $900$  [ $\text{J (kg K)}^{-1}$ ] and the dry thermal conductivity:  $\lambda_{dry} = 0.03$  [ $\text{W m kg}^{-1} \text{ m}^{-3}$ ] and the hydraulic conductivity at saturation  $k_{sat} = 1.25 \cdot 10^{-6}$  [ $\text{m s}^{-1}$ ].

Then the SVAT parameters that could not be directly measured were calibrated to best fit the measured fluxes and observed radiative temperatures at  $0^\circ$  and at  $55^\circ$ . In particular, the parameters of the soil resistance to evaporation, were calibrated at the beginning of the measurements when the wheat was short. The following coefficients were found  $A_{rss} = 11$  and  $B_{rss} = 11$ . The roughness length of the substrate was found to be  $z_{0,s} = 0.03$  [ $\text{m}$ ].

After installation of the canopy, the calibration of the vegetation parameters was done. The minimum stomatal resistance was found to be:  $r_{sc,min} = 90$  [ $\text{m s}^{-1}$ ], the water vapor deficit stress factor parameter of the Jarvis formulation:  $D_P = 1.5 \cdot 10^{-4}$  [ $\text{Pa}^{-1}$ ] and the parameter of the temperature stress factor  $D_T = 0.004$  [ $\text{K}^{-2}$ ]. All those parameters were calibrated on R3-B123 in 2003 and validated on R3-B130 during the same period. The best set of parameters matching both the calibration and validation was selected.

Variable	Definition	Value/Units
$A_{rss}$	First parameter of the stomatal resistance dependency on soil moisture	11 (-)
$B_{rss}$	First parameter of the stomatal resistance dependency on soil moisture	11 (-)
$z_{0,s}$	Roughness length of the substrate	0.03 m
$r_{sc,min}$	Minimum stomatal resistance	90 s m <sup>-1</sup>
$D_P$	Water vapor deficit parameter of the Jarvis formulation	1.5 · 10 <sup>-4</sup> Pa <sup>-1</sup>
$D_T$	Temperature deficit parameter of the Jarvis formulation	0.004 K <sup>-2</sup>

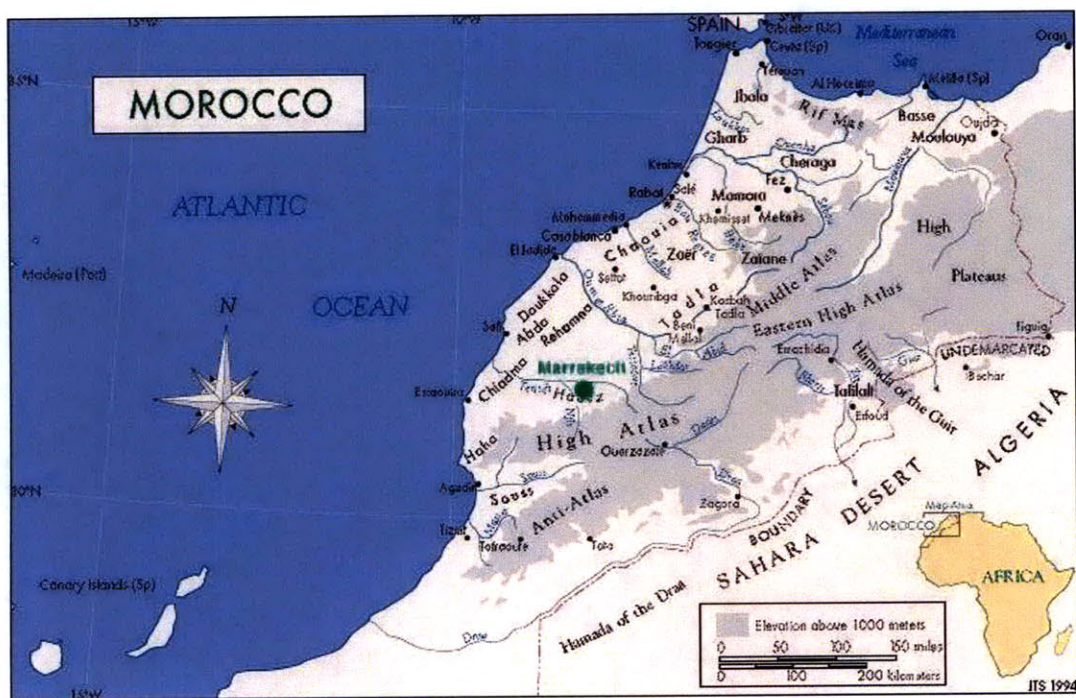


Figure 3-1: Map of Morocco

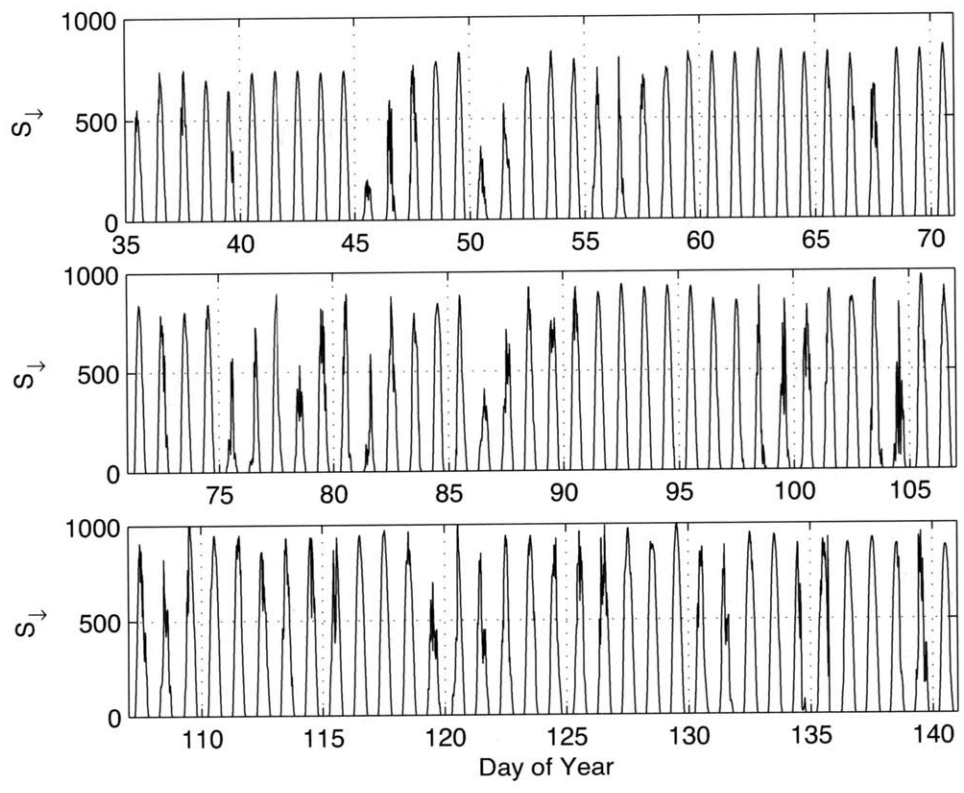


Figure 3-2: Solar incoming radiation measured over parcel R3-B123 in 2003

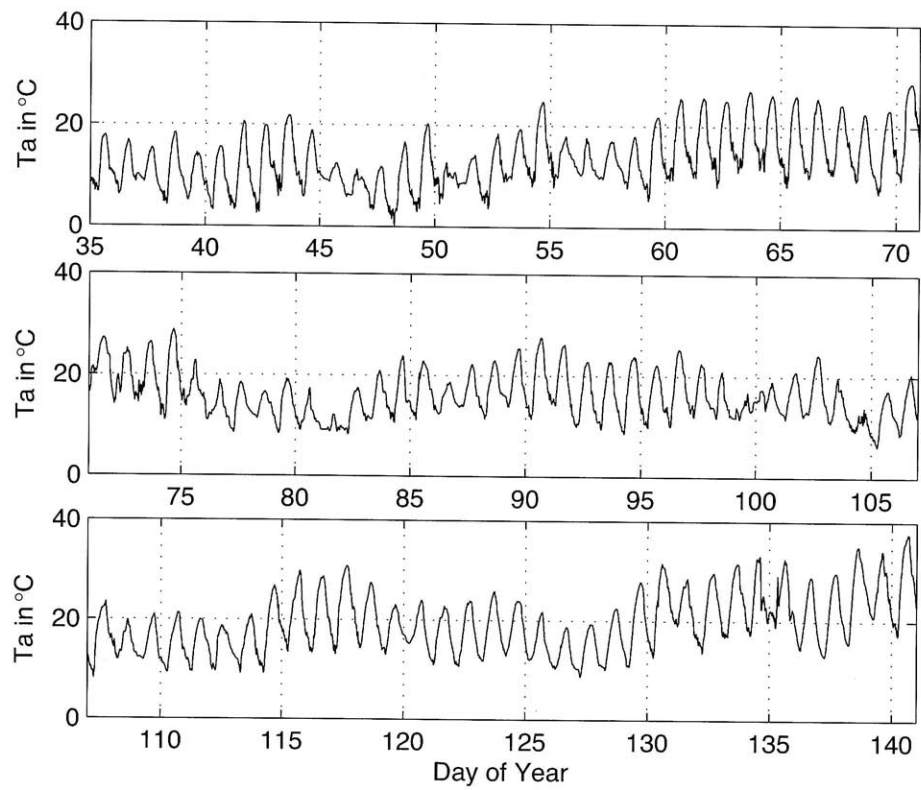


Figure 3-3: Air temperature measured over parcel R3-B123 in 2003

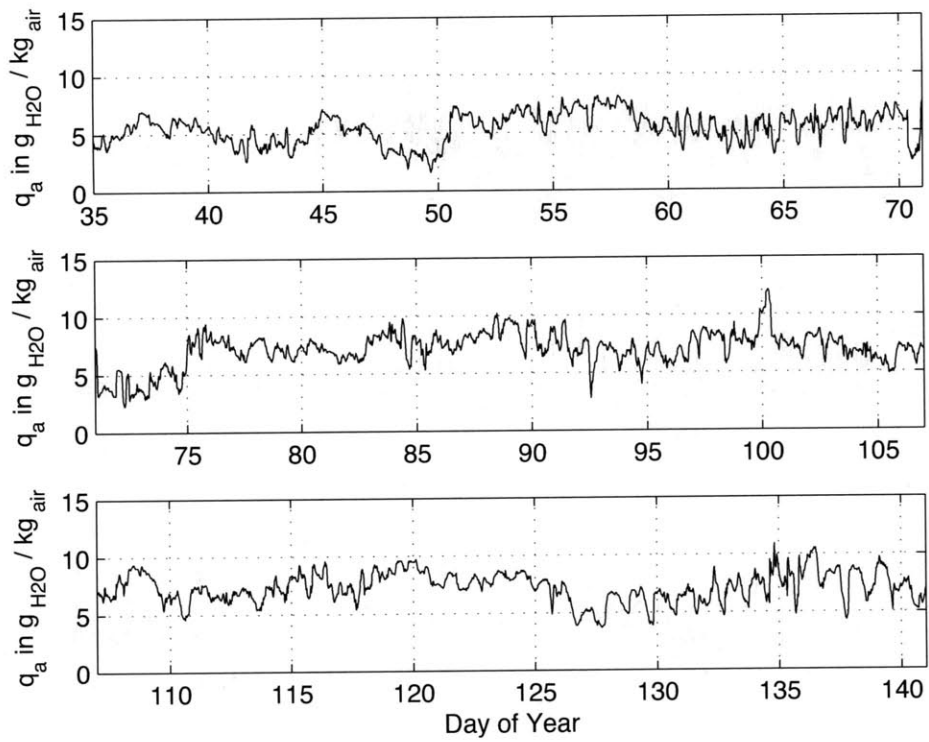


Figure 3-4: Air specific humidity measured over parcel R3-B123 in 2003

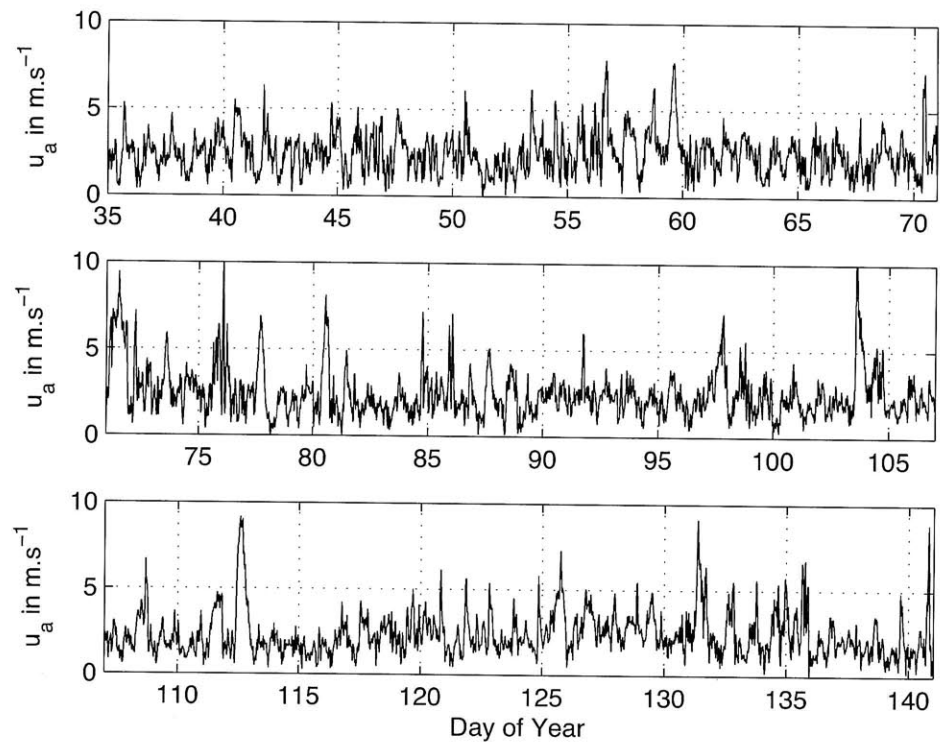


Figure 3-5: Wind speed measured over parcel R3-B123 in 2003



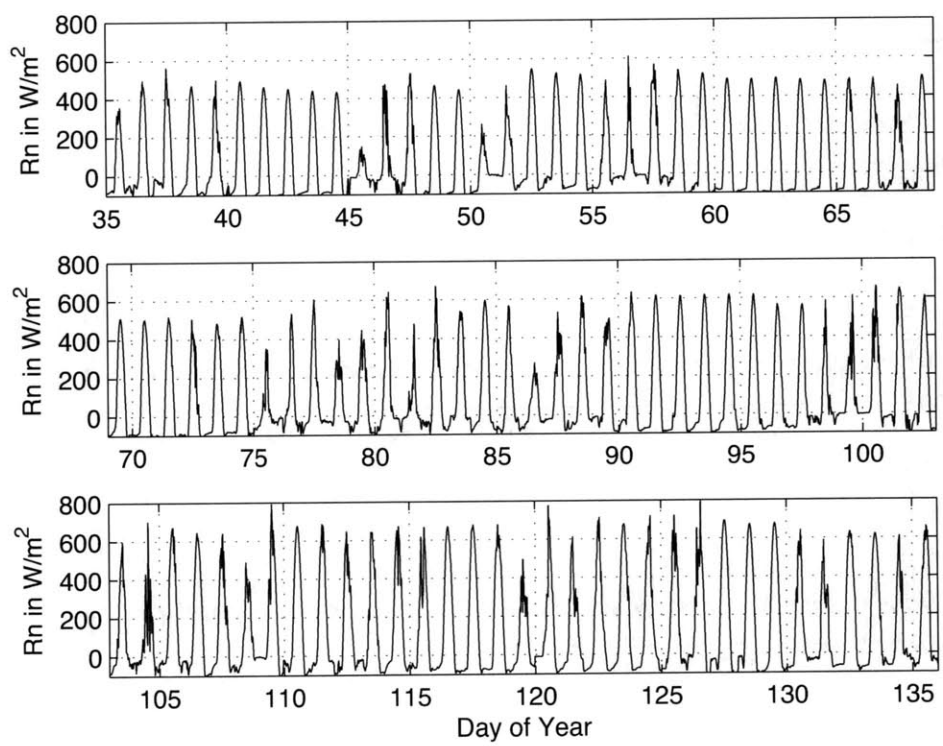


Figure 3-6: Net radiation measured at 2m high over parcel R3-B123 in 2003

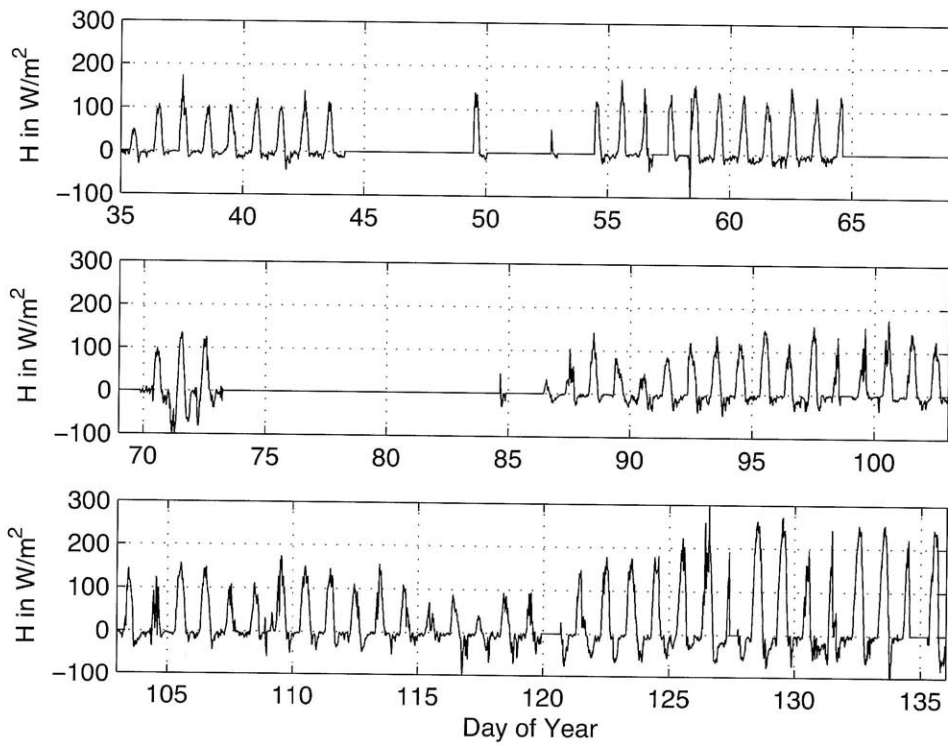


Figure 3-7: Sensible Heat Flux measured using eddy correlation over parcel R3-B123 in 2003

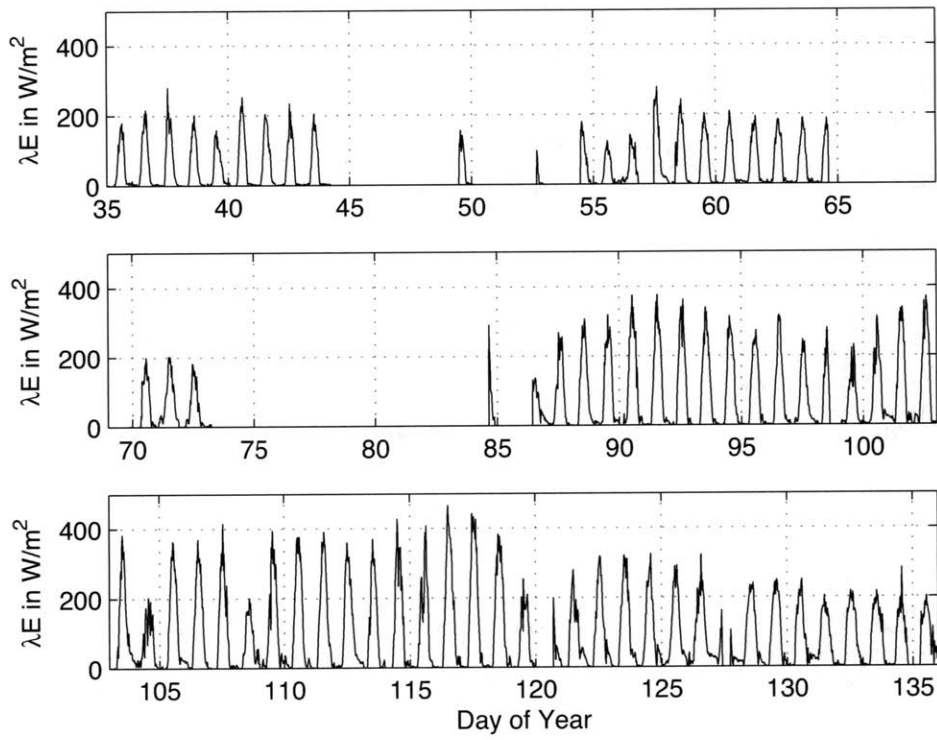


Figure 3-8: Latent Heat Flux measured using eddy correlation over parcel R3-B123 in 2003

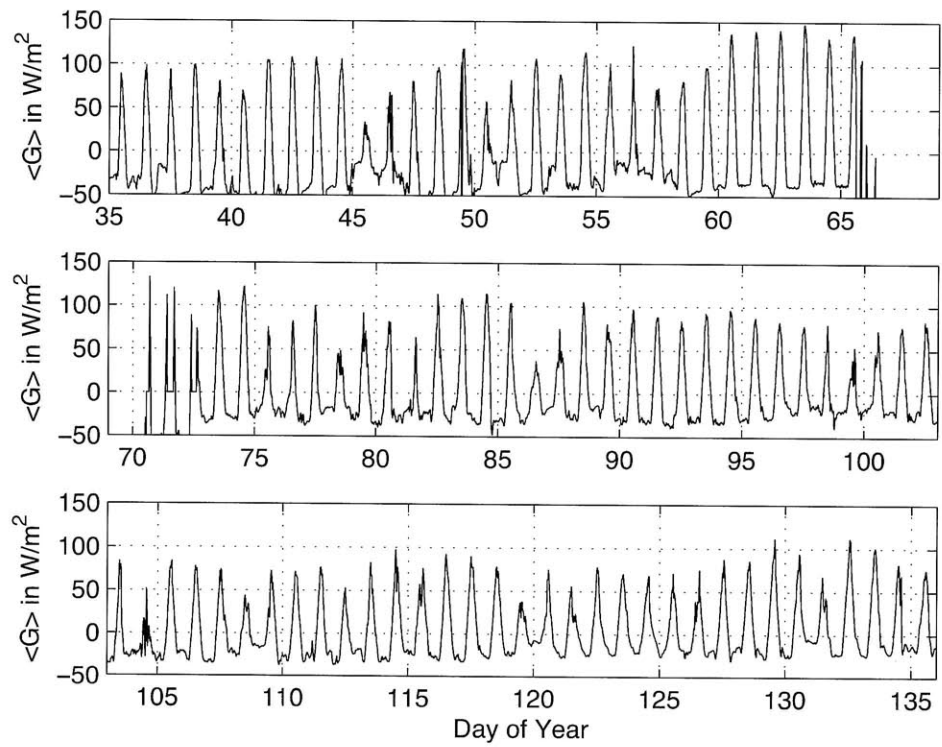


Figure 3-9: Mean ground heat flux measured using 3 flux plates over parcel R3-B123 in 2003

## Chapter 4

# Spectral behavior of a coupled land-surface and boundary-layer system

**Abstract:**

The temporal spectral response of a coupled land-atmosphere system to daily forcing of net radiation at the land surface is investigated using the analytic approach. The original definition of the problem dates back to an early study by Lettau (1951). The present study builds on the problem and introduces some important additions, with a focus on the propagation of heat flux and temperature waves in both the soil and the atmospheric boundary layer. The study highlights the dependence of the complex amplitude of surface temperature and heat fluxes on the different land-surface parameters, such as friction velocity, evaporative fraction, aerodynamic resistance and vegetation height. Finally, the dependency of surface state variables to the frequency of the forcing is analyzed.

**Key words:** Diurnal cycle; Ground heat flux; Fourier series; Land-atmosphere interactions

## List of symbols

$\lambda$	Latent heat of vaporization at the triple point ( $2.45 \times 10^6 \text{ J kg}^{-1}$ )
$\lambda_G$	Penetration depth of the soil heat wave (m)
$\lambda_H$	Penetration depth of the sensible heat flux wave (m)
$\lambda_s$	Soil thermal conductivity ( $\text{W m}^{-1} \text{K}^{-1}$ )
$\lambda_\theta$	Penetration depth of the potential temperature wave (m)
$\lambda E(z)$	Latent heat flux at height $z$ ( $\text{W m}^{-2}$ )
$\lambda E(h)$	Latent heat flux above the canopy height $h$ ( $\text{W m}^{-2}$ )
$\omega$	Angular frequency of the harmonic ( $\text{rad s}^{-1}$ )
$\rho$	Surface air density ( $1.2 \text{ kg m}^{-3}$ )
$\theta$	Mean potential temperature in the boundary layer (K)
$E_F$	Evaporative fraction at the land surface (nominal value is 0.6)
$C_s$	Soil heat capacity (nominal value is $1.42 \times 10^6 \text{ J m}^{-3} \text{K}^{-1}$ )
$C_p$	Specific heat capacity of the air at constant pressure ( $1012 \text{ J kg}^{-1} \text{K}^{-1}$ )
$d$	Displacement height (m)
$G$	Ground heat flux ( $\text{W m}^{-2}$ )
$h$	Vegetation height (nominal value is 0.5 m)
$H$	Turbulent (sensible) heat flux of potential temperature $\overline{w'\theta'}$ ( $\text{K m s}^{-1}$ )
$K_s$	Soil thermal diffusivity (nominal value is $2.5 \times 10^{-7} \text{ m}^2 \text{s}^{-1}$ )
$k$	Von Karman's constant (0.4)
$r_a^c$	Canopy aerodynamic resistance (nominal value is $50 \text{ s m}^{-1}$ )
$R_n$	Net radiation at the land surface (nominal peak value is $500 \text{ W m}^{-2}$ )
$T_{deep}$	Deep soil temperature (K)

$T_s$	Soil temperature (K)
$T_{surf}$	Soil surface temperature (K)
$T_{day}$	Duration of a day (s)
$u_*$	Friction velocity at the land surface (nominal value is $0.2 \text{ m s}^{-1}$ )
$z_I$	Measurement height (nominal value is 2 m)
$z_i$	Boundary-layer height (m)



## Introduction

The dynamics and predictability of the lower atmosphere are significantly affected by radiative heating at the land surface. The response of the land surface to the large-amplitude solar radiative forcing is dependent on the heat storage and diffusion as well as on the coupling of the soil and atmospheric boundary-layer systems. Characteristics of the land surface such as soil moisture and roughness significantly affect surface energy balance and heat fluxes in the soil and in the boundary layer.

There have been only limited theoretical studies investigating the influence of surface incoming radiation and land-surface parameters on the coupled land-atmosphere system. In particular, the diurnal cycle of temperature and heat-flux profiles in a coupled land-surface and atmospheric boundary layer is not understood well. An early study of the coupled system behavior, (Lettau 1951), defined the coupled system and obtained analytic solutions for temperature and heat-flux profiles under one daily harmonic of net radiation forcing.

In Lettau (1951) the role of the different land-surface parameters is investigated under several strong assumptions: (i) the atmospheric boundary layer (ABL) is near-neutral with infinite height, (ii) the surface friction velocity is a daily constant, (iii) the latent heat flux is also a daily constant, and (iv) there is no surface temperature discontinuity between the air and the land. Kimura and Shimizu (1994) also used an equivalent approach but introduced a

temperature discontinuity at the land surface through the resistance formulation of sensible heat flux. More recently Van de Wiel et al. (2002) focused on the behavior of the nocturnal and dry stable atmospheric boundary layer.

The goal of the present study is to improve the approach introduced by Lettau in order to investigate the spectral response of a land-atmosphere model to a range of harmonics and with less restrictive assumptions. Several assumptions used by Lettau are removed. Firstly, the latent heat flux is not considered to be a daily constant. We choose to use a constant daily evaporative fraction, defined as the instantaneous ratio between latent heat flux and available energy at the land surface. Evaporative fraction ( $E_f$ ) is meant to effectively isolate, as much as possible, the micrometeorological factors controlling latent heat flux from the soil water availability factor. Secondly, whereas Lettau used only one harmonic here we approach the problem with the full spectrum for the daily net radiation forcing. Thirdly, a temperature discontinuity at the land surface is introduced through the relation between sensible heat flux and air-surface temperature difference. Finally, the atmospheric boundary layer is considered to have finite height during daytime. This is important in that it allows base solutions for the harmonics, i.e. solutions under the steady-state conditions.

The resulting analytical model is used to diagnose the harmonic response of surface heat flux or temperature to incident radiation forcing at the land surface. First, the role of the frequency of the forcing on the heat and

temperature response is studied. The propagation of heat flux harmonics across the soil and ABL domains is characterized. The role of the land-surface parameters on the amplitude and phase of the harmonics for both temperature and heat fluxes are investigated.

#### 4.1. Model description

Our main interest is to describe the diurnal behavior of soil-atmosphere interactions. A simplified analytical model has thus been defined with a behavior resembling that of more complex numerical models. The coupled soil-atmosphere model is based on the following assumptions:

- 1) The land surface is covered with vegetation of height  $h$ , with turbulent heat fluxes modeled using the resistance approach.
- 2) The ABL is assumed to be in a near-neutral to unstable state and the whole atmospheric domain is assumed to be subject to K-theory, i.e. the turbulent heat flux of potential temperature is dependent on the gradient of potential temperature  $\theta$  as:

$$H = -K_H(z) \frac{\partial \theta}{\partial z}. \quad (1)$$

In the surface layer, the eddy-diffusion coefficient  $K_H(z)$  for heat is linearly varying with height  $z$ , as characterized by Lettau (1951):

$$K_H(z) = ku_*(z - d). \quad (2)$$

The displacement height appearing in (2) can be expressed as fraction

of obstacle height  $h$ , using Brutsaert (1982):

$$d = \frac{2h}{3}. \quad (3)$$

Above the surface layer and within the turbulently mixed layer the potential temperature is nearly constant. Sensible heat flux decreases with height and vanishes at the height of the ABL. In the mixed layer this decreasing sensible heat flux is usually accompanied by negligible potential temperature gradients, which contradicts the use of an eddy-diffusion parameterization and requires more sophisticated turbulence modelling such as the countergradient approach (see Hotslag and Moeng 1991, Zilitinkevich et al. 1999 and Van Dop and Verver 2001 for recent studies). In addition the eddy-diffusion coefficient of the sensible heat flux  $K_H(z)$  is usually decreasing in the upper ABL.

In order to obtain an analytical solution in the entire ABL domain, we here extend the surface-layer parameterization of the eddy-diffusion coefficient across the ABL. This is a major assumption of our work and should be improved in future studies. Yet in our near-neutral turbulent case the extension of the eddy-diffusion parameterization in the whole ABL gives reasonable characteristic mixed-layer profiles with negligible potential temperature gradients accompanied by linearly decreasing sensible heat flux with height (see Sect. 4.5).

- 3) The ABL is assumed to have a constant height.

- 4) At ABL top, there is no transfer of heat and moisture through turbulence between the free atmosphere and the ABL, so that the turbulent heat fluxes vanish.
- 5) Radiative cooling in the ABL is assumed to be negligible when compared to turbulence on the daily time scale.
- 6) The ratio between latent heat and available energy at the land surface is assumed to be constant throughout the day; that is the evaporative fraction is considered as a daily constant (see discussion in Sect. 4.2.3).
- 7) The surface stress is assumed to remain constant throughout the day (see discussion in Sect. 4.2.3).

The above assumptions limit the range of applicability of the results as it is underscored throughout this study. Yet this model is shown to adequately describe the main features of the diurnal land-atmosphere interactions. Moreover the above-described model can be analytically solved in both spectral and temporal domains, leading to a spatial and temporal continuous solution for the temperature and heat-flux profiles. The resolution in spectral domain provides new insights on the response of the coupled system to radiative forcing at the land surface.

#### **4.1.1. Atmospheric boundary layer**

The system considered here is composed of an atmospheric boundary layer with finite depth and a soil layer, which is assumed to be semi-infinite. Vertical heat fluxes in the system are considered to be far larger and more important than

those in the horizontal directions. Effectively the system is considered to be homogeneous horizontally and horizontal advection in the atmospheric boundary layer is assumed to be negligible. Consequently, only the vertical variations within the system are considered. The two layers interact and are coupled through a vegetation layer with height  $h$  as shown in Figure 1.

Assuming that there is no condensation and radiative heating/cooling on short time scales in the boundary layer, the conservation of dry static energy is:

$$\frac{\partial \theta}{\partial t} = -\frac{\partial H}{\partial z}. \quad (4)$$

With equations (1), (2) and (4), the evolution of sensible heat flux and potential temperature in the boundary layer is:

$$\frac{\partial H}{\partial t} = K_H(z) \frac{\partial^2 H}{\partial z^2} = K_*(z-d) \frac{\partial^2 H}{\partial z^2} \quad (5)$$

where  $K_* = ku_*$ .

In conjunction with (4), the mean potential temperature equation follows:

$$\frac{\partial \theta}{\partial t} = \frac{\partial}{\partial z} \left( K_H(z) \frac{\partial \theta}{\partial z} \right) = K_* \frac{\partial^2 \theta}{\partial z^2} + K_*(z-d) \frac{\partial \theta}{\partial z}. \quad (6)$$

Then the two diffusion equations governing the evolution of the potential temperature and sensible heat flux are linearized using an assumption similar to that introduced by Lettau (1951): the friction velocity at the bottom of the boundary layer remains constant throughout the day. Even though the time series of friction velocity usually exhibit two distinct regimes during day and

night, the assumption is required to obtain an analytical solution: the coefficient  $K_*$  of the diffusion equation thus becomes a daily constant and the equations are linear. This assumption can be justified since we are mainly interested in the daylight hours, during which friction velocity can often be assumed constant. Moreover comparison with observations (see Sect. 4.6.2) shows that this assumption remains valid over a relatively wide range of meteorological conditions.

#### 4.1.2. Soil medium

In the soil, the water vapor flux has been assumed to be negligible and the soil properties are supposed to be uniform and constant. These strong assumptions allow us to decouple the soil water content and the soil temperature  $T_s$  dynamics. Ground heat flux  $G$  is expressed as:

$$G = \lambda_s \frac{\partial T_s}{\partial z} \quad (7)$$

where  $\lambda_s$  is the soil thermal conductivity ( $G$  is taken as positive downward).

The conservation of energy leads to the following equation for soil temperature:

$$C_s \frac{\partial T_s}{\partial t} = \frac{\partial G}{\partial z} \quad (8)$$

where  $C_s$  is the soil thermal capacity.

The soil temperature  $T_s$  and ground heat flux  $G$  are solutions of the following two equations:

$$\frac{\partial G}{\partial t} = K_s \frac{\partial^2 G}{\partial z^2} \quad (9)$$

$$\frac{\partial T_s}{\partial t} = K_s \frac{\partial^2 T_s}{\partial z^2} \quad (10)$$

where  $K_s = \lambda_s / C_s$  is the soil thermal diffusivity.

#### 4.1.3. Fourier decomposition

Lettau (1951) studied the response of the coupled system to the forcing of net radiation at the soil surface. Here we extend the approach and characterize the phase and amplitude response of the soil-atmospheric boundary-layer continuum to radiative forcing at the surface. We derive the response of the coupled system to any daily-periodic radiative forcing at the land surface. The height-dependent heat flux or temperature profiles at any height or depth are rewritten in the form of a Fourier series:

$$Y(t) = \bar{Y} + \sum_{\substack{n=-\infty \\ n \neq 0}}^{+\infty} \tilde{Y}(n\omega_0) \exp(jn\omega_0 t). \quad (11)$$

Each harmonic, corresponding to the angular frequency  $\omega_n = n\omega_0$  can be studied independently from the others. The results presented herein are the response to any angular frequency, except for the zero-order daily harmonic  $\bar{A}$  (steady-state solution) which is considered as a special case.



The temporal Fourier transform of the atmospheric and soil equations can be derived using the fact that the temporal derivative becomes a simple multiplicative coefficient:  $\frac{\partial}{\partial t} \rightarrow j\omega$ . The ABL equations (5) and (6) then become the following ordinary differential equations for their respective Fourier amplitudes:

$$\tilde{H}(\omega) = -\left(j\frac{K_*(z-d)}{\omega}\right)\frac{d^2\tilde{H}}{dz^2}(\omega) \quad (12)$$

$$\tilde{\theta}(\omega) = -\left(\frac{jK_*(z-d)}{\omega}\right)\frac{d^2\tilde{\theta}}{dz^2}(\omega) - \left(\frac{jK_*}{\omega}\right)\frac{d\tilde{\theta}}{dz}(\omega) \quad (13)$$

at any harmonic  $\omega \neq 0$ . The soil equations (9) and (10) can equivalently be rewritten in terms of their Fourier amplitudes:

$$\tilde{G}(\omega) = -\frac{jK_s}{\omega}\frac{d^2\tilde{G}}{dz^2}(\omega) \quad (14)$$

$$\tilde{T}_s(\omega) = -\frac{jK_s}{\omega}\frac{d^2\tilde{T}_s}{dz^2}(\omega). \quad (15)$$

#### 4.1.4. Boundary conditions

The atmosphere and the soil interact through the exchange of energy and water at their common interface. In this problem there is no explicit use of initial conditions, since they are implicit when using the daily periodicity of all variables. The problem is governed by the following boundary conditions:

1) The daily forcing of net radiation  $R_n(t)$  at the land surface, i.e. on top of the canopy at height  $h$ , is specified.

2) The ground heat flux vanishes at very large depth:  $\lim_{z \rightarrow -\infty} G(z) = 0$ . The steady-state solution of the soil temperature thus verifies  $\lim_{z \rightarrow -\infty} \overline{T_s}(z) = T_{deep}$ , i.e. an isothermal condition. The temperature of this isothermal condition does not need to be specified for harmonics outside of zero. It only applies to the zero-order harmonic or steady-state conditions and it is obtained by the steady-state solution of sensible heat at the land surface. It follows that the boundary condition of the soil temperature at infinity is for all non-zero harmonic:

$$\lim_{z \rightarrow -\infty} \widetilde{T}_s(z, \omega_n) = 0.$$

3) The atmospheric boundary layer (ABL) is assumed to have a height:

$$z_i = c \frac{u_*}{|f|} \quad (16)$$

where  $c = 0.2$  as suggested by Plate (1971) and  $f$  is the Coriolis parameter. This height corresponds to the elevation where the sensible heat flux vanishes. For a complete review of the different neutral ABL height formulations see Garratt (1992). Thus a boundary condition on the atmospheric domain is

$$H(z_i) = 0. \quad (17)$$

Note that in our case the friction velocity is considered as a daily constant so that the near-neutral ABL height is a daily constant too, using expression (16).

In his paper Lettau (1951) assumed that the sensible heat flux was null at

infinity, which precludes the steady-state or  $\omega = 0$  solution because of the singularity of equations (12) to (15) in this case. This constant ABL height certainly represents the main assumption of our approach since the ABL height exhibits a strong diurnal cycle overland under clear skies. In particular, at night, regimes of strongly stably stratified turbulence are poorly represented by our model. Our main focus is the daylight hours, which can be reasonably represented so long as this ABL “height”, with vanishing heat fluxes, is high.

To determine the steady-state solutions of both sensible heat flux and potential temperature profiles in the atmosphere, one single daily-mean temperature value must be known at any given height  $z_1$  above the vegetation. In the following section we show that that this is sufficient to solve the steady-state profiles of both potential temperature and sensible heat flux in the ABL.

4) Contrary to the approach used by Lettau (1951), which assumed continuity of surface potential and soil temperatures, a temperature discontinuity is introduced between the land surface and the air just above the surface. Potential temperature at the base of the ABL differs from the land-surface temperature. Hence, the difference between the land-surface temperature,  $T_{surf} = T_s(z = 0)$ , and the potential temperature at the height of the canopy  $\theta(h)$  is given by:

$$H(h) = \frac{T_{surf} - \theta(h)}{r_a^c} \quad (18)$$

where  $r_a^c$  is the canopy aerodynamic resistance and  $H(h)$  is the sensible heat flux

just above the canopy. The canopy aerodynamic resistance is assumed to be a daily constant as with friction velocity. Moreover the reference pressure for the calculation of potential temperature is taken as the instantaneous pressure at the surface. The introduction of a canopy aerodynamic resistance with a transfer coefficient differing from that within the ABL allows the introduction of discontinuity at the land surface.

Evaporative fraction, which is defined as the ratio of latent heat flux over available energy at the land surface, has been shown to have a tendency for self-preservation during the daytime. Shuttleworth et al. (1989), Nichols and Cuenca (1993), Crago (1996a) and Crago and Brutsaert (1996) have observed that this diagnostic is an effective way to separate, as much as it is at all possible, the micrometeorological from the hydrological factors influencing the evaporation process. The partitioning diagnostic, evaporative fraction, is strongly related to soil moisture and plant controls on the evaporation regime. When evaporative fraction approaches or is equal to unity the surface evaporation regime is energy limited, as is the case with a well-watered surface. When water becomes a limiting factor in the evaporation process, the turbulent heat partitioning shifts from the latent to sensible heat flux, and the evaporative fraction falls below unity. Since it is more related to soil and eco-hydrological factors, evaporative fraction diurnal variations are less than that of turbulent fluxes. Evaporative fraction has also been theoretically analyzed in Lhomme and Elguero (1999) and Gentine et al. (2007). They find that evaporative fraction can be considered as a

diurnal constant in most vegetation and soil moisture conditions. This assumption generally leads to small evapotranspiration estimation error over a day. Therefore in this study a constant daily evaporative fraction at the land surface is imposed:

$$E_F = \frac{\lambda E(h)}{R_n - G(0)} = \text{constant} . \quad (19)$$

In Lettau (1951) the latent heat flux itself was assumed to remain constant during the day.

Finally we assume that the heat capacity of the relatively thin vegetation layer is negligible so that the energy budget at the land surface is:

$$R_n - G(0) = \rho C_p H(h) + \lambda E(h) . \quad (20)$$

We linearize the problem to obtain a harmonic and analytical representation. This allows us to gain insights into the phase and amplitude of heat fluxes and temperatures across the soil-vegetation-boundary layer continuum. Net radiation is considered to be the forcing of our coupled system and is assumed to be a known time-series.

## 4.2. Steady-state solution

First the steady-state solution of the problem is sought since it is different from the solutions at other harmonics. In the ABL, the steady-state sensible heat flux is solution of:

$$\frac{d^2 \overline{H}(z)}{dz^2} = 0. \quad (21)$$

That is simply:

$$\overline{H}(z) = A_1 z + A_2. \quad (22)$$

Using boundary condition (17) the steady-state sensible heat flux becomes:

$$\overline{H}(z) = A_1 (z - z_i). \quad (23)$$

This linear behavior has been observed in many field experiments and large-eddy simulations e.g. Stevens (2000). Moreover the mean potential temperature at steady-state can be expressed as a function of turbulent potential temperature flux:

$$-K_* (z - d) \frac{d\overline{\theta}}{dz} = \overline{H}(z) = A_1 (z - z_i) \quad (24)$$

so that the steady-state temperature profile is:

$$\overline{\theta}(z) = -\frac{A_1}{K_*} [z - (z_i - d) \ln(z - d)] + A_2 \quad (25)$$

where the subscript  $A$  is a constant of integration. In the near-neutral formulation the integration coefficient  $A_1$  can be found via the mean-diurnal value of sensible heat:  $\rho C_p \overline{H}(h) = (1 - E_F) \overline{R}_n$  and  $A_2$  can be obtained from the measurement of the mean daily temperature at level  $z_1$ .

Similarly the steady-state solution of the ground heat flux follows:

$$\frac{d^2 \bar{G}}{dz^2} = 0. \quad (26)$$

Using  $\lim_{z \rightarrow -\infty} G(z) = 0$  the steady-state ground heat flux has to vanish everywhere, i.e.  $\bar{G}(z) = 0$ . Similarly the soil temperature is solution of the same equation and the steady-state soil temperature gives:

$$\bar{T}(z) = T_{deep} \quad (27)$$

where  $T_{deep}$  is the constant soil temperature far below the surface. Note that  $T_{deep}$  does not need to be specified, as it can be obtained from the steady-state expression of the sensible heat flux at the land surface:

$$\bar{H}(h) = \frac{1}{r_a^c} (T_{deep} - \bar{\theta}(h)) \quad (28)$$

so that:

$$T_{deep} = r_a^c A_1 (h - z_i) + \frac{A_1}{K_*} [h + (d - z_i) \ln(h - d)] + A_2. \quad (29)$$

Thus, using equations (25), (27) and (29) the measurement of the mean-daily potential temperature at level  $z_i$  is sufficient to determine the steady-state profiles of temperatures and heat fluxes in the soil and in the ABL.

The steady-state profiles of sensible heat flux and potential temperature (not shown) are physically realistic and correspond to the results of Stevens (2000). The steady-state potential temperature exhibits a logarithmic profile with a strong gradient in the lower part of the ABL (surface layer). In the upper ABL,

the steady-state potential temperature remains almost uniform, corroborating the behavior of the well-mixed layer. The daily-mean value of potential temperature at the surface is higher than in the rest of the ABL since the solar heating at the land surface strongly impacts the overlying air. The steady-state sensible heat flux is linearly varying with height as in the case of instantaneous profiles. As it is discussed later, the heat fluxes in the atmospheric boundary layer behave as in quasi steady state i.e. the influence of the surface is so rapid that it is almost instantaneously transmitted throughout the ABL, leading to profiles in quasi-equilibrium.

### 4.3. Harmonic solution

The solution to the  $n^{\text{th}}$  daily harmonic forcing with angular frequency  $\omega_n$  can be derived. The harmonics for negative values of  $n$  can be deduced from the positive ones, using the fact that the heat fluxes and temperatures are real function of time and space; therefore the negative Fourier coefficients can be expressed as:

$$Y_{-n} = (Y_n)^* \quad (30)$$

where  $(.)^*$  denotes the complex conjugate. The solution to the soil diffusion equation is well known (see Carslaw and Jaeger 1967 or Crank 1956 for more detailed and classical reviews). Using the fact that the ground heat flux and the soil temperature amplitudes vanish at infinite depth, the complex amplitude of ground heat flux at frequency  $\omega_n$  is:



$$\tilde{G}(\omega_n, z) = G_0 \exp(j\gamma) \exp(z / \tilde{\lambda}_G). \quad (31)$$

The decay with depth is exponential and has the length scale parameter:

$$\tilde{\lambda}_G = (1-j) \sqrt{\frac{K_s}{2\omega_n}} \quad (32)$$

where  $G_0(\omega_n)$  and  $\gamma(\omega_n)$  are respectively the amplitude and phase of ground heat flux at frequency  $\omega_n$ .

In the soil, the conservation of internal energy (8) in the Fourier domain becomes:

$$j\omega_n C_s T_s = \frac{d\tilde{G}}{dz} \quad (33)$$

so that the complex amplitude of soil temperature can be expressed as a function of depth:

$$\tilde{T}_s(\omega_n, z) = \frac{G_0 \exp(j\gamma)}{C_s} (1-j) \sqrt{\frac{1}{2\omega_n K_s}} \exp(z / \tilde{\lambda}_G). \quad (34)$$

To solve the sensible heat flux equation, which is a diffusion equation with non-constant parameters, the variable  $x = 2\sqrt{-\frac{j\omega_n(z-d)}{K_*}}$  is introduced and the sensible heat flux is written as:  $H(z, t) = h(z) \exp(j\omega_n t) = h(x) \exp(j\omega_n t)$ . Then the atmospheric equation can be transformed into a modified Bessel equation of zero order:

$$x^2 \frac{d^2 h}{dx^2} - x \frac{dh}{dx} + x^2 h(x) = 0. \quad (35)$$

The solution to this equation can be written:

$$h(x) = x(C_1 H_1^1(x) + C_2 H_1^2(x)) \quad (36)$$

where  $H_1^1$  denotes the Hankel function of the first order and first kind, representing an inward wave for the  $z$  coordinate and  $H_1^2$  is the Hankel function of the first order and second kind, which represents an outward wave. However, the sensible heat flux is zero at the top of the ABL:  $z = z_i = c \frac{u_*}{|f|}$ . Since  $z_i$  is

much larger than  $d$  so that to a very good approximation:

$$x_i = 2\sqrt{-\frac{j\omega_n(z_i - d)}{K_s}} \approx 2\sqrt{\frac{j\omega_0 nc}{2K_s \sin(\phi)}},$$

where  $\phi$  is latitude and  $\omega_0$  is the Earth's angular rotation rate. Since the effect of the daily frequency (or Earth's rotation frequency) cancels out, it has no influence on the depth of the neutral ABL height. The only influence of the Earth's rotation on the ABL height appears through the latitude of the location.

The sensible heat flux  $H(h) = \overline{w'\theta'}(h)$  at height  $h$  is written as a complex exponential  $h_h \exp(j\beta)$  with  $h_h \in \mathbb{R}^+$ . The boundary condition at the land surface thus becomes  $h(x_h) = h_h \exp(j\beta)$  and at the top of the ABL the vanishing flux reads:  $h(x_i) = 0$ . Finally, the following linear system is obtained:

$$\begin{bmatrix} x_i H_1^1(x_i) & x_i H_1^2(x_i) \\ x_h H_1^1(x_h) & x_h H_1^2(x_h) \end{bmatrix} \begin{bmatrix} C_1 \\ C_2 \end{bmatrix} = \begin{bmatrix} 0 \\ h_h \end{bmatrix}. \quad (37)$$

By a matrix inversion:

$$\begin{bmatrix} C_1 \\ C_2 \end{bmatrix} = \begin{bmatrix} \frac{H_1^2(x_i)}{x_h [H_1^1(x_i)H_1^2(x_h) - H_1^2(x_i)H_1^1(x_h)]} h_h \\ \frac{H_1^1(x_i)}{x_h [H_1^1(x_i)H_1^2(x_h) - H_1^2(x_i)H_1^1(x_h)]} h_h \end{bmatrix}. \quad (38)$$

However in most conditions  $|H_1^2(x_i)| \ll |H_1^1(x_i)|$  by at least two orders of magnitude so that a good approximation of the coefficients  $C_1$  and  $C_2$  are:

$$\begin{bmatrix} C_1 \\ C_2 \end{bmatrix} = \begin{bmatrix} 0 \\ \frac{1}{x_h H_1^2(x_i)} h_h \end{bmatrix}. \quad (39)$$

This resembles the solution obtained by Lettau (1951). The main advantage of the introduction of an ABL height is the possibility to obtain a steady-state solution.

Finally, the complex amplitude of sensible heat flux can be rewritten:

$$\tilde{h}(\omega_n, z) = \frac{H_1^1(x_i)H_1^2(x) - H_1^2(x_i)H_1^1(x)}{H_1^1(x_i)H_1^2(x_h) - H_1^2(x_i)H_1^1(x_h)} \sqrt{\frac{z-d}{h-d}} h_h \exp(j\beta) \quad (40)$$

where  $h_h(\omega_n)$  and  $\beta(\omega_n)$  are respectively the amplitude and phase of sensible heat flux and  $\tilde{h}(\omega_n, z)$  is the complex amplitude of sensible heat flux at height  $z$  and frequency  $\omega_n$ .

The conservation of dry static energy in the atmosphere, (4), can be rewritten:

$$j\omega_n \tilde{\theta}(\omega_n, z) = -\frac{d\tilde{H}}{dz}(\omega_n, z). \quad (41)$$

Consequently the complex amplitude of potential temperature at height  $z$  becomes:

$$\tilde{\theta}(\omega_n, z) = \frac{1+j}{\sqrt{2\omega_n Ku_*^0 (h-d)}} \frac{H_1^1(x_i)H_0^2(x) - H_1^2(x_i)H_0^1(x)}{H_1^1(x_i)H_1^2(x_h) - H_1^2(x_i)H_1^1(x_h)} h_h \exp(j\beta). \quad (42)$$

These expressions of the complex amplitudes of temperature and heat-flux profiles are the fundamental building blocks of this study. They are invaluable for the analysis of the phase and amplitude of the heat-flux and temperature dependence at the land surface in the coupled soil-vegetation-atmosphere continuum framework.

#### 4.4. Vertical spectral structure

In order to study the propagation of the surface forcing into the soil and the ABL, a characteristic length scale of the wave penetration is introduced. This length scale is defined as the distance to which the wave is attenuated by an exponential factor.

For the soil heat wave, the penetration depth can be derived from (31) as:

$$\lambda_G(\omega_n) = \sqrt{\frac{2K_s}{\omega_n}}. \quad (43)$$

Indeed the absolute complex amplitude of ground heat flux can be rewritten:

$|G(\omega_n, z)| = G_0(\omega_n) \exp(z / \lambda_G(\omega_n))$ , with  $z$  below land surface taking on negative values.

A typical value for  $\lambda_G$ , for a daily sinusoidal forcing, is of the order of a few centimeters for most soil conditions and typical values of  $K_s$ . Moreover, the penetration depth of the soil temperature wave is the same as that of the ground heat flux.

The propagation depth of both potential temperature  $\lambda_\theta$  and sensible heat flux  $\lambda_H$  are defined as:

$$\lambda_\theta(\omega_n) = \arg \min_{z>h} \left\| \frac{\tilde{\theta}(\omega_n, z)}{\tilde{\theta}(\omega_n, h)} - e^{-1} \right\| \quad (44)$$

and

$$\lambda_H(\omega_n) = \arg \min_{z>h} \left\| \frac{\tilde{H}(\omega_n, z)}{\tilde{H}(\omega_n, h)} - e^{-1} \right\|. \quad (45)$$

These two propagation depths are rapidly decreasing functions of frequency. They become small at higher frequencies as shown in Figure 2. The scale  $\lambda_\theta$  is always smaller than  $\lambda_H$  by two orders of magnitude. The effect of the potential temperature wave remains relatively shallow (of the order of a few tenths of meters) compared to that of the sensible heat flux (which is of the order of a kilometer) and remains concentrated in a small layer right above the vegetation. This is an interesting result as potential temperature and sensible heat flux are two linked physical variables, yet the surface does not affect both quantities in the same way. It also confirms that our simplified model exhibits a realistic behavior in the whole ABL domain, with a distinct surface layer at its base

capped by a mixed layer as illustrated by Figure 3. Even with our simple linearly-varying eddy-diffusion coefficients, the surface layer displays strong potential temperature gradients accompanied by relatively small sensible heat flux gradients. On top of this bottom layer, the mixed layer possesses negligible potential temperature gradients as well as a sensible heat flux linearly varying with height, i.e. a sensible heat flux in quasi steady-state.

The important difference in the behavior of  $\lambda_\theta$  and  $\lambda_H$  is due to the assumption about linearly increasing eddy diffusion-coefficient in the ABL. For a given value of sensible heat flux, the magnitude of the potential temperature gradient in the surface layer has to be high in order to compensate for the low eddy-diffusion coefficient. In the upper ABL the eddy-diffusion coefficient is high and smaller potential temperature gradients are needed to maintain the sensible heat flux profile. In our near-neutral turbulent case, the potential temperature gradient is stronger at the surface since it is closer to the heat source and the eddy-diffusion coefficients are generally small. In highly unstable conditions large eddies tend to improve the mixing of the mixed layer since turbulence is characterized by larger, more energetic eddies. The result is larger eddy-diffusion coefficients and large-scale motions, which cannot be modeled by a local closure.

The influence of four parameters, namely evaporative fraction, canopy aerodynamic resistance  $r_a^c$ , vegetation height  $h$ , and friction velocity  $u_*$ , can easily be studied with our analytical solution. The influence of these parameters is studied for the main daily harmonic  $\omega_0$  only for the sake of simplicity.

In our near-neutral turbulent case,  $\lambda_\theta$  is independent on the value of evaporative fraction and  $r_a^c$  but is very dependent on  $h$  and  $u_*$ , as seen on Figure 4. Indeed the latter two factors drive the eddy diffusion near the surface and are consequently determinants for the propagation of the potential temperature wave.

On the contrary, the propagation depth of sensible heat flux, normalized by  $z_i$ , is insensitive to the surface parameters, as long as the normalization includes the dependence on friction velocity:  $z_i(u_*)$ . Indeed the friction velocity tremendously impacts the value of the propagation depth, since it is the main factor driving the turbulence in our near-neutral case. Moreover the relationship between friction velocity and  $\lambda_H$  is linear because the propagation depth of sensible heat flux is proportional to the eddy-diffusion coefficient, which is itself linearly dependent on the friction velocity. Because the neutral ABL height parameterization is also linearly varying with friction velocity, the propagation depth of sensible heat normalized by the ABL height remains constant for all values of friction velocity.

These results emphasize the theoretical existence of the well-known diurnal atmospheric surface layer as described by Lettau (1949). This surface layer is located right above the canopy and has a size of the order of  $\lambda_\theta$ . This study provides a framework for decomposing the sensitivity of key features of the surface layer to different diurnal harmonics and key surface parameters. The

surface layer is commonly used in resistance models of the surface energy balance and ABL coupling (see e.g., Monteith 1973; Thom 1975; Choudhury 1988). One caveat is that our study is restricted to near-neutral conditions and that it should be improved in forthcoming studies to include the effect of stability and alternative eddy-diffusion profile parameterizations. Indeed these changes modify the structure of the ABL and lead to changes in  $\lambda_H$  and  $\lambda_\theta$ .

## 4.5. Surface heat-flux and temperature harmonics

### 4.5.1. Amplitude expressions

Here we introduce two variables that simplify the representation of the spectral amplitudes of the surface energy balance components:

$$\Delta(\omega_n) = \frac{1}{C_s} (1-j) \sqrt{\frac{1}{2\omega_n K_s}} \quad (46)$$

and

$$\Sigma(\omega_n) = \frac{1+j}{\sqrt{2\omega_n Ku_* (h-d)}} \frac{H_1^1(x_i)H_0^2(x_n) - H_1^2(x_i)H_0^1(x_n)}{H_1^1(x_i)H_1^2(x_n) - H_1^2(x_i)H_1^1(x_n)} + r_a^c. \quad (47)$$

Now the energy balance components can be rewritten as a function of the net radiation harmonic at the land surface:

$$G_0 \exp(j\gamma) = \frac{1}{1 + \frac{1}{1-E_F} \frac{\rho c_p \Delta(\omega_n)}{\Sigma(\omega_n)}} r_n \exp(j\alpha) \quad (48)$$



$$h_n \exp(j\beta) = \frac{1 - E_F}{1 + \frac{1 - E_F \Sigma(\omega_n)}{\rho C_p \Delta(\omega_n)}} r_n \exp(j\alpha) \quad (49)$$

$$\lambda E_h \exp(j\epsilon) = \frac{E_F}{1 + \frac{1 - E_F \Sigma(\omega_n)}{\rho c_p \Delta(\omega_n)}} r_n \exp(j\alpha) \quad (50)$$

where  $r_n(\omega_n)$  and  $\alpha(\omega_n)$  are respectively the amplitude and phase of net radiation,  $\lambda E_h(\omega_n)$  and  $\epsilon(\omega_n)$  are the amplitude and phase of latent heat flux,  $h_h(\omega_n)$  and  $\beta(\omega_n)$  the amplitude and phase of sensible heat flux and  $G_0(\omega_n)$  and  $\gamma(\omega_n)$  the amplitude and phase of ground heat flux, all at frequency  $\omega_n$ . Moreover the complex amplitudes of the surface temperatures can also be rewritten as functions of the incoming radiation forcing:

$$\tilde{T}_{surf} = \frac{1}{1 + \frac{1 - E_F \Sigma(\omega_n)}{\rho c_p \Delta(\omega_n)}} \frac{1 - j}{C_s} \sqrt{\frac{1}{2\omega_n K_s}} r_n \exp(j\alpha) \quad (51)$$

$$\tilde{\theta}_h = \frac{\Sigma(\omega_n)}{\rho c_p} \frac{1 - E_F}{1 + \frac{1 - E_F \Sigma(\omega_n)}{\rho C_p \Delta(\omega_n)}} r_n \exp(j\alpha) \quad (52)$$

where  $\tilde{T}_{surf}(\omega_n)$  is the complex amplitude of land-surface temperature at frequency  $\omega_n$  and  $\tilde{\theta}_h(\omega_n)$  is the complex amplitude of air potential temperature at height  $h$  and frequency  $\omega_n$ . These equations form the basis for the analysis of the spectral behavior (gain and phase difference) of the surface heat fluxes and

temperatures as functions of key land-surface parameters in a land-atmosphere coupled framework.

#### **4.5.2. Tests using field observations**

We test various aspects of the framework presented here by comparing the surface energy balance components against observations and output from a numerical Soil-Vegetation-Atmosphere Transfer (SVAT) model (described in Gentine et al. 2007) that is calibrated and validated using 101 days of field observations at the SudMed experiment site (Chehbouni et al. 2008 and Duchemin et al. 2006). The land-surface model allows continuous outputs that fill gaps in measurements. Continuous time-series are required for Fourier decomposition. The analytical model estimates of air temperature, soil, sensible and latent heat fluxes are shown in Figure 5 and compared with the measurements as well as the outputs of the calibrated land-surface model. Even though the analytic model has simplified representation of the soil-vegetation-atmosphere continuum, it nonetheless captures the main amplitude and phase features of the surface heat fluxes and surface temperatures.

#### **1.3 Response to daily sinusoidal forcing**

The response of the land-atmosphere coupled model to harmonic forcing of net radiation at the surface is investigated using the derived amplitude and phase spectra. The peak of the surface net radiation forcing is taken to be local solar noon. The response of surface heat fluxes and temperatures to incoming radiation

sinusoidal forcing at frequency  $\omega_0$  is shown in Figure 6. The soil heat flux at the surface leads net radiation in phase by  $\pi/6$  which is about 2 hours for a daily fundamental frequency. This result is consistent with observations and SVAT simulated values as shown in Gentine et al. (2007) among many others.

The soil surface temperature has a phase lag of  $\pi/4$  with respect to ground heat flux i.e.  $\pi/12$  with respect to net radiation. This result holds for any forcing frequency because of the presence of the  $(1-j)$  factor between the soil surface temperature and the surface ground heat flux. This effect has also both been observed and theoretically investigated for general heat diffusion problems (Carslaw and Jaeger 1967). Consequently the soil surface temperature reaches its peak around one hour after solar noon, since the soil thermal inertia delays the dynamics of soil temperature. We note that the soil profile of this study has uniform conductivity and capacity thermal properties. The approach neglects heterogeneity that influences the propagation of soil heat waves. Non-uniform soil thermal diffusivity can introduce multiple reflections of ground heat-flux waves as shown in Karam (2000).

The difference between the air potential temperature  $\theta_h$  and the surface temperature  $Ts_0$  is also evident on Figure 6. The daily amplitude of the surface potential temperature is smaller compared to that of  $Ts_0$ . Even if the magnitude of the surface ground heat flux and sensible heat flux are comparable in this case, the penetration depth of the soil heat wave  $\lambda_G$ , which is of the order of a few

centimeters for most soil conditions, is much smaller than  $\lambda_\theta$ , which is of the order of a few tenths of meters. The heat wave is consequently limited to a much shallower layer in the soil than in the atmosphere.  $T_{s_0}$  exhibits more diurnal variations than  $\theta_h$  since the elevated soil heat capacity is not sufficient to compensate for the length scale difference in the penetration of heat in the soil and in the ABL.

#### 4.5.3. Influence of Forcing Frequency

Equations (48) through (52) are used to characterize the influence of the land-surface parameters on the land-surface energy partitioning, and on the air and soil temperatures. The gain (as represented by the ratio of spectral amplitudes) and phase spectra with respect to the net radiation forcing are shown in Figure 7 and Figure 8 for the fluxes and temperatures respectively. The turbulent and ground heat fluxes exhibit very different gain responses over the whole frequency domain. At high frequencies, the importance of the ground heat flux in the surface energy budget increases sharply in contrast to the turbulent fluxes. This is evident in the higher gain values. This result demonstrates the relative importance of the high-frequency component in the ground heat flux spectrum and its role in absorbing weather noise i.e. high-frequency radiative forcing induced by, for example, intermittent clouds. Indeed rapid changes in net radiation primarily influence ground heat flux and have less impact on the turbulent fluxes. This result is compared with the SVAT numerical simulation of

the 101-day period in the SudMed field experiment. Figure 9 shows that soil heat flux has a stronger amplitude gain at higher frequencies when compared with turbulent heat fluxes. Even with varying environmental conditions, the amplitude ratio between soil heat flux and turbulent fluxes matches the theoretical curve well. This is of importance since it proves that soil heat flux always acts as a high-pass filter of the incoming radiation compared to turbulent heat fluxes, which act as low-pass filter, since their response is limited by the temporal delay of the land-surface temperature changes.

The theoretical phase spectrum in Figure 7b shows that the ground heat flux always leads in phase with respect to net radiation and that this phase remains almost constant regardless of frequency. Similarly the sensible heat flux always lags in phase with respect to net radiation and its phase remains nearly constant across frequencies. The surface latent heat flux is directly proportional to the sensible heat flux but modulated through the constant evaporative fraction as in  $\lambda E = \frac{E_F}{1 - E_F} H$ . Therefore its phase spectrum behaves similarly to sensible heat flux.

The spectral responses of the surface soil and near-surface air potential temperatures are shown in Figure 8. The gain spectra of the two temperatures exhibit a broad spectrum which only slowly decays at higher frequencies. The difference in amplitudes demonstrate the relatively larger impact of weather noise (high frequency variations in net radiation) on the instantaneous value of soil temperature when compared with surface air potential surface temperature.

Moreover the phase spectra show that  $Ts_0$  and  $\theta_h$  both always lag in phase with respect to net radiation forcing.

#### 4.5.4. Dependency on parameters

Evaporative fraction ( $E_f$ ), canopy aerodynamic resistance  $r_a^c$ , surface friction velocity  $u_*$  and vegetation height  $h$  are among the key factors controlling the model partitioning of net radiation into sensible, latent and ground heat flux. Here we use the analytic framework introduced in this study to analyze their effect on the amplitude and phase of the surface fluxes and temperatures. The results apply only to near-neutral-to-unstable atmospheric conditions.

The influence of these parameters on the amplitude of the surface heat fluxes is shown in Figure 10. The phase differences are shown in Figure 11. As evaporative fraction increases, the proportion of net radiation transformed into latent heat flux naturally rises, since it controls the partitioning between surface turbulent heat fluxes. Evaporative fraction impacts the ground heat flux as well because ground heat flux compensates for the reduction of latent heat flux, a more efficient heat dissipation mechanism than sensible heat flux (see Gentine et al. 2007). A larger evaporative fraction leads to a reduction of surface temperature. A stronger evaporative fraction consequently reduces the temperature gradient in the near-surface soil and hence reduces the surface ground heat flux at the surface. Finally, a higher evaporative fraction tends to increase the phase lead of ground heat flux with respect to net radiation;

conversely it decreases the phase lag of turbulent heat fluxes with respect to net radiation. When evaporative fraction increases, available energy is favourably partitioned towards latent heat flux which leads to a faster temperature equilibration that closely follows the net radiation forcing.

The role of the canopy aerodynamic resistance  $r_a^c$  is shown in Figure 10b. A stronger aerodynamic resistance naturally reduces the turbulent heat fluxes and also noticeably increases ground heat flux, since this latter compensates the reduced heat dissipation through turbulence. The phase difference between sensible heat flux and net radiation in Figure 11b shows that a larger aerodynamic resistance tends to increase the sensible heat flux delay with net radiation. An increasing aerodynamic resistance reduces the efficiency of heat dissipation through sensible heat flux at the land surface. This consequently both reduces and delays the response of sensible heat flux and of surface potential temperature to net radiation changes.

Vegetation height displays little influence on the heat-flux partitioning but has an indirect role since it modifies aerodynamic resistance. This is evident in the relatively constant gain and phase spectra shown in Figure 10c and Figure 11c.

Friction velocity influence (Figure 10d) on the turbulent fluxes is large because it scales them by magnitude. Therefore a larger surface friction velocity increases the magnitude of both the sensible and latent heat flux, and ground heat flux decreases due to the surface energy balance constraint. Friction velocity

also exerts a control on the phase of the ground and turbulent heat fluxes as evident in Figure 11d. Larger friction velocities induce a more efficient and rapid land-surface energy dissipation through turbulent heat release, resulting in a reduced phase lag with respect to net radiation. Correspondingly the residual ground heat flux exhibits an increased phase lead with respect to net radiation.

The surface parameters also influence the gain and phase of soil surface and near-surface air potential temperatures. The amplitude influence is displayed on Figure 12. A larger evaporative fraction tends to decrease the amplitude of both the surface potential and soil temperatures. Indeed a stronger evaporative fraction decreases the harmonic amplitude of both potential and soil temperature. Again this is principally due to the fact that evaporation is a more efficient mechanism to dissipate energy than sensible heat flux.

The canopy aerodynamic resistance  $r_a^c$  controls the gradient of temperature in the canopy and therefore a larger  $r_a^c$  tends to decouple the variations of land-surface potential temperature and soil temperature as evident in Figure 12b. The amplitude of soil surface temperature is increased for larger  $r_a^c$  values.

Finally the increase in friction velocity tends to decrease the amplitude of both the potential and soil temperatures. A stronger friction velocity increases turbulence, which reduces the amplitude of soil surface temperature. The increased turbulence diminishes the amplitude of potential temperature because it leads to closer ABL and soil coupling.



## Conclusions

This study extends the remarkable work of Lettau (1951) with the shared aim to understand the harmonic response of a coupled land-atmosphere system to periodic surface net radiation forcing. A one-dimensional model of the soil-vegetation-atmospheric boundary layer continuum is used to characterize the dynamic response of soil and air temperature and heat flux profiles. The formulation of the problem has several important features: 1) latent heat flux is now included whereas Lettau (1951) assigned it to be constant and independent of model states, 2) a vegetation layer without heat capacity is included to improve the fidelity of the treatment of the surface layer and matching of temperature boundary conditions, 3) a finite height is imposed on the boundary layer in order to derive the steady-state profiles of temperatures and heat fluxes, and 4) the problem is solved for all daily harmonics whereas Lettau (1951) only solved one leading harmonic. The latter enhancement allows us to analyze the spectral gain and phase responses of heat fluxes and temperatures across the spectrum of net radiation forcing.

The first conclusion is that heat waves exhibit very different behaviors in the soil and in the boundary layer. In particular the harmonic influence of net radiation on soil temperature and heat flux is concentrated in a shallow soil layer of a few tens of centimeters and varies considerably with frequency. The boundary-layer potential temperature profile is affected by the surface net radiation harmonics on a layer of several tenths of meters that also varies with

frequency. In contrast, sensible heat flux wave penetration depth is on the order of a kilometer that is comparable to the depth of the boundary layer. This penetration depth is also a strong function of spectral frequency.

The influence of the surface radiation forcing spectrum underscores the importance of high-frequency observations since the soil and air potential temperatures are both characterized by broad gain spectra and respond to weather noise (high frequency variations in net radiation). Soil heat flux dominates in absorbing much of the high-frequency forcing, whereas turbulent fluxes are mostly influenced by the lower (daily) frequencies. Finally evaporative fraction, canopy aerodynamic resistance  $r_a^c$  and friction velocity  $u_*$  influence the gain and phase spectra of heat fluxes and temperatures in complex ways that relate to the relative efficiency of the fluxes in dissipating heat and to the surface energy balance constraint.

In order to derive closed-form spectral representation, this study is limited to linear parameterization of components such as eddy-diffusion profiles, invariant soil and boundary layer properties (e.g., soil thermal conductivity, soil thermal heat capacity, ABL friction velocity, canopy sensible heat flux resistance, etc.). Follow-on studies need to account for the effects of thermal stratification and convection. Moreover the inclusion of specific humidity profile in the ABL can lead to the relaxation of the evaporative fraction self-preservation assumption. Since the analytic framework for gain and phase spectra with respect to surface net radiation spectrum is now available, future studies can include

stochasticity in the surface energy balance and analyze the effects of errors in characterization of surface process in the coupled land-atmosphere system.

Figures:

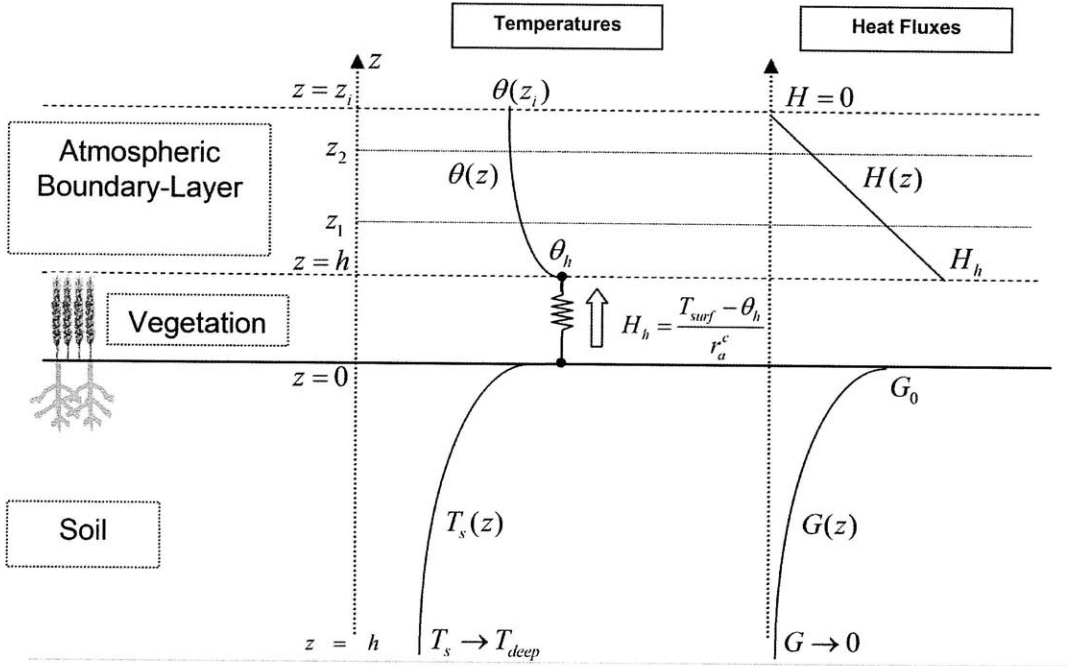


Figure 1: Schematic representation of the soil-vegetation-atmospheric boundary layer continuum with temperature (on the left) and heat fluxes (on the right).

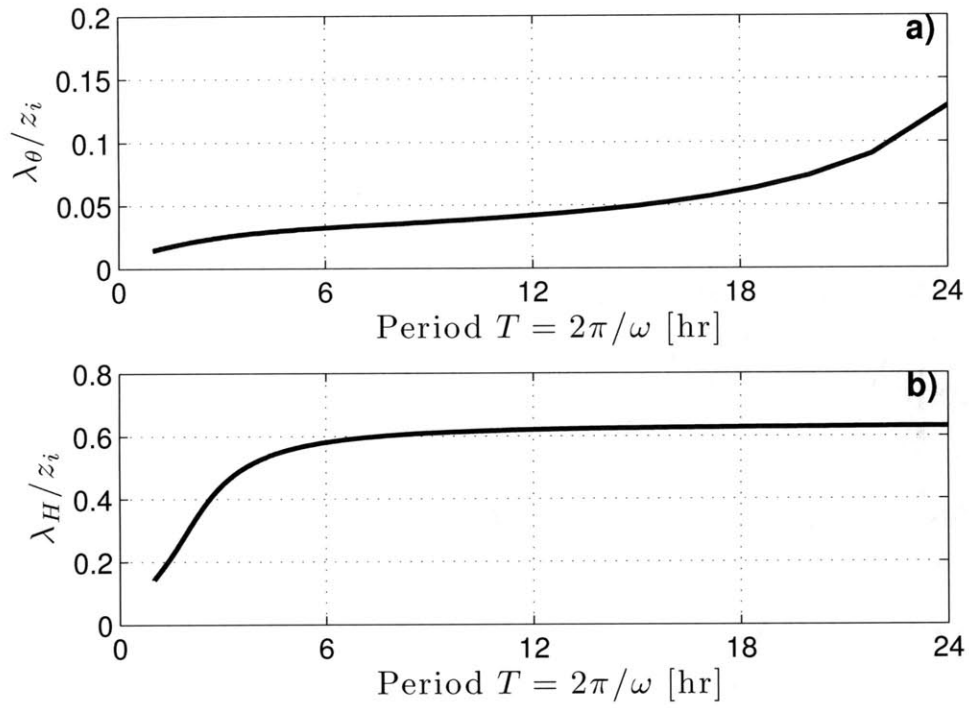


Figure 2: Spectral dependency of the normalized propagation depth of the atmospheric wave for potential temperature (top) and sensible heat flux (bottom).

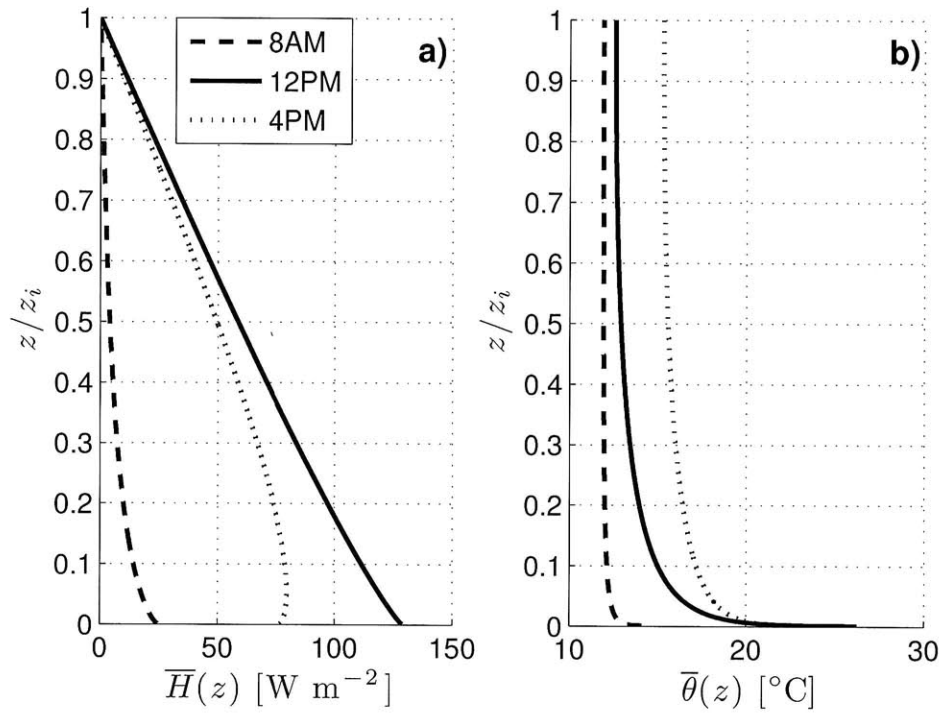


Figure 3: Simulated profiles of sensible heat flux (a) and potential temperature (b).

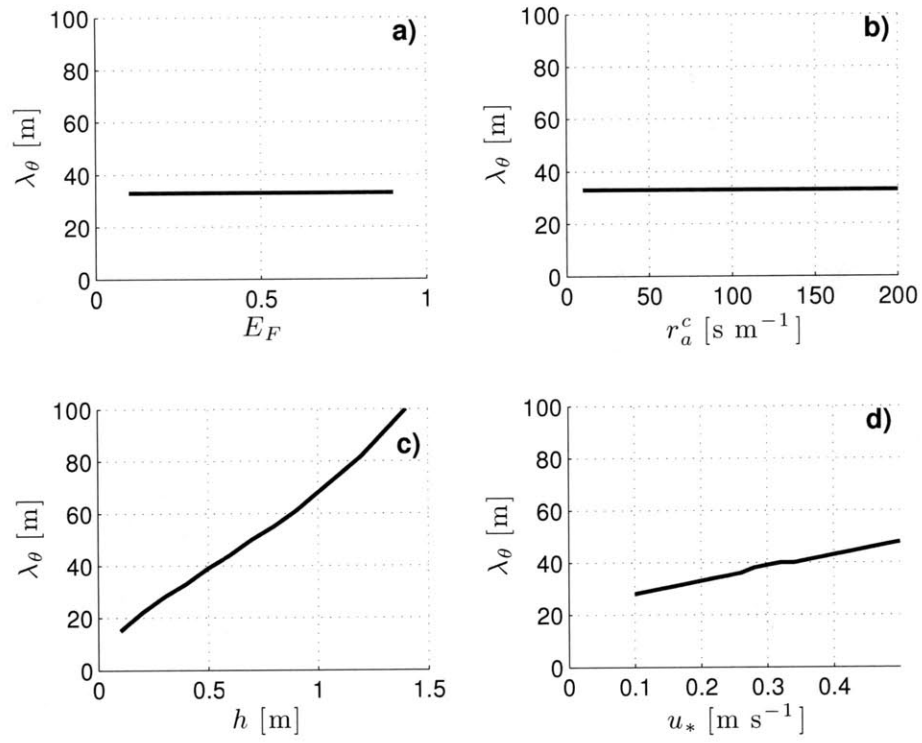


Figure 4: Dependency of the penetration depth of the potential temperature wave to evaporative fraction (a), aerodynamic resistance (b), vegetation height (c) and friction velocity (d).

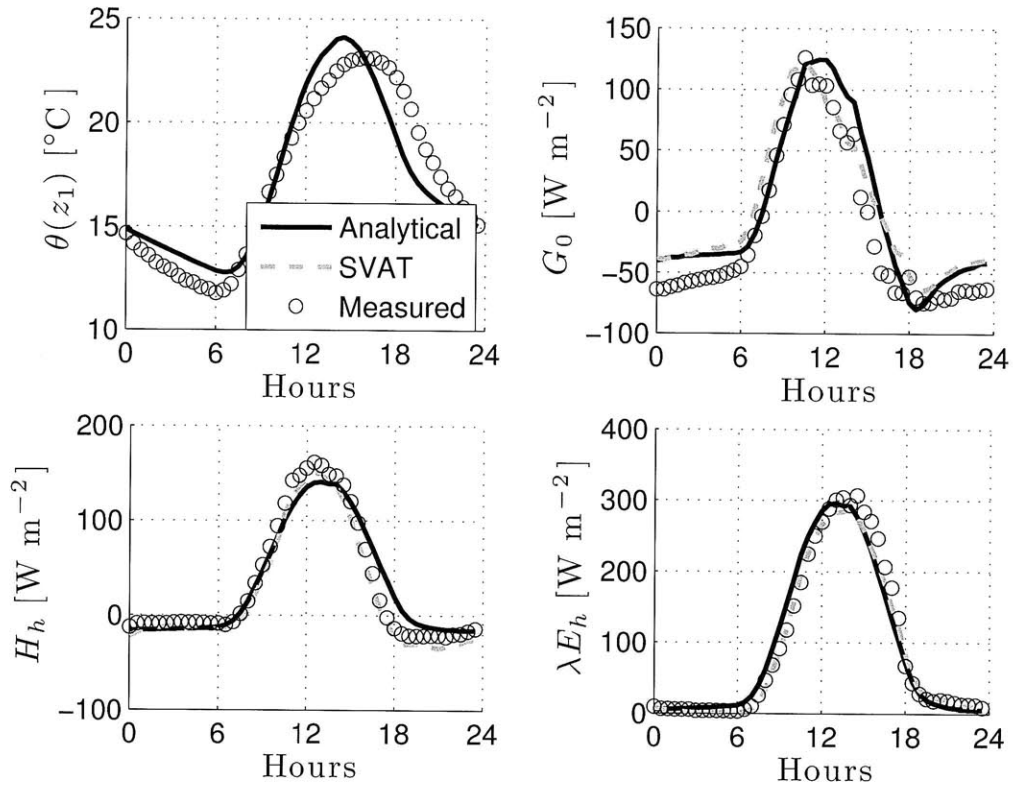


Figure 5: Comparison between theoretical (this study; black continuous), SVAT (grey dash line) and measured (circles) air temperature (a), soil heat flux (b), sensible heat flux (c) and latent heat flux (d) for the daily cycle averaged over 101 days of measurements from the SudMed experiment in Marrakech, Morocco.



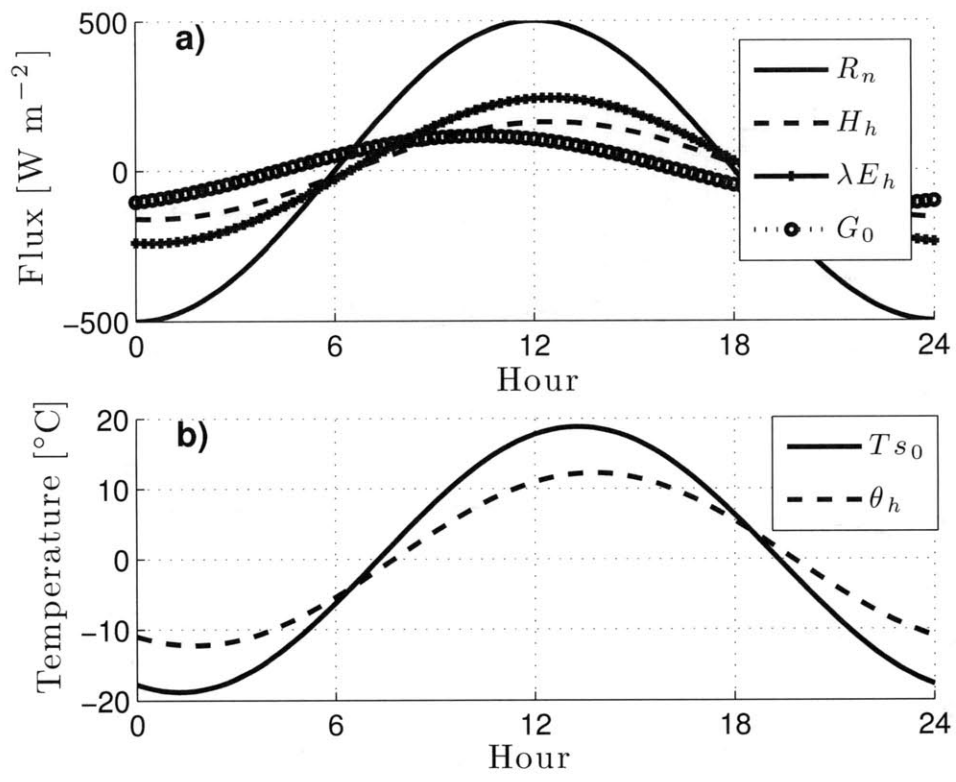


Figure 6: Response of the surface heat fluxes (a) and surface temperatures (b) to diurnal forcing of net radiation at the surface.

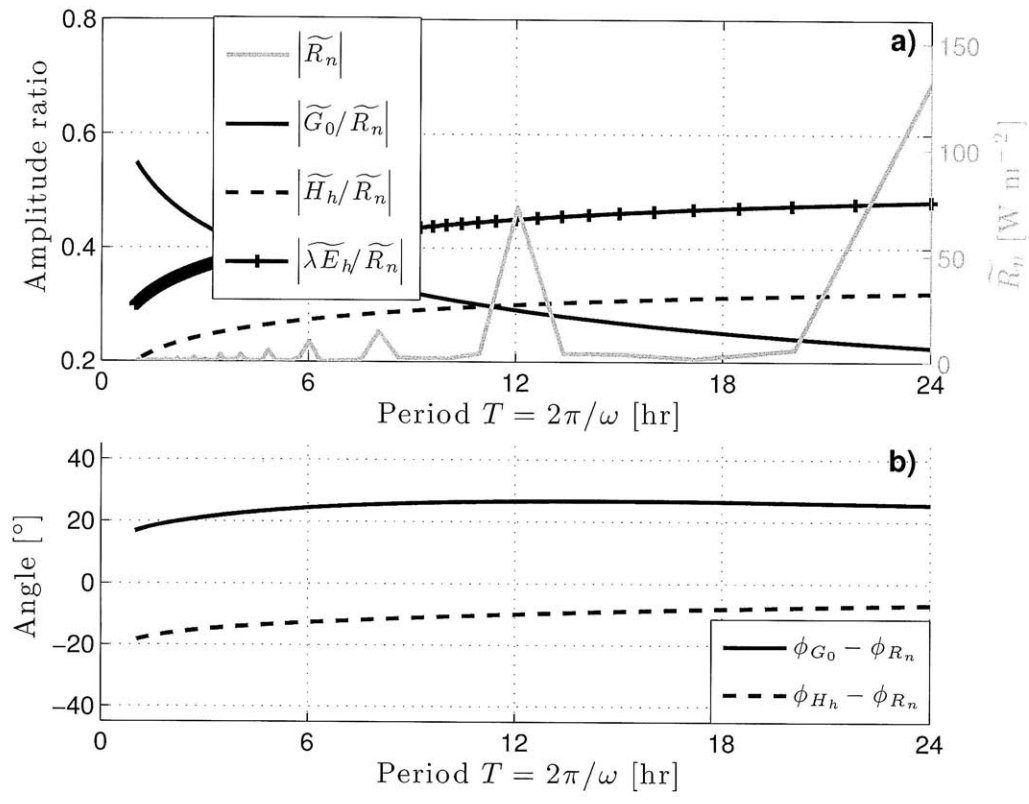


Figure 7: Spectral dependency of the amplitude (a) and phase (b) of the surface heat fluxes

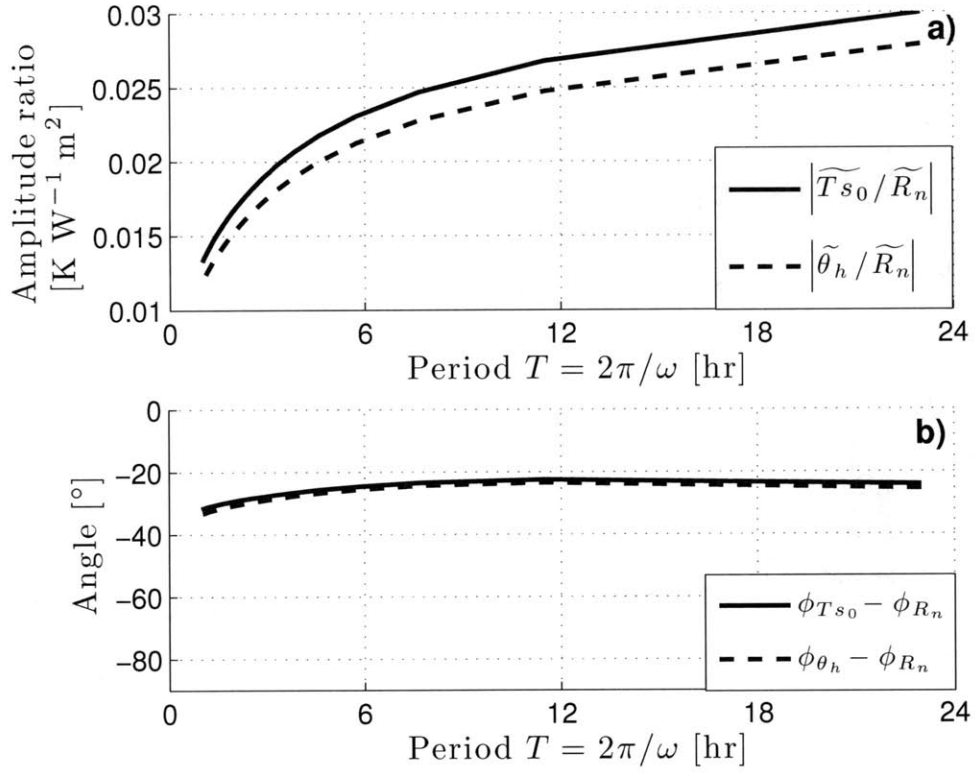


Figure 8: Spectral dependency of the amplitude (a) and phase (b) of the surface temperatures.

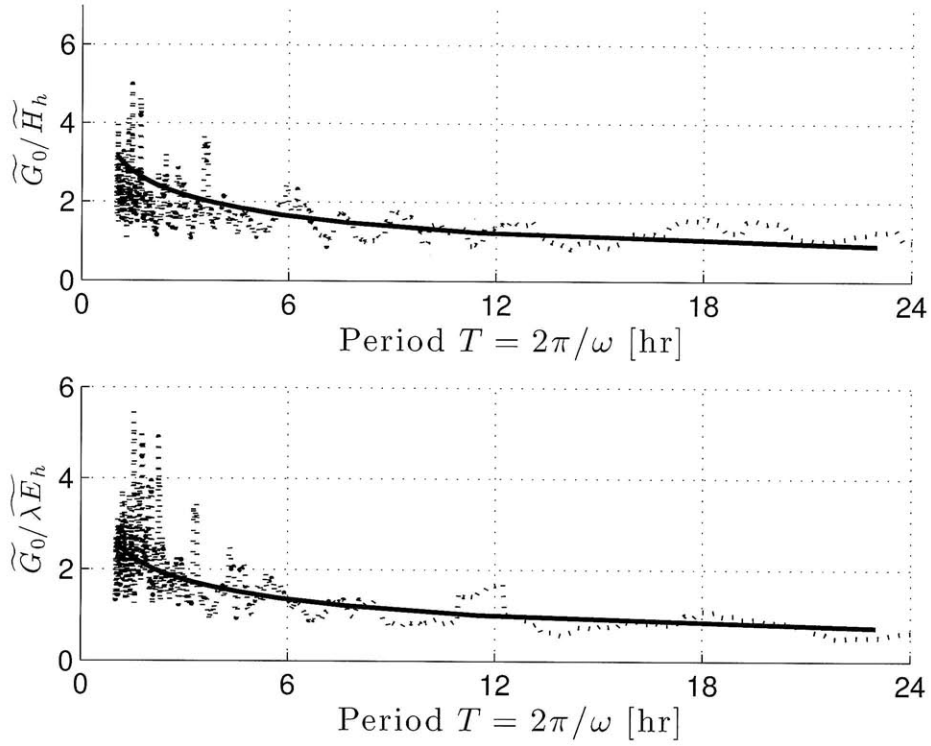


Figure 9: Relative amplitude spectrum of the SVAT (dash line) and theoretical (this study; continuous line) surface soil heat flux over sensible heat flux a) and latent heat flux b) for 101 days of measurements from the SudMed experiment in Marrakech, Morocco. A moving average of 25 frequencies has been used for the SVAT outputs.

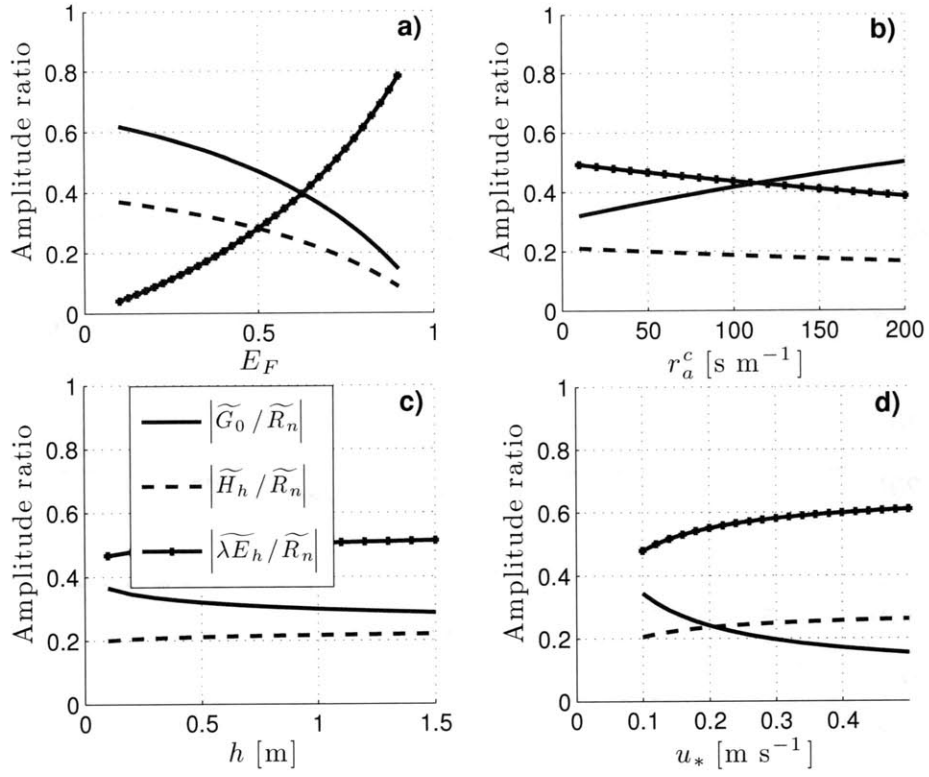


Figure 10: Dependency of the amplitude of the surface heat fluxes on evaporative fraction (a), aerodynamic resistance (b), vegetation height (c) and friction velocity (d).

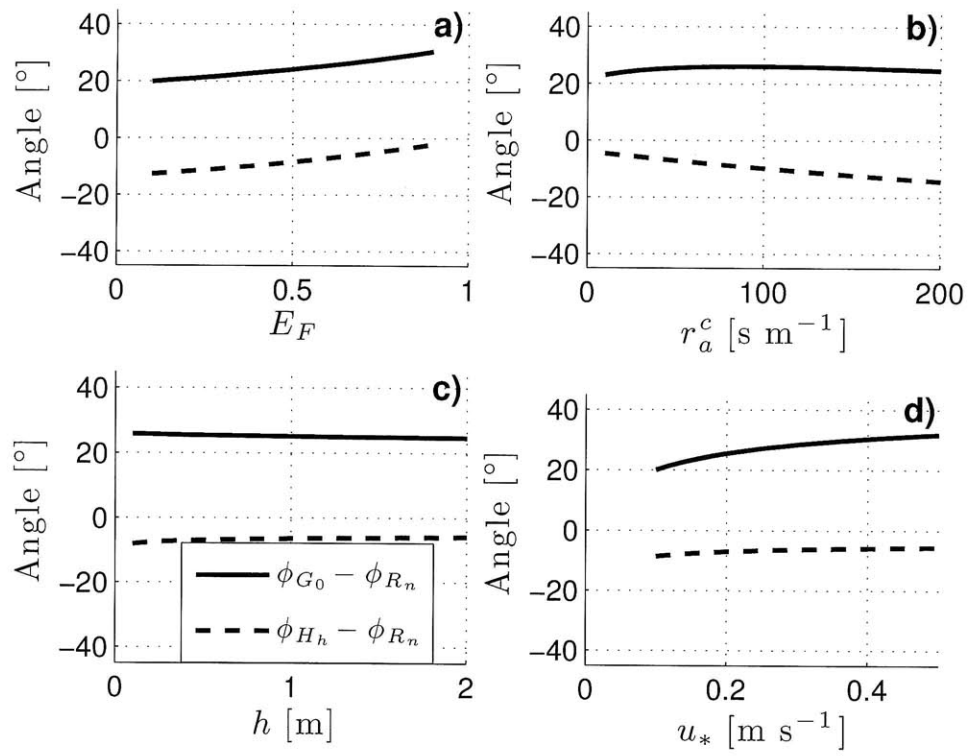


Figure 11: Dependency of the phase of the surface heat fluxes on evaporative fraction (a), aerodynamic resistance (b), vegetation height (c) and friction velocity (d).

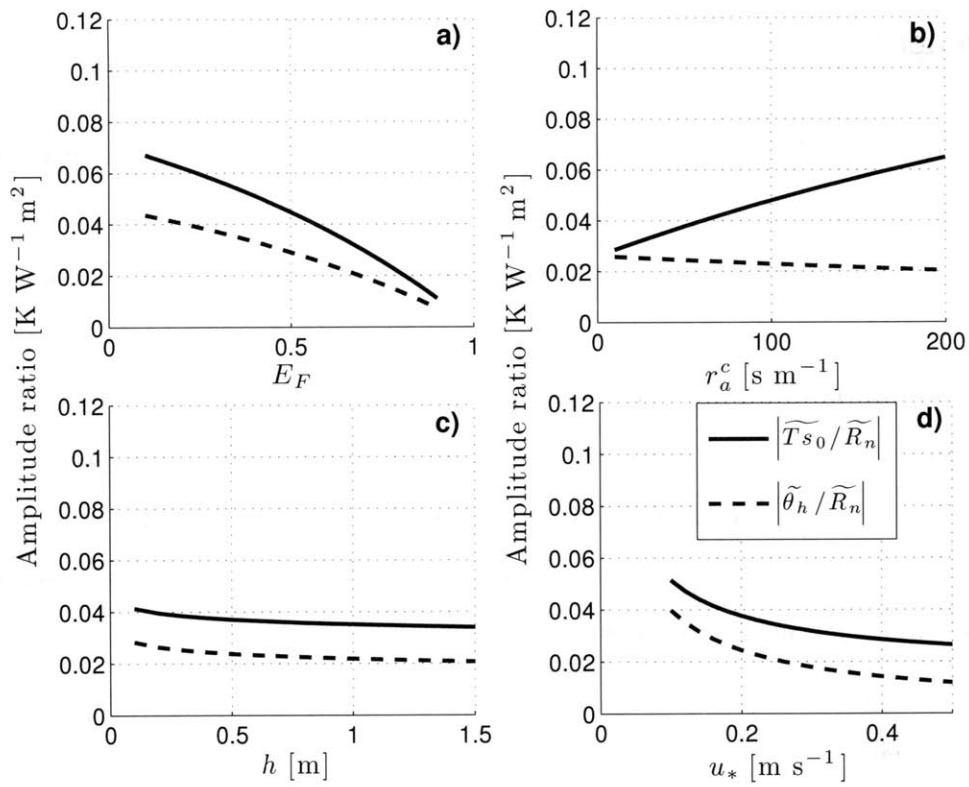


Figure 12: Dependency of the amplitude of surface temperatures on evaporative fraction (a), aerodynamic resistance (b), vegetation height (c) and friction velocity (d).

## References

- Brutsaert WH (1982) *Evaporation into the Atmosphere*. Kluwer Acad Publ, Dordrecht, Holland, 299 pp
- Caparrini F, Castelli F, Entekhabi D (2003) Mapping of land-atmosphere heat fluxes and surface parameters with remote sensing data. *Boundary-Layer Meteorol* 107: 605-633
- Caparrini F, Castelli F, Entekhabi D (2004) Estimation of surface turbulent fluxes through assimilation of radiometric surface temperature sequences. *J Hydrometeorol* 5: 145-159
- Caparrini F, Castelli F, Entekhabi D (2004) Variational estimation of soil and vegetation turbulent transfer and heat flux parameters from sequences of multisensor imagery. *Water Resour Res*: 40.doi: 10.1029/2004WR003358
- Carslaw HS and Jaeger JC (1967) *Conduction of Heat in Solids*. Oxford University Press, New York, 353 pp
- Chebouni A Escadafal R, Duchemin B, Boulet G, Simonneaux V, Dedieu G, Mougenot B, Khabba S, Kharrou MH, Maisongrande P, Merlin O, Chaponnière A, Ezzahar J, Er-Raki S, Hoedjes J, Hadria R, Abourida A, Cheggour A, Raibi F, Boudhar A, Benhadj I, Hanich L , Benkaddour A, Guemouria N, Chebouni AH, Lahrouni A, Oliosio A, Jacob F, Williams DG, Sobrino J (2008) An integrated modelling and remote sensing approach for hydrological study in arid and semi-arid regions: the SUDMED Program. *Int J Remote Sens* 29: 5161-5181
- Choudhury BJ and Monteith JL (1988) A four-layer model for the heat budget of homogeneous land surfaces. *Q J Roy Meteorol Soc* 114: 373-398
- Crago R (1996) Conservation and variability of the evaporative fraction during the daytime. *J Hydrol* 180: 173-194
- Crago R Brutsaert W (1996) Daytime evaporation and the self-preservation of the evaporative fraction and the Bowen ratio. *J Hydrol* 178: 241-255



- Crank J (1956) *The Mathematics of Diffusion*. Oxford University Press, New York, 356 pp
- Duchemin B et al. (2006) Monitoring wheat phenology and irrigations in Central Morocco: On the use of relationships between evapotranspiration, crops coefficients, leaf area index and remotely-sensed vegetation indices. *Agr Water Manage* 79: 1-27
- Garratt JR (1992) *The Atmospheric Boundary Layer*. Cambridge, UK, 316 pp
- Gentine P, Entekhabi D et al (2007) Analysis of evaporative fraction diurnal behaviour. *Agric For Meteorol* 143: 13-29
- Holtslag AAM and Moeng CH (1991) Eddy Diffusivity and Countergradient Transport in the Convective Atmospheric Boundary Layer. *J Atmos Sci* 48: 1690-1698
- Karam MA (2000) A Thermal Wave Approach for Heat Transfer in a Nonuniform Soil. *Soil Sci Soc Am J* 64: 1219-1225
- Kimura F, Shimizu Y (1994) Estimation of Sensible and Latent Heat Fluxes from Soil Surface Temperature using a Linear Air-Land Heat Transfer Model. *J Appl Meteorol* 33: 477-489
- Lettau H (1949) Isotropic and non-isotropic turbulence in the atmospheric surface layer. *Geophys Res Lett* 1: 13-84
- Lettau H (1951) Theory of surface temperature and heat-transfer oscillations near level ground surface. *EOS* 32: 189-200
- Lhomme J-P, Elguero E (1999) Examination of evaporative fraction diurnal behaviour using a soil-vegetation model coupled with a mixed-layer model. *Hydrol Earth Syst Sc* 3: 259 – 270
- Monin AS and Obukhov AM (1954) Basic Laws of Turbulent Mixing in the Ground Layer of the Atmosphere. *Trans Geophys Inst Akad Nauk USSR* 151: 163-187
- Monteith JL (1973) *Principles of Environmental Physics*. Arnold, London, UK, 241 pp
- Nichols WE, Cuenca RH (1993) Evaluation of the evaporative fraction for parameterization of the surface energy-balance. *Water Resour Res* 29: 3681-3690
- Plate EJ (1971) *Aerodynamic Characteristics of Atmospheric Boundary Layers*. US Atomic Energy Commission Division of Technical Information, Oak Ridge, TN, 190 pp

- Shuttleworth WJ, Gurney RJ, Hsu AY, Ormsby JP (1989) FIFE: The variation in energy partition at surface flux sites. IAHS Publ 186: 67-74
- Stevens B (2000) Quasi-Steady Analysis of a PBL Model with an Eddy-Diffusivity Profile and Nonlocal Fluxes. Mon Weather Rev 128: 824-836
- Stull RB (1988) An introduction to Boundary Layer Meteorology. Kluwer Acad Publ, Dordrecht, Holland, 666 pp
- Thom AS, Stewart JB, Oliver HR, Gash JHC (1975) Comparison of Aerodynamic and Energy Budget Estimates of Fluxes over a Pine Forest. Q J Roy Meteorol Soc 101: 93-105
- Van De Wiel BJH, Moene AF, Ronda RJ, De Bruin HAR, Holtslag AAM (2007) Intermittent Turbulence and Oscillations in the Stable Boundary Layer Over Land Part II: A System Dynamics Approach. J Atmos Sci 59: 2567-2581
- Van Dop H and Verver G (2001) Countergradient Transport Revisited. J Atmos Sci 58: 2240-2247
- Zilitinkevich S, Gryanick VM, Lykossov VN and Mironov DV (1999) Third-order transport and nonlocal turbulence closures for convective boundary layers. J Atmos Sci 56: 3463-3477

## Chapter 5

# Harmonic Characteristics of Land Surface Evaporation in the Soil-Atmosphere Continuum

**Abstract.** The components of the land-surface energy balance respond to periodic net radiation forcing with complex amplitude and phase characteristics. In this study a linearized model of the soil-vegetation-atmospheric boundary layer continuum is used to study the harmonics in the energy balance components.

The influence of the incident radiation spectrum on the heat fluxes (sensible, latent) and scalars (temperature, specific humidity) in the atmospheric boundary layer is investigated. In addition, the roles of the major land-surface parameters on the land-surface energy partitioning and temperatures are further studied.

Evaporative fraction is shown to exhibit a much wider spectrum than surface heat fluxes. This behavior is linked to inherent non-linearities in the system. Also evaporative fraction possesses an asymptotical diurnal lower limit, which is derived as function of surface parameters. In regions experiencing strong solar radiative forcing, dry and fair weather conditions, evaporative fraction is demonstrated to remain constant and approach its asymptotical value during daylight hours.

**Keywords:** Evaporative fraction, Fourier transform, Soil heat flux, Diurnal, Turbulent heat fluxes, Land-atmosphere interaction.

## 5.1. Introduction

Land surface control on evaporation results in adjustments in the components of surface energy balance. The effects of these adjustments extend to the soil and atmosphere profiles of moisture, energy states and heat fluxes. The changes in the profiles in turn affect the surface energy balance. Coupling of the soil profiles and atmospheric boundary layer (ABL) profiles of temperature and heat fluxes can be strong and they can also be cause for the emergence of feedback mechanisms.

The soil and the ABL systems, as well as the processes of surface energy balance that link them at their common interface, respond to the periodic (radiative) forcing. The phase and amplitude attributes of their responses are key to the working of the feedback mechanisms and land-atmosphere coupling. In this study we seek to decompose the states and fluxes in the soil-vegetation-atmosphere continuum into harmonics that reveal their characteristic phase and amplitude response to diurnal forcing.

Many studies of land-atmosphere interactions have been performed using numerical models that can capture nonlinearities and threshold behaviors. Harmonic decomposition of the soil-vegetation-atmosphere continuum however requires simpler models that capture the essential physics and links, yet that can be solved using Fourier decomposition. There is a history of using simpler and analytical models to gain insights into the coupled system [e.g., see *Mangian and*

*Jinjun* 1993, *Brubaker and Entekhabi* 1994, *Kim and Entekhabi* 1998, *Margulis and Entekhabi* 1998, *Zeng and Neelin* 1999, *Wang and Mysak* 2000]. In the present study we pose a linear model of the soil-vegetation-ABL continuum in order to analyze the phase and amplitude responses at different spectral frequencies.

The present study extends the seminal work of *Lettau* [1951]. The original model is extended in several important ways. First, *Lettau* [1951] formulated and solved the problem for only one harmonic. Here we extend the model so that it resolves all harmonics. Second, *Lettau* [1951] assumed that surface latent heat flux is a constant. Here we allow it to be a dynamic component of the surface energy balance through introducing humidity profiles in the model. Thirdly, *Lettau* [1951] assumed that the ABL height is infinite whereas a finite ABL height is more realistic and furthermore allows characterization of steady-state profiles. We make this important extension to the original model. Finally, we introduce a vegetation layer that is key to characterizing a surface layer and transition zone between the surface and the atmosphere. Although the model introduced in this study is largely different from *Lettau* [1951], the influence and inspiration of that original and seminal work cannot be underestimated.

In this study we place special emphasis on the partitioning of available energy at the surface into turbulent fluxes and ground heat flux. These components of the surface energy balance have gain and phase spectra with respect to radiative forcing that are important for insights into land-atmosphere

coupling. Clearly they are strongly periodic on diurnal time scales. There are however diagnostics, such as the Evaporative Fraction ( $EF$ ), that aim to isolate the highly periodic from the constant factors affecting surface energy balance. Evaporative fraction is defined as the fraction of available energy partitioned towards latent heat flux:

$$EF = \frac{\lambda E_h}{A} = \frac{\lambda E_h}{R_n - G_0}. \quad (1.1)$$

Surface latent heat flux is governed by available energy (highly periodic) and surface control (less periodic). Surface control refers to soil moisture and water available to plants that vary on longer time scales than daytime. If  $EF$  truly isolates the surface control on turbulent heat flux and is nearly constant during daytime, it has major implications for sampling and estimation. For example *Boni et al.* [2001a, 2001b], *Caparrini et al.* [2004], *Kustas et al.* [2001], and *Margulis et al.* [2002] map surface energy balance components from the diurnal march of the remotely-sensed land surface temperature. What makes their estimation procedure well-conditioned is due to the assumption of a constant value for daytime  $EF$ . They essentially use the amplitude of the LST response to radiation as implicitly indicative of surface control on surface energy balance.

Several studies based on field experiment data [e.g., *Shuttleworth et al.* 1989, *Nichols and Cuenca* 1993, *Crago* 1996 and *Crago and Brutsaert* 1996] have shown that  $EF$  could often be considered to be a constant during daytime (self-preservation). However recent theoretical studies by *Lhomme* [1999] and *Gentine et al.* [2007] have shown that  $EF$  is nearly constant during daytime under very

limited surface conditions and only in fair weather. This study delves deeper into the underlying causes and degree of the apparent near self-preservation of  $EF$  during daytime. We use the analytical and linearized model of the soil-vegetation-ABL continuum to decompose the profiles of temperature, humidity and heat flux into harmonics with phase and amplitude information at each frequency. We analyze the dependence of these spectral characteristics on surface physical parameters. There are limits to the self-preservation assumption that are shown using the analytic framework.

## 5.2. Description of A Model for the Soil-Vegetation-Atmosphere Continuum

A schematic representation of the land-atmosphere system is shown in Figure 1. The model links the one-dimensional soil-vegetation-boundary layer continuum for the heat and moisture state variables and fluxes. The only source of energy and periodic forcing for the system is incident radiation at the surface.

The representation of the atmosphere and soil are inspired by the work of *Lettau* [1951] extended by *Gentine et al.* [2009]. The studies use similar linear diffusion equations for the evolution of temperature. The major difference here with *Lettau's* [1951] approach is in the treatment of the coupling between the two media. For tractability reasons, *Lettau* [1951] assumed that latent heat was constant throughout the day, which was a major limitation of his model. Here we relax that assumption since the interplay between latent and sensible heat fluxes (as well as ground heat flux) are key to the goals of this study. *Lettau* [1951]



assumed that temperature was continuous at the interface between the land and the atmosphere: there is however evidence for strong gradients and even discontinuity between the soil and the surface air layer due to the presence of the vegetation canopy. This discontinuity can result in major phase shift between the responses of both soil and ABL temperatures induced by diurnal solar forcing. Finally *Lettau* [1951] assumed an infinite height for the ABL. Here we formulate the model to have a finite ABL height which also allows us to solve for the steady-state solution. Unlike *Lettau* [1951] who only solved for one harmonic, here we solve for all harmonics because the goal of the study is to find the degree to which there are harmonic shifts and harmonic broadening in the response of surface energy balance components and their diagnostics to periodic solar forcing.

### 5.2.1. The boundary-layer medium

The dynamics of the atmospheric boundary layer and soil temperature in the vertical are assumed to dominate over the horizontal. The ABL and land surface are assumed to be uniform horizontally and the effect of lateral advection is considered to be negligible compared to that of incident radiation forcing. The ABL extends from the surface to a finite height  $z_i$  where the turbulent heat fluxes vanish. More importantly the atmosphere is assumed to be in near-neutral to unstable turbulent conditions, so that small eddies dominate the sensible and latent heat flux. Turbulent fluxes in the surface layer can therefore be expressed as functions of gradients of passive scalars (respectively potential temperature and specific humidity) using the eddy-diffusion theory. Above the surface layer

the mechanism of turbulent heat transport are more complex. The larger turbulently mixed layer is characterized by small temperature gradient and linearly decreasing sensible heat flux. Sensible heat flux diminishes to zero at height  $z_r$ . The application of linearly-increasing eddy-diffusion coefficient through the depth of the ABL does achieve these requirements for flux parameterization. Gradients of potential temperature approach zero and sensible heat flux linearly decreases to zero at the ABL height. We adopt this approach for both the surface layer and the ABL.

The turbulent fluxes are thus written as:

$$\phi_\theta = -K_H(z) \frac{\partial \theta}{\partial z} \quad (2.1)$$

$$\phi_q = -K_V(z) \frac{\partial q}{\partial z}. \quad (2.2)$$

The eddy-diffusion coefficients for near-neutral to slightly unstable conditions are assumed to be linearly varying with height

$$K_{H,V}(z) = ku_*(z - d). \quad (2.3)$$

This assumption is common with *Lettau* [1951] and takes friction velocity  $u_*$  to be constant throughout the daytime. The expression for turbulent heat fluxes within the ABL become:

$$\phi_\theta = -ku_*(z - d) \frac{\partial \theta}{\partial z} \quad (2.4)$$

$$\phi_q = -ku_*(z - d) \frac{\partial q}{\partial z}. \quad (2.5)$$

The displacement height  $d$  is related to the height of the vegetation layer using the expression introduced by *Brutsaert* [1982]:

$$d = \frac{2h}{3}. \quad (2.6)$$

There is no condensation within the boundary-layer depth of the model. With negligible lateral advection and condensation, the conservation of mean potential temperature within the ABL becomes:

$$\frac{\partial \theta}{\partial t} = -\frac{\partial \phi_\theta}{\partial z}. \quad (2.7)$$

Similarly the conservation of mean water mass in the ABL is:

$$\frac{\partial q}{\partial t} = -\frac{\partial \phi_q}{\partial z}. \quad (2.8)$$

Using scalar conservation equations (2.7) and (2.8), in conjunction with eddy diffusivity parameterizations in (2.4) and (2.5), the potential temperature and specific humidity are solutions of

$$\frac{\partial \theta}{\partial t} = \frac{\partial}{\partial z} \left( K(z) \frac{\partial \theta}{\partial z} \right) = K_*(z-d) \frac{\partial^2 \theta}{\partial z^2} + K_* \frac{\partial \theta}{\partial z} \quad (2.9)$$

$$\frac{\partial q}{\partial t} = \frac{\partial}{\partial z} \left( K(z) \frac{\partial q}{\partial z} \right) = K_*(z-d) \frac{\partial^2 q}{\partial z^2} + K_* \frac{\partial q}{\partial z}. \quad (2.10)$$

Similarly, operating  $K(z) \frac{\partial}{\partial z}$  on both equations (2.9) and (2.10) leads to the

following governing relationships for the evolution of turbulent fluxes in the ABL:

$$\frac{\partial \phi_\theta}{\partial t} = K(z) \frac{\partial^2 \phi_\theta}{\partial z^2} = K_*(z-d) \frac{\partial^2 \phi_\theta}{\partial z^2} \quad (2.11)$$

$$\frac{\partial \phi_q}{\partial t} = K(z) \frac{\partial^2 \phi_q}{\partial z^2} = K_*(z-d) \frac{\partial^2 \phi_q}{\partial z^2} \quad (2.12)$$

where  $K_* = Ku_*$ . These partial differential equations are linear and can be solved analytically. We use spectral methods that give harmonics of states and fluxes.

The spectral method allows us to find the phase (lag-lead) spectra with respect to the periodic radiative forcing at the land surface. The amplitude gain spectra are defined as the response amplitudes normalized by the amplitude spectrum of the surface radiative forcing.

### 5.2.2. The Soil Medium

Heat flux and temperature state dynamics within the soil medium are also assumed to be dominated by vertical diffusion. The soil thermal diffusivity and heat capacity are taken to be constant and uniform throughout the profile so that the dynamics of soil water content and soil temperature redistribution are decoupled. Without this simplifying assumption the problem becomes non-tractable and can only be solved numerically.

Using Fourier's law the soil heat flux can be expressed as a function of the soil temperature gradient ( $G$  is positive downward):

$$G = \lambda_s \frac{\partial T_s}{\partial z}. \quad (2.13)$$

The conservation of internal energy leads to the following relationship for soil temperature profile evolution:

$$C_s \frac{\partial T_s}{\partial t} = \frac{\partial G}{\partial z}. \quad (2.14)$$

Substituting (2.13) into (2.14) leads to the partial differential equations for soil temperature  $T_s$  evolution:

$$\frac{\partial T_s}{\partial t} = K_s \frac{\partial^2 T_s}{\partial z^2} \quad (2.15)$$

where  $K_s$  is the soil heat diffusivity. Operating  $\lambda_s \frac{\partial}{\partial z}$  on (2.15) and using the expression for soil heat flux (2.13) leads to a related diffusion equation for soil heat flux evolution:

$$\frac{\partial G}{\partial t} = K_s \frac{\partial^2 G}{\partial z^2}. \quad (2.16)$$

### 5.2.3. Boundary conditions

The soil and ABL evolution equations are coupled through the land surface energy balance. Surface energy balance serves as the common boundary for both systems. The incident solar and thermal radiative fluxes at the land surface force the entire system. At the top of the ABL the boundary condition is defined through vanishing turbulent fluxes. Below the surface and at the far-field of the surface boundary where the forcing is imposed, the soil heat flux similarly vanishes. The boundary conditions can be summarized as:

I/ At the land surface, the incident radiation is composed of incoming solar  $S_\downarrow$  and thermal components  $L_\downarrow$  as  $I_\downarrow(t) = (1 - \alpha_s)S_\downarrow(t) + L_\downarrow(t)$ . The parameter  $\alpha_s$  is the surface solar albedo.

II/ The soil heat flux is zero at the far-field:  $\lim_{z \rightarrow -\infty} G(z, t) = 0$ .

III/ The sensible and latent heat fluxes vanish at the top of the ABL, i.e.:  $\phi_\theta(z_i) = 0$  and  $\phi_q(z_i) = 0$ . The height is modeled using *Plate's* [1971] formulation

$z_i = \frac{cu_*}{|f|}$  with  $c = 0.2$ . The ABL height scales with the Coriolis parameter  $f$  and

friction velocity  $u_*$ .

The sensible heat flux at the land surface is parameterized using aerodynamic resistance  $r_a^c$  at the vegetation canopy and ABL interface:

$$\phi_\theta(h,t) = \frac{T_s(z=0,t) - \theta(h,t)}{r_a^c}. \quad (2.17)$$

The resistance parameter is considered to be constant throughout the solution period  $T$ . Similarly the latent heat flux at the same boundary is modeled as :

$$\phi_q(h,t) = \frac{\beta}{r_a^c} \{q^*(T_s(0,t)) - q(h,t)\} \quad (2.18)$$

The parameter  $\beta$  reduces the evaporation below its limiting potential value corresponding to a moist surface. This parameter is related to the soil moisture in the root zone and it is assumed to be constant throughout the period  $T$ .

IV/ A common assumption in land-surface modeling is that there is negligible storage of heat within the vegetation layer (compared to the other energy balance components) so that the energy budget at the land surface is:

$$R_n(t) - G(0,t) = H(h,t) + \lambda E(h,t) = \rho C_p \phi_\theta(h,t) + \rho \lambda \phi_q(h,t) \quad (2.19)$$

### 5.3. Fourier Development

The flux profiles as well as state (potential temperature and specific humidity) profiles are assumed to be periodic over the period  $T$  so that the different variables can be expanded using Fourier basis functions. Any variable  $A(t, z)$  is then developed as a weighted sum of harmonics:

$$A(t, z) = \bar{A}(z) + \sum_{\substack{n=-\infty \\ n \neq 0}}^{+\infty} \tilde{A}(n\omega_0, z) e^{jn\omega_0 t} \quad (2.20)$$

with fundamental pulsation  $\omega_0 = \frac{2\pi}{T}$ . By projecting on Fourier bases, the problem can be solved component-wise, i.e. each complex amplitude  $\tilde{A}(n\omega_0, z)$  is solved independently from the others and the time derivative operator becomes a simple multiplicative factor  $\frac{\partial}{\partial t} \rightarrow jn\omega_0$ . The atmospheric boundary layer evolution partial differential equations (2.9), (2.10), (2.11) and (2.12) reduce to simple ordinary differential equations. After removing the subscript  $n$  notation for simplicity and for non zero harmonics  $\omega \neq 0$ , the Fourier amplitudes are governed by:

$$\tilde{\phi}_\theta(\omega, z) = -j \frac{K_*(z-d)}{\omega} \frac{d^2 \tilde{\phi}_\theta}{dz^2}(\omega, z) \quad (2.21)$$

$$\tilde{\phi}_q(\omega, z) = -j \frac{K_*(z-d)}{\omega} \frac{d^2 \tilde{\phi}_q}{dz^2}(\omega, z) \quad (2.22)$$

$$\tilde{\theta}(\omega, z) = -\frac{jK_*(z-d)}{\omega} \frac{d^2 \tilde{\theta}}{dz^2}(\omega, z) - \frac{jK_*}{\omega} \frac{d\tilde{\theta}}{dz}(\omega, z) \quad (2.23)$$

$$\tilde{q}(\omega, z) = -\frac{jK_*(z-d)}{\omega} \frac{d^2 \tilde{q}}{dz^2}(\omega, z) - \frac{jK_*}{\omega} \frac{d\tilde{q}}{dz}(\omega, z). \quad (2.24)$$

The corresponding zero-th harmonic is the steady-state solution that obeys the following original relations:

$$\frac{d^2 \overline{\phi}_\theta}{dz^2}(z) = 0 \quad (2.25)$$

$$\frac{d^2 \overline{\phi}_q}{dz^2}(z) = 0 \quad (2.26)$$

$$(z-d) \frac{d^2 \bar{\theta}}{dz^2}(z) + \frac{d\bar{\theta}}{dz}(z) = 0 \quad (2.27)$$

$$(z-d) \frac{d^2 \bar{q}}{dz^2}(z) + \frac{d\bar{q}}{dz}(z) = 0. \quad (2.28)$$

Similarly in the soil, (2.15) and (2.16) reduce to:

$$\tilde{G}(\omega, z) = -\frac{jK_s}{\omega} \frac{d^2 \tilde{G}}{dz^2}(\omega, z) \quad (2.29)$$

$$\tilde{T}_s(\omega, z) = -\frac{jK_s}{\omega} \frac{d^2 \tilde{T}_s}{dz^2}(\omega, z) \quad (2.30)$$

and the steady-state solutions follow:

$$\frac{d^2 \bar{G}}{dz^2}(z) = 0 \quad (2.31)$$

$$\frac{d^2 \bar{T}_s}{dz^2}(z) = 0 \quad (2.32)$$

for  $\omega \neq 0$ .

The coupled boundary conditions are also expressed in the Fourier domain.

Because of the linearity, in the Fourier domain for  $\omega \neq 0$  the sensible heat flux expression at the surface (2.17) simply becomes:

$$\tilde{\phi}_\theta(\omega, h) = \frac{\tilde{T}_{s_0}(\omega) - \tilde{\theta}_h(\omega)}{r_a^c} \quad (2.33)$$

And the steady-state solution is:

$$\bar{\phi}_\theta(h) = \frac{\bar{T}_{s_0} - \bar{\theta}_h}{r_a^c} \quad (2.34)$$

The main difficulty of the latent heat flux boundary condition is that the saturated specific humidity is a non-linear function of temperature. To the first



order approximation, this equation can be linearized around the mean surface temperature, over period  $T$  :

$$q_*(T_s(0,t)) = q_*(\bar{T}_{s_0}) + (T_s(0,t) - \bar{T}_{s_0}) \left[ \frac{dq_*(T)}{dT} \right]_{T=\bar{T}_{s_0}} = q_*(\bar{T}_{s_0}) + \gamma_{\bar{T}_{s_0}} (T_s(0,t) - \bar{T}_{s_0}). \quad (2.35)$$

Using the daily Fourier series of the surface temperature, this can be rewritten:

$$q_*(T_s(0,t)) = q_*(\bar{T}_{s_0}) + \gamma_{\bar{T}_{s_0}} \sum_{\substack{n \in \mathbb{Z} \\ n \neq 0}} \tilde{T}_{s_0}(\omega_n) e^{j\omega_n t}. \quad (2.36)$$

Note that with this linearization:

$$\overline{q_*(T_s(0,t))} = q_*(\bar{T}_{s_0}) \quad (2.37)$$

so that the mean daily value of the saturated specific humidity at the surface equals the saturated specific humidity of the mean surface temperature.

After projection on the Fourier basis, boundary condition (2.18) is written as:

$$\forall n \in \mathbb{Z}^* \quad \tilde{\phi}_q(n\omega_0, h) = \frac{\beta}{r_a^c} \left( \gamma_{\bar{T}_{s_0}} \tilde{T}_{s_0}(n\omega_0) - \tilde{q}_h(n\omega_0) \right). \quad (2.38)$$

For the steady-state component:

$$\bar{\phi}_q(h) = \frac{\beta}{r_a^c} \left( q_*(\bar{T}_{s_0}) - \bar{q}_{h,0} \right). \quad (2.39)$$

The outgoing thermal radiation component in net radiation is characterized by the Stefan-Boltzmann law. It depends on the fourth power of surface temperature. Even though this is a strongly nonlinear function, over the range of temperatures (Kelvin) experienced at the land surface, the linearized function adequately represents the flux.

If the surface temperature is linearized around its mean daily value, the difference

between the actual surface temperature and the daily mean temperature is only due to the influence of the harmonics of surface temperature:

$$T_{s_0}(t) = \bar{T}_{s_0} + \sum_{\substack{n=-\infty \\ n \neq 0}}^{\infty} \widetilde{T}_{s_0}(\omega_n) e^{jn\omega_0 t} = \bar{T}_{s_0} + \Delta T_{s_0} \quad (3.1)$$

The net radiation can consequently be divided into a steady-state term plus the influence of all non-zero harmonics:

$$R_n(t) = \underbrace{(1 - \alpha_s) \bar{S} + \bar{L}_\downarrow - \varepsilon_s \sigma \bar{T}_{s_0}^4}_{\bar{R}_n} + \underbrace{\sum_{\substack{k=-\infty \\ k \neq 0}}^{\infty} \left[ (1 - \alpha_s) \widetilde{S}_\downarrow(k\omega_0) + \widetilde{L}_\downarrow(k\omega_0) - 4\varepsilon_s \sigma \bar{T}_{s_0}^3 \widetilde{T}_{s_0}(k\omega_0) \right] e^{jk\omega_0 t}}_{\Delta R_n} \quad (3.2)$$

Thus the non-zero harmonics of net radiation are:

$$\forall k \in \mathbb{Z}^*, \quad \widetilde{R}_n(k\omega_0) = \underbrace{(1 - \alpha_s) \widetilde{S}_\downarrow(k\omega_0) + \widetilde{L}_\downarrow(k\omega_0)}_{\triangleq \widetilde{I}_\downarrow(k\omega_0)} - 4\varepsilon_s \sigma \bar{T}_{s_0}^3 \widetilde{T}_{s_0}(k\omega_0) \quad (3.3)$$

and the steady-state component is:

$$\bar{R}_n = \underbrace{(1 - \alpha_s) \bar{S}_\downarrow + \bar{L}_\downarrow}_{\triangleq \bar{I}_\downarrow} - \varepsilon_s \sigma \bar{T}_{s_0}^4. \quad (3.4)$$

These relations are necessary to impose energy balance at the land surface in the Fourier domain.

### 5.3.1. Steady-State Solution

In order to obtain the full Fourier series development of the solution, the steady-state solution needs to be obtained first. This is due to the fact that the non-zero harmonic governing the equations contain terms linearized around the steady-state conditions.

The steady-state profiles of turbulent flux of potential temperature and specific humidity are obtained by integrating (2.25) and (2.26) as:

$$\forall z \in (h, z_i) \quad \bar{\phi}_\theta(z) = A_1 (z - z_i) \quad (3.5)$$

$$\forall z \in (h, z_i) \quad \bar{\phi}_q(z) = B_1(z - z_i) \quad (3.6)$$

where  $A_1$  and  $B_1$  are coefficients of integration. They can be evaluated using (2.34) and (2.39) as:

$$A_1 = -\frac{\bar{T}_{s_0} - \bar{\theta}_h}{r_a^c(z_i - h)} \quad (3.7)$$

$$B_1 = -\beta \frac{q^*(\bar{T}_{s_0}) - \bar{q}_h}{r_a^c(z_i - h)}. \quad (3.8)$$

The profiles of potential temperature and specific humidity are given by equations (2.27) and (2.28). Using the boundary conditions (2.34) and (2.39), their solutions are:

$$\bar{\theta}(z) - \bar{\theta}_h = (\bar{T}_{s_0} - \bar{\theta}_h) \underbrace{\frac{1}{Ku_* r_a^c} \left[ \frac{z-h}{z_i-h} - \left( \frac{z_i-d}{z_i-h} \right) \ln \left( \frac{z-d}{h-d} \right) \right]}_{\triangleq \alpha(z)} \quad (3.9)$$

$$\bar{q}(z) - \bar{q}_h = (q^*(\bar{T}_{s_0}) - \bar{q}_h) \underbrace{\frac{\beta}{Ku_* r_a^c} \left[ \frac{z-h}{z_i-h} - \left( \frac{z_i-d}{z_i-h} \right) \ln \left( \frac{z-d}{h-d} \right) \right]}_{\triangleq \beta \alpha(z)}. \quad (3.10)$$

Here  $\alpha(z)$  is the nondimensional collection of terms characterizing solutions dependence on height.

The soil temperature steady-state governing relation has a boundary condition that requires vanishing soil heat flux at infinity. Therefore the steady-soil temperature has to be uniform throughout the soil profile and equals to:

$$\bar{T}(z) = T_{deep} = \bar{T}_{s_0} \quad (3.11)$$

where  $T_{deep}$  is the constant soil temperature at great depth.  $T_{deep} = \bar{T}_{s_0}$  can be obtained using the steady-state equation of the land-surface energy balance (3.4) in combination with (3.9) and (3.10).

Finally the steady-state surface energy balance at the land-surface becomes:

$$\bar{T}_\downarrow = \varepsilon_s \sigma \bar{T}_{s_0}^4 + \frac{\rho C_p}{r_a^c} \frac{1}{1-\alpha(z_1)} (\bar{T}_{s_0} - \bar{\theta}(z_1)) + \frac{\rho \lambda \beta}{r_a^c} \frac{1}{1-\beta\alpha(z_1)} (q^*(\bar{T}_{s_0}) - \bar{q}(z_1)), \quad (3.12)$$

evaluated at height  $z_1$  corresponding to the height of air temperature and humidity measurements. Note that because we are using the value of mean potential temperature at height  $z_1$  instead of height  $h$ , the aerodynamic resistance is increased by a factor  $1-\alpha(z_1)$ , to compensate for the change in elevation. Similarly for specific humidity the total resistance is increased by a factor  $1-\beta\alpha(z_1)$ .

### 5.3.2. Higher non-zero harmonics

The solution of (2.29) for each soil heat flux harmonic is:

$$\tilde{G}(n\omega_0, z) = g_0 e^{j\gamma} (n\omega_0) \exp\left((1+j)\sqrt{\frac{\omega_n}{2K_s}} z\right) \quad (3.13)$$

where  $g_0 e^{j\gamma} (n\omega_0)$  is the complex amplitude of the soil heat flux at the origin and  $g_0 \in \mathbb{R}^+$ . In the soil the conservation of heat (2.14) becomes:

$$j\omega_n C_s \tilde{T}_s(\omega_n, z) = \frac{\partial \tilde{G}}{\partial z}(\omega_n, z) \quad (3.14)$$

so that the soil temperature profile harmonics are:

$$\tilde{T}_s(\omega_n, z) = \frac{g_0 e^{j\gamma}(\omega_n)}{C_s} (1-j) \sqrt{\frac{1}{2\omega_n K_s}} \exp\left((1+j)\sqrt{\frac{\omega_n}{2K_s}} z\right). \quad (3.15)$$

In the ABL, the sensible heat flux is solved similarly but using the change of variables  $x = 2\sqrt{-\frac{j\omega_n(z-d)}{K_*}}$  and rewriting the fluxes as

$A(z, t) = \tilde{A}(\omega_n, z) e^{j\omega_n t} = a(\omega_n, x) e^{j\omega_n t}$ . On top of the ABL, the variable  $x$  becomes:

$x_i = 2\sqrt{-\frac{j\omega_n(z_i-d)}{K_*}} \approx 2\sqrt{-\frac{jnc}{2K \sin(\phi)}} \triangleq \sqrt{n}x_{i,0}$  and right above the canopy its value

$$\text{is: } x_h = 2\sqrt{-\frac{j\omega_n(h-d)}{K_*}}.$$

The turbulent flux amplitudes (potential temperature and specific humidity) at height  $h$  are written as complex amplitudes  $h_h e^{j\beta}$  with  $h_h \in \mathbb{R}^+$  and  $E_h e^{j\epsilon}$  with  $E_h \in \mathbb{R}^+$  are:

$$\tilde{\phi}_\theta(\omega_n, z) = h_h e^{j\beta}(\omega_n) \sqrt{\frac{z-d}{h-d}} \frac{H_1^1(x_i)H_1^2(x) - H_1^2(x_i)H_1^1(x)}{H_1^1(x_i)H_1^2(x_h) - H_1^2(x_i)H_1^1(x_h)} \quad (3.16)$$

$$\tilde{\phi}_q(\omega_n, z) = E_h e^{j\epsilon}(\omega_n) \sqrt{\frac{z-d}{h-d}} \frac{H_1^1(x_i)H_1^2(x) - H_1^2(x_i)H_1^1(x)}{H_1^1(x_i)H_1^2(x_h) - H_1^2(x_i)H_1^1(x_h)}. \quad (3.17)$$

The conservation of mean enthalpy and water mass in the atmosphere (2.7) and (2.8) can be rewritten with the use of temporal Fourier transform:

$$j\omega_n \tilde{\theta}(\omega_n, z) = -\frac{\partial \tilde{\phi}_\theta}{\partial z}(\omega_n, z) \quad (3.18)$$

$$j\omega_n \tilde{q}(\omega_n, z) = -\frac{\partial \tilde{q}}{\partial z}(\omega_n, z). \quad (3.19)$$

These conservation equations are used to determine the complex amplitudes of the profiles of potential temperature and specific humidity in the ABL:

$$\tilde{\theta}(\omega_n, z) = \frac{1+j}{\sqrt{2\omega_n Ku_*^0 (h-d)}} \frac{H_1^1(x_i)H_0^2(x) - H_1^2(x_i)H_0^1(x)}{H_1^1(x_i)H_1^2(x_h) - H_1^2(x_i)H_1^1(x_h)} h_h e^{j\beta}(\omega_n) \quad (3.20)$$

$$\tilde{q}(\omega_n, z) = \frac{1+j}{\sqrt{2\omega_n Ku_*^0 (h-d)}} \frac{H_1^1(x_i)H_0^2(x) - H_1^2(x_i)H_0^1(x)}{H_1^1(x_i)H_1^2(x_h) - H_1^2(x_i)H_1^1(x_h)} E_h e^{j\epsilon}(\omega_n). \quad (3.21)$$

The only unknowns that remain are the amplitudes of the surface flux terms.

They can be obtained using the land-surface boundary conditions.

#### 5.4. Land-Surface Variables

The two following variables are introduced to simplify the expressions of the surface temperatures and fluxes:

$$\Delta(\omega_n) = \frac{1}{C_s} (1-j) \sqrt{\frac{1}{2\omega_n K_s}} \quad (4.1)$$

$$\Sigma(\omega_n) = \frac{1+j}{\rho \sqrt{2K_* \omega_n} (h-d)} \frac{H_1^1(x_i) H_0^2(x_h) - H_1^2(x_i) H_0^1(x_h)}{H_1^1(x_i) H_1^2(x_h) - H_1^2(x_i) H_1^1(x_h)}. \quad (4.2)$$

The amplitude and phase spectra of surface fluxes are expressed as function of incoming net radiation spectrum. The complex amplitudes of soil heat flux  $G_0$ , turbulent transport of potential temperature  $\phi_\theta$  and specific humidity  $\phi_q$  are:

$$g_0 e^{j\gamma}(\omega_n) = \frac{1}{1 + 4\varepsilon_s \sigma \bar{T}_{s_0}^3 \Delta(\omega_n) + \rho \Delta(\omega_n) \left( \frac{C_p}{r_a^c + \rho \Sigma(\omega_n)} + \frac{\lambda \beta \gamma_{\bar{T}_{s_0}}}{r_a^c + \rho \beta \Sigma(\omega_n)} \right)} I_\downarrow e^{j\alpha}(\omega_n) \quad (4.3)$$

$$h_\theta e^{j\beta}(\omega_n) = \frac{\Delta(\omega_n)}{(r_a^c + \rho \Sigma(\omega_n)) \left\{ 1 + 4\varepsilon_s \sigma \bar{T}_{s_0}^3 \Delta(\omega_n) + \rho \Delta(\omega_n) \left( \frac{C_p}{r_a^c + \rho \Sigma(\omega_n)} + \frac{\lambda \beta \gamma_{\bar{T}_{s_0}}}{r_a^c + \rho \beta \Sigma(\omega_n)} \right) \right\}} I_\downarrow e^{j\alpha}(\omega_n) \quad (4.4)$$

$$E_h e^{j\epsilon}(\omega_n) = \frac{\beta \gamma_{\bar{T}_{s_0}} \Delta(\omega_n)}{(r_a^c + \rho \beta \Sigma(\omega_n)) \left\{ 1 + 4\varepsilon_s \sigma \bar{T}_{s_0}^3 \Delta(\omega_n) + \rho \Delta(\omega_n) \left( \frac{C_p}{r_a^c + \rho \Sigma(\omega_n)} + \frac{\lambda \beta \gamma_{\bar{T}_{s_0}}}{r_a^c + \rho \beta \Sigma(\omega_n)} \right) \right\}} I_\downarrow e^{j\alpha}(\omega_n) \quad (4.5)$$

where  $I_\downarrow(\omega_n)$  and  $\alpha(\omega_n)$  are respectively the amplitude and phase of incident

radiation at the land-surface at frequency  $\omega_n$ .

Similarly the complex amplitudes of the soil surface temperature, the potential temperature and the specific humidity, the latter two at height  $h$ , become:

$$\widetilde{T}_{surf}(\omega_n) = \frac{1}{1/\Delta(\omega_n) + 4\varepsilon_s \sigma \bar{T}_{s_0}^3 + \rho \left( \frac{C_p}{r_a^c + \rho \Sigma(\omega_n)} + \frac{\lambda \beta \gamma_{\bar{T}_{s_0}}}{r_a^c + \rho \beta \Sigma(\omega_n)} \right)} I_{\downarrow} e^{j\alpha}(\omega_n) \quad (4.6)$$

$$\widetilde{\theta}_h(\omega_n) = \frac{\rho \Sigma(\omega_n)}{(r_a^c + \rho \Sigma(\omega_n)) \left\{ 1/\Delta(\omega_n) + 4\varepsilon_s \sigma \bar{T}_{s_0}^3 + \rho \left( \frac{C_p}{r_a^c + \rho \Sigma(\omega_n)} + \frac{\lambda \beta \gamma_{\bar{T}_{s_0}}}{r_a^c + \rho \beta \Sigma(\omega_n)} \right) \right\}} I_{\downarrow} e^{j\alpha}(\omega_n) \quad (4.7)$$

$$\widetilde{q}_h(\omega_n) = \frac{\beta \gamma_{\bar{T}_{s_0}} \rho \Sigma(\omega_n)}{(r_a^c + \rho \beta \Sigma(\omega_n)) \left\{ 1/\Delta(\omega_n) + 4\varepsilon_s \sigma \bar{T}_{s_0}^3 + \rho \left( \frac{C_p}{r_a^c + \rho \Sigma(\omega_n)} + \frac{\lambda \beta \gamma_{\bar{T}_{s_0}}}{r_a^c + \rho \beta \Sigma(\omega_n)} \right) \right\}} I_{\downarrow} e^{j\alpha}(\omega_n) \quad (4.8)$$

These expressions allow the study of the harmonic response of the soil-vegetation-ABL continuum to any periodic forcing of incident radiation at the land-surface. Observations of this forcing from an intensive field experiment are used to characterize them in this study. They are shown in Figure 2. The observations also serve to provide partial tests of the model in capturing the diurnal dynamics of surface energy balance components.

### 5.5. Forcing and Test Dataset

The observational dataset corresponds to 101 days of measurements from the SUDMED 2002 field campaign in Marrakech, Morocco as described in *Duchemin et al.* [2006] and *Chehbouni et al.* [2008]. In this dataset, five continuous days of intensive measurements from March 1<sup>st</sup> to March 5<sup>th</sup> were selected because the flux measurements were free of gaps. Furthermore, the synoptic conditions over this five-day period were clear-skies fair weather with near-steady (calm) wind conditions. The study site is a wheat field with relatively sparse vegetation ( $LAI=0.4 \text{ m}^2 \text{ m}^{-2}$  and vegetation height of 40 cm).

The theoretical coupled land-surface and boundary-layer model developed in this study is forced with the incident radiation observed during the intensive experiment days (March 1<sup>st</sup> to March 5<sup>th</sup>). The model is assumed to be periodic over the five-day period  $T$ . The root-zone soil water content did not change appreciably during this period and the synoptic conditions were similar during the duration.

Continuous and long-duration records are required for statistical estimation of the amplitude and phase spectra based on experimental data. The entire 101 days of the SUDMED project do contain some gaps in measurements and missing data. A more extensive dataset on land-atmosphere exchange for this study is developed using a Soil Vegetation Atmosphere Transfer (SVAT) model that is calibrated using the extended 101-day period of the experiment over the wheat field site [*Gentine et al.* 2007]. The value of this gap-free and longer albeir



partially model-based data set is that spectral behavior of variables can be estimated, since measurements are gap free.

## 5.6. Results

As a partial test of the model presented here based on the five-day observation period, the surface energy balance components resulting from the application of the model to the period of the intense field campaign are compared with observations. The forcing is the series contained in Figure 2. Figure 3 shows the net radiation and surface ground heat flux comparisons between the model and observations. Figure 4 extends the comparison to the two turbulent heat fluxes. The simple linearized model effectively captures the diurnal course of the surface energy balance components in terms of relative partitioning and dynamic pattern.

Figure 5 shows that the linearized model is also able to represent well both soil surface temperature and potential temperature at the height of reference  $z_l = 2\text{m}$ . The diurnal course of the two temperatures is realistic and could be used as the lower boundary condition for the ABL domain.

In order to further evaluate the dynamical behaviors inherent in the model, we take some asymptotic limits of the analytical solutions in the following subsections. These correspond to extreme limits and should provide physical insights into the consistency of the model as well as its range.

### 5.6.1. Asymptotic behavior for large aerodynamic resistance

The case of very large canopy aerodynamic resistance, i.e.  $r_a^c \gg 1$ , is first

studied. It effectively represents the suppression of turbulent transfer of energy and water from the land-surface to the ABL. In this case the surface fluxes amplitudes (4.3), (4.4) and (4.5) asymptotically reach:

$$G_0 e^{j\gamma}(\omega_n) = \frac{1}{1 + 4\varepsilon_s \sigma \bar{T}_{s_0}^3 \Delta(\omega_n)} I_{\downarrow} e^{j\alpha}(\omega_n) \quad (6.1)$$

$$h_h e^{j\beta}(\omega_n) = E_h e^{j\varepsilon}(\omega_n) = 0 \quad (6.2)$$

for  $r_a^c \gg 1$ . These signify the disappearance of turbulent surface flux and the increased amplitude of the ground heat flux. Note that through the  $\Delta(\omega_n)$  term, there is still phase shift between the forcing and the ground heat flux response.

When the aerodynamic resistance tends to infinity, the land-surface state variable solutions (4.6) to (4.8) asymptote to:

$$\widetilde{T}_{surf}(\omega_n) = \frac{1}{1 / \Delta(\omega_n) + 4\varepsilon_s \sigma \bar{T}_{s_0}^3} I_{\downarrow} e^{j\alpha}(\omega_n) \quad (6.3)$$

$$\widetilde{\theta}_h(\omega_n) = \widetilde{q}_h(\omega_n) = 0. \quad (6.4)$$

It is interesting to find that the land-surface temperature still exhibits a T-periodic cycle influenced by longwave radiation and soil characteristics alone, thus introducing a phase lag in the response to incoming radiation forcing. The near-surface ABL potential temperature and specific humidity, however, have only the steady-state component. Thus when the aerodynamic resistance becomes very large, there is total decoupling between aerodynamic temperature and land-surface temperature. More precisely, when the aerodynamic resistance is large there is decoupling between the soil and atmosphere systems, except for the radiative transfer component and the land surface has no control on the ABL

profiles.

### 5.6.2. Surface layer behavior

The analytical solutions of turbulent flux, potential temperature, and specific humidity profiles can be expanded in series form for small values of  $z-d$ . This also represents the asymptotic behavior in the lower part of the surface layer, i.e. in the lower part of the ABL close to the surface, where the gradients in stress and turbulent fluxes are negligible. In the surface layer the gradients in potential temperature and specific moisture are, however, important and influential.

The series expansion of the sensible heat flux and potential temperature near the surface gives:

$$\begin{aligned}
\tilde{\phi}_o(\omega, z) = & \frac{(-1+j)}{\pi} \sqrt{\frac{K_*}{2\omega_n(h-d)}} \frac{H_1^1(x_i) + H_1^2(x_i)}{H_1^1(x_i)H_1^2(x_f) - H_1^2(x_i)H_1^1(x_h)} \\
& + \frac{(1-j)}{\pi} \sqrt{\frac{\omega_n}{K_*(h-d)}} \frac{1}{H_1^1(x_i)H_1^2(x_f) - H_1^2(x_i)H_1^1(x_h)} (z-d) \\
& \times \left\{ H_1^1(x_i) \left[ \pi - j \ln \left( -\frac{j\omega_n(z-d)}{K_*} \right) + j(1-2\gamma) \right] + H_1^2(x_i) \left[ -\pi - j \ln \left( -\frac{j\omega_n(z-d)}{K_*} \right) + j(1-2\gamma) \right] \right\} \\
& + O((z-d)^2)
\end{aligned} \tag{6.5}$$

and

$$\begin{aligned}
\tilde{\theta}(\omega, z) = & \frac{(1+j)}{\pi} \frac{1}{H_1^1(x_i)H_1^2(x_f) - H_1^2(x_i)H_1^1(x_h)} \\
& \times \left\{ H_1^1(x_i) [\pi - 2j\gamma] + H_1^2(x_i) [-\pi - 2j\gamma] - j(H_1^1(x_i) + H_1^2(x_i)) \ln \left( -\frac{j\omega_n(z-d)}{K_*} \right) \right\} \\
& \times \left\{ \frac{1}{\sqrt{2K_*\omega_n(h-d)}} + \sqrt{\frac{\omega_n}{2K_*^3(h-d)}} (z-d) \right\} \\
& + O((z-d)^2)
\end{aligned} \tag{6.6}$$

These expansions show that sensible heat flux is indeed slowly varying in the surface layer and is close to constant in the near-surface layer, which is given by

the first term on the right-hand-side of (6.5). The variations of sensible heat flux remain small i.e.  $\left| \frac{H(z) - H_h}{H_h} \right| \ll 1$ , even at heights on the order of tens of meters above the surface. This series expansion also shows that in the near-surface layer, the potential temperature amplitude is described by a logarithmic  $(z-d)\ln(z-d)$  profile and thus amplitude changes rapidly with height compared to that of sensible heat flux. Given the similarities in the sensible and latent heat flux solutions, as well the correspondence between the potential temperature and specific humidity profiles, similar conclusions hold for latent heat flux and specific moisture logarithmic height dependency.

### 5.6.3. Responses as a function of frequency

We begin examining the responses as a function of frequency by first considering the extreme limits. For very low values of frequency, i.e.  $\omega \rightarrow 0$  or slowly-varying components just above the steady-state, the amplitude of potential temperature tends toward infinity and for very large frequency, i.e.  $\omega \rightarrow +\infty$  or fast-changing components, the potential temperature complex amplitude tends to 0. This means that high frequency forcing impacts the temperature profile of the ABL to a limited degree and tends to remain confined to a very shallow layer near the surface. We refer to high frequency forcing in incident radiation as weather noise and it can be induced by passing clouds or effectively wind variability. Thus the ABL potential temperature is really responding to lower frequency factors and mostly immune to weather noise. The

boundary-layer profile is therefore mostly an indicator of slowly daily varying forcing at the surface but it cannot capture high frequency forcing. This result, or more specifically the result in between these two extreme limits, can be important guides for the sampling and interpretation of measurements. The low frequencies part of the ABL potential temperature and specific humidity spectra are mostly due to surface incoming radiation whereas higher frequency spectra will be mostly influenced by advection at regional scale. This interpretation echoes *Claussen* [1995]: “Far above the blending height, modifications of air flow owing to changes in surface conditions will not be recognizable individually, but an overall stress or heat flux profile will exist, representing the surface conditions of a large area”. When  $\omega \rightarrow 0$ , the profile of potential temperature is linear and corresponds to the steady state solution:  $\frac{z-z_i}{z-h} h_h e^{j\beta}$ .

We now turn to the behavior away from these extreme limits. First we introduce the penetration depth that is defined as the characteristic length scale of a wave penetration. It corresponds to the depth at which the wave is attenuated by an exponential factor. The penetration depths are part of the profiles solutions as evident in the complex exponential dependencies in (3.13) to (3.21). Examination of the penetration depth for the state variables and the fluxes as a function of frequency provides valuable and new insights into the relative roles of each component of the soil-vegetation-ABL continuum as they adjust to the complex spectrum of radiative forcing. The penetration depth at each frequency is accompanied by phase spectra indicating, lag-lead behavior. As

a length scale the penetration depths are normalized by the ABL height so that it is dimensionless in the presentations.

Figure 6 shows the normalized penetration depth for a) potential temperature and specific humidity and b) sensible and latent heat flux as a function of the forcing frequency. Sensible heat flux and latent heat flux change only very slightly in the lower tens of meters of the boundary-layer whereas the specific humidity and potential temperature exhibit sharp gradients. These behaviors are characteristic identifiers of the development of a surface layer linking the near-surface (right above canopy) air and the ABL. It is actually the very definition of the surface layer. Then above a few tens of meters away from the land-surface, the potential temperature and specific humidity profiles reach values converging and very close to their upper boundary value. Consequently, in a near-neutral case, the gradient of both potential temperature and specific humidity are mostly located in a layer of a few tens of meters above the land-surface. This is consistent with both experimental and numerical results [see *Stull* 1988 and *Garratt* 1992 for a review]. Above this surface layer the gradients of both quantities become negligible. On the other hand, the gradients of sensible and latent heat flux are small in the surface layer, i.e. in the first few ten meters over the land surface the fluxes can be considered to remain constant. Above the surface layer and reaching to the upper parts of the ABL the fluxes smoothly decrease with height until they reach zero at the exact height of the ABL. Indeed, larger scale eddies tend to propagate further from the surface

(corresponding to an increased eddy-diffusivity) and mix the passive scalars. Therefore far away from the surface, there are still considerable magnitudes of heat fluxes associated with very small passive scalar gradients. It is important to note that a simple eddy diffusion parameterization is adequate to capture these characteristic profiles of potential temperature and sensible heat flux. Nonetheless more sophisticated and physically-consistent parameterizations of turbulent heat transfer coefficient need to replace K-theory based approach adopted in this study.

#### 5.6.4. Responses as a function of parameters

The key parameters of the model that affect surface energy balance as well as the profiles of states and flux in the soil and the ABL are: 1) water availability control  $\beta$ , 2) aerodynamic resistance  $r_a^c$ , 3) vegetation height  $h$ , and 4) friction velocity  $u_*$ . Figure 7 shows the dependency of the penetration depth for potential temperature or specific humidity on these four parameters. The flux penetration depth is not shown and it is constant for the parameters.

It is evident that  $\beta$  does not influence the penetration depth of the scalar wave since it only scales the input of heat flux at the land surface. It does not impact the way fluxes and scalars vary in the ABL. Similar results hold for the canopy aerodynamic resistance that will equally influence the magnitude of the sensible and latent heat flux at the land surface. This in turn determines how temperature and specific humidity will transport from the surface into the overlying atmosphere. However aerodynamic resistance is a quantity closely

related to the surface friction velocity. The magnitude of the resistance is largely due to shear stress at the surface.

Figure 7 also shows that vegetation height has a very different impact on turbulent fluxes than on specific humidity and potential temperature. An increasing vegetation height acts as a change in the height of the source of potential temperature and specific moisture, the penetration depth is thus changed. The penetration depth is taken from the soil surface with abscissa  $z=0$ , which is now displaced. There is however no fundamental physical changes as long as the other surface parameters remain constant. It is also interesting to note that a change in vegetation height has almost no influence on both the latent and sensible heat flux penetration depths. The penetration depth scale of the fluxes is two or three order of magnitude larger than vegetation height. A displacement of the source of sensible or latent heat flux of a few meters will not appreciably affect the profile. Consequently a change of vegetation height, with all other surface parameters remaining constant, has negligible impact on the profile of turbulent fluxes but strongly affects the profiles of both potential temperature and specific humidity. It will displace the potential temperature and specific humidity profiles by a distance equals to the change of the vegetation height and comparable to the surface layer.

Friction velocity plays a strong influence on the propagation of humidity and latent heat flux waves. Indeed even though the ratio  $\lambda_{H,AE} / z_i$  remains constant, the ABL height  $z_i$  is a strongly increasing function of friction velocity.



The propagation depth of latent heat flux will consequently increase with friction velocity.

Finally, friction velocity is shown to have the strongest influence on all near-neutral penetration depths since the surface shear stress drives the profile of wind speed and turbulence. It consequently influences all passive scalars of the fluid be it enthalpy or water content. In a near-neutral atmosphere, the stronger the shear stress at the surface, i.e. the stronger the forced convection at the land-surface, the larger the penetration depth for any atmospheric variable or flux.

#### 5.6.5. Gain and phase amplitudes

The state and flux profiles in the soil-vegetation-ABL continuum are all forced by incident radiation (and friction velocity) at the surface. Incident radiation has a spectrum and all other system variables have amplitude whose value relative to the radiative forcing is the gain spectrum. The corresponding phase spectra indicate the lag-lead relationships at the same frequencies. Figure 8 presents the gain spectra of the surface fluxes. The first panel shows a strong dependency of all surface fluxes to the frequency of incoming radiation. In particular the amplitude of the soil heat flux is rapidly decreasing with period. After the period reaches one hour, it then remains fairly constant for lower frequencies. On the other hand, the amplitude of both latent and sensible heat flux is slowly increasing and their relative magnitude is determined by the value of  $\beta$ , which has been fixed at 0.6 in this study.

Several insights may be gained from this result. First, the soil heat flux captures a large fraction of the high frequency (low period) forcing, therefore soil heat flux will be sensitive to rapid changes in incident radiation. Relative to the turbulent fluxes, soil heat flux is compensating for weather noise. The diurnal shape of the soil heat flux appears noisy because it captures any rapid variations in forcing. Turbulent fluxes behave differently: sensible heat flux displays a relatively flat gain spectrum for all forcing frequencies. Therefore it will not amplify any particular frequency and high frequencies will have the same influence as low frequencies. In our slightly water-limited case, latent heat flux behaves slightly differently: the response to low frequencies (high period) is slightly stronger than to high frequencies and this explains the relatively smooth diurnal shape of surface evaporation compared to sensible heat flux in wet conditions.

### 5.7. Evaporative Fraction spectral behavior

Whereas sensible and latent heat have strong periodicities originating in their direct dependence on the periodic radiative forcing, the Evaporation Fraction,  $EF$ , diagnostic has less direct dependence on radiative forcing and hence may exhibit less pronounced periodicity. The spectrum of  $EF$  is now investigated using the framework introduced in this study.

Contrary to latent and sensible heat flux, there is no simple relationship between each harmonic of  $EF$  and their counterpart in the forcing of incident

radiation. Since  $EF$  is a fraction defined through (1.1), i.e.  $EF(t) = \frac{\lambda E_h(t)}{H_h(t) + \lambda E_h(t)}$

or  $EF(t)(H_h(t) + \lambda E_h(t)) = \lambda E_h(t)$ , its spectral solution involves a convolution in the frequency domain:

$$\widetilde{EF}(\omega) * (\widetilde{H}_h(\omega) + \lambda \widetilde{E}_h(\omega)) = \lambda \widetilde{E}_h(\omega) \quad (7.1)$$

equivalent to:

$$\sum_{m=-\infty}^{+\infty} [\widetilde{H}_h((n-m)\omega_0) + \lambda \widetilde{E}_h((n-m)\omega_0)] \widetilde{EF}(m\omega_0) = \lambda \widetilde{E}_h(n\omega_0). \quad (7.2)$$

The fractions:  $\frac{\widetilde{H}_h(\omega)}{\widetilde{I}_\downarrow(\omega)}$  and  $\frac{\lambda \widetilde{E}_h(\omega)}{\widetilde{I}_\downarrow(\omega)}$  are known from (4.4) and (4.5). Therefore the

Fourier transform of incoming radiation is required to determine the spectrum of  $EF$ . Because of the non linearity, the spectrum of both sensible and latent heat flux will impact and diffuse across the whole spectrum of  $EF$  because it results in a convolution in the spectral domain. The power spectrum of  $EF$  will consequently necessarily be much broader than that of sensible and latent heat flux.

To investigate the  $EF$  spectrum and compare its shape to the spectra of surface fluxes ( $R_n$ ,  $H_h$  and  $\lambda E_h$ ) we introduce the daytime energy spectrum for each variable. The daytime energy spectrum is the average, over 101 days, of the daytime-only Fourier decomposition of the variable for each day. It is introduced in lieu of multi-day time-series Fourier transform because the full series contain discontinuities at dawn and dusk and the nighttime values should not be mixed with daytime values.

In order to obtain comparable values for any variable of interest, the energy spectrum is normalized by its total spectral power or integral across frequencies. The square root of the normalized energy spectrum is shown in Figure 9 for observed a) net radiation b) evaporative fraction c) sensible and d) latent heat flux at the land surface during daytime. These energy spectra show that most of the daytime energy spectrum of net radiation and turbulent fluxes is located at high periods (low frequencies). Therefore the major part of the diurnal cycle of surface fluxes is explained by these low diurnal frequency harmonics components. Consequently most of the diurnal spectrum of the surface energy fluxes is due to the influence of the main solar radiation harmonic, which has a (nearly) semi-day period. On the other hand, evaporative fraction displays a relatively flat energy spectrum, which again emphasizes the implications of nonlinearities: the relatively localized spectrum of  $H_h$  and  $\lambda E_h$  evenly influence the whole  $EF$  energy spectrum.

### 5.8. $EF$ asymptotes

More insights into the diurnal shape of  $EF$  may be gained by writing the limiting expressions for  $EF$  and examining the amplitude spectra of its fundamental constitutive elements. Evaporative fraction can be rewritten as:

$$EF = \frac{1}{1 + \frac{C_p}{\lambda\beta} \frac{T_{s_0} - \theta_h}{q^*(T_{s_0}) - q_h}} \quad (7.3)$$

using its definition and expressions for the turbulent fluxes, (2.17) and (2.18).

This expression shows that  $EF$  mostly removes the effects of turbulence and

isolates surface controls, as stated in *Gentine et al.* [2007].  $EF$  is a function of soil water availability through  $\beta$ , surface temperature deficit  $T_{s_0} - \theta_h$  and water vapor deficit  $q^*(T_{s_0}) - q_h$ .  $EF$  is consequently a complex function of water availability, near surface temperature and humidity conditions. It can be related to the surface resistance to evaporation only if the surface temperature and the near surface meteorological state are known. More concisely the  $EF$ -soil moisture control relationship is mediated through micrometeorology.

The diurnal shape of  $EF$  can be diagnosed using (7.3). The surface temperature and water vapor deficits, resp.  $T_{s_0} - \theta_h$  and  $q^*(T_{s_0}) - q_h$ , can be characterized with our linearized land-atmosphere model using (4.6), (4.7) and (4.8). Figure 10 (a) and (b) show that the temperature and water vapor deficit at the land surface respond similarly to a forcing of incoming radiation at the land surface. Moreover, except for their mean components, the ratio of their amplitude remains relatively constant over the whole spectrum as presented on Figure 10 (c). The differences  $T_{s_0} - \theta_h$  and  $q^*(T_{s_0}) - q_h$  are in phase, which explains why their harmonic behavior is almost identical. Finally the evaporative fraction can be rewritten using the harmonic decomposition of the temperature deficit at the surface:

$$T_{s_0} - \theta_h = \delta T_0 + \sum_{\substack{n=-\infty \\ n \neq 0}}^{+\infty} \delta T_n \cos(n\omega_0 t + \varphi_n) \triangleq \delta T_0 + \delta T(t) \quad (7.4)$$

and the water vapor deficit at the land surface can be rewritten using the Taylor expansion to the first order:

$$q^*(T_{s_0}) - q_h = \delta q_0 + \sum_{\substack{n=-\infty \\ n \neq 0}}^{+\infty} \delta q_n \cos(n\omega_0 t + \varphi_n) \approx \delta q_0 + \delta q_1 \sum_{\substack{n=-\infty \\ n \neq 0}}^{+\infty} \delta T_n \cos(n\omega_0 t + \varphi_n). \quad (7.5)$$

Yet  $\delta q_0$  represents the mean steady-state specific humidity influenced by large-scale weather systems, whereas the harmonic variations are mostly due to changes influenced by the surface, acting as a source of moisture through the release of moisture at the land-surface. Thus regarding the proportional harmonic response of the temperature and humidity deficit to a very good approximation:

$$q^*(T_{s_0}) - q_h \approx \delta q_0 + \gamma_{\bar{T}_{s_0}} \sum_{\substack{n=-\infty \\ n \neq 0}}^{+\infty} \delta T_n \cos(n\omega_0 t + \varphi_n) \quad (7.6)$$

where  $\gamma_{\bar{T}_{s_0}}$  is the slope of the saturation specific humidity at temperature  $T_{s_0}$ .

Then  $EF$  becomes:

$$EF \approx \frac{1}{\delta T_0 + \sum_{\substack{n=-\infty \\ n \neq 0}}^{+\infty} \delta T_n \cos(n\omega_0 t + \varphi_n)} = \frac{1}{1 + \frac{C_p}{\lambda\beta} \frac{\delta T_0 + \delta T(t)}{\delta q_0 + \gamma_{\bar{T}_{s_0}} \delta T(t)}}. \quad (7.7)$$

$$1 + \frac{C_p}{\lambda\beta} \frac{\delta T_0 + \delta T(t)}{\delta q_0 + \gamma_{\bar{T}_{s_0}} \sum_{\substack{n=-\infty \\ n \neq 0}}^{+\infty} \delta T_n \cos(n\omega_0 t + \varphi_n)}$$

When  $|\delta T(t)| \gg \max(|\delta T_0|, |\delta q_0| / \gamma_{\bar{T}_{s_0}})$ ,  $EF$  tends to:

$$EF_{min} = \frac{1}{1 + \frac{1}{\gamma_{\bar{T}_{s_0}}} \frac{C_p}{\lambda\beta}}. \quad (7.8)$$

This condition is approached around solar noon in the SUDMED data as shown in Figure 11. Indeed at noon the principal daily harmonic of temperature difference reaches its maximum value and the temperature deficit  $\delta T(t)$  becomes large compared to the other parameters. Thus  $EF$  reaches its asymptotical minimum value. Moreover in our field experiment dataset, the surface and air temperatures above the canopy are equal at 7AM and 4.15PM, at these times  $EF$

equals 1. Before 7AM and after 4.15PM,  $T_{s_0} - \theta_h$  is negative while  $q^*(T_{s_0}) - q_h$  remains always positive, therefore  $EF$  is larger than 1. Then for very negative surface temperature differences, the evaporative fraction will become negative, this behavior is generally observed at night, when the radiative cooling of the surface will lower the surface temperature compared to the air temperature, leading at some point to a negative value of  $EF$ . The single diurnal harmonic of incident radiation forcing is broadened in frequency and results in the characteristics diurnal shape of  $EF$  as shown in Figure 11.

Therefore in fair-weather conditions with strong solar radiative forcing, such as in semi-arid regions,  $EF$  approaches its asymptotic value  $EF_{min}$  during most of the day. The water vapor pressure deficit also plays a strong role on  $EF$ : in humid regions evaporation is not limited by the surface soil and vegetation. Instead it is limited by atmospheric aridity and available energy. The limiting condition defined for  $EF$  cannot be reached in humid regions.

The power spectrum of incident radiation has a fundamental impact on the  $EF$  spectrum and on its diurnal behavior. Indeed any high order harmonic of incident radiation will strongly influence  $EF$ . In the SUDMED dataset used in this study, the main harmonic actually corresponds to the principal daily harmonic. The second daily harmonic also reaches its maximum around noon and contributes to the asymptotic behavior of  $EF$  at that time. The effect of the other harmonics on  $EF$  is negligible. This behavior is due to the fact that the influence of the first daily harmonic is almost sufficient to explain the diurnal

shape of  $EF$ . However, any noticeable changes in the power spectrum of solar incoming radiation, such as those induced by clouds, will strongly influence the diurnal shape of  $EF$ .

The use of the diurnal constant  $EF$  assumption will only hold under very restrictive conditions: fair, relatively dry weather and with elevated incoming radiation.

Finally we recognize that the present interpretations remain valid for near-neutral turbulent conditions where the eddy-diffusion coefficients  $K_{H,V}$  for heat and water vapor are similar. Highly unstable ABL conditions lead to departures from similarity for potential temperature and specific humidity transport. Potential temperature is no longer a passive tracer but actively induces turbulence through buoyancy.

## 5.9. Conclusions

This study uses the general framework originally introduced by *Lettau* [1951] and extended by *Gentine et al.* [2009] to model the soil-atmosphere continuum as one system subject to periodic incoming radiation forcing at the land surface. We extend the framework in several important new directions and apply it to understand the harmonic response of the land surface to periodic radiative forcing. An analytical solution of the problem is found for any forcing of incident radiation at the land surface. In particular, the land-surface fluxes and temperatures are expressed as function of the surface parameters and are used to investigate the role of land-surface parameters on the atmospheric profiles and on



surface variables.

First asymptotic expressions of turbulent fluxes, specific humidity and potential temperature are found, describing the variations of the respective profile in the few first meters above the canopy height. Among the surface parameters,  $\beta$  and  $r_a^c$  are shown not to modify the profiles but only to scale the magnitude of the surface turbulent heat fluxes. The surface friction velocity, however, influences the whole profile and not only the surface fluxes. Finally, a change in vegetation height acts as a change in elevation of the source of temperature and humidity and is shown to have very minor influence on the profiles of turbulent fluxes but strongly affects the specific humidity and potential temperature profiles.

Secondly the impact of the frequency of the incoming radiation forcing is investigated. At the land surface, soil heat flux absorbs most of the high-frequency component of the incoming radiation forcing and is thus considerably influenced by weather noise. The turbulent fluxes act at all frequencies with preponderance in the lower frequencies. Since the incoming radiation spectrum is mainly composed of the principal daily harmonic, the spectra of the turbulent heat fluxes is mostly responding to this daily cycle. In contrast, Evaporative Fraction possesses a broad spectrum with no clear diurnal harmonic. This is because it is fundamentally a convolution of periodic signals.

Even though the spectral study of  $EF$  is rendered difficult by its non-linear dependence on surface heat fluxes, the study of the near-surface temperature and

specific humidity spectra allows derivation of the asymptotical minimum diurnal value of  $EF$  as a function of key land-surface parameters. In addition,  $EF$  is demonstrated to remain a diurnal constant only under limiting meteorological conditions: fair and dry weather accompanied by strong solar radiation.

The present study, which develops new insight on the Evaporative Fraction diurnal behavior, has several shortcomings that should be addressed in future studies. First, there is no direct inclusion of stability/instability effects in the ABL and the modeling of turbulence through an eddy diffusion approach is limited to relatively specific conditions. Moreover the ABL height was assumed to be constant; yet it clearly exhibits a strong daily cycle, which should be taken into account to correctly model the near-surface scalar and fluxes values. Introducing these complexities will prohibit analytical solution, which was preferred in this first study.

## List of Figures

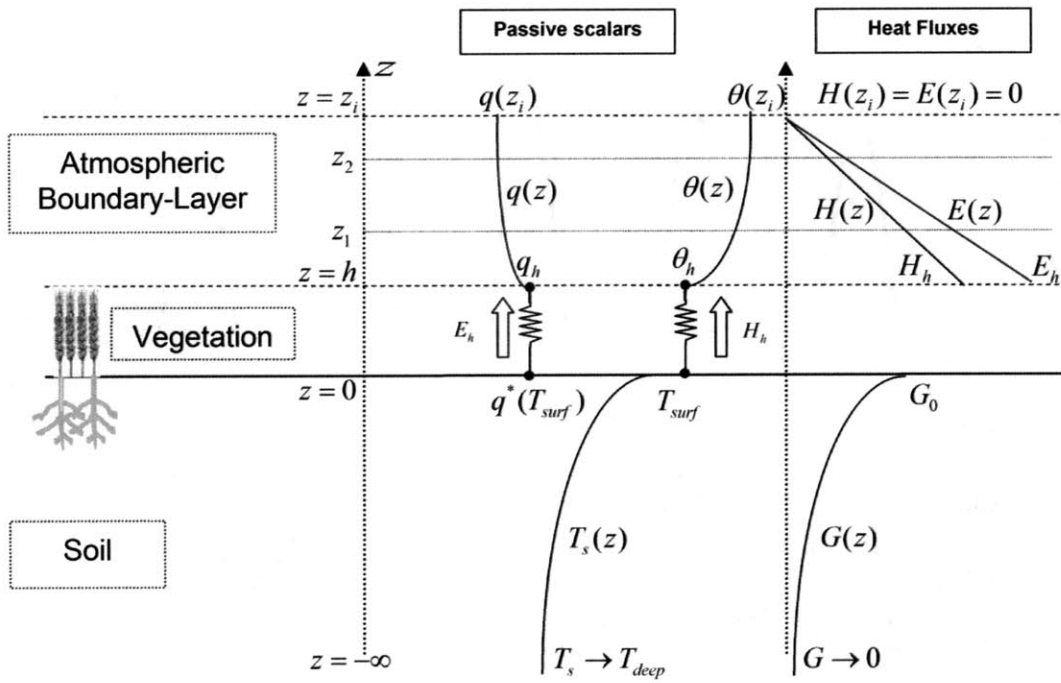


Figure 1. Representation of the soil-vegetation-atmospheric boundary layer continuum for states and fluxes in the coupled land-atmosphere.

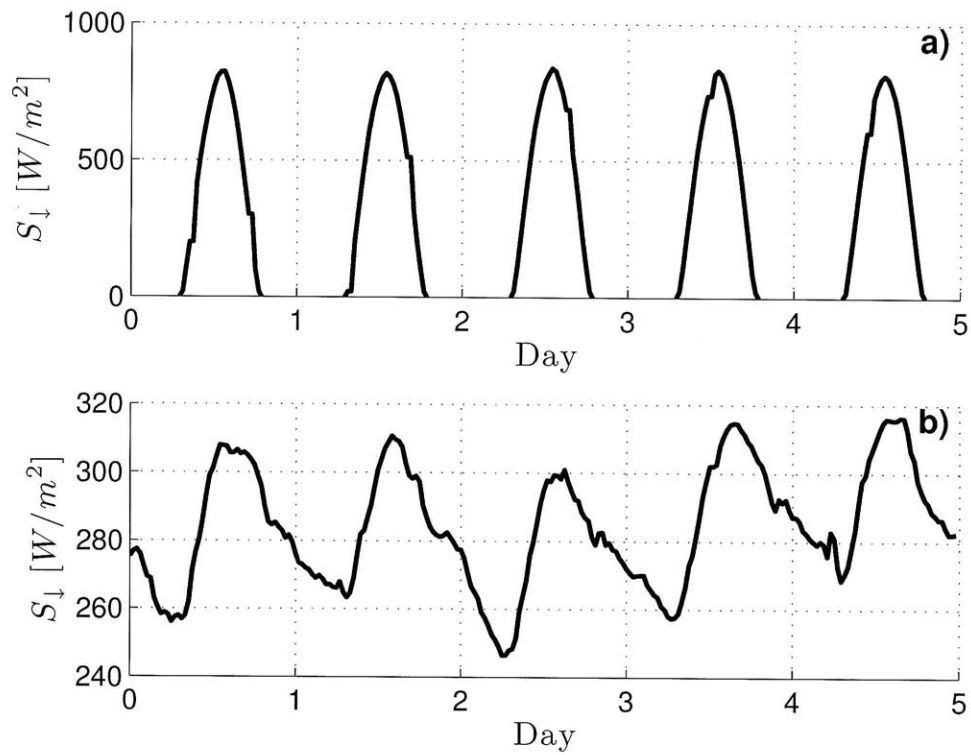
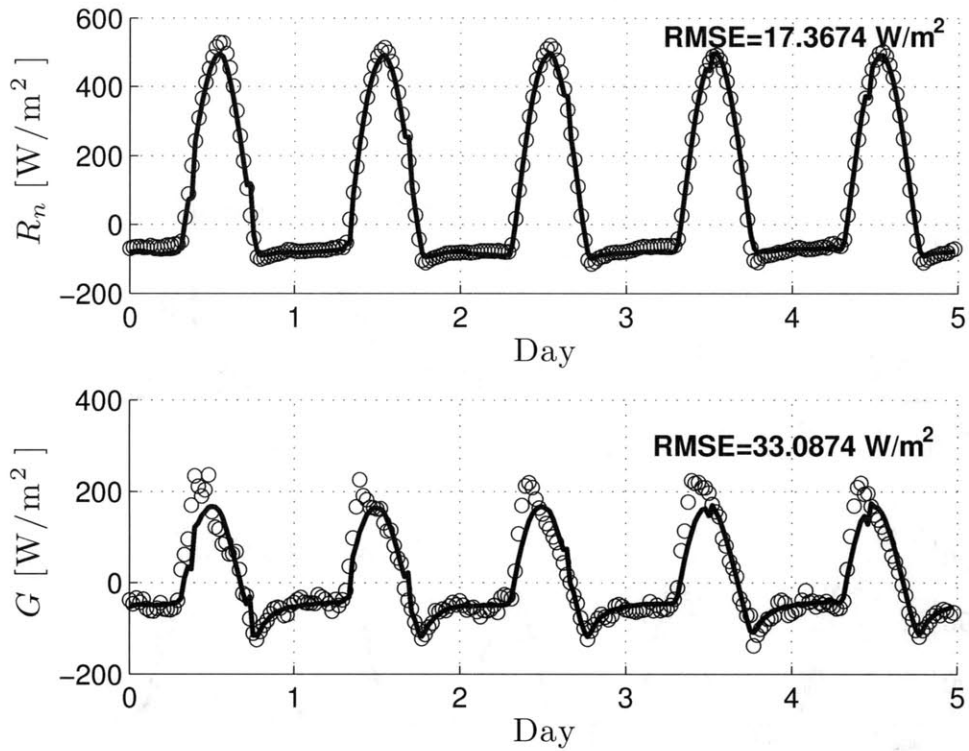


Figure 2. Sample forcing of shortwave incoming radiation (a) and longwave radiation (b) at the land surface, from in-situ measurements spanning March 1<sup>st</sup> to March 6<sup>th</sup> 2003. from the total SUDMED experiment covered 101 days and was located nearby Marrakech, Morocco.



**Figure 3.** Comparison of net radiation (top panel) and soil heat flux at the surface (bottom panel) for in-situ measurements (circles) and the model in this study (lines) from March 1<sup>st</sup> to March 6<sup>th</sup> 2003, using reference values of surface parameters as shown in appendix.

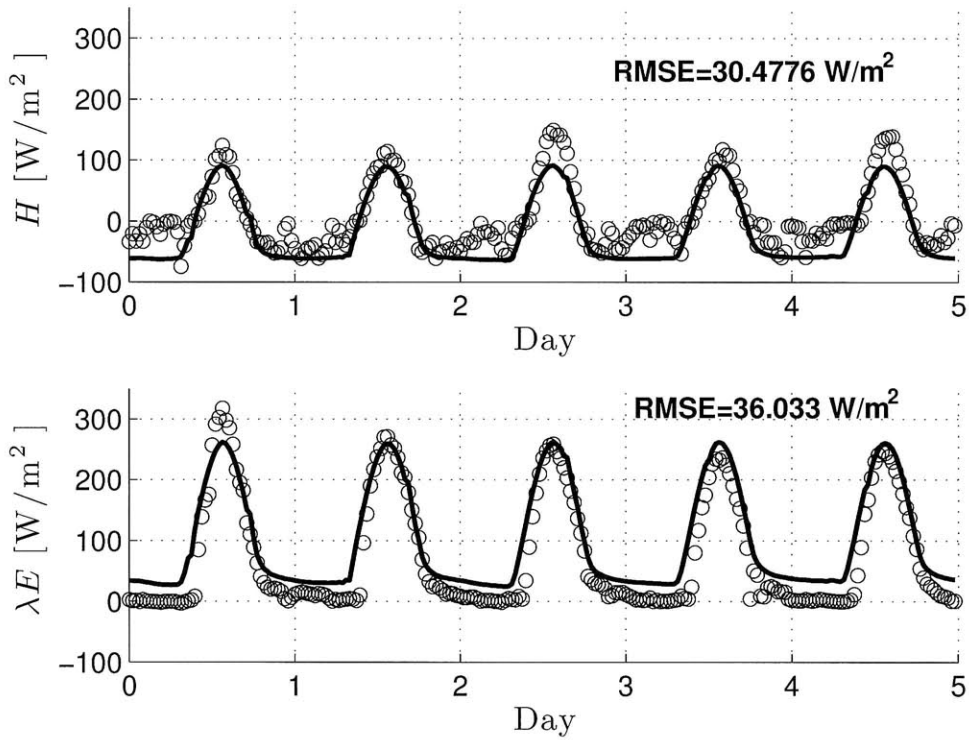
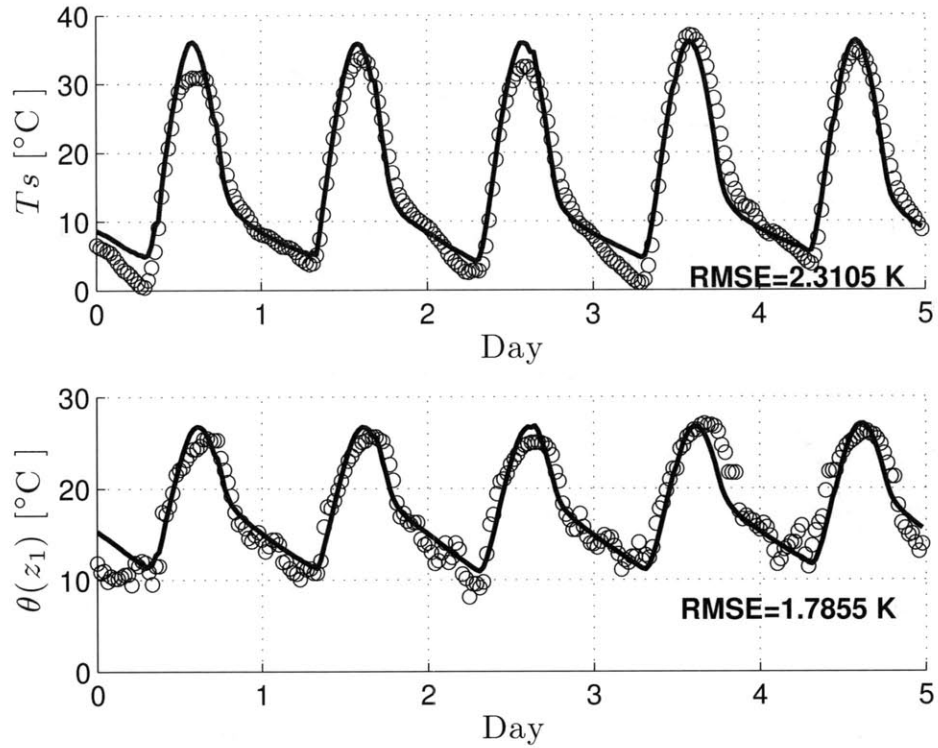
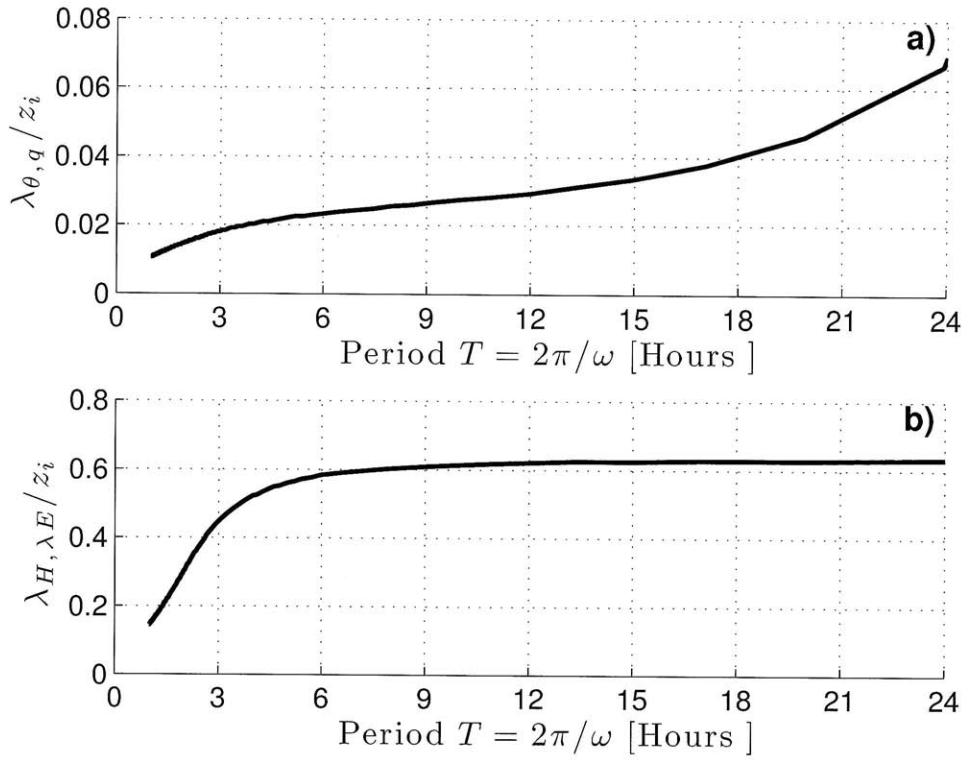


Figure 4. Comparison of sensible heat flux (top panel) and latent heat flux at the surface (bottom panel) for in-situ measurements (circles) and the model in this study (lines) from March 1<sup>st</sup> to March 6<sup>th</sup> 2003, using reference values of surface parameters as shown in appendix.



**Figure 5.** Comparison of land surface temperature (top panel) and air potential temperature at 2m (bottom panel) for in-situ measurements (circles) and the model in this study (lines) from March 1<sup>st</sup> to March 6<sup>th</sup> 2003, using reference values of surface parameters as shown in appendix.



**Figure 6.** Penetration depth of potential temperature and specific humidity (a) and sensible and latent heat flux (b) as a function of the period of incident radiative forcing.



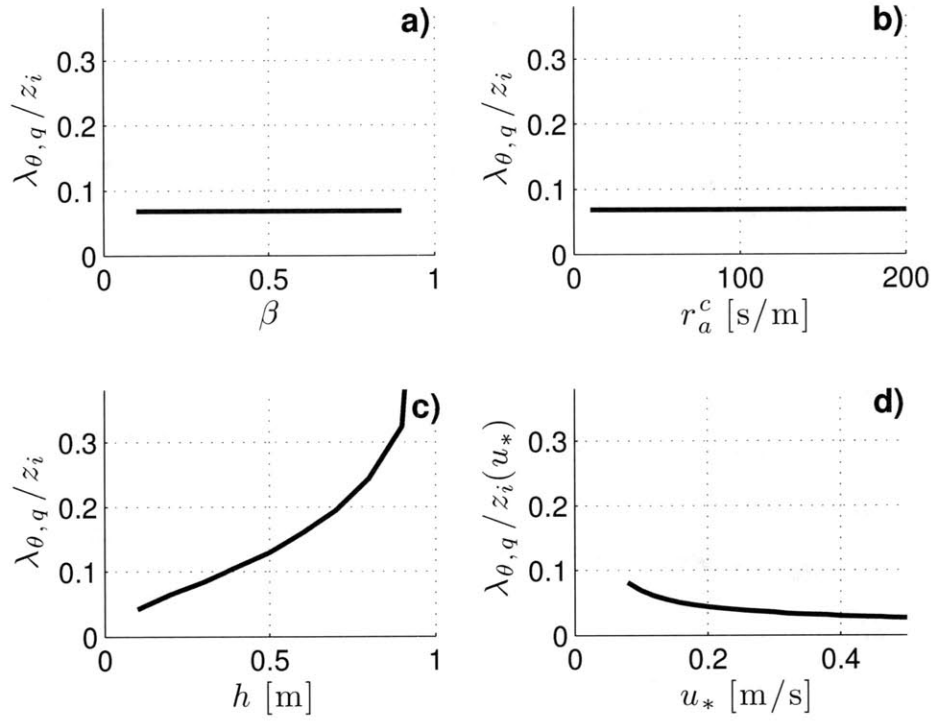


**Figure 7.** Influence of surface parameters on the penetration depth of potential temperature or specific humidity for a change in a) evaporation reduction factor  $\beta$ , b) aerodynamic canopy resistance  $r_a^c$ , c) vegetation height  $h$ , d) friction velocity at the surface  $u_*$ .

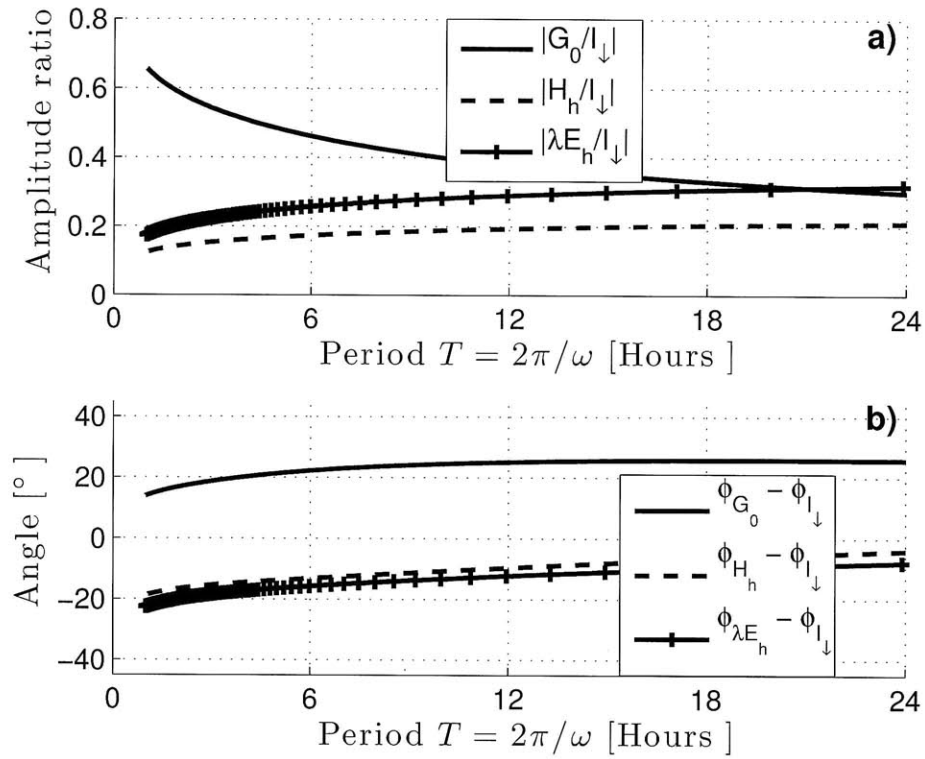


**Figure 8.** The frequency dependence of the gain and phase spectra of surface heat fluxes.

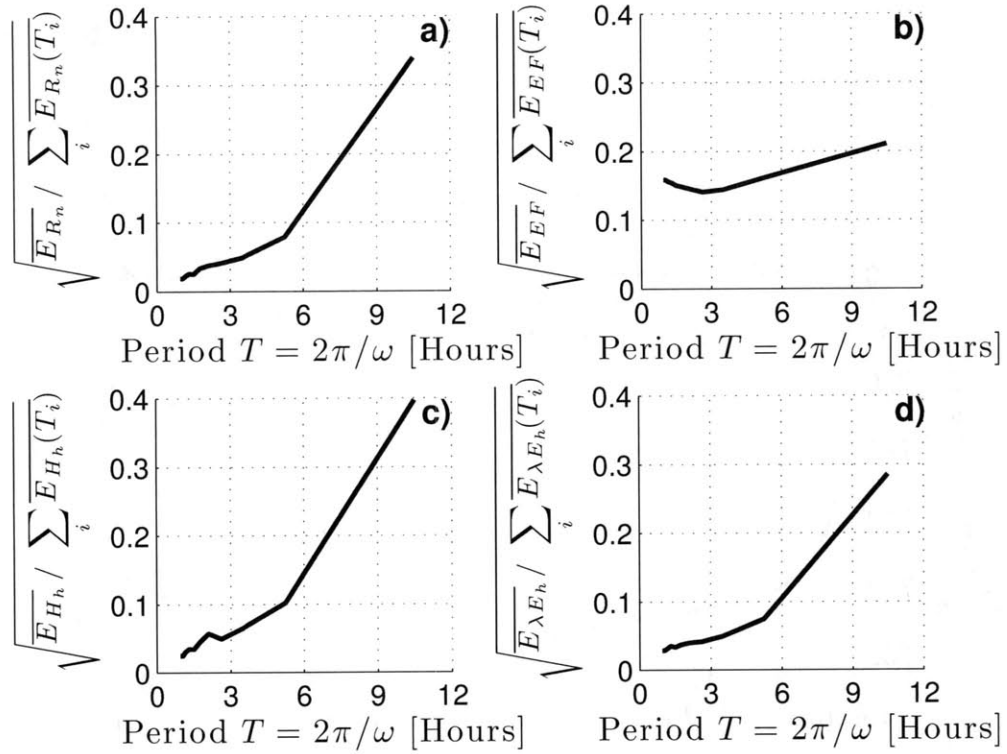


**Figure 9.** Square root of the normalized energy spectrum (squared amplitude of the harmonics) for day-time a) net radiation, b) Evaporative Fraction c) sensible heat flux and d) latent heat flux using flux measurements averaged over the 101-day extensive period, except for days with missing measurement.

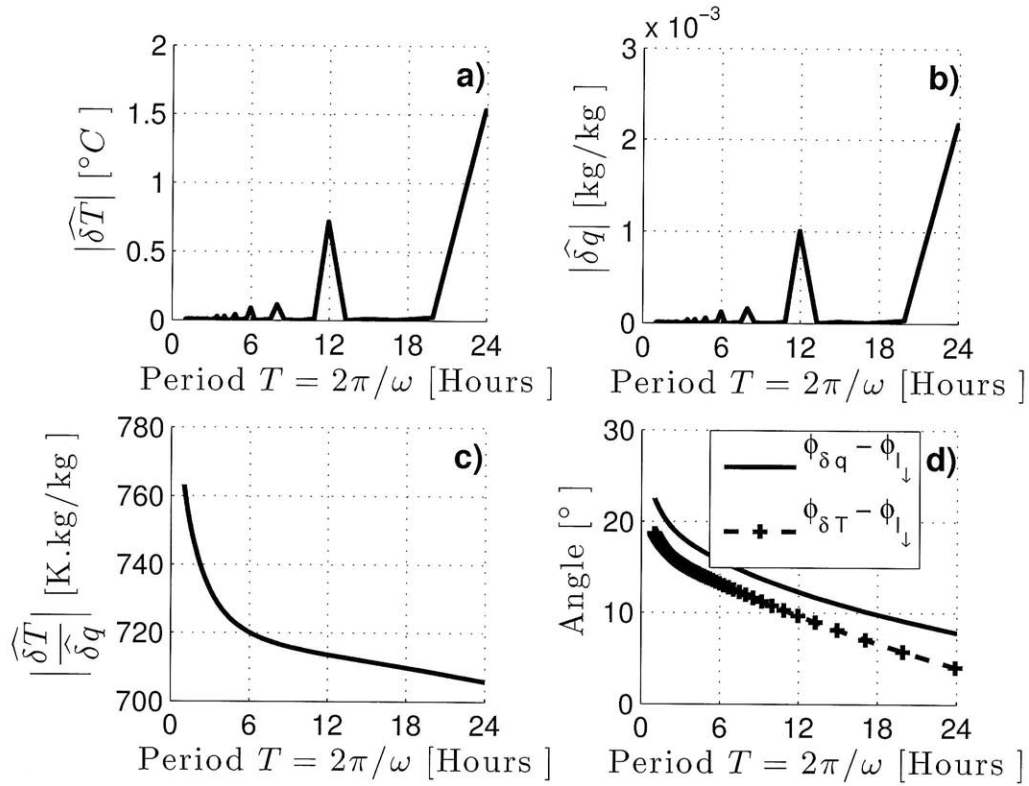
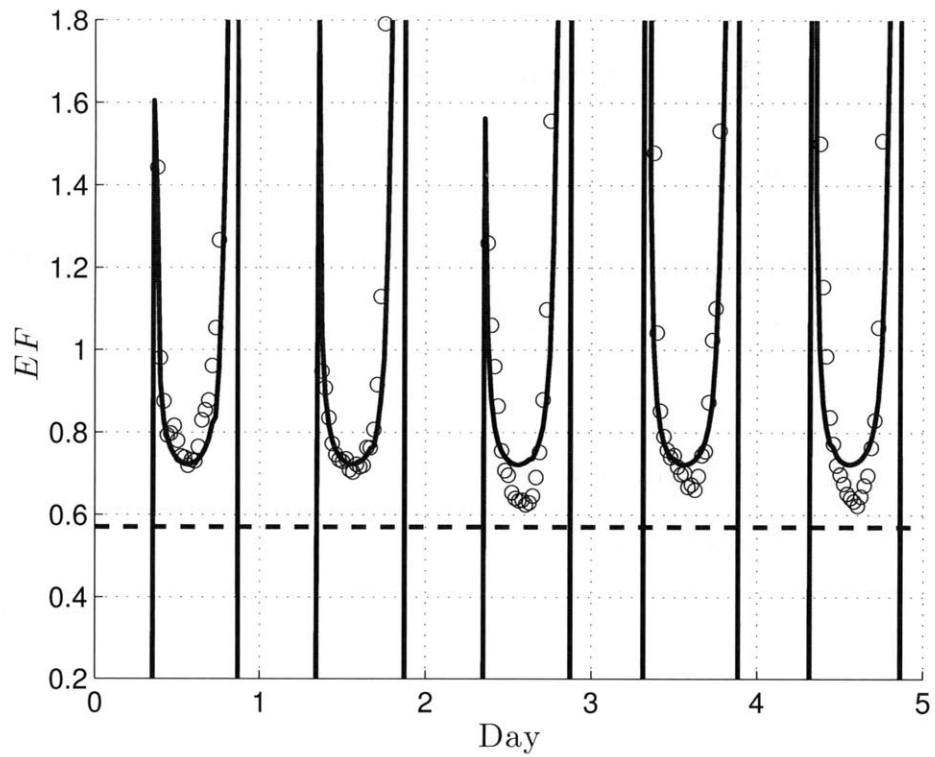


Figure 10. Absolute spectrum of temperature deficit  $\delta T = T_{s_0} - \theta_h$  (a), water vapor pressure deficit  $\delta q = q^*(T_{s_0}) - q_h$  (b), ratio between both (c) and phase difference with incoming radiation (d).



**Figure 11.** Evaporative fraction diurnal cycle (solid line) obtained from theoretical land-atmosphere coupled model compared to in-situ measurements (circles) and minimum value  $EF_{min}$  (dashed-line).

## APPENDIX A

### List of Variables and Units

$\alpha_s$	<i>Albedo of the land surface (0.16)</i>
$\beta$	<i>Beta factor in the Deardorff [1978] parameterization of latent heat flux at the land surface (0.6 dimensionless)</i>
$\gamma$	<i>Gamma constant (0.577215)</i>
$\gamma_T$	<i>Partial derivative of saturation specific humidity with respect to temperature taken at temperature <math>T</math> (<math>\text{kg kg}^{-1} \text{K}^{-1}</math>)</i>
$\lambda$	<i>Latent heat of vaporisation at triple point <math>T_t=273.16\text{K}</math> (<math>2.45 \times 10^6 \text{ J kg}^{-1}</math>)</i>
$\lambda_E$	<i>Penetration depth of the evapotranspiration wave (m)</i>
$\lambda_G$	<i>Penetration depth of the soil heat wave (m)</i>
$\lambda_H$	<i>Penetration depth of the sensible heat flux wave (m)</i>
$\lambda_q$	<i>Penetration depth of specific humidity wave (m)</i>
$\lambda_s$	<i>Soil thermal conductivity (<math>\text{W m}^{-1} \text{K}^{-1}</math>)</i>
$\lambda_\theta$	<i>Penetration depth of the potential temperature wave (m)</i>
$\lambda E(z)$	<i>Latent heat flux at given height <math>z</math> (<math>\text{W m}^{-2}</math>)</i>
$\lambda E_h$	<i>Latent heat flux at the land-surface, at canopy height <math>h</math> (<math>\text{W m}^{-2}</math>)</i>
$\lambda E_p$	<i>Potential latent heat flux at the land-surface, at canopy height <math>h</math> (<math>\text{W m}^{-2}</math>)</i>

$\omega$	<i>Pulsation of the harmonic (rad s<sup>-1</sup>)</i>
$\omega_0$	<i>Fundamental pulsation <math>2\pi / T</math> (rad s<sup>-1</sup>)</i>
$\phi_\theta$	<i>Turbulent heat flux of potential temperature <math>\phi_\theta = \overline{w'\theta'} = \frac{H}{\rho C_p}</math> (K m s<sup>-1</sup>)</i>
$\phi_q$	<i>Turbulent heat flux of specific humidity <math>\phi_q = \overline{w'q'} = \frac{\lambda E}{\rho \lambda}</math> (kg kg<sup>-1</sup> m s<sup>-1</sup>)</i>
$\rho$	<i>Density of air (1.2 kg m<sup>-3</sup>)</i>
$\theta$	<i>Mean potential temperature in the boundary-layer (K)</i>
$\theta_s$	<i>Surface layer Potential scale (K)</i>
$A$	<i>Available energy at the land surface (W m<sup>-2</sup>)</i>
$C_s$	<i>Soil heat capacity (1.42×10<sup>6</sup> J m<sup>-3</sup> K<sup>-1</sup>)</i>
$C_p$	<i>Specific heat of air at constant pressure (1012 J kg<sup>-1</sup> K<sup>-1</sup>)</i>
$d$	<i>Displacement height (m)</i>
<i>Day</i>	<i>Duration of a day in s (86400 s)</i>
<i>EF</i>	<i>Evaporative fraction at the land surface (dimensionless)</i>
$f$	<i>Coriolis parameter <math>2\Omega \sin(\phi)</math> (rad s<sup>-1</sup>), with <math>\Omega</math> : rotation rate of the Earth (7.2921×10<sup>-5</sup> rad/s) and <math>\phi</math> latitude of Marrakech: 31°37'N</i>
$G$	<i>Ground heat flux (W m<sup>-2</sup>)</i>
$G_0$	<i>Ground heat flux at the land surface (W m<sup>-2</sup>)</i>
$h$	<i>Vegetation height (0.45 m)</i>

$H$	<i>Sensible heat fluxes at the land surface right above the canopy (<math>W m^{-2}</math>)</i>
$K_s$	<i>Soil thermal diffusivity (<math>2.5 \times 10^{-7} m^2 s^{-1}</math>)</i>
$k$	<i>Von Karman's constant (0.4 dimensionless)</i>
$K_H$	<i>Eddy diffusion for heat (<math>m^2 s^{-1}</math>)</i>
$K_V$	<i>Eddy diffusion for water vapor (<math>m^2 s^{-1}</math>)</i>
$L_{MO}$	<i>Monin-Obukhov length (m)</i>
$LAI$	<i>Leaf Area Index (<math>0.4 m^2 m^{-2}</math>)</i>
$q$	<i>Mean specific humidity in <math>kg kg^{-1}</math></i>
$q^*$	<i>Specific humidity at saturation in <math>kg kg^{-1}</math></i>
$r_a^c$	<i>Canopy aerodynamic resistance between canopy and within canopy source height (<math>50 s m^{-1}</math>)</i>
$R_n$	<i>Net radiation at the land surface (<math>500 W m^{-2}</math>)</i>
$T$	<i>Time period of the whole experiment in s.</i>
$T_s$	<i>Soil temperature (K)</i>
$T_{surf}$	<i>Soil surface temperature (K)</i>
$T_{day}$	<i>Duration of a day (86400 s)</i>
$u_*$	<i>Friction velocity (<math>0.2 m s^{-1}</math>)</i>
$u_a$	<i>Wind speed (<math>m s^{-1}</math>)</i>
$z$	<i>Height/Depth (m)</i>
$z_i$	<i>Boundary-layer height (m)</i>
$z_1$	<i>Measurement height (2m)</i>



## References

- Brutsaert W.H., *Evaporation into the atmosphere*, Kluwer Academic Publishers, 299 pp, 1982.
- Boni, G., Castelli F., and Entekhabi D., Sampling strategies and assimilation of ground temperature for the estimation of surface energy balance components, *IEEE Trans. Geosci. Remote Sens.*, *39*, 165-172, 2001.
- Boni, G., Entekhabi D., and Castelli F., Land data assimilation with satellite measurements for the estimation of surface energy balance components and surface control on evaporation, *Water Resour. Res.*, *37*, 1713-1722, 2001.
- Caparrini F., Castelli F., Entekhabi D., Mapping of land-atmosphere heat fluxes and surface parameters with remote sensing data. *Bound.-Lay. Meteorol.*, *107* (3), 605-633, 2003.
- Caparrini F., Castelli F., Entekhabi D., Estimation of surface turbulent fluxes through assimilation of radiometric surface temperature sequences. *J. Hydrometeorology*, *5* (1), 145-159, 2004.
- Caparrini F., Castelli F., Entekhabi D., Variational estimation of soil and vegetation turbulent transfer and heat flux parameters from sequences of multisensor imagery. *Water Resour. Res.*, *40* (12) Paper No. 10.1029/2004WR003358, 2004.
- Carslaw H.S. and J. C. Jaeger. *Conduction of heat in solids*. Oxford University

Press, New York, pp. 54-56, 1967.

Chehbouni A., Escadafal R., Duchemin B., Boulet G., Simonneaux V., Dedieu G., Mougnot B., Khabba S., Kharrou M.H., Maisongrande P., Merlin O., Chaponnière A., Ezzahar J., Er-Raki S., Hoedjes J., Hadria R., Abourida A., Cheggour A., Raibi F., Boudhar A., Benhadj I., Hanich L. , Benkaddour A., Guemouria N., Chehbouni A.H., Lahrouni A., Oliosio A., Jacob F, Williams D.G., Sobrino J., An integrated modelling and remote sensing approach for hydrological study in arid and semi-arid regions: the SUDMED Program. *Int. J. Remote Sens.*, *29*, 5161-5181, 2008.

Crago R., Conservation and variability of the evaporative fraction during the daytime. *J. Hydrol.*, *180* (1-4), 173-194, 1996.

Crago R., Brutsaert W., Daytime evaporation and the self-preservation of the evaporative fraction and the Bowen ratio. *J. Hydrol.*, *178* (1-4), 241-255, 1996.

Crank J., *The mathematics of diffusion*. Oxford University Press, New York, 356 pp, 1956.

Choudhury B.J. and Monteith J.L., A four-layer model for the heat budget of homogeneous land surfaces. *Q. J. Roy. Meteor. Soc.*, *114*, 373-398, 1988.

Duchemin B., Hadria R., Erraki S., et al., Monitoring wheat phenology and irrigation in Central Morocco: On the use of relationships between evapotranspiration, crops coefficients, leaf area index and remotely-sensed vegetation indices. *Agr. Water Manage.*, *79* (1), 1-27, 2006.

Entekhabi D., Asrar G.R, Betts A.K., et al., An agenda for land surface

hydrology research and a call for the second international hydrological decade, *B. Am. Meteorol. Soc.*, *80*, (10), 2043-2058, 1999.

Gentine P., Entekhabi D., Chehbouni A., Boulet G. and Duchemin B., Analysis of evaporative fraction diurnal behaviour, *Agric. For. Meteorol.*, *143* (1-2), 13-29, 2007.

Gentine P., Entekhabi D. and Polcher J., Spectral behaviour of a coupled land-surface and boundary-layer system. *Bound.-Lay. Meteorol.*, In press, 2009.

Karam M.A., A Thermal Wave Approach for Heat Transfer in a Nonuniform Soil. *Soil Sci. Soc. Am. J.*, *64*, 1219-1225, 2000.

Kustas, W., T. Jackson, A. French, and J. MacPherson, Verification of patch- and regional-scale energy balance estimates derived from microwave and optical remote sensing during SGP97, *J. Hydrometeorol.*, *2*, 254-273, 2001.

Lettau H., Isotropic and non-isotropic turbulence in the atmospheric surface layer. *Geophys. Res. Pap.*, *1*, 13-84, 1949.

Lettau H., Theory of surface temperature and heat-transfer oscillations near level ground surface. *EOS* *32* (2), 189 – 200, 1951.

Margulis, S., McLaughlin D., Entekhabi D., and Dunne S., Land data assimilation and estimation of soil moisture using measurements from the southern great plains 1997 field experiment, *Water Resour. Res.*, *38*, 1299, 2002.

Monin, A. S. and Obukhov, A. M., Basic Laws of Turbulent Mixing in the Ground Layer of the Atmosphere, *Trans. Geophys. Inst. Akad. Nauk. USSR* *151*,

163–187, 1954.

Monteith J.L., *Principles of Environmental Physics*. Arnold, London, 241 pp, 1973.

Nichols W.E., Cuenca R.H., Evaluation of the evaporative fraction for parameterization of the surface, energy-balance. *Water Resour. Res.*, 29 (11), 3681-3690., 1993

Plate E.J., *Aerodynamic Characteristics of Atmospheric Boundary Layers*. US Atomic Energy Commission, Division of Technical Information, Oak Ridge, TN., 190 pp, 1971.

Shuttleworth W.J., Gurney R.J., Hsu A.Y., Ormsby J.P., FIFE: The variation in energy partition at surface flux sites. *IAHS Publ. 186*, 67-74, 1989.

Shuttleworth W.J., *Evaporation models in hydrology*. In T.J. Schmugge and J. André, eds. Land surface evaporation, Springer, New York. pp. 93-120, 1991.

Thom, A.S., Stewart, J.B., Oliver, H.R., and Gash, J.H.C., Comparison of Aerodynamic and Energy Budget Estimates of Fluxes over a Pine Forest, *Q. J. Roy. Meteor. Soc.*, 101, 93–105, 1975.

## Chapter 6

Impact of noise in the surface energy budget on screen-level and land-surface variables within a coupled land-atmosphere model

## **Abstract**

The response of a coupled land-atmosphere model to noise in the surface energy budget at the land surface is investigated. The noise is assumed to be a brownian bridge, which is a brownian motion conditioned to peak at mid-day and vanish at midnight. The noise represents inherent modeling or measurement errors in the components of the surface energy balance.

An analytical solution of the problem is sought using a linearization of the land-atmosphere system. This allows to analytically derive the statistics (variance, covariances) of the fluxes and scalars in the soil and in the atmospheric boundary layer as a function of height and time. The statistics of the energy partitioning at the land surface are then studied in response to the surface energy balance. This highlights the very different responses of soil heat flux and turbulent heat fluxes.

In a second part, the analytical model is used to determine what land-surface or screen-level observable variables are strongly affected by surface noise. In particular, the potential use and quality of these variables within a data assimilation scheme is discussed, highlighting fundamental differences between screen-level and surface variables on the one side and passive scalar (specific humidity) and active scalar (potential temperature) in the atmosphere on the other side.

## 6.1 Introduction and background

The land surface represents the interface between the soil and the Atmospheric Boundary Layer (ABL), which are coupled through the fluxes of energy, mass and chemicals. This interface thus plays a key role for the prediction of weather, climate and hydrology of continental surfaces. It is well-recognized that there is the need to better understand and model the way the soil and atmosphere interact through this common boundary. Indeed better characterization of these mutual interactions would lead to better representation of both the soil and atmospheric state, which will in turn improve meteorological and hydrological predictions at both the regional and global scales.

Accurate estimation of the land-surface energy and moisture state at the regional scale is required to better predict hydrological extremes or to improve land-surface forcing in numerical weather prediction models. Soil moisture represents a key parameter toward these improvements as it couples the energy and water budgets, and regulates the partitioning of energy at the land surface. Surface fluxes cannot be directly measured over large areas but only locally using in situ measurements. Fortunately observable variables (air and surface temperature, albedo, ...), which are measurable over large areas through remote sensing or dense meteorological stations, can be related to the land-surface state (soil moisture, temperature and heat fluxes). Using these observables to estimate the land-surface state is referred to as an inverse problem.

Recent studies have propose new methods to estimate the land-surface state from available or future data streams. Yet none of the currently available techniques possesses all required qualities: retrieval accuracy, high temporal and spatial resolution. Many have used remote sensing to determine soil moisture and land-surface fluxes. The most promising route toward global and frequent estimation of soil moisture from space remains the use of passive microwave imagery, with L-band (1.4 GHz) radiometer. Indeed because of

the strong sensitivity of soil microwave dielectric properties to soil moisture content, the potential of soil moisture retrieval from microwave brightness temperature has been clearly demonstrated [see *Entekhabi et al.*, 1994, 2004; *Schmugge and Jackson*, 1994; *Njoku and Entekhabi*, 1996; *Jackson et al.*, 1999; *Kerr et al.*, 2001; *Margulis et al.*, 2002; *Schmugge et al.*, 2002]. Current retrieval techniques however still require further developments for accurate soil moisture determination in any region of the world because of its strong dependency on soil properties and vegetation water content. In addition L-band satellites: Soil Moisture Ocean Salinity (SMOS) [*Kerr et al.*, 2001] and Soil Moisture Active Passive (SMAP) [*Entekhabi et al.*, 2008] are not in orbit yet and the operational use of this data will not be possible before a few more years. Finally, L-band microwave imagery suffers important spatial limitation and can only acquire images at a resolution of 10 km or more.

Consequently, a first group of researchers has tried to use currently available remote sensing measurements, such as infrared radiometric temperature, to estimate soil moisture and land-surface fluxes mostly at the regional scale. [see *Bastiaanssen et al.*, 1998; *Boegh et al.*, 2002; *Boni et al.*, 2001a, b; *Burke et al.*, 2003; *Caparrini et al.*, 2003, 2004a, b; *Castelli et al.*, 1999; *Friedl*, 1995; *Gillies et al.*, 1997; *Kustas and Daughtry*, 1990; *Kustas et al.*, 1996, 2001; *Jiang and Islam*, 1999; *Mecikalski et al.*, 1999; *Moran et al.*, 1994; *Su*, 2002; *van den Hurk et al.*, 1997; *Zhan et al.*, 1996]. These studies use the fact that soil moisture availability exerts a strong control on the diurnal cycle of land-surface temperature (LST), through the control of evapotranspiration, a more efficient process than the sensible release of heat, and through the strong sensitivity of soil thermal capacity on soil moisture content. Because these studies make use of inverse problems that are strongly ill-conditioned, they rely on drastic assumptions (such as empirical energy closure) and on limiting environmental and instrumental conditions (fair weather, very accurate sensing of radiometric surface temperature, low vegetation cover,...), which reduce their range of applicability.



A second group of study, inspired by the pioneer work of *Mahfouf* [1991], have used screen-level measurements of meteorological stations as an indicator of soil moisture availability and state [see *Bouttier et al.*, 1993b, a; *Ruggiero et al.*, 1996; *Callies et al.*, 1998; *Bouyssel et al.*, 1999; *Rhodin et al.*, 1999; *Douville et al.*, 2000; *Giard and Bazile*, 2000; *Alapaty et al.*, 2001; *Hess*, 2001; *Margulis et al.*, 2002; *Seuffert et al.*, 2004]. Indeed on water-limited surface receiving sufficient radiative energy, soil water availability controls the energy partitioning and in particular that between sensible and latent heat flux. The idea behind the use of screen-level temperature and humidity is that these surface turbulent heat fluxes strongly influence the structure and profiles of the ABL, thus impacting the diurnal course of air temperature and humidity at screen level. In regions with dense meteorological network, these methods have been successfully used by operational weather forecast centers (e.g. Météo France, European Centre for Medium-range Weather Forecast, Deutscher Wetterdienst...) to initialize or update soil moisture content in numerical weather prediction models. Despite its numerous assets (accuracy, operational, high temporal resolution and good spatial resolution since the footprint of these scalars is restrained), this methodology suffers important limitations that should be addressed to obtain more reliable estimates of soil moisture in an operational framework. Most of these issues are related to the update equation during the assimilation (filtering) of screen-level measurements to obtain better estimate of soil moisture. For the assimilation to be optimal the correct characterization of the variance of the error of both soil moisture and meteorological measurements has to be accurately characterized. In fact, this issue could be divided into two parts, with possible feedbacks: (i) "internal" model errors such as soil moisture variability, which are often characterized through the histogram of historical model runs. (ii) "external" sources of errors, such as misspecification of the large-scale dynamics, cloud cover or atmospheric radiation. As emphasized by *Callies et al.* [1998] and *Hess* [2001] incorrect specification of cloud cover and radiation at the land surface is regarded as most

detrimental for the assimilation of soil moisture. In their studies, *Deardorff* [1978]; *Callies et al.* [1998] were the first researchers looking at the influence of incoming radiation error, yet this effect constituted only a short part of their studies and they did not treat it in detail.

The objective of the present theoretical study are: (i) to quantify the impact of an error in the surface energy budget at the land surface and in particular the resulting variance of the partitioned flux error, (ii) to characterize the optimal frequency sampling of air measurements in order to achieve accurate land-surface state characterization (iii) to theoretically determine the "information" and the reliability added by observable variables such as radiometric temperature, air specific humidity and temperature according to the limitations of current data acquisition platforms, (iv) to investigate the impact of the inverse problem too: i.e. what is the link between fluctuations in screen-level measurements and identifiability in land-surface flux partitioning, and (v) to provide a theoretical underpinning of the use of non-perfect measurements in a coupled land-atmosphere system.

## 6.2 Description

The present study builds on the works of *Lettau* [1951] and *Gentine et al.* [2009] that introduced a simplified linearized land-atmosphere model. The model has been shown to adequately represent the daily evolution of surface and screen-level variables based on the input of land-surface incoming radiation alone. This model is solved analytically and used to obtain the profiles of temperatures and heat fluxes in the soil and in the ABL. The advantage of this simple model is that it captures the main features of the soil-ABL two-way interactions and allows for an analytical solution, highlighting the control and impact of the coupling. Furthermore, the model does not require any specification of initial profiles, which is of great interest as most previous studies investigating the diurnal evolution of

screen-level statistics were very much conditioned by the specification of the initial profiles [such as *Mahfouf*, 1991]. Indeed there can be a lasting artificial decorrelation between variables because of this imposed initial profiles, which actually depend on the surface state. In this case, the lasting decorrelation can be seen by the strong non-periodicity of the daily evolution of the variances. When weather and surface conditions undergo small changes, atmospheric profiles should remain relatively similar from one day to another.

### 6.2.1 Model outline

The land-ABL model used in this study is the one introduced in previous chapter. The main equations for the evolution of the turbulent heat fluxes of potential temperature  $\phi_\theta = \overline{w'\theta'}$  and moisture  $\phi_q = \overline{w'q'}$  are:

$$\frac{\partial \phi_\theta}{\partial t} = K(z) \frac{\partial^2 \phi_\theta}{\partial z^2} = K_*(z-d) \frac{\partial^2 \phi_\theta}{\partial z^2} \quad (6.1)$$

$$\frac{\partial \phi_q}{\partial t} = K(z) \frac{\partial^2 \phi_q}{\partial z^2} = K_*(z-d) \frac{\partial^2 \phi_q}{\partial z^2} \quad (6.2)$$

where  $K(z) = ku_*(z-d)$  represents the eddy diffusion in the ABL. Potential temperature and specific humidity are related to those equations through the K-theory:

$$\frac{\partial \theta}{\partial t} = \frac{\partial}{\partial z} \left( K(z) \frac{\partial \theta}{\partial z} \right) = K_*(z-d) \frac{\partial^2 \theta}{\partial z^2} + K_* \frac{\partial \theta}{\partial z} \quad (6.3)$$

$$\frac{\partial q}{\partial t} = \frac{\partial}{\partial z} \left( K(z) \frac{\partial q}{\partial z} \right) = K_*(z-d) \frac{\partial^2 q}{\partial z^2} + K_* \frac{\partial q}{\partial z}. \quad (6.4)$$

Moreover the soil heat flux and temperature are solutions of the following diffusion equations:

$$\frac{\partial G}{\partial t} = K_s \frac{\partial^2 G}{\partial z^2} \quad (6.5)$$

$$\frac{\partial T_s}{\partial t} = K_s \frac{\partial^2 T_s}{\partial z^2}. \quad (6.6)$$

The main assumptions behind the model are that friction velocity at the land surface is assumed to be a daily constant, changes induced by advection are considered to be small compared to the influence of surface radiative heating, the ABL height is assumed to remain constant throughout the day, and the boundary layer is assumed to be in a neutral toward unstable case with an eddy-diffusion representation of the turbulence in the whole ABL, [see *Gentine et al.*, 2009, for a complete review of the hypotheses].

The boundary conditions of this system of partial differential equations are also similar to the ones presented in the previous chapter. The only change with the preceding deterministic study lies in the formulation of the energy budget at the land surface. Indeed the energy closure is now assumed to be imperfect and equal to a brownian bridge  $B_{T_{day}}(t)$ , representing surface energy budget errors. Indeed the surface energy budget error represents inherent modeling errors of heat fluxes at the land surface, be it induced by radiation mispecification, turbulent heat flux inaccurate representation or incorrect soil heat flux. All of these error components in the surface energy budget are added into one single error term, which is the brownian bridge  $B_{T_{day}}(t)$ . Consequently, the energy budget at the land-surface now is:

$$\underbrace{I_1(t) - \epsilon_s S T_s(0, t)^4}_{R_n(t)} - G(0, t) - \underbrace{H(h, t)}_{\rho C_p \phi_\theta(h, t)} - \underbrace{\lambda E(h, t)}_{\rho \lambda \phi_q(h, t)} = B_{T_{day}}(t). \quad (6.7)$$

In this study we are only interested in the energy errors induced at the land surface, but we are not considering the addition of error within the atmosphere nor in the soil.

### 6.2.2 Brownian bridge forcing (Dirichlet white-noise boundary condition)

The Brownian Bridge (BB) is a continuous stochastic process, with probability distribution being the conditional distribution of the brownian motion given that  $B_{T_{day}}(0) = B_{T_{day}}(T_{day}) = 0$ . This BB will represent the error induced by the misrepresentation of surface energy balance components in the land-surface budget, inherent to any modeling or measurement of reality. As discussed in the introduction it is important to quantify the repercussion of this error onto the soil and atmospheric profiles, in particular for an optimal assimilation of screen-level measurements for soil moisture retrieval.

The BB has been selected to model the error in the land-surface energy budget, as it is a natural representation of the diurnal error. Indeed measurements or model errors are usually considered to be Gaussian, moreover because of the strong daily cycle of incoming radiation due to its solar component the variance is maximum at solar noon and minimum at midnight. Hence we take the noise to be patterned after the incoming radiation as a random walk conditioned to vanish at midnight, i.e.  $t = 0$  and  $t = T_{day}$ .

In addition the brownian bridge preserves a natural periodicity when atmospheric and surface conditions are unchanged from day to day. Its variance is maximal at noon, which is also realistic as land-surface errors are generally highest at solar noon when incoming solar radiation is the strongest. Moreover it is unbiased, so that the energy budget is closed on average over all realizations of the random walk at any time. This average could represent different model runs or different sensor measurements, i.e. different realizations of the process. The forcing error is thus assumed to be unbiased on average. In essence the BB is a good theoretical representation of a constant error relative to the intensity of incoming solar radiation at the surface. Finally, it should be noted that the BB has a natural Fourier series development. Several realizations (trajectories) of the BB are displayed on Figure 1

and its daily variance is depicted on Figure 2, exhibiting a strong diurnal cycle.

### 6.2.3 Brownian bridge properties

In this section, the main properties of the BB are described; in particular we focus on the Fourier transform, which is required for the rest of this study. First of all for simplification the BB is rewritten as a modified brownian motion:

$$\sigma \widehat{B}_{T_{day}}(t) = \sigma \left\{ \widehat{W}_t - \frac{t}{T_{day}} \widehat{W}_{T_{day}} \right\} \quad (6.8)$$

with  $\widehat{B}_{T_{day}}(t)$  : normalized BB,  $\widehat{W}_t$ : normalized Brownian Motion and  $\sigma$  is the volatility of the process. The covariance function of the BB is given by:

$$\text{cov} \left( \sigma \widehat{B}_{T_{day}}(s), \sigma \widehat{B}_{T_{day}}(t) \right) = \sigma^2 \left( s \wedge t - \frac{st}{T} \right). \quad (6.9)$$

So that the variance of the process is  $\sigma^2 \left( t - \frac{t^2}{T_{day}} \right)$ , which is null at midnight (i.e.  $t = 0$  or  $T_{day}$ ) and is maximum at noon ( $T_{day}/2$ ) and equal to  $\sigma^2 T_{day}/4$ . Moreover the BB has a natural Fourier decomposition with random coefficients:

$$B_{T_{day}} = \sum_{k=-\infty}^{+\infty} \widetilde{B}_k e^{j\omega_k t} = \langle B_0 \rangle + \sum_{k=1}^{+\infty} \left( \widetilde{B}_k e^{j\omega_k t} + \widetilde{B}_k^* e^{-j\omega_k t} \right) \quad (6.10)$$

with  $\widetilde{B}_k$ ,  $k \neq 0$  being (pairwise) independent complex Gaussian random variables (r.v.) distributed as  $N(0; \sigma^2 T_{day}/4n^2\pi^2)$  and  $\langle B_0 \rangle$  being a real Gaussian r.v. distributed as  $N(0; \sigma^2 T_{day}/12)$ .

Since the Fourier coefficients are normally distributed r.v., their pairwise covariances

are sufficient to determine any moments. These covariances are:

$$\forall n \geq 1 : \quad \text{var } \widetilde{B}_n = \mathbb{E} \widetilde{B}_n \widetilde{B}_n^* = \frac{\sigma^2 T_{day}}{4n^2 \pi^2} \quad (6.11)$$

$$\forall (n_1, n_2) : n_1 \neq 0 \neq n_2, n_1 \neq n_2 : \\ \text{cov} \left( \widetilde{B}_{n_1}, \widetilde{B}_{n_2} \right) = \mathbb{E} \left( \widetilde{B}_{n_1} \widetilde{B}_{n_2}^* \right) = 0 = \mathbb{E} \left( \widetilde{B}_{n_1} \widetilde{B}_{n_2} \right) = \text{cov} \left( \widetilde{B}_{n_1}, \widetilde{B}_{n_2}^* \right) \quad (6.12)$$

$$\text{cov} \left( \widetilde{B}_n, \widetilde{B}_n^* \right) = \mathbb{E} \widetilde{B}_n \widetilde{B}_n^* = 0. \quad (6.13)$$

Most of the noise energy (variance) is concentrated in the low-frequency part of the spectrum,  $\omega_n$   $n \leq 6$  (not shown). Indeed the BB, which is a conditioned brownian motion, can be thought of as an integral of the white noise, which spectrum is flat. An integral is a division by a factor  $j\omega_n$  in the spectral domain, explaining that the spectrum of the BB harmonics is mostly located in the low frequencies. In the presence of noise with different spectral representations (for instance more red), the results highlighted in this study could somewhat differ.

The correlation between the steady-state Fourier coefficient  $\langle B_0 \rangle$  and the different harmonics  $\widetilde{B}_n$  is plotted on Figure 3. Harmonics of low frequency (high period  $T$ ) are negatively correlated with the steady-state coefficient, whereas high-frequency (low- $T$ ) harmonics are almost uncorrelated and thus independent (as Gaussian r.v.) of the steady-state value. The periodicity of the BB creates these correlations as the bridge is constrained to reach a null value in both 0 and  $T_{day}$ . Indeed a diurnal bias (zero harmonic) will be compensated by diurnal harmonics in order for the bridge to vanish at midnight. Lower harmonics are the major compensator of the bias as they are more energetic (more variance) they will thus be more correlated with the steady-state harmonic, i.e. with the diurnal bias.

These statistics form the base forcing of our soil-ABL coupled model and are used to

express the variance and correlations of the different state variables. These statistics can thus be analytically derived.

## 6.3 Data set and deterministic response

### 6.3.1 Data set

The data set is similar to the one presented in *Gentine et al.* [2009] and further described in *Duchemin et al.* [2006], except that in the present study only one single day was isolated. The measurements of March 3rd 2003 were extracted from the SUDMED field campaign [*Gentine et al.*, 2007; *et al.*, 2008], which took place in the region of Marrakech, Morocco. As presented in *Gentine et al.* [2009] and in previous chapter, the linearized land-ABL model is able to reproduce the diurnal cycle of both surface and screen-level fluxes and scalars. Even though the modeling remains fairly simple, the atmospheric scalar profiles exhibit a surface layer, capped by a well-mixed region, in which scalars tend to be uniform. Moreover turbulent heat fluxes are mostly linearly varying with height in the boundary layer, in agreement with well-know results [see for a review: *Stull*, 1988; *Garratt*, 1992]. In the lower part of the ABL (surface layer) turbulent heat fluxes display either a slightly convex or concave shape, as observed by *Young* [1988] or *Wulfmeyer* [1999], then in the upper part of the ABL the flux is linearly varying with height.

### 6.3.2 Deterministic response

In this section we rapidly recall some of the deterministic results partly discussed in *Gentine et al.* [2009]. They will help better comprehend the soil and ABL response to noisy incoming radiation forcing.

The deterministic response of the complex amplitude of the land-surface temperatures



to the deterministic incoming radiation forcing is depicted on Figure 4. In response to incoming radiation heating, land-surface temperature rises with a delay induced by the high heat capacity of the soil. The land-surface temperature phase increases for high-frequency forcing since the slow response of the surface compared to the period of the forcing  $T$  introduces more relative delay. The heating of the land-surface leads to dissipation through the release of sensible heat flux in the ABL, which will increase the potential temperature right above the canopy  $\theta_h$ . The screen-level potential temperature  $\theta_{z_{meas}}$  will consequently increase, but because of the small heat capacity and high conductivity of the ABL (due to convective motion) and consecutive small heat flux divergence, this change will be attenuated and delayed.

While the land-surface temperature increases, the surface dissipates energy into the ABL through turbulent heat transfer (sensible and latent). Latent heat responds more vigorously because evapotranspiration is a more efficient dissipation mechanism than sensible heat over non-water limited surfaces as seen on Figure 5. Turbulent heat transfer and longwave surface outgoing radiation  $L_{\uparrow}$  are less efficient at high frequencies, ie. low periods  $T$ , since they are limited by the slow and delayed LST change, induced by the elevated soil heat capacity. Their amplitude and (negative) phase consequently decrease at high frequencies. Soil heat flux on the opposite side has to compensate for this attenuation, because of the balanced energy budget at the land surface. Therefore soil heat flux responds more vigorously to high-frequency incoming radiation forcing as demonstrated by *Gentine et al.* [2009] and has a positive phase.

## 6.4 Stochastic solution

The land-atmosphere model is linear so that the solution to the full stochastic problem can be thought as the superposition of the solution of a deterministic problem, forced by the

incoming radiation at the land surface and of the solution of a stochastic problem, forced by the BB. The solution of the deterministic problem is similar to the one presented in the previous chapter. The solution is solved in the Fourier domain and requires the specification of the mean-daily value of potential temperature and specific humidity at any height  $z_1$ . Any variable of interest: temperature, specific humidity, heat fluxes is then expressed in terms of a Fourier series, with coefficients dependent on the frequency of the forcing and on height. The determination of the mean-daily land-surface temperature is fundamental as all equations involving non-linear transformation of the soil temperature are linearized around this value (e.g. outgoing radiation from the surface, specific humidity at saturation at the surface). It has been shown in *Gentine et al.* [2009] and in the previous chapter, that the linearization of the equations still gives very satisfactory results when compared to measurements, in various conditions, and is consequently justifiable.

In this section, the solution to the stochastic part of the problem is sought. It is assumed here after that the amplitude of the BB is small compared to the deterministic incoming radiation forcing at the land surface. In this experiment the noise has to remain small enough so that the linearization remains a good approximation of the problem. Indeed for larger values of the incoming radiation noise the effect of non-linearities could become important. This effect has been evaluated using Monte-Carlo simulations (not shown) and this transition toward non-linear processes will be studied in further details in a forthcoming study. In the present study the maximum standard deviation of the BB is assumed to be  $25 \text{ W m}^{-2}$ , which should be compared to the amplitude of shortwave incoming radiation:  $800 \text{ W m}^{-2}$  and longwave incoming radiation:  $300 \text{ W m}^{-2}$ , and is well within the linearity assumption. Moreover, since the perturbation is small the periodicity assumption remains valid. Indeed the effect of the non-linearities will consequently be small and the forcing at one frequency will mainly have repercussions at the same frequency. For instance, long-term soil heat storage induced by the perturbation is negligible since the noise is small enough

so that the linear approximation is valid.

All stochastic variables resulting from the BB perturbation are denoted with prime superscripts and sought as Fourier series:

$$X'(t, z) = \langle X'(z) \rangle + \sum_{n \in \mathbf{Z}^*} \widetilde{X}_n'(z) e^{j\omega_n t}. \quad (6.14)$$

By linearity the perturbed variables are solution of equations (6.1) through (6.6) and the boundary conditions are:

1. The surface energy budget error at the land surface is given by:  $B_{T_{day}}(t)$
2. The soil heat flux is null at infinite depth:  $\lim_{z \rightarrow -\infty} G'(z, t) = 0$
3. turbulent heat fluxes are null on top of the ABL:  $\phi_\theta'(z_i) = 0$  and  $\phi_q'(z_i) = 0$
4. The perturbed sensible heat flux at the land surface is given by:

$$\phi_\theta'(h, t) = \frac{T_s'(z = 0, t) - \theta'(z = h, t)}{r_a^c}. \quad (6.15)$$

5. The perturbed latent heat flux at the land-surface boundary is linearized as:

$$\phi_q'(h, t) = \frac{\beta}{r_a^c} \{ \gamma_{T_{deep}} T_s'(z = 0, t) - q'(h, t) \} \quad (6.16)$$

where the specific humidity at saturation has been linearized around the mean land-surface deterministic temperature  $T_{deep}$

6. The last boundary condition assumes that the land-surface energy budget is perturbed

at the land-surface:

$$B_{T_{day}}(t) - 4\epsilon_s S T_{deep}^3 T'_s(z=0, t) - G'(z=0, t) = \rho C_p \phi_{\theta'}(z=h, t) + \rho \lambda \phi_q'(z=h, t). \quad (6.17)$$

### 6.4.1 Steady-state stochastic solution

As in the deterministic case the steady-state solution first needs to be found to express the full harmonic solution. The resolution of the steady-state ordinary differential equations is very similar to the deterministic case. It should be emphasized that the steady-state solutions represent the random bias in the daily-mean values. The influence of daily biases can thus be studied. Using equations (6.5) and (6.6), the steady-state stochastic soil temperature and heat flux solutions are:

$$\langle G' \rangle(z) = 0 \quad (6.18)$$

$$\langle T'_s(z) \rangle = \langle T'_{s0} \rangle \quad (6.19)$$

Consequently, there is no diurnal random bias in soil heat flux as its steady-state component is null. This constitutes an important result for modeling as there is no mean daily bias induced by the incoming radiation noise at the land surface. Yet we want to emphasize that this result is dependent on the spectrum of the noise.

In the ABL, the following steady-state temperature and humidity random profiles are obtained:

$$\langle \theta' \rangle(z) = -\frac{\Phi_1}{Ku_*^0} [z + (d - z_i) \ln(z - d)] + \Phi_2 \quad (6.20)$$

$$\langle q' \rangle(z) = -\frac{\Psi_1}{Ku_*^0} [z + (d - z_i) \ln(z - d)] + \Psi_2. \quad (6.21)$$

Notice that the unknown coefficients  $\Phi_i$  and  $\Psi_i$  are random variables. Using both the expression of sensible and latent heat flux at the land surface, boundary conditions (4) and (5), the coefficients can be expressed as a function of the air temperature and specific humidity perturbations away from deterministic equilibrium (resp.  $\langle\theta'\rangle(z)$  and  $\langle q'\rangle(z)$  at height  $z$ ):

$$\langle\theta'\rangle(z) - \langle\theta'\rangle(h) = (\langle T_{s_0}' \rangle - \langle\theta'\rangle(h)) \underbrace{\frac{1}{Ku_* r_a^c} \left[ \frac{z-h}{z_i-h} - \left( \frac{z_i-d}{z_i-h} \right) \ln \left( \frac{z-d}{h-d} \right) \right]}_{\triangleq \alpha(z)} \quad (6.22)$$

$$\langle q'\rangle(z) - \langle q'\rangle(h) = (\gamma_{T_{deep}} \langle T_{s_0}' \rangle - \langle q'\rangle(h)) \underbrace{\frac{\beta}{Ku_* r_a^c} \left[ \frac{z-h}{z_i-h} - \left( \frac{z_i-d}{z_i-h} \right) \ln \left( \frac{z-d}{h-d} \right) \right]}_{\triangleq \beta\alpha(z)}. \quad (6.23)$$

The stochastic surface steady-state budget can be rewritten as a function of these latter:

$$\langle B_0 \rangle - 4\epsilon_s S T_{deep}^3 \langle T_{s_0}' \rangle = \frac{\rho C_p \langle T_{s_0}' \rangle - \langle\theta'\rangle(z_1)}{r_a^c} + \frac{\rho \lambda \beta \gamma_{T_{deep}} \langle T_{s_0}' \rangle - \langle q'\rangle(z_1)}{r_a^c}. \quad (6.24)$$

To entirely solve the problem the steady-state stochastic soil temperature  $\langle T_{s_0}' \rangle$  has to be found first, and the random variables  $\langle q'\rangle(z_1)$  and  $\langle\theta'\rangle(z_1)$  should be specified. These two random variables will be assumed to be jointly independent, independent from the land-surface noise, and normally distributed with respective distribution:  $\langle\theta'\rangle(z_1) \sim N(0, \sigma_\theta^2)$  and  $\langle q'\rangle(z_1) \sim N(0, \sigma_q^2)$ , where  $\sigma_\theta^2$  and  $\sigma_q^2$  represent the daily-mean error of potential temperature and specific humidity at height  $z_1$ . These errors represent the modeling or measurements dispersion, such as the variance of ensemble forecasts in operational meteorological models. In this study the height  $z_1$  was assumed to be  $z_i$ , the ABL height, whereas in previous studies the value was imposed at the measurement height.

All random variables are normally distributed, since all input variables are normally distributed and the problem is linear. In particular the steady-state soil temperature error

can be written as:  $\langle T_{s_0}' \rangle \sim N(0, \sigma_{T_{s_0}}^2)$ . The variance of this random variable can easily be obtained using equations (6.22), (6.23) and (6.24):

$$\sigma_{T_{s_0}}^2 = \frac{\frac{\sigma^2 T}{12} + \sigma_\theta^2 \left[ \frac{\rho C_p}{r_{ac}(1-\alpha(z_1))} \right]^2 + \sigma_q^2 \left[ \frac{\rho \lambda \beta \gamma_{T_{deep}}}{r_{ac}(1-\beta\alpha(z_1))} \right]^2}{\left[ 4_s S T_{deep}^3 + \frac{\rho C_p}{r_{ac}(1-\alpha(z_1))} + \frac{\rho \lambda \beta \gamma_{T_{deep}}}{r_{ac}(1-\beta\alpha(z_1))} \right]^2}. \quad (6.25)$$

There is consequently a correlation between  $\langle \theta' \rangle(z_1)$  and  $\langle T_{s_0}' \rangle$  and their covariance can be written as:

$$\text{cov}(\langle \theta' \rangle(z_1), \langle T_{s_0}' \rangle) = \frac{\sigma_\theta^2}{1 + \frac{4_s S T_{deep}^3 r_{ac}(1-\alpha(z_1))}{\rho C_p} + \frac{\lambda \beta \gamma_{T_{deep}}(1-\alpha(z_1))}{C_p(1-\beta\alpha(z_1))}} \quad (6.26)$$

Similarly between  $\langle q' \rangle(z_1)$  and  $\langle T_{s_0}' \rangle$ :

$$\text{cov}(\langle q' \rangle(z_1), \langle T_{s_0}' \rangle) = \frac{\sigma_q^2}{\gamma_{T_{deep}} + \frac{4_s S T_{deep}^3 r_{ac}(1-\beta\alpha(z_1))}{\rho \lambda \beta} + \frac{C_p(1-\beta\alpha(z_1))}{\lambda \beta(1-\alpha(z_1))}} \quad (6.27)$$

Finally for  $\langle B_0 \rangle$  and  $\langle T_{s_0}' \rangle$ :

$$\text{cov}(\langle B_0 \rangle, \langle T_{s_0}' \rangle) = \frac{\frac{\sigma^2 T_{day}}{12}}{4_s S T_{deep}^3 + \frac{\rho C_p}{r_{ac}(1-\alpha(z_1))} + \frac{\rho \lambda \beta \gamma_{T_{deep}}}{r_{ac}(1-\beta\alpha(z_1))}} \quad (6.28)$$

. These covariances are required to express the steady-state variance of respectively sensible and latent heat:

$$\sigma_{\langle H_h \rangle}^2 = \frac{\rho C_p}{r_{ac}} (\sigma_{T_{s_0}}^2 + \sigma_{\theta_h}^2 - 2 \text{cov}(\langle T_{s_0}' \rangle, \langle \theta_h' \rangle)) \quad (6.29)$$

$$\sigma_{\langle \lambda E_h \rangle}^2 = \frac{\rho \lambda}{r_{ac}} \left( \gamma_{T_{deep}}^2 \sigma_{T_{s_0}}^2 + \sigma_{q_h}^2 - 2 \gamma_{T_{deep}} \text{cov}(\langle T_{s_0}' \rangle, \langle q_h' \rangle) \right) \quad (6.30)$$

where

$$\sigma_{\langle \theta_h' \rangle}^2 = \frac{\sigma_\theta^2 + \alpha^2(z_1) \sigma_{T_s}^2 - 2\alpha(z_1) \text{cov}(\langle \theta(z_1)' \rangle, \langle T_{s_0}' \rangle)}{(1 - \alpha(z_1))^2} \quad (6.31)$$

$$\sigma_{\langle q_h' \rangle}^2 = \frac{\sigma_q^2 + [\gamma_{T_{deep}} \beta \alpha(z_1)]^2 \sigma_{T_s}^2 - 2\gamma_{T_{deep}} \beta \alpha(z_1) \text{cov}(\langle \theta(z_1)' \rangle, \langle T_{s_0}' \rangle)}{(1 - \alpha(z_1))^2} \quad (6.32)$$

$$\text{cov}(\langle \theta_h' \rangle, \langle T_{s_0}' \rangle) = \frac{\text{cov}(\langle \theta(z_1)' \rangle, \langle T_{s_0}' \rangle) - \alpha(z_1) \sigma_{T_{s_0}}^2}{1 - \alpha(z_1)} \quad (6.33)$$

$$\text{cov}(\langle q_h' \rangle, \langle T_{s_0}' \rangle) = \frac{\text{cov}(\langle q(z_1)' \rangle, \langle T_{s_0}' \rangle) - \beta \alpha(z_1) \gamma_{T_{deep}} \sigma_{T_{s_0}}^2}{1 - \beta \alpha(z_1)}. \quad (6.34)$$

Then using the steady-state relations:

$$\langle \theta' \rangle(z) = \alpha(z) \langle T_{s_0}' \rangle + (1 - \alpha(z)) \langle \theta_h' \rangle \quad (6.35)$$

$$\langle q' \rangle(z) = \beta \alpha(z) \gamma_{T_{deep}} \langle T_{s_0}' \rangle + (1 - \beta \alpha(z)) \langle q_h' \rangle \quad (6.36)$$

$$\langle \phi_{\theta'} \rangle(z) = \langle \phi_{\theta'} \rangle(h) \frac{z - z_i}{h - z_i} \quad (6.37)$$

$$\langle \phi_{q'} \rangle(z) = \langle \phi_{q'} \rangle(h) \frac{z - z_i}{h - z_i}. \quad (6.38)$$

The steady-state variances at any height read:

$$\sigma_{\langle \theta' \rangle(z)}^2 = \alpha^2(z) \sigma_{T_{s_0}}^2 + (1 - \alpha(z))^2 \sigma_{\theta_h}^2 + 2\alpha(z) (1 - \alpha(z)) \text{cov}(\langle \theta_h' \rangle, \langle T_{s_0}' \rangle) \quad (6.39)$$

$$\begin{aligned} \sigma_{q(z)}^2 &= (\gamma_{T_{deep}} \beta \alpha(z))^2 \sigma_{T_{s_0}}^2 + (1 - \beta \alpha(z))^2 \sigma_{q_h}^2 \\ &+ 2\gamma_{T_{deep}} \beta \alpha(z) (1 - \beta \alpha(z)) \text{cov}(\langle q_h' \rangle, \langle T_{s_0}' \rangle) \end{aligned} \quad (6.40)$$

$$\sigma_{H(z)}^2 = \sigma_{\langle H_h \rangle}^2 \left( \frac{z - z_i}{h - z_i} \right)^2 \quad (6.41)$$

$$\sigma_{\lambda E(z)}^2 = \sigma_{\langle \lambda E_h \rangle}^2 \left( \frac{z - z_i}{h - z_i} \right)^2. \quad (6.42)$$

We also have:

$$\text{cov} \left( \langle T_{s_0} \rangle, \widetilde{B}_n \right) = \frac{\text{cov} \left( \widetilde{B}_0, \widetilde{B}_n \right)}{4_s S T_{deep}^3 + \frac{\rho C_p}{r_g^c (1 - \alpha(z_1))} + \frac{\rho \lambda \beta \gamma T_{deep}}{r_g^c (1 - \beta \alpha(z_1))}} \quad (6.43)$$

$$\text{cov} \left( \langle \theta_h' \rangle, \widetilde{B}_n \right) = - \frac{\alpha(z_1)}{1 - \alpha(z_1)} \text{cov} \left( \langle T_{s_0}' \rangle, \widetilde{B}_n \right) \quad (6.44)$$

$$\text{cov} \left( \langle q_h' \rangle, \widetilde{B}_n \right) = - \frac{\beta \alpha(z_1) \gamma T_{deep}}{1 - \beta \alpha(z_1)} \text{cov} \left( \langle T_{s_0}' \rangle, \widetilde{B}_n \right). \quad (6.45)$$

These expressions are the basis for the study of the error propagation in the ABL. Indeed the definition of these steady-state statistics is necessary to investigate the stochastic diurnal behavior of any variables throughout the day.

## 6.4.2 Stochastic Harmonic Solution

The harmonic solution of the stochastic problem and its derivation are in essence equivalent to the deterministic solution, except that the Fourier transform of the BB replaces that of the incoming radiation forcing at the land surface. Even though the time-derivative is ill-defined as stochastic variables are considered, the partial differential equations in the soil and in the ABL are well-defined, as diffusion (heat) equations with no pole in the domain of interest. Theoretically the use of the heat Kernel (Green's function) with stochastic forcing (brownian bridge) can be justified as well as the use of a Fourier decomposition of the daily periodic variables. This has to be emphasized, since the soil and ABL partial differential equations forced by a stochastic boundary noise become stochastic partial differential equations, in which time derivatives are undefined and for which solution is in general more complicated. Moreover the use of the projection on the Fourier basis is justifiable because of the pathwise convergence. The Fourier harmonics of the perturbed



surface variables can thus be written:

$$\tilde{G}'(\omega_n, z = 0) = \frac{1}{1 + 4\epsilon_s ST_{deep}^3 \Delta(\omega_n) + \rho \Delta(\omega_n) \left( \frac{C_p}{r_a^c + \rho \Sigma(\omega_n)} + \frac{\lambda \beta \gamma_T_{deep}}{r_a^c + \rho \beta \Sigma(\omega_n)} \right)} \tilde{B}(\omega_n) \quad (6.46)$$

$$\tilde{\phi}'_\theta(\omega_n, z = h) = \frac{\Delta(\omega_n)}{(r_a^c + \rho \Sigma(\omega_n)) \left\{ 1 + 4\epsilon_s ST_{deep}^3 \Delta(\omega_n) + \rho \Delta(\omega_n) \left( \frac{C_p}{r_a^c + \rho \Sigma(\omega_n)} + \frac{\lambda \beta \gamma_T_{deep}}{r_a^c + \rho \beta \Sigma(\omega_n)} \right) \right\}} \tilde{B}(\omega_n) \quad (6.47)$$

$$\tilde{\phi}'_q(\omega_n, z = h) = \frac{\beta \gamma_{(T_{s0})} \Delta(\omega_n)}{(r_a^c + \rho \beta \Sigma(\omega_n)) \left\{ 1 + 4\epsilon_s ST_{deep}^3 \Delta(\omega_n) + \rho \Delta(\omega_n) \left( \frac{C_p}{r_a^c + \rho \Sigma(\omega_n)} + \frac{\lambda \beta \gamma_T_{deep}}{r_a^c + \rho \beta \Sigma(\omega_n)} \right) \right\}} \tilde{B}(\omega_n) \quad (6.48)$$

$$\tilde{T}'_s(\omega_n, z = 0) = \frac{1}{1/\Delta(\omega_n) + 4\epsilon_s ST_{deep}^3 + \rho \left( \frac{C_p}{r_a^c + \rho \Sigma(\omega_n)} + \frac{\lambda \beta \gamma_T_{deep}}{r_a^c + \rho \beta \Sigma(\omega_n)} \right)} \tilde{B}(\omega_n) \quad (6.49)$$

$$\tilde{\theta}'(\omega_n, z = h) = \frac{\rho \Sigma(\omega_n)}{(r_a^c + \rho \Sigma(\omega_n)) \left\{ 1/\Delta(\omega_n) + 4\epsilon_s ST_{deep}^3 + \rho \left( \frac{C_p}{r_a^c + \rho \Sigma(\omega_n)} + \frac{\lambda \beta \gamma_T_{deep}}{r_a^c + \rho \beta \Sigma(\omega_n)} \right) \right\}} \tilde{B}(\omega_n) \quad (6.50)$$

$$\tilde{q}'(\omega_n, z = h) = \frac{\beta\gamma(T_{s0})\rho\Sigma(\omega_n)}{(r_a^c + \rho\beta\Sigma(\omega_n)) \left\{ 1/\Delta(\omega_n) + 4\epsilon_s S T_{deep}^3 + \rho \left( \frac{C_p}{r_a^c + \rho\Sigma(\omega_n)} + \frac{\lambda\beta\gamma T_{deep}}{r_a^c + \rho\beta\Sigma(\omega_n)} \right) \right\}} \tilde{B}(\omega_n). \quad (6.51)$$

And the stochastic solutions in the ABL are expressed as a function of land-surface values:

$$\tilde{\phi}'_{\theta}(\omega_n, z) = \tilde{\phi}'_{\theta}(\omega_n, z = h) \sqrt{\frac{z-d}{h-d}} \frac{H_1^1(x_i)H_1^2(x) - H_1^2(x_i)H_1^1(x)}{H_1^1(x_i)H_1^2(x_h) - H_1^2(x_i)H_1^1(x_h)} \quad (6.52)$$

$$\tilde{\phi}'_q(\omega_n, z) = \tilde{\phi}'_q(\omega_n, z = h) \sqrt{\frac{z-d}{h-d}} \frac{H_1^1(x_i)H_1^2(x) - H_1^2(x_i)H_1^1(x)}{H_1^1(x_i)H_1^2(x_h) - H_1^2(x_i)H_1^1(x_h)} \quad (6.53)$$

$$\tilde{\theta}'(\omega_n, z) = \tilde{\phi}'_{\theta}(\omega_n, z = h) \frac{1+j}{\sqrt{2\omega_n K u_*^0 (h-d)}} \frac{H_1^1(x_i)H_0^2(x) - H_1^2(x_i)H_0^1(x)}{H_1^1(x_i)H_1^2(x_h) - H_1^2(x_i)H_1^1(x_h)} \quad (6.54)$$

$$\tilde{q}'(\omega_n, z) = \tilde{\phi}'_q(\omega_n, z = h) \frac{1+j}{\sqrt{2\omega_n K u_*^0 (h-d)}} \frac{H_1^1(x_i)H_0^2(x) - H_1^2(x_i)H_0^1(x)}{H_1^1(x_i)H_1^2(x_h) - H_1^2(x_i)H_1^1(x_h)} \quad (6.55)$$

And similarly in the soil:

$$\tilde{G}'(\omega_n, z) = \tilde{G}'(\omega_n, z = 0) \exp \left( (1+j) \sqrt{\frac{\omega_n}{2K_s}} z \right) \quad (6.56)$$

$$\tilde{T}'_s(\omega_n, z) = \tilde{G}'(\omega_n, z = 0) \frac{1-j}{C_s} \sqrt{\frac{1}{2\omega_n K_s}} \exp \left( (1+j) \sqrt{\frac{\omega_n}{2K_s}} z \right). \quad (6.57)$$

The stochastic problem is thus entirely solved with the specifications of the steady-state and harmonic solutions. The dependence on height or depth can be investigated, as well as its time dependency. Because of the linearity of the soil-ABL model, all r.v. are normally distributed and all stochastic processes are Gaussian, therefore the specification of the covariance function alone is sufficient to entirely determine the distribution of the variables of interest. Moreover, since the BB and measurement at height  $z_1$  are centered, all variables will also be centered (zero-mean processes and variables) so that the study of the mean value can be neglected.

### 6.4.3 Time-varying variance and correlations

Because all soil and ABL variables can be expressed linearly as a function of the BB harmonics, the time-varying covariance between two variables can be expressed as a Fourier series using the covariance of their Fourier coefficients:

$$\begin{aligned} \text{cov}(X(t), Y(t)) &= \text{cov}(\langle X_0 \rangle, \langle Y_0 \rangle) \\ &+ 2\text{Re} \left[ \sum_{n=1}^{+\infty} \left( \text{cov}(\langle X_0 \rangle, \widetilde{Y}_n) + \text{cov}(\langle Y_0 \rangle, \widetilde{X}_n) \right) e^{-j\omega_n t} + \text{cov}(\widetilde{X}_n, \widetilde{Y}_n) \right]. \end{aligned} \quad (6.58)$$

And in particular the variance of any stochastic process will be expressed as:

$$\text{var}(X(t)) = \text{var}(\langle X_0 \rangle) + 2\text{Re} \left[ \sum_{n=1}^{+\infty} 2\text{cov}(\langle X_0 \rangle, \widetilde{X}_n) e^{-j\omega_n t} + \text{var}(\widetilde{X}_n) \right]. \quad (6.59)$$

The correlations can then easily be deduced. Those expressions will be fundamental to understand the influence of the land-surface error on the variability of the soil and ABL scalars and fluxes.

## 6.5 Quantifying the variance of the partitioned error

The phase of the Fourier coefficients of any process of the system is random, i.e. is uniformly distributed. Indeed the coefficients of the BB error forcing are uncorrelated with their own conjugate: leading to the independence of the real and imaginary part of the normally distributed coefficient. Since any land-atmosphere variable is a linear combination of this land-surface forcing and thus of the Fourier coefficients of the BB, its Fourier coefficients will exhibit a random, uniformly distributed, phase. This observation has important consequences: the effect of high (respectively low) frequency noise will be uniformly distributed throughout the day, whereas in the deterministic case a given harmonic of incoming solar

radiation forcing had a repercussion characterized by a specific phase lag. This illustrates a fundamental difference between the stochastic and deterministic case. This will have a strong influence on the response of the land-atmosphere coupled system to land-surface energy error.

To better understand the diurnal influence of land-surface energy error on surface variables, the relative frequency distribution of the energy (variance) as a function of frequency is of great importance. More precisely, we define the Square Root Residual Energy (*SRRE*) as a function of the Fourier coefficients of a given stochastic process  $X(t)$ :

$$SRRE(\omega_n) = \sqrt{\sum_{i=0}^{+\infty} \text{var}\tilde{X}(\omega_i) - \sum_{k=0}^{n-1} \text{var}\tilde{X}(\omega_k)} = \sqrt{\sum_{i=n}^{+\infty} \text{var}\tilde{X}(\omega_i)} \quad (6.60)$$

This represents the amount of energy (variance) located above the considered harmonic frequency  $\omega_n$  and is thus an indicator of the influence of higher harmonics on the total energy noise of  $X(t)$ , moreover it has the same dimension as  $X(t)$ . When  $SRRE(\omega_n) \approx 0$ , the harmonics higher or equal to  $\omega_n$  (periods lower or equal to  $T = T_n = 2\pi/\omega_n$ ) have negligible contribution to the total variance of the noise. Thus the noise influence is mostly captured below this frequency and corresponding time period  $T$ . This latter timescale will have a fundamental role for modeling, as it will specify the maximum possible period of model integration or measure repetition, required to avoid systemic errors due to incoming radiation.

We also define the Relative Residual Energy (*RRE*) of the process  $X(t)$  as:

$$RRE(\omega_n) = 1 - \frac{\sum_{k=0}^{n-1} \text{var}\tilde{X}(\omega_k)}{\sum_{i=0}^{+\infty} \text{var}\tilde{X}(\omega_i)} = \frac{SRRE^2(\omega_n)}{\sum_{i=0}^{+\infty} \text{var}\tilde{X}(\omega_i)} \quad (6.61)$$

which is a dimensionless equivalent to the *SRRE*.

### 6.5.1 Land-surface heat fluxes

As evident in Figure 6, the high frequency (short term) part of the land-surface noise mostly influences soil heat flux compared to surface turbulent heat fluxes. This corroborates the erratic aspect of the measured time series of soil heat flux. High-frequency (long-term) land-surface noise mostly influences turbulent heat, i.e. is mostly dissipated through turbulent release of heat. This behavior is comparable to the deterministic case presented in *Gentine et al.* [2009]: deterministic soil heat flux was shown to highlight the high frequencies of solar incoming radiation forcing. When forced by stochastic surface energy budget noise, soil heat flux plays an equivalent role and mostly emphasizes high frequency (low period) noise. It has been previously shown, while solving the steady-state stochastic solution, that soil heat flux had no steady-state component i.e. soil heat flux has no daily-mean bias induced by the land-surface budget error contrary to turbulent heat fluxes, as seen on equation (6.18). This means that the repercussion of incoming radiation noise does not bias soil heat flux but other fluxes only. This result is linked to the linearization hypothesis as well as to the color of the noise: with a different spectral repartition of the incoming radiation noise, this result could be modified, in particular when modeled incoming radiation exhibits a strong morning or afternoon bias. Yet Monte-Carlo simulations (not displayed) show that this result is relatively insensitive to the color of the incoming radiation noise, because soil heat flux mainly acts as a high-pass filter. Therefore surface turbulent heat fluxes and, to less extend, longwave incoming radiation tend to mostly concentrate the low-frequency spectrum of surface energy budget noise. In contrast, soil heat flux noise is mainly influenced by high frequencies, and is even unbiased in our specific case (brownian bridge forcing), underscoring this effect.

It is also interesting to look at the *SRRE* of the surface heat fluxes on Figure 7. Outgoing longwave radiation  $L_{\uparrow}$  exhibits a smooth an almost linear increase through its whole spectrum. There is little energy (variance) accumulated at high frequencies (low  $T$ ).

Thus outgoing longwave radiation mostly emphasizes low- and medium-frequency diurnal noise and will be little sensitive to high-frequency incoming radiation forcing noise, referred from here on as weather noise. This is correlated with the observations of the relatively stable and smooth shape of measured or modeled outgoing longwave radiation throughout the day.

Turbulent heat fluxes behave similarly: their respective *SRRE* is slightly more elevated at high frequencies (low periods), they thus respond slightly more to weather noise than net radiation. The overall spectrum of these fluxes is correspondingly little influenced by high-frequency noise. Land-surface noise thus reverberates mostly on middle and low frequencies. This constitutes an important result as turbulent heat fluxes modeled at an hourly time scale will be little sensitive to land-surface incoming radiation errors (see Figure 7), since their *SRRE* is negligible below this period.

Soil heat flux behaves much differently. Figure 7 confirms that soil heat flux noise is mostly influenced by high-frequency incoming radiation noise. The contribution of the low frequencies to the total variance is almost negligible, as evident in the lower rate of the *SRRE* growth at low frequencies. This emphasizes that modeling of soil heat flux is very much prone to radiation errors. Moreover numerical integration of soil heat flux modeling will need to be performed with a very short time step, in order to capture all rapid changes in incoming radiation as shown in *Gentine et al.* [2009]. Soil heat flux has often been considered a second-order term of the energy budget, frequently modeled as a proportion of net radiation when assimilating infrared brightness temperature. Yet because of its specific spectral response, its accurate modeling is fundamental to obtain better estimates of the surface state and in particular of the LST. This important role of soil heat flux was emphasized by *Deardorff* [1978]: "any assumption that it is proportional to any particular component, or partial set of such components, seems dangerously non-general".

Physically, the rapid, high-frequency, will principally impact the soil heat flux since

the delayed response of land-surface temperature induced by the soil high heat capacity limits the rapidity of response of surface turbulent heat fluxes and outgoing radiation. The elevation in LST also induces a fast response of screen-level temperature and humidity. This rapid propagation of the LST changes onto the lower air temperature (induced by the air small heat capacity and efficient convective heat transfer) and humidity will lead to a negative feedback on surface turbulent heat fluxes. This effect will consequently limit the change of these latter in response to rapid incoming radiation noise. In addition, for high-frequency (low-period) forcing, LST changes are small since the temperature does not have sufficient time to adjust its value and there is consequently only a little relative modification of turbulent heat fluxes. In fact, this result further explains why the ABL fluxes are always in quasi steady state: the land-surface temperature acts as a low-pass filter of incoming radiation, the changes in LST are consequently small compared to the very efficient and rapid transport of heat in the whole ABL. The use of land-atmosphere coupling is necessary to analyze this phenomenon, as the different temporal response within the coupled system help understand this quasi steady state for turbulent heat fluxes. Soil heat flux, which compensates the other surface heat fluxes through the energy budget at the land surface, consecutively exhibits a very strong response to high-frequency noise.

Finally, Figure 8 displays the standard deviation of surface heat fluxes in response to surface energy budget noise. These figures shows that the surface outgoing radiation error exhibits a strong diurnal cycle with a peak at around 1PM, similar to the peak of LST as will be shown next. Moreover the error in outgoing radiation is almost vanishing at midnight. This results helps us to understand the effect of the different variance harmonics on outgoing radiation. The random harmonics tend to either attenuate (at night) or increase (during daytime) the steady-state component of the variance. This results in a strong diurnal cycle of outgoing radiation error throughout the day. Turbulent heat fluxes behave differently: the error is never vanishing and remains relatively large through the whole day with a peak

at noon. As a result, daytime incoming radiation errors will have repercussions on nighttime estimated values of turbulent heat fluxes. In our slightly water-limited case ( $\beta = 0.6$ ), the variance of latent heat flux exhibits a strong diurnal cycle compared to sensible heat flux. Indeed the harmonics of the latent heat flux variance are relatively important compared to the steady-state component, they consequently attenuate or amplify the steady-state variance.

It is striking to see that the variance of the soil heat flux error remains constant throughout the day. Even though soil heat flux errors have no steady-state component, the variance harmonics add together and create a constant standard deviation throughout the day, which is a consequence of the BB spectrum. The incoming radiation error, with its strong diurnal cycle, leads to the same soil heat flux error at night or during daytime. Accurate nighttime estimate of soil heat flux is consequently rendered difficult. In addition, with the BB forcing and with our hypotheses, soil heat flux is unbiased. Even though this is specific to our experiment it emphasizes the tendency of soil heat flux to act as a high-pass filter, with regards to incoming radiation noise, thus decorrelating long-term trends, making the noise act as random instantaneous and uncorrelated with previous values.

Such simple estimates of the daily evolution of surface heat fluxes could be used in a simplified assimilation scheme, in order to obtain more reliable time-varying heat flux statistics matrices. This model is very simple and has inherent limitations, however it has proven to be able to reproduce relatively well the evolution of deterministic surface heat fluxes and temperatures, both at the surface and at screen level. The main advantage of this approach is that there is no need to specify initial profiles, which could lead to erroneous statistics estimates, as they introduce a strong constrain on the surface state (fluxes and temperatures). Moreover an analytical solution can be sought leading to negligible computer burden.

Operationally an improved version of such kind of coupled model forced by an estimated



incoming radiation error could be used to obtain fast, relatively reliable estimate of variance and covariance matrices induced by incoming radiation error. As these covariance matrices are dependent on surface state and on meteorological conditions, accurate estimates of these covariance matrices are required to obtain an optimal land-surface data assimilation scheme, in return such approach could help obtain better soil moisture and surface heat flux updates.

### 6.5.2 Surface and screen-level variables at $z_{meas} = 2\text{m}$

In this section the effect of surface energy budget noise on surface and screen-level scalars is investigated. In particular, we focus on a) potential temperature  $\theta_{z_{meas}}$  and b) specific humidity  $q_{z_{meas}}$  at screen level, and on c) land-surface temperature  $T_{s0}$  and d) soil temperature at a 5cm-depth  $T_{5cm}$ . This latter temperature is used as a simplified proxy to microwave brightness temperature in the L-band.

First, the standard deviation of these four variables is depicted on Figure 9. The standard deviation of all four variables exhibits a strong daily cycle, with a minimum at night, about one hour after the minimum of incoming radiation noise. The LST noise is maximum at around 1PM whereas the standard deviation of  $T_{5cm}$  is maximum much later, at 3PM, as it takes time for the incoming radiation noise to propagate into the soil, because of the soil elevated heat capacity and low conduction. Potential temperature and specific humidity noise has a peak located even later at about 4PM. This should be compared with the deterministic results of *Gentine et al.* [2009], which showed only a very slight delay between the deterministic response of land-surface temperature and air potential temperature, leading to a peak at around 1PM for both.

The difference between the stochastic and deterministic behavior of screen-level variables is further highlighted in Figure 10. The daily cycle of the standard deviation of screen-level variables relative to the deterministic value does not exhibit a daytime plateau

as in the case of soil temperature. Indeed the daytime response of the standard deviation of soil temperature is nearly proportional to the deterministic value. This result emphasizes the very different behavior of the ABL and the soil in response to the stochastic incoming radiation noise as opposed to the deterministic case. As evident on Figure 4, the response of potential temperature at screen level  $\theta_{z_{meas}}$  to deterministic incoming radiation lags that of land-surface temperature  $T_{s_0}$ . This effect is emphasized at high frequencies (low periods  $T$ ) because high-frequency changes in incoming radiation do not have sufficient time to propagate into the ABL. Since the power spectrum of the BB emphasizes high frequencies compared to the deterministic forcing, the ABL is not able to respond rapidly enough to the fast stochastic changes in incoming radiation. This will result in a delayed peak of the standard deviation of screen-level temperature compared to the deterministic case.

Figure 10 is also of great importance to determine the sensitivity of soil and screen-level variables to incoming radiation noise. First, Figure 10 a) shows that the impact of noise on screen-level potential temperature remains fairly small, in addition it is maximum and relatively constant throughout daytime. Indeed the ratio of its standard deviation on the deterministic value attains a maximum value of only 0.2 %, or 0.6 K (see Figure 9 a). Therefore screen-level temperature is relatively insensitive to incoming radiation noise, because this latter has difficulty propagating far away from the surface. As emphasized in *Gentine et al.* [2009], the ABL temperature acts as a low-pass filter, thus damping high-frequency, weather, noise.

Finally the inspection of the spectral repartition of the noise on screen-level potential temperature can be highlighted using the *RRE*, as shown on Figure 11. The contribution of the harmonics is small for any period  $T$ , this underscores the principal contribution of the mean-daily noise to the total variability. In consequence, surface energy budget noise is mostly present in the form of a daily bias in the screen-level temperature. This suggests that the use of anomalies of potential temperature at screen level would further reduce the

impact of incoming radiation noise. Moreover the *RRE* is almost negligible for periods below 6 hours, implying that acquisition of screen-level air temperature at a 6h time-step is able to almost fully reduce the effect of incoming radiation noise as well as to capture the daily cycle of the land surface state. In this respect, the assimilation scheme introduced by *Mahfouf* [1991] ,with a 6h time step, is optimal in terms of temporal acquisition resolution to reduce screen-level temperature variability.

Furthermore Figure 12 depicts the correlation of screen-level potential temperature with turbulent heat fluxes at 8AM, 12PM and 4PM. Sensible heat flux noise is only slightly correlated with screen-level temperature. As expected, sensible heat flux quickly responds to land-surface temperature changes triggered by surface energy budget noise (see next section). Yet screen-level temperature only experience an attenuated and (slightly) delayed version of this surface modification because of the strong "conductivity" and low heat capacity of the ABL. Because of this latter ABL properties, turbulent heat fluxes propagate almost instantaneously throughout the ABL and are in quasi steady state. As a result the instantaneous correlation between sensible heat flux and screen-level temperature is relatively small. Latent heat flux is more correlated with potential temperature, in our slightly water-limited case. An increase in incoming radiation leads to a land-surface temperature rise, thus intensifying both sensible and latent heat flux. This is accompanied by a rise of the lower ABL potential temperature, which creates a negative feedback on sensible heat flux, as this latter results from the temperature difference between the land surface and the lower ABL temperature. As specific humidity is a passive scalar, it exerts almost no feedback on the lower ABL potential temperature. Since there is no feedback, the rise in potential temperature, induced by sensible heat increase, is more strongly correlated with the increase in latent heat. This represents an important result: potential temperature at screen level is a better indicator of latent heat rather than sensible heat in non-water-limited regimes. This results should be further confirmed in various meteorological conditions.

Screen-level specific humidity, on the other hand, behaves much differently. The incoming radiation noise has a very strong effect on specific humidity with a peak of the error relative to the deterministic value of the order of 5%, see Figure 10. Indeed as emphasized by *Albertson and Parlange* [1999], specific humidity, which acts as a passive scalar, exerts little feedbacks on the ABL field contrary to air temperature. Moreover, the nonlinearity of specific humidity at the land surface induces a strong high-frequency response to land-surface temperature changes. Our result gives theoretical underpinning to the observed or assumed difficulty to operationally use specific humidity as a reliable variable in a data assimilation scheme [see *Hess*, 2001]. This suggests that specific humidity is very sensitive to radiation noise. This also serves as one explanation for the erratic aspect of specific humidity, often missing any clear diurnal cycle contrary to air temperature. It is unfortunate that specific humidity be a poor indicator of the land-surface state because it tends to blend lower than air temperature (and turbulent heat fluxes) over heterogeneous surfaces [see *Albertson and Parlange*, 1999]. This latter property would have been useful, as screen-level humidity measured at the very bottom of the ABL could have served as an indicator of the integrated land-surface state over a relatively large area, induced by its footprint.

### **Soil temperatures**

Figure 9 and 10 show that noise has a stronger repercussion on soil temperatures than on screen-level temperature. The standard deviation for both land-surface and 5cm-deep temperature exhibits a daytime-peak plateau of about 0.4 % or 1.25 K. This emphasizes that soil temperatures are strongly influenced by incoming radiation noise. Moreover the change in soil conductivity and heat capacity, which could be induced by soil water content changes (not shown) have very little impact on this result. This has important consequence for the use of brightness temperature in an assimilation scheme, as these temperatures will

be very much influenced by inaccurate specification of incoming radiation at the land surface. However the study of the *RRE* of the noise of both temperatures, Figure 11, gives crucial understanding of the spectral repartition of the noise. Indeed, the land-surface temperature noise is shown to be mostly present as a steady-state term, since the harmonics contribute to only 25% to the total noise. This again emphasizes that land-surface temperature and thus infrared brightness temperature will be very much influenced by high-frequency incoming radiation noise i.e. weather noise. Since the *RRE* for a period of 12 hours is of the order of 5% and less than 1% for a period of 6 hours, it suggests that the influence of incoming radiation noise could be reduced when acquired at a 6h-resolution.

Inspection of Figure 13 shows that land-surface temperature is almost perfectly correlated with the turbulent heat fluxes in the ABL. As already discussed, the heated land surface leads to an increase of land-surface temperature that rapidly propagates into the ABL. Therefore the turbulent heat fluxes in the ABL almost instantaneously respond to the land-surface modifications. This will lead to a very strong correlation between turbulent fluxes and land-surface temperature. In our slightly water-limited case ( $\beta = 0.6$ ), the surface is in an energy-limited case. If the surface experiences moisture stress, there will be little adjustment in evapotranspiration induced by changes in land-surface temperature. This will lead to a much lower correlation between  $\lambda E$  and  $T_{s_0}$ , which could even vanish in extremely dry cases. Finally, we can state that infrared brightness temperature would be the most reliable estimates of the instantaneous land-surface and ABL state, yet this would require temporal resolutions and precisions that are not compatible with common atmospheric conditions (e.g. no clouds at each acquisition).

The spectral repartition of noise on the 5cm-deep temperature displays a contrasting result, as seen on Figure 11. Indeed its *RRE* is small (less than 8% for periods greater than 12 hours) thus pointing out that incoming radiation mostly result in long-term noise (greater than 12 hours). Moreover this means that the noise component in  $T_{5cm}$  is mostly

present as a random bias. This two results are of great interest for the use of microwave brightness temperatures because they suggest that using anomalies of brightness temperature to remove random bias, [as in *Reichle et al., 2008*], along with a 12h-acquisition repetition would lead to a highly reduced impact of incoming radiation errors. Moreover as emphasized by Figure 10, images acquisition in the early morning and late afternoon, would reduce the impact of incoming radiation variability. This acquisition times are in good agreement with SMOS and SMAP overpass times [*Kerr et al., 2001; Barre et al., 2008; Cros et al., 2008*]. Our results further confirms that the chosen acquisition time of those sensors will diminish errors induced by land-surface incoming radiation. Yet because of the diurnal cycle of incoming radiation in Northern latitudes, the late-afternoon sampling errors would be reduced in the wintertime and increased in the summertime. As the variability of  $T_{5cm}$  is reduced after sunset (6.30 PM in this experiment), microwave brightness temperature would be even less influenced by incoming radiation variability when sampled after that time. We wish to emphasize that the model used in this study is a simplified version of the system. A more detailed and precise determination of the optimal sampling satellite time could be achieved with this methodology applied to state-of-the-art numerical coupled land-atmosphere model.

## 6.6 Inverse problem

In this final section, the authors are investigating the inverse problem, i.e. what is the link between observable variables and identifiability of the land-surface energy partitioning. Figure 14 shows that net radiation as well as surface turbulent heat fluxes are very much correlated with the instantaneous value of land-surface temperature as well as the temperature at a 5cm-depth. This results stresses that these two temperatures are very good indicator of the instantaneous land-surface partitioning and consequently of the land-

surface state (fluxes, temperatures, soil water content...). However as previously discussed, the use of land-surface temperature in a data assimilation scheme will be complicated by the need for very high-temporal resolution, which is not compatible with sampling possibilities. Temperature at 5 cm within the soil is also an accurate estimator of the land-surface energy partitioning as it is very much correlated with land-surface heat fluxes. In addition the temporal resolution of soon-to-be launched sensors, SMOS and SMAP, is compatible with both a good assimilation quality and inferment of land-surface partitioning. This constitutes an important advantage of this new generation of microwave sensors.

As expected, screen-level potential temperature is less correlated with the instantaneous land-surface energy fluxes. It indeed takes time for the land-surface "information" to propagate into the lower ABL scalars, as emphasized earlier. Consequently, the assimilation of screen-level temperature alone will not be an accurate measure of the instantaneous land-surface partitioning. Nevertheless, screen-level temperature has been shown to provide strong insights on the land-surface state, through its diurnal cycle and coupling with the land surface. As a result, the use of screen-level temperature in current operational assimilation scheme remains of great importance, as the temporal frequency of acquisition of current sensors is compatible with its operational use, as highlighted previously. This result also suggests that screen-level temperature is a significant observable and that data-assimilation schemes based on coupled land-ABL models have a strong advantage over stand-alone land-surface models to estimate the surface energy partitioning in a data assimilation scheme. Indeed the information they contain can be used in conjunction with the coupling, which induces strong constrain from the land-surface energy budget on the ABL state and in particular on screen-level temperature. Moreover screen-level temperature provide land-surface information at a higher spatial resolution than L-band sensors, since the extend of their footprint is generally much smaller than that of L-band sensors.

Consequently, the authors suggest that any future operational data assimilation scheme

should use a synergy of both L-band microwave brightness temperature and screen-level temperature within a coupled land-atmosphere model, in order to better estimate the surface state and in particular the diurnal energy partitioning at the land surface. This statement further confirms the idea of *Seuffert et al.* [2004], who tried to assimilate microwave brightness temperature and screen-level temperature, with current available microwave sensors.

## 6.7 Conclusion

In this study we present a new methodology to estimate the impact of surface energy budget noise on the soil and the ABL. We use a simplified linearized land-atmosphere model forced by surface energy budget noise, in the form of a daily brownian bridge. This simple procedure allows to analytically investigate the impact of noise on the land-surface energy partitioning as well as on land-surface and screen-level variables, which can be used in an operational land-surface data assimilation scheme.

Within this framework, soil heat flux at the land-surface was shown to mostly concentrate high-frequency incoming radiation noise whereas turbulent heat fluxes were mostly impacted by low daily frequencies. Moreover because of the constrained periodicity, soil heat flux was shown to be daily-unbiased, leading to a constant standard deviation throughout the day. Turbulent heat fluxes and longwave outgoing radiation on the opposite side are mostly impacted through a random daily bias.

In a second stage screen-level temperature and specific humidity were demonstrated to display very different responses to surface energy budget noise. Specific humidity is impacted by this noise. In contrast, screen-level temperature acquired at a 6h-resolution seems to yield much information about the land-surface state and is only slightly impacted by incoming radiation noise.



Finally, infrared and 5-cm deep temperatures are very good indicators of the land-surface instantaneous state. However land-surface temperature demonstrates strong sensitivity to high-frequency noise and its operational use is complicated by the presence of clouds. The acquisition time (6AM and 6PM) of future microwave L-band sensors (SMOS and SMAP) seem to strongly reduce the impact of incoming radiation noise and to provide very important knowledge on the land-surface energy partitioning and surface state.

Finally, this study suggests using the synergy of screen-level temperature with soonly-available microwave L-band brightness temperature in order to obtain a robust estimate of the surface state (e.g. soil moisture).

The present study has inherent limitations owing to the reliance on a simplified linearized model. The results highlighted in this study should thereby be further investigated in various meteorological and surface conditions along with a more detailed land-atmosphere coupled model. In particular, the numerical resolution of a coupled land-atmosphere system using a state of the art model along with more precise characterization of surface energy budget noise would help obtain reliable estimates of the covariance matrices required in a land-surface assimilation scheme. It will also give a more precise characterization of the diurnal cycle of the land-surface errors, which in turn could help determine the best sampling times of future satellites.

## List of variables and units

Variable	Definition	Value/Units
$\alpha$	Albedo of the land surface	0.16 (–)
$\beta$	Beta parameterization of latent heat flux as introduced by Deardorff (1978)	0.6 (–)
$\epsilon_s$	Emissivity of the surface	0.99 (–)
$\gamma$	Gamma constant	0.577215 (–)
$\gamma_T$	$\frac{\partial q_s}{\partial T}(T, P_0)$	kg kg <sup>-1</sup> K <sup>-1</sup>
$\lambda$	Latent heat of vaporisation at triple point	$2.45 \cdot 10^6$ J kg <sup>-1</sup>
$\lambda_s$	Soil thermal conductivity	W m <sup>-1</sup> K <sup>-1</sup>
$\lambda E(z)$	Latent heat flux at height $z$	W m <sup>-2</sup>
$\lambda E_h$	Latent heat flux at the land-surface, i.e. at canopy height $h$	W m <sup>-2</sup>
$\omega$	Angular frequency of the harmonic	rad s <sup>-1</sup>
$\Omega$	Rotation rate of the Earth	rad s <sup>-1</sup>
$\omega_0$	Fundamental pulsation $2\pi/T$	$7.29 \cdot 10^{-5}$ rad s <sup>-1</sup>
$\phi$	Latitude of Marrakech	31°37'N
$\phi_\theta$	Turbulent heat flux of potential temperature $\phi_\theta = \overline{w'\theta'} = \frac{H}{\rho C_p}$	K m s <sup>-1</sup>
$\phi_q$	Turbulent heat flux of specific humidity $\phi_q = \overline{w'q'} = \frac{\lambda E}{\rho \lambda}$	kg kg <sup>-1</sup> m s <sup>-1</sup>
$\rho$	Density of the air	1.2 kg m <sup>-3</sup>
$\sigma$	Volatility of the brownian bridge such that $\sigma\sqrt{T}/2 = 25\text{Wm}^{-2}$	W m <sup>-2</sup> s <sup>-1/2</sup>

$\theta$	Mean potential temperature in the boundary layer	K
$A$	Available energy at the land surface	$\text{W m}^{-2}$
$B_{T_{day}}$	Brownian bridge at the land surface	$\text{W m}^{-2}$
$\widetilde{B}_n$	Fourier harmonic of the Brownian bridge	$\text{W m}^{-2}$
$C_s$	Soil heat capacity	$1.42 \cdot 10^6 \text{ J m}^{-3} \text{ K}^{-1}$
$C_p$	Specific heat of air at constant pressure	$1012 \text{ J kg}^{-1} \text{ K}^{-1}$
$d$	Displacement height	m
$Day$	Duration of a day in s	86400 s
$EF$	Evaporative fraction at the land surface	(-)
$f$	Coriolis parameter	(-)
$G$	Ground heat flux	$\text{W m}^{-2}$
$G_0$	Ground heat flux at the land surface	$\text{W m}^{-2}$
$h$	Vegetation height	0.45 m
$H(z)$	Sensible heat flux at height $z$	$\text{W m}^{-2}$
$H_h$	Sensible heat flux at the land surface i.e. at canopy height $h$	$\text{W m}^{-2}$
$K_s$	Soil thermal diffusivity	$2.5 \cdot 10^{-7} \text{ m}^2 \text{ s}^{-1}$
$k$	Von Karman constant	0.4 (-)
$K_H$	Eddy diffusion for heat	$\text{m}^2 \text{ s}^{-1}$
$K_V$	Eddy diffusion for water vapor	$\text{m}^2 \text{ s}^{-1}$

$I_{\downarrow}$	Incoming radiation at the land surface	$\text{W m}^{-2}$
$P_0$	Reference pressure	$1.01310^6 \text{ Pa}$
$q$	Mean specific humidity	$\text{kg kg}^{-1}$
$q_*$	Specific humidity at saturation	$\text{kg kg}^{-1}$
$r_{ac}$	Canopy aerodynamic resistance	$50 \text{ s m}^{-1}$
$S$	Stefan-Boltzmann's constant	$5.67 \cdot 10^{-8} \text{ W m}^{-2} \text{ K}^{-4}$
$R_n$	Net radiation at the land surface	$500 \text{ W m}^{-2}$
$T_{day}$	Time period of the whole experiment $T = Day$	$86400 \text{ s}$
$T_s$	Soil temperature	$\text{K}$
$T_{surf}$	Soil surface temperature	$\text{K}$
$T_{day}$	Duration of a day	$86400 \text{ s}$
$T_{deep}$	Soil temperature at infinite depth	$\text{K}$
$u_*$	Friction velocity	$0.2 \text{ m s}^{-1}$
$W_T$	Brownian motion at the land surface	$\text{W m}^{-2}$
$z$	Height/Depth	$\text{m}$
$z_i$	Boundary-layer height	$\text{m}$
$z_1$	Height of mean values specification $z_1 = z_i$	$\text{m}$
$z_{meas}$	Measurement height	$2 \text{ m}$

# Bibliography

Alapaty, K., N. Seaman, D. Niyogi, and A. Hanna, Assimilating surface data to improve the accuracy of atmospheric boundary layer simulations, *Journal of Applied Meteorology*, *40*, 2068–2082, 2001.

Albertson, J., and M. Parlange, Natural integration of scalar fluxes from complex terrain, *Advances in Water Resources*, *23*, 239–252, 1999.

Barre, H. M. J. P., B. Duesmann, and Y. H. Kerr, Smos: The mission and the system, *IEEE Transactions on Geoscience and Remote Sensing*, *46*, 587–593, 2008.

Bastiaanssen, W., M. Menenti, R. Feddes, and A. Holtslag, A remote sensing surface energy balance algorithm for land (sebal) - 1. formulation, *Journal of Hydrology*, *213*, 198–212, 1998.

Boegh, E., H. Soegaard, and A. Thomsen, Evaluating evapotranspiration rates and surface conditions using landsat tm to estimate atmospheric resistance and surface resistance, *Remote Sensing of Environment*, *79*, 329–343, 2002.

Boni, G., F. Castelli, and D. Entekhabi, Sampling strategies and assimilation of ground temperature for the estimation of surface energy balance components, *IEEE Transactions on Geoscience and Remote Sensing*, *39*, 165–172, 2001a.

- Boni, G., D. Entekhabi, and F. Castelli, Land data assimilation with satellite measurements for the estimation of surface energy balance components and surface control on evaporation, *Water Resources Research*, *37*, 1713–1722, 2001b.
- Bouttier, F., J. Mahfouf, and J. Noilhan, Sequential assimilation of soil-moisture from atmospheric low-level parameters .1. sensitivity and calibration studies, *Journal of Applied Meteorology*, *32*, 1335–1351, 1993a.
- Bouttier, F., J. Mahfouf, and J. Noilhan, Sequential assimilation of soil moisture from atmospheric low-level parameters .2. implementation in a mesoscale model, *Journal of Applied Meteorology*, *32*, 1352–1364, 1993b.
- Bouyssel, F., V. Casse, and J. Pailleux, Variational surface analysis from screen level atmospheric parameters, *Tellus A*, *51*, 453–468, 1999.
- Burke, E., W. Shuttleworth, and R. Harlow, Using micro-sweat to model microwave brightness temperatures measured during sgp97, *Journal of Hydrometeorology*, *4*, 460–472, 2003.
- Callies, U., A. Rhodin, and D. Eppel, A case study on variational soil moisture analysis from atmospheric observations, *Journal of Hydrology*, *213*, 95–108, 1998.
- Caparrini, F., F. Castelli, and D. Entekhabi, Mapping of land-atmosphere heat fluxes and surface parameters with remote sensing data, *Boundary-Layer Meteorology*, *107*, 605–633, 2003.
- Caparrini, F., F. Castelli, and D. Entekhabi, Estimation of surface turbulent fluxes through assimilation of radiometric surface temperature sequences, *Journal of Hydrometeorology*, *5*, 145–159, 2004a.

- Caparrini, F., F. Castelli, and D. Entekhabi, Variational estimation of soil and vegetation turbulent transfer and heat flux parameters from sequences of multisensor imagery, *Water Resources Research*, 40, W12,515, 2004b.
- Castelli, F., D. Entekhabi, and E. Caporali, Estimation of surface heat flux and an index of soil moisture using adjoint-state surface energy balance, *Water Resources Research*, 35, 3115–3125, 1999.
- Cros, S., A. Chanzy, M. Weiss, T. Pellarin, J.-C. Calvet, and J.-P. Wigneron, Synergy of smos microwave radiometer and optical sensors to retrieve soil moisture at global scale, *IEEE Transactions on Geoscience and Remote Sensing*, 46, 835–845, 2008.
- Deardorff, J., Efficient prediction of ground surface temperature and moisture, with inclusion of a layer of vegetation, *J Geophys Res-Oc Atm*, 83, 1889–1903, 1978.
- Douville, H., P. Viterbo, J. Mahfouf, and A. Beljaars, Evaluation of the optimum interpolation and nudging techniques for soil moisture analysis using fife data, *Monthly Weather Review*, 128, 1733–1756, 2000.
- Duchemin, B., et al., Monitoring wheat phenology and irrigation in central morocco: On the use of relationships between evapotranspiration, crops coefficients, leaf area index and remotely-sensed vegetation indices, *Agricultural Water Management*, 79, 1–27, 2006.
- Entekhabi, D., H. Nakamura, and E. Njoku, Solving the inverse problem for soil moisture and temperature profiles by sequential assimilation of multifrequency remotely sensed observations, *IEEE Transactions on Geoscience and Remote Sensing*, 32, 438–448, 1994.
- Entekhabi, D., E. Njoku, P. O'Neill, M. Spencer, T. Jackson, J. Entin, E. Im, and K. Kellogg, The Soil Moisture Active/Passive Mission (SMAP), in *IEEE International Geoscience and Remote Sensing Symposium, 2008. IGARSS 2008*, vol. 3, 2008.

- Entekhabi, D., et al., The hydrosphere state (Hydros) satellite mission: An Earth system pathfinder for global mapping of soil moisture and land freeze/thaw, *IEEE Transactions on Geoscience and Remote Sensing*, 42, 2184–2195, 2004.
- et al., A. C., An integrated modelling and remote sensing approach for hydrological study in arid and semi-arid regions: the sudmed programme, 2008.
- Friedl, M., Modeling land surface fluxes using a sparse canopy model and radiometric surface temperature measurements, *Journal of Geophysical Research-Atmospheres*, 100, 25,435–25,446, 1995.
- Garratt, J., *The atmospheric boundary layer*, Cambridge University Press Cambridge, 1992.
- Gentine, P., D. Entekhabi, A. Chehbouni, G. Boulet, and B. Duchemin, Analysis of evaporative fraction diurnal behaviour, *Agricultural and Forest Meteorology*, 143, 13–29, 2007.
- Gentine, P., D. Entekhabi, and J. Polcher, Spectral behaviour of a coupled land-surface and boundary-layer system, *Boundary-Layer Meteorology*, p. In press., 2009.
- Giard, D., and E. Bazile, Implementation of a new assimilation scheme for soil and surface variables in a global nwp model, *Monthly Weather Review*, 128, 997–1015, 2000.
- Gillies, R., T. Carlson, J. Cui, W. Kustas, and K. Humes, A verification of the 'triangle' method for obtaining surface soil water content and energy fluxes from remote measurements of the normalized difference vegetation index (ndvi) and surface radiant temperature, *International Journal of Remote Sensing*, 18, 3145–3166, 1997.
- Hess, R., Assimilation of screen level observations by variational soil moisture analysis, *Meteorology and Atmospheric Physics*, 77, 145–154, 2001.
- Jackson, T., D. Le Vine, A. Hsu, A. Oldak, P. Starks, C. Swift, J. Isham, and M. Haken, Soil moisture mapping at regional scales using microwaveradiometry: the Southern Great



- Plains Hydrology Experiment, *IEEE transactions on geoscience and remote sensing*, *37*, 2136–2151, 1999.
- Jiang, L., and S. Islam, A methodology for estimation of surface evapotranspiration over large areas using remote sensing observations, *Geophysical Research Letters*, *26*, 2773–2776, 1999.
- Kerr, Y., P. Waldteufel, J. Wigneron, J. Martinuzzi, J. Font, and M. Berger, Soil moisture retrieval from space: the Soil Moisture and OceanSalinity (SMOS) mission, *IEEE transactions on Geoscience and remote sensing*, *39*, 1729–1735, 2001.
- Kustas, W., and C. Daughtry, Estimation of the soil heat-flux net-radiation ratio from spectral data, *Agricultural and Forest Meteorology*, *49*, 205–223, 1990.
- Kustas, W., K. Humes, J. Norman, and M. Moran, Single- and dual-source modeling of surface energy fluxes with radiometric surface temperature, *Journal of Applied Meteorology*, *35*, 110–121, 1996.
- Kustas, W., T. Jackson, A. French, and J. MacPherson, Verification of patch- and regional-scale energy balance estimates derived from microwave and optical remote sensing during sgp97, *Journal of Hydrometeorology*, *2*, 254–273, 2001.
- Lettau, H., Theory of surface temperature and heat-transfer oscillations near level ground surface., *EOS*, *32*, 189D200, 1951.
- Mahfouf, J., Analysis of soil-moisture from near-surface parameters - a feasibility study, *Journal of Applied Meteorology*, *30*, 1534–1547, 1991.
- Margulis, S., D. McLaughlin, D. Entekhabi, and S. Dunne, Land data assimilation and estimation of soil moisture using measurements from the southern great plains 1997 field experiment, *Water Resources Research*, *38*, 1299, 2002.

- Mecikalski, J., G. Diak, M. Anderson, and J. Norman, Estimating fluxes on continental scales using remotely sensed data in an atmospheric-land exchange model, *Journal of Applied Meteorology*, *38*, 1352–1369, 1999.
- Moran, M., T. CLARKE, Y. Inoue, and A. Vidal, Estimating crop water-deficit using the relation between surface-air temperature and spectral vegetation index, 1994.
- Njoku, E., and D. Entekhabi, Passive microwave remote sensing of soil moisture, *Journal of Hydrology*, *184*, 101–129, 1996.
- Reichle, R. H., W. T. Crow, R. D. Koster, H. O. Sharif, and S. P. P. Mahanama, Contribution of soil moisture retrievals to land data assimilation products, *Geophys Res Lett*, *35*, L01,404, 2008.
- Rhodin, A., F. Kucharski, U. Callies, D. Eppel, and W. Wergen, Variational analysis of effective soil moisture from screen-level atmospheric parameters: Application to a short-range weather forecast model, *Quarterly Journal of the Royal Meteorological Society*, *125*, 2427–2448, 1999.
- Ruggiero, F., K. Sashegyi, R. Madala, and S. Raman, The use of surface observations in four-dimensional data assimilation using a mesoscale model, *Monthly Weather Review*, *124*, 1018–1033, 1996.
- Schmugge, T., and T. Jackson, Mapping surface soil moisture with microwave radiometers, *Meteorology and Atmospheric Physics*, *54*, 213–223, 1994.
- Schmugge, T., W. Kustas, J. Ritchie, T. Jackson, and A. Rango, Remote sensing in hydrology, 2002.
- Seuffert, G., H. Wilker, P. Viterbo, M. Drusch, and J. Mahfouf, The usage of screen-level

- parameters and microwave brightness temperature for soil moisture analysis, *Journal of Hydrometeorology*, 5, 516–531, 2004.
- Stull, R., *An Introduction to Boundary Layer Meteorology*, Springer, 1988.
- Su, Z., The surface energy balance system (sebs) for estimation of turbulent heat fluxes, *Hydrology and Earth System Sciences*, 6, 85–99, 2002.
- van den Hurk, B., W. Bastiaanssen, H. Pelgrum, and E. van Meijgaard, A new methodology for assimilation of initial soil moisture fields in weather prediction models using meteosat and noaa data, *Journal of Applied Meteorology*, 36, 1271–1283, 1997.
- Wulfmeyer, V., Investigation of Turbulent Processes in the Lower Troposphere with Water Vapor DIAL and Radar–RASS, *Journal of the Atmospheric Sciences*, 56, 1055–1076, 1999.
- Young, G., Turbulence Structure of the Convective Boundary Layer. Part I. Variability of Normalized Turbulence Statistics, *Journal of the Atmospheric Sciences*, 45, 719–726, 1988.
- Zhan, X., W. Kustas, and K. Humes, An intercomparison study on models of sensible heat flux over partial canopy surfaces with remotely sensed surface temperature, *Remote Sensing of Environment*, 58, 242–256, 1996.

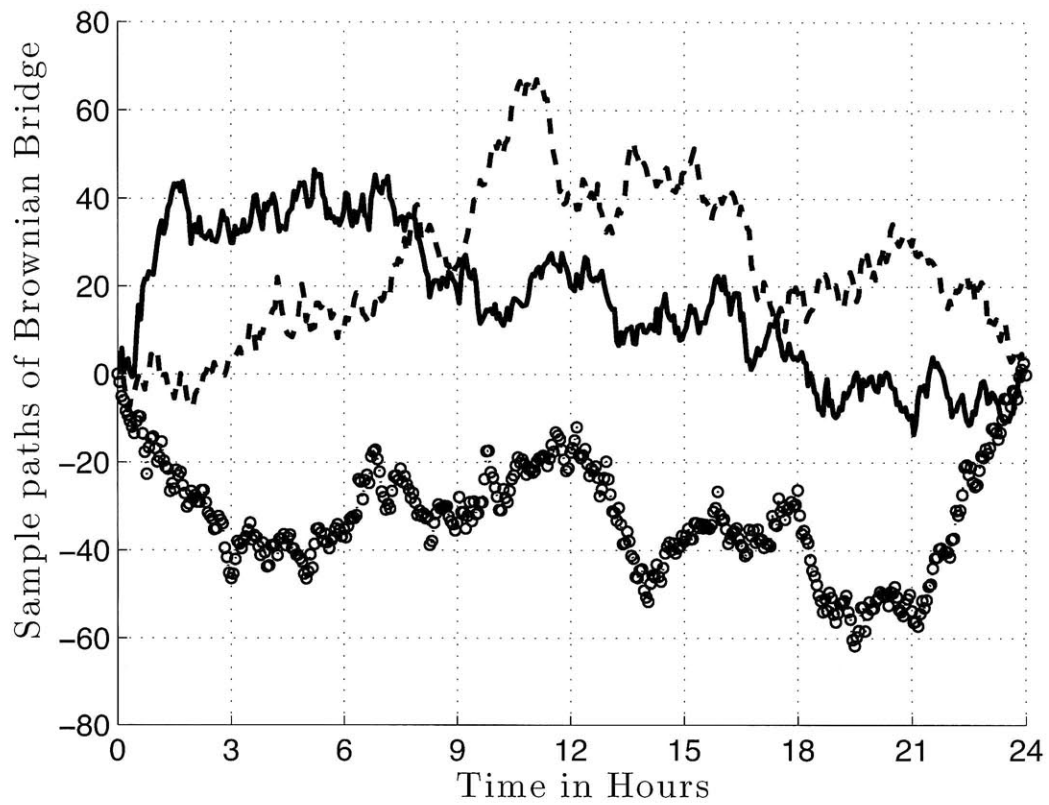


Figure 1: Three random trajectories of the brownian bridge, with 30-mn time step increments and standard deviation at noon  $\sigma\sqrt{T}/2 = 25 \text{ W m}^{-2}$

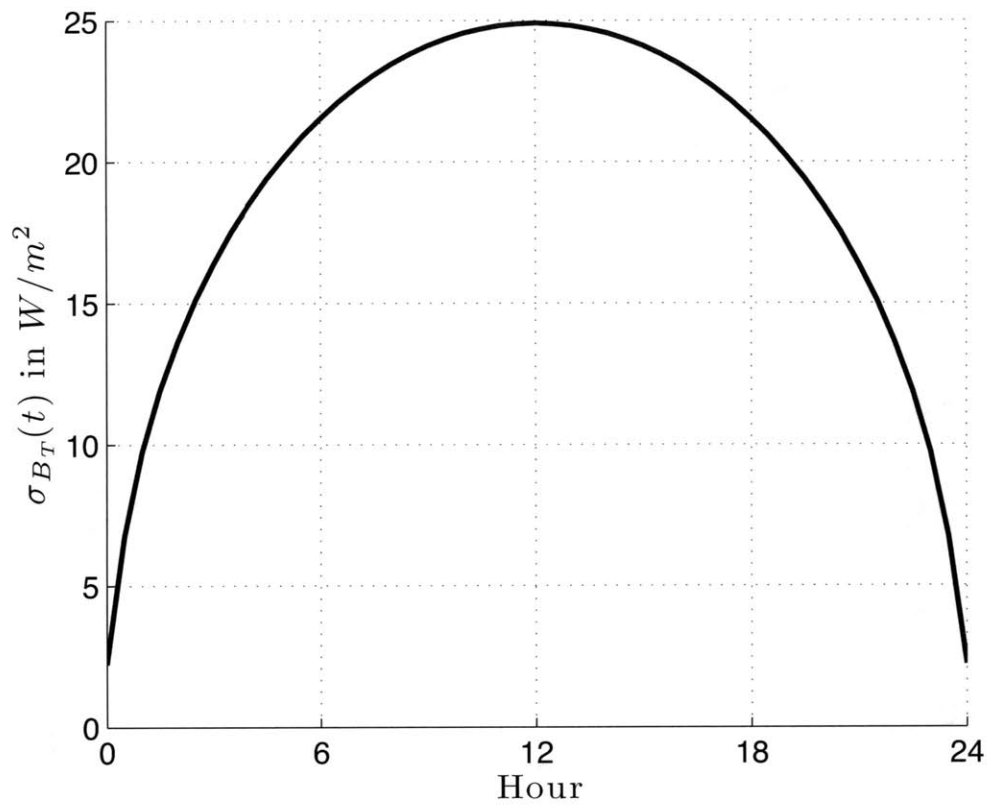


Figure 2: Standard deviation of brownian bridge for a maximum value at noon equal to  $\sigma\sqrt{T}/2 = 25 \text{ W m}^{-2}$

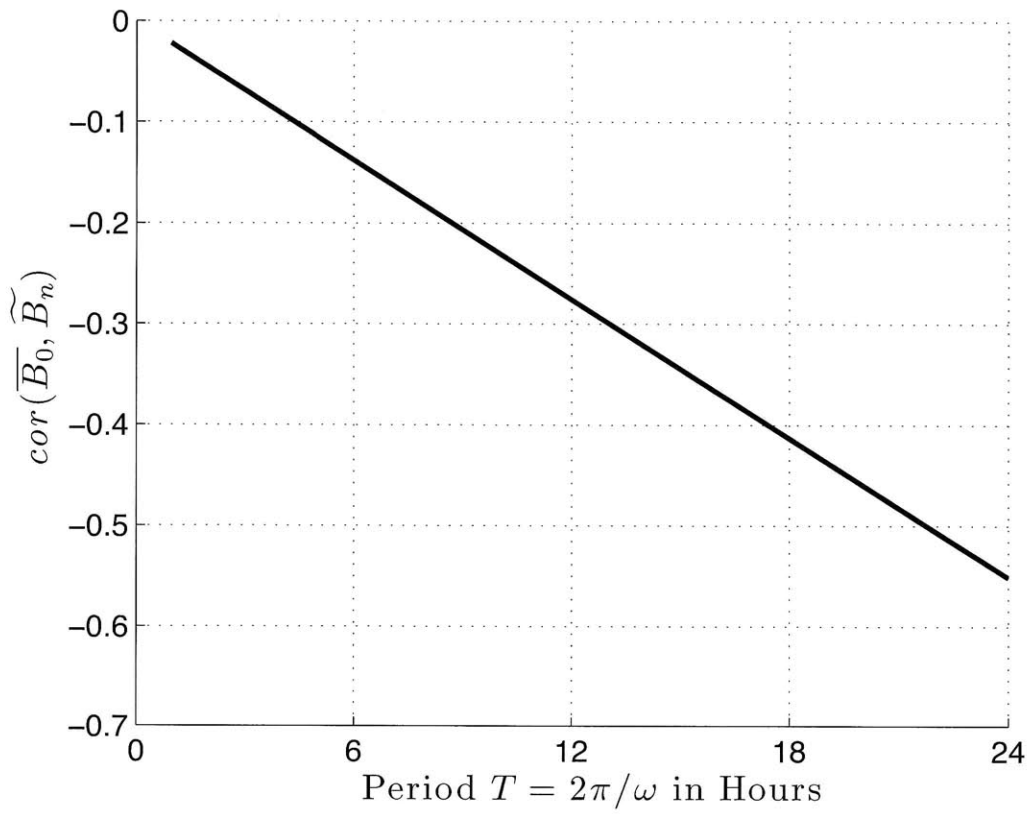


Figure 3: Correlation of the brownian bridge Fourier coefficients  $\widetilde{B}_n$  with the steady-state value  $\langle B_0 \rangle$  as a function of the harmonics period  $T$

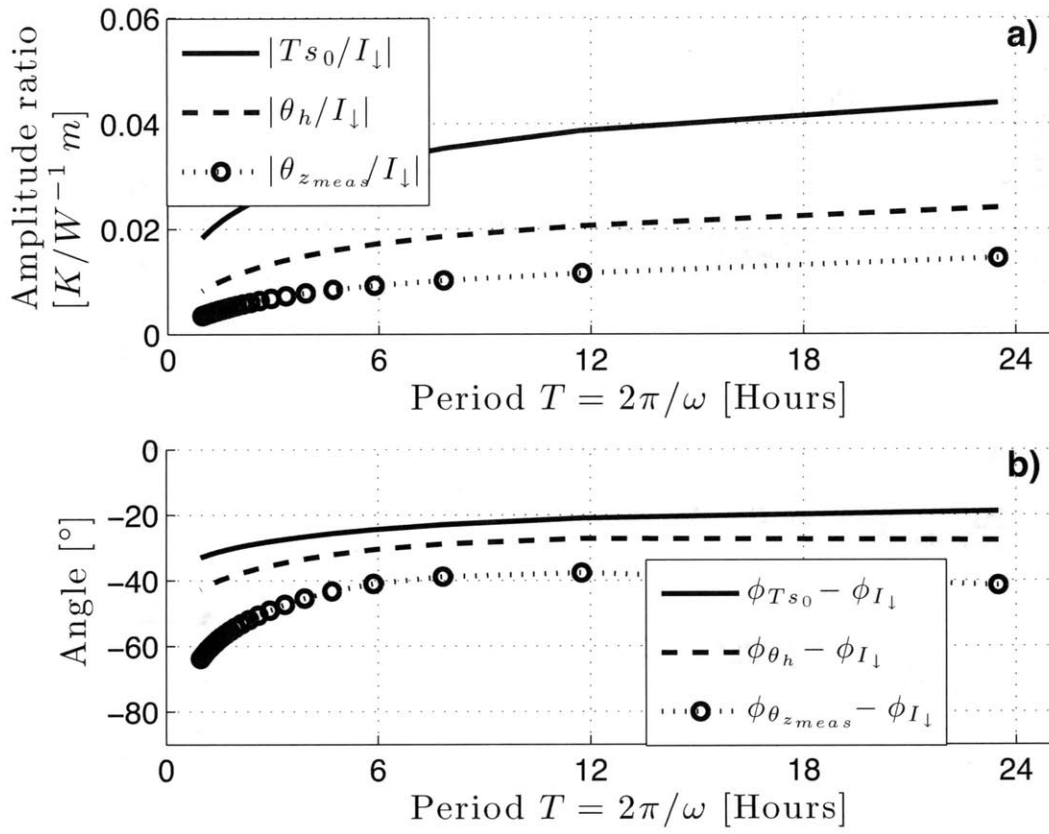


Figure 4: Deterministic spectral dependency of the amplitude (a) and phase (b) of the surface and screen-level temperatures as a function of the harmonics period  $T$

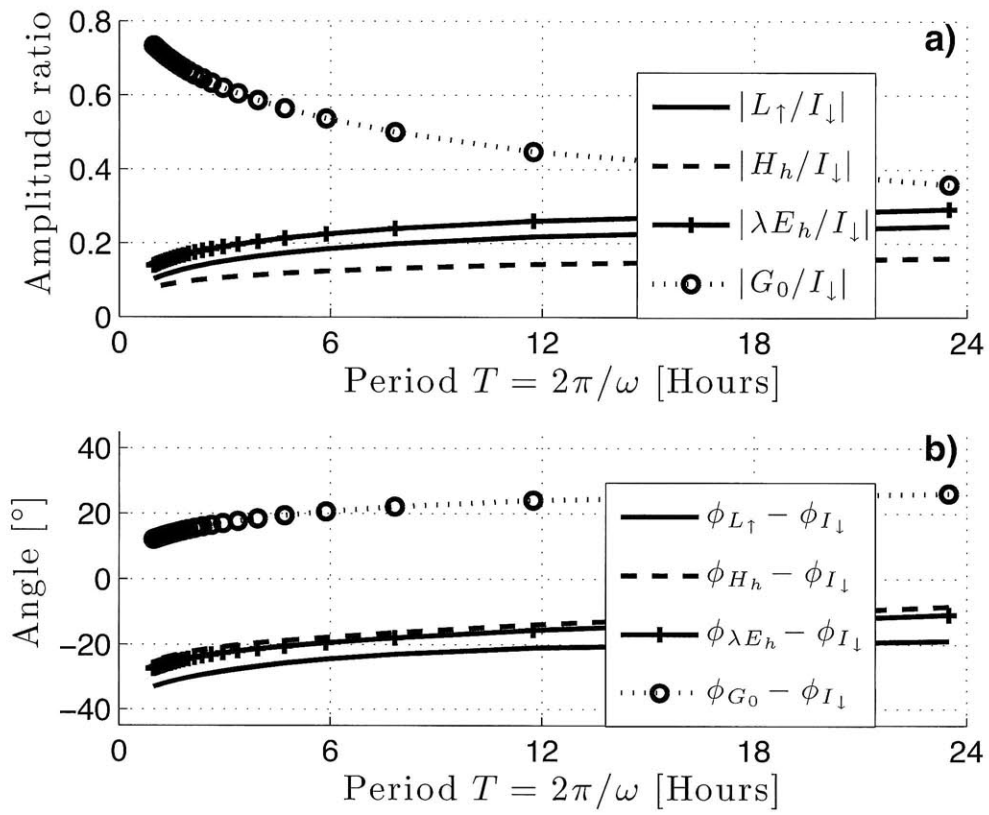


Figure 5: Deterministic spectral dependency of the amplitude (a) and phase (b) of the surface heat fluxes as a function of the harmonics period  $T$



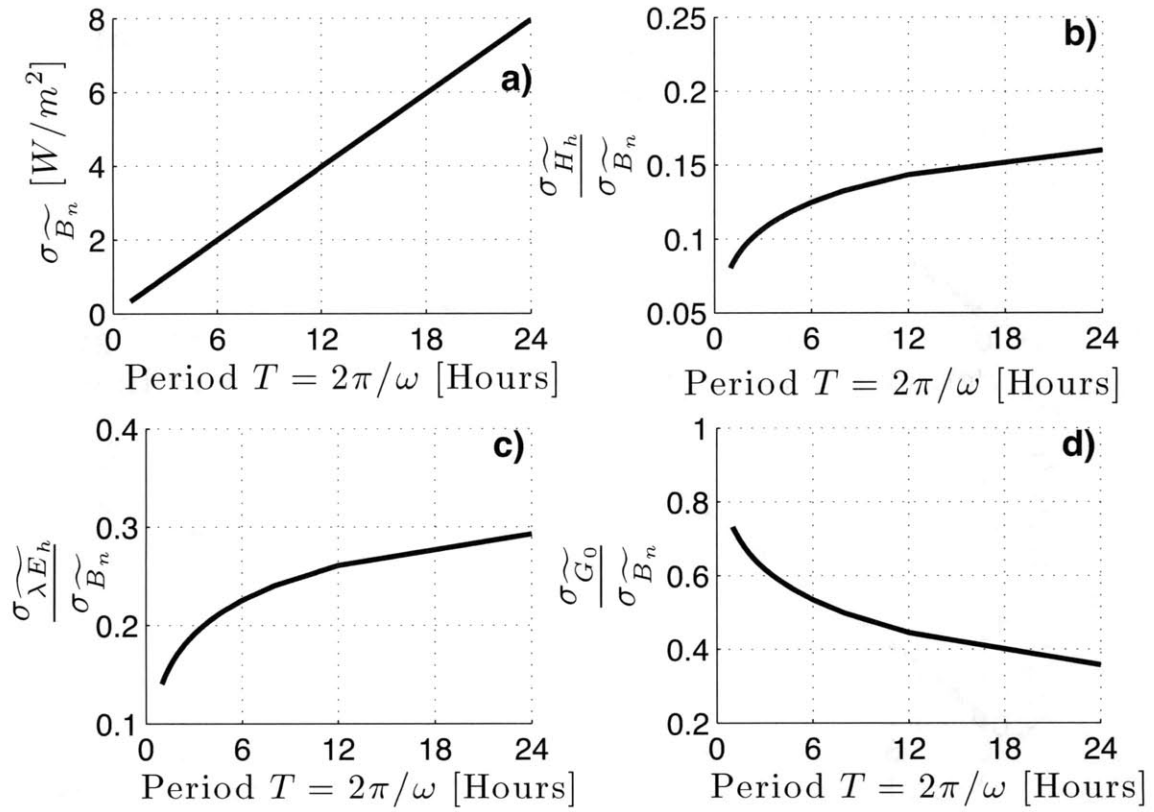


Figure 6: Standard deviation of a) brownian bridge, b) surface sensible heat flux, c) surface latent heat flux, d) surface soil heat flux relative to that of brownian bridge, as a function of the harmonics period  $T$

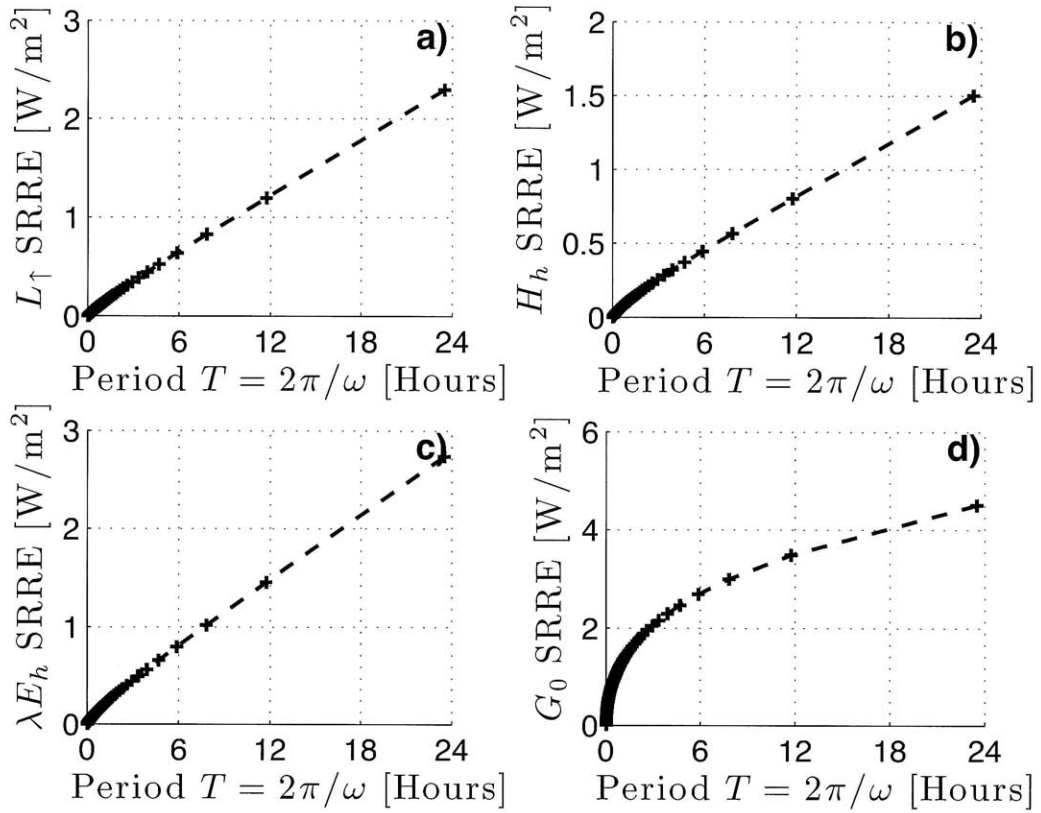


Figure 7: SRRE of a) surface longwave outgoing radiation, b) surface sensible heat flux, c) surface latent heat flux, d) surface soil heat flux as a function of the harmonics period  $T$

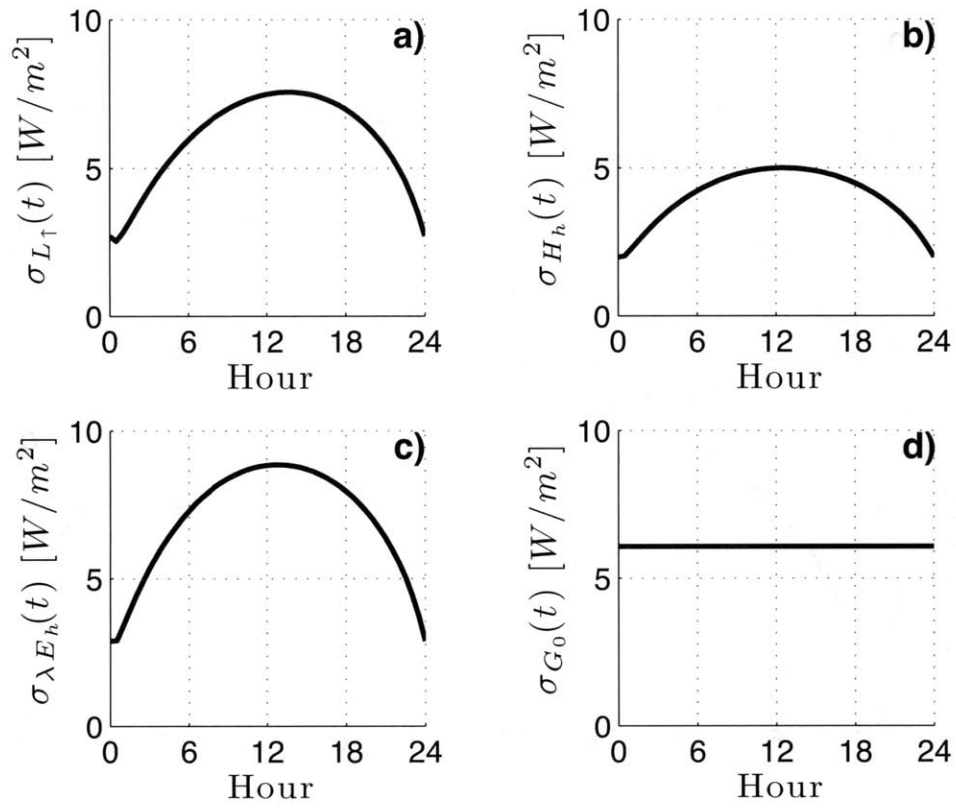


Figure 8: Standard deviation of a) surface longwave outgoing radiation, b) surface sensible heat flux, c) surface latent heat flux, d) surface soil heat flux as a function of time

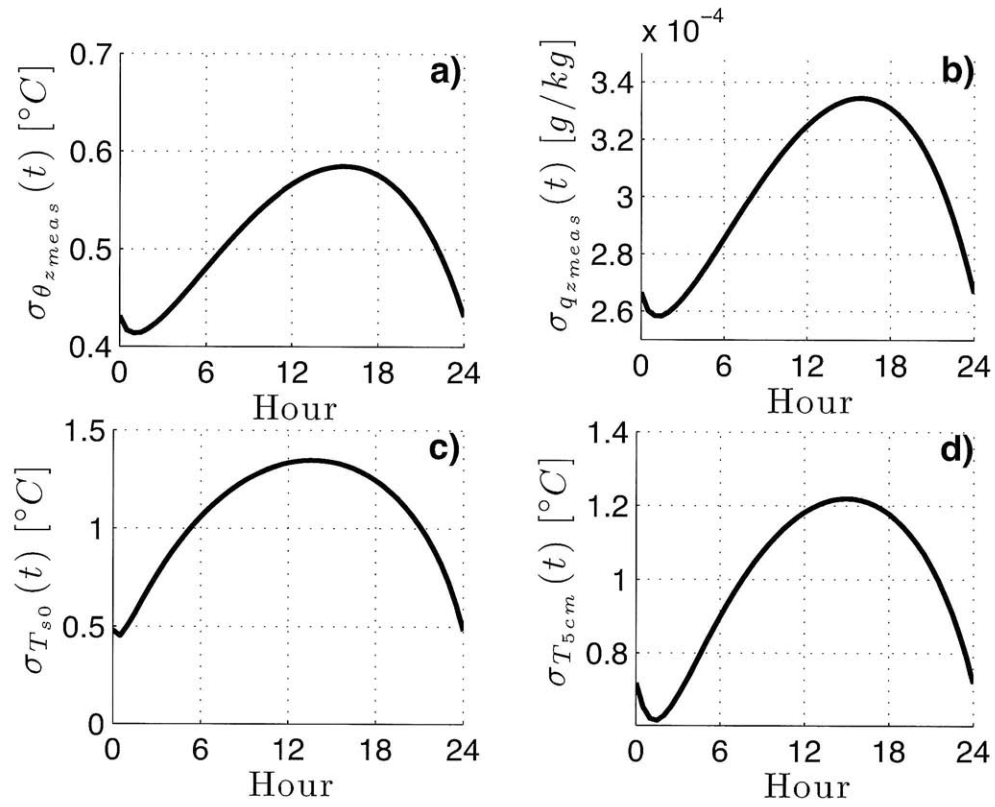


Figure 9: Standard deviation of a) potential temperature at 2m, b) specific humidity at 2m, c) land-surface temperature, d) soil temperature at 5cm as a function of time

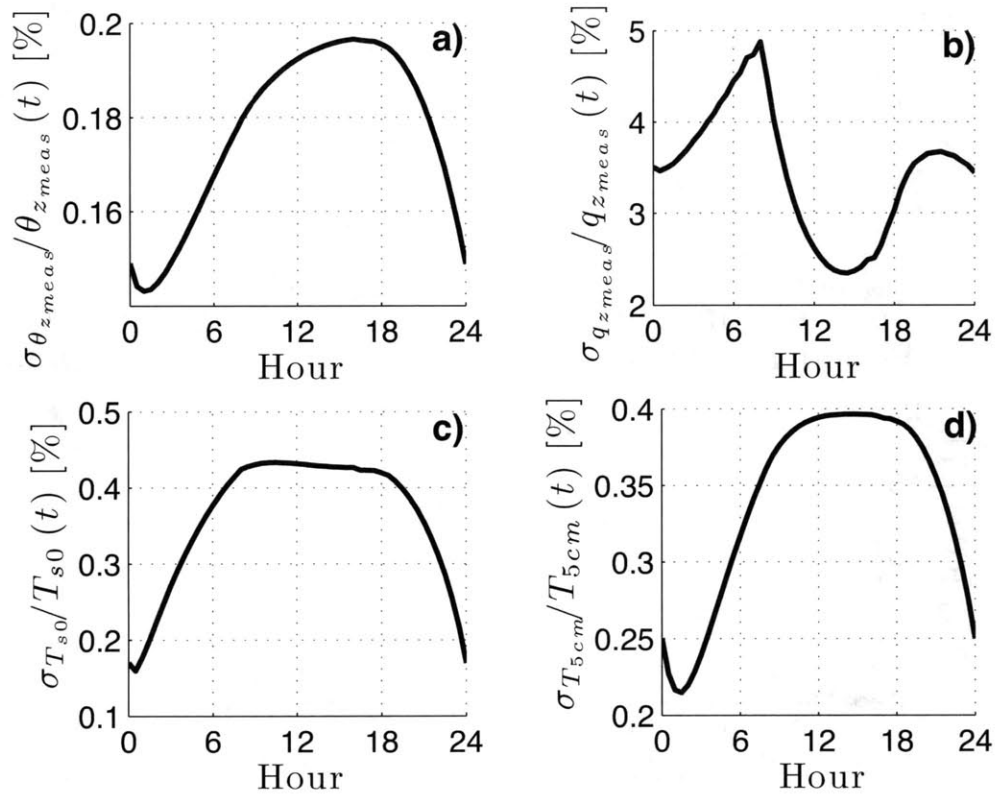


Figure 10: Coefficient of variation of a) potential temperature at 2m, b) specific humidity at 2m, c) land-surface temperature, d) soil temperature at 5cm relative to deterministic value as a function of time

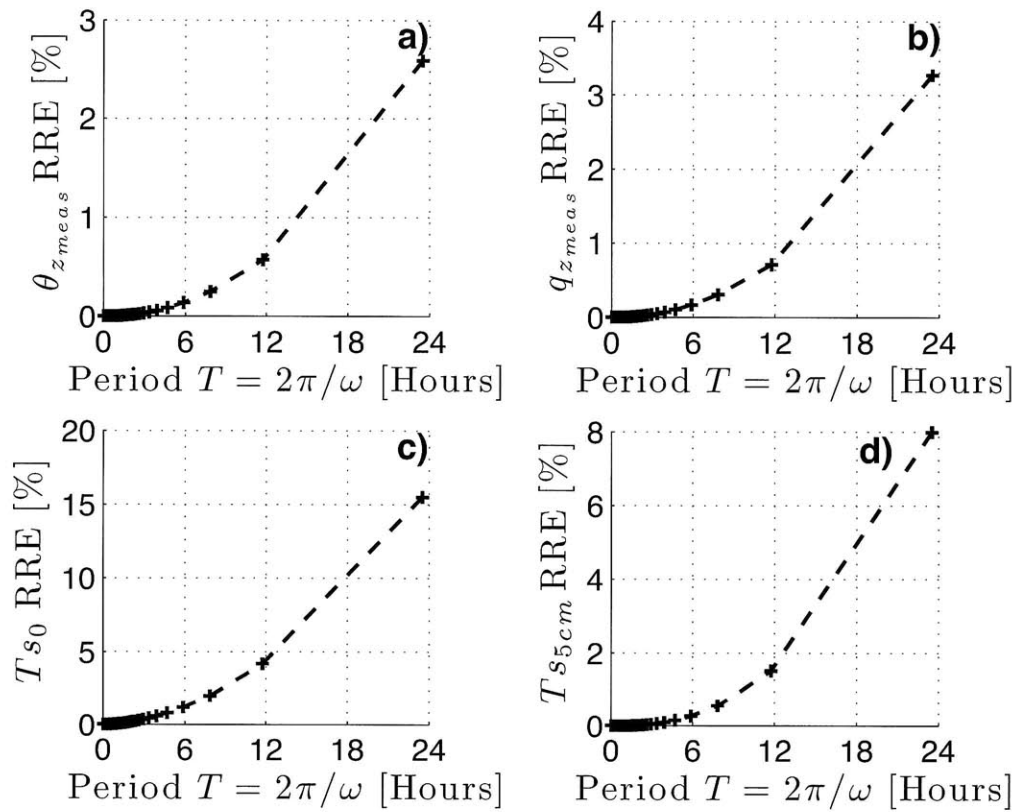


Figure 11: RRE of a) potential temperature at 2m, b) specific humidity at 2m, c) land-surface temperature, d) soil temperature at 5cm as a function of the harmonics period  $T$

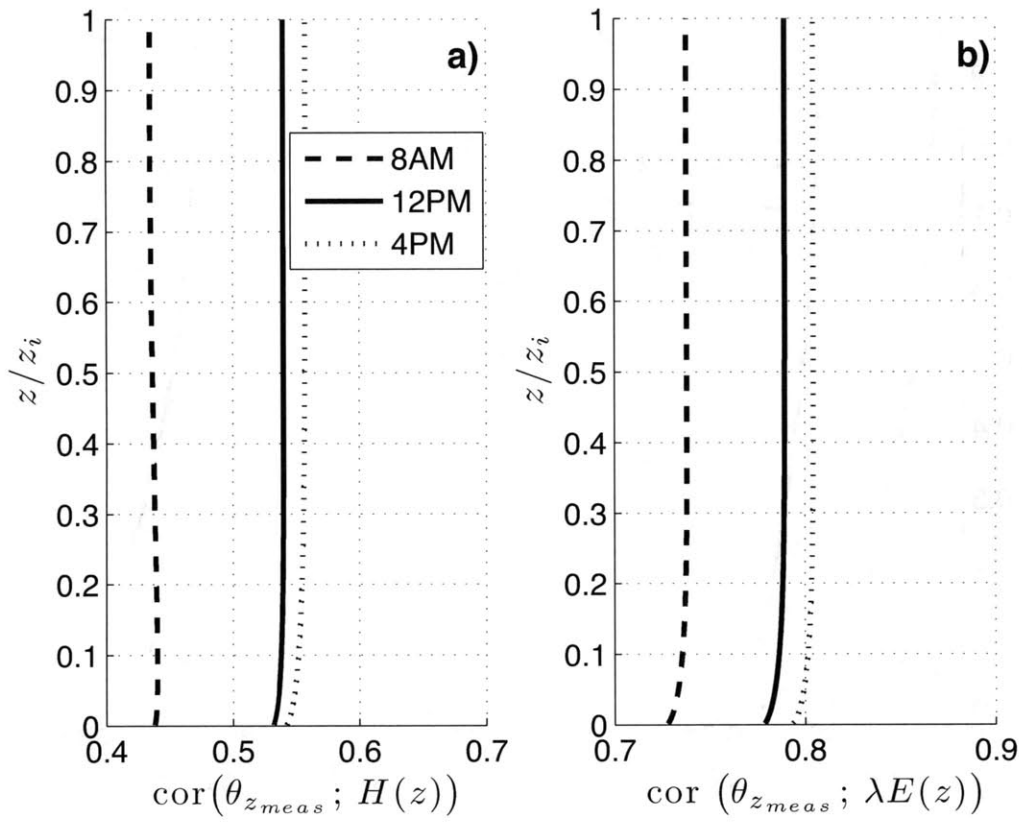


Figure 12: Correlation of a) sensible heat flux and b) latent heat flux with potential temperature at 2m as a function of height at 8AM, 12PM and 4PM

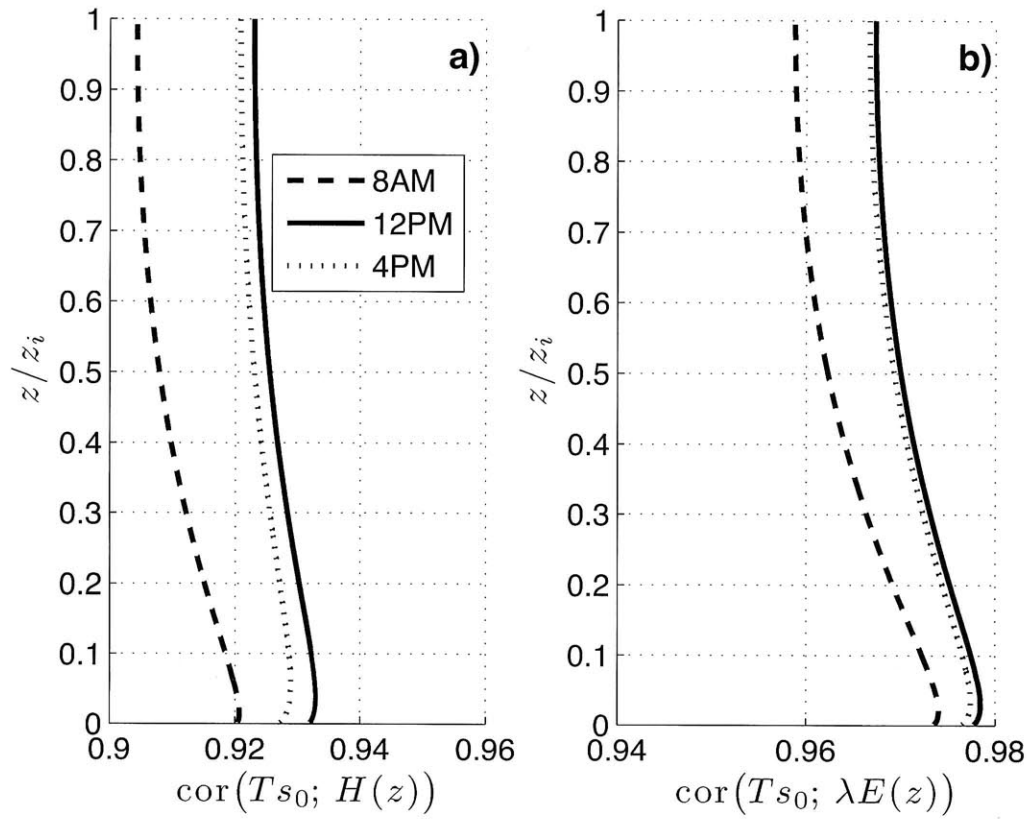


Figure 13: Correlation of a) sensible heat flux and b) latent heat flux with land-surface temperature as a function of height at 8AM, 12PM and 4PM



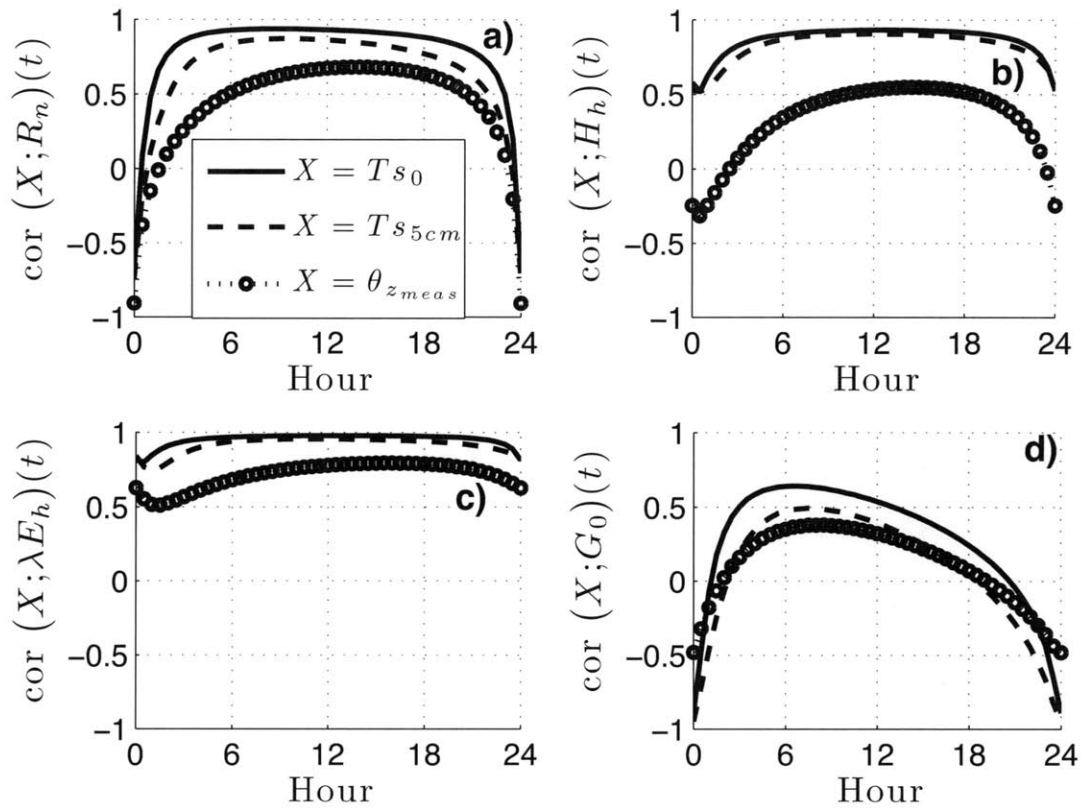


Figure 14: Correlation between land-surface temperature (solid line), soil temperature at 5 cm (dashed lined), screen-level temperature (circles) and a) net radiation, b) surface sensible heat flux, c) surface latent heat flux, d) surface soil heat flux as a function of time



# Chapter 7

## Future research

We have seen in the preceding papers that our modeling suffers important shortcomings. A short list of these issues is:

- i) Potential temperature, specific humidity profiles in the free troposphere should be given by a constant and uniform lapse rate  $\gamma_{\theta,q}$ , which is in general positive for potential temperature  $\gamma_{\theta} \approx 5[K km^{-1}]$  and negative for specific humidity  $\gamma_q \approx -1[g km^{-1}]$ . This lapse rates can have important repercussion on the ABL profiles as it will induce a non-local flux of temperature and humidity (modeled as a counter-gradient term, see next section) throughout the ABL, as well as control or limit the development of the ABL height.
- ii) The effect of stability and instability (using for instance the Monin-Obukhov similarity) has not been taken into account in this study. Yet the coupled land-atmosphere model is able to reproduce realistic values near the surface, since during daytime the ABL height is very high compared to the screen-level height. At night the behavior is much different in the sense that the nighttime stable ABL is relatively shallow, leading to much impact on screen-level and surface temperature and humidity. Therefore to obtain realistic surface and screen-level values throughout the day, it is important to take into account the stability/instability effect. Moreover the inclusion of this stability/instability can be used to obtain realistic daily ABL height evolution.
- iii) Friction velocity at the surface has been considered as a constant. However in reality there could be changes induced by large scale wind change or by stability and

instability effect.

iu) Turbulent transport of scalar has been represented by an eddy-diffusivity approach. A counter-gradient approach would be more realistic to take into account non-local mixing in the ABL (see next section).

u) There was no inclusion of radiative transfer in the ABL. However the effect of radiative transfer can be important near the surface or near the top of the ABL (where gradients of potential temperature are strong) but also at night, as described by André et al. (1978).

ui) Finally, ABL height should be variable throughout the day as it exhibits a strong diurnal cycle.

With these additions the daily evolution of the ABL height could be a diagnostic of the system and could be compared to soundings. However the system will not be analytically solvable and will require a numerical solution. Yet one of the main advantage of this system is that it would only require the specification of measurable incoming radiation at the land-surface and no specification of the initial profiles of potential temperature and specific humidity. The profiles will be obtained through the assumed periodicity (removing the large-scale effect).

## 7.1 Non-local closure: countergradient formulation

Following the approach introduced by Troen and Mahrt (1986) [34]: in the ABL, in unstable and convective situations, large eddies can transport scalars far away from their origin, without intermediate diffusion of the scalar through the neighboring cells. Hence, K-theory is not suitable for such conditions, as these large eddies cannot be modeled by a diffusion process. One way to keep a first order closure modeling is to introduce a non-local closure to include the effect of large eddies that act as a countergradient. For instance in the mixed layer, potential temperature is almost uniform  $\frac{\partial \theta}{\partial z} \approx 0$ , but the sensible heat flux is non-null which contradicts the K-theory. Therefore Erstel (1942) [14], Deardorff (1966) [8], (1972) [9], (1974) [10] and Holtslag and Moeng (1991) [19] introduced a non-local term in the transport equation of any

scalar  $c$  by turbulence.

$$-\overline{c'w'} = K_C \left( \frac{\partial \bar{c}}{\partial z} - \gamma_C \right) \quad (7.1)$$

where  $K_C$  is the eddy diffusivity of scalar  $c$  and  $\gamma_C$  represents the "non-local" transport of  $c$  by dry convection. This applies to heat, water vapor and passive scalars, but it does not apply to the momentum transport. Moreover the counter-gradient term can be neglected in stable and near-neutral conditions.

One such parameterization was introduced by Troen and Mahrt 1986 [34] or Holtslag et al. 1990 [18]. The non-local eddy-diffusivity term was given by:

$$K_C(z) = K w_s (z - d) \left( 1 - z/h \right)^2 \quad (7.2)$$

where  $h$  is the ABL height, and  $w_s$  is the turbulent velocity scale. With this parameterization, (7.1) behaves very well for both stable and unstable condition. In unstable conditions,  $w_s$  is proportional to the convective velocity scale  $w_*$ , while for stable and neutral case  $w_s$  is proportional to the friction velocity  $u_*$ :  $w_s = u_*/\phi_m(z/L)$ . For unstable conditions the ABL is divided into two parts: the surface layer  $z/h \ll 1$  (defined as the layer less than  $\epsilon h$ , with  $\epsilon = 0.1$ ) where  $w_s = u_*/\phi_m(z/L)$  and above the surface layer the velocity scale  $w_s$  is arbitrarily assumed to be uniform:  $w_s = ((u_*)^3 + 7\epsilon K (w_*)^3)^{1/3} = u_*/\phi_m(z/L)$ , with  $z = \epsilon h$ . The convective velocity scale is given by  $w_* = (g/\theta_s (\overline{\theta'w'})_s h)^{1/3}$  and  $\theta_s$  is the air potential temperature at the surface. More precisely in stable and near-neutral conditions, above the ABL,  $\gamma_C = 0$ . In unstable conditions,  $\gamma_C$  can be modelled as proposed by Holtslag and Moeng (1991) [19]:

$$\gamma_C = a \frac{w_* \overline{(c'w')}_s}{w_m^2 h} \quad (7.3)$$

where  $w_m$  is the turbulent velocity scale for momentum. Or an alternative formulation can be the one introduced in Troen and Mahrt (1986) [34]:

$$\gamma_C = C \frac{\overline{(c'w')}_s}{w_s h} \quad (7.4)$$

with  $C$  of the order of 6.5. Maybe this value could be inferred from temperature sounding or reanalysis on top of the ABL. (This boundary condition gives a constant gradient to the potential temperature: constant lapse rate  $\gamma_\theta$  in the free troposphere right above the top of the ABL.)

Notice that in neutral conditions  $w_* = 0$ , this thus explains the vanishing of the countergradient. For stable  $(\overline{\theta'w'})_s < 0$  and near-neutral conditions  $|(\overline{\theta'w'})_s| \ll 1$ , the velocity scale for scalar transport is  $w_s = \frac{u_*}{\phi_m}$ . The stability correction functions are given by Dyer (1974) [13] or Businger 1971[5]. Taking into account the non-local effect of large eddies and thermals would improve the representation of convective boundary layers. The existence of the countergradient has a theoretical justification, which is described in the following section.

## 7.2 Eddy-diffusivity and counter-gradient approximation: theoretical justification

Following the approach of Holtslag and Moeng (1991) [19] with horizontally homogeneous conditions, the turbulent equation for sensible heat flux  $\overline{\theta'w'}$  reads in the Boussinesq approximation:

$$\begin{aligned} \frac{\partial \overline{\theta'w'}}{\partial t} = & \underbrace{-\frac{\partial \overline{\theta'w'^2}}{\partial z}}_{\text{Turbulent flux of sensible heat flux}} \quad \underbrace{-\frac{1}{\rho_0} \overline{\theta' \frac{\partial p'}{\partial z}}}_{\text{Pressure covariance}} \\ & \underbrace{-\overline{w'^2} \frac{\partial \overline{\theta}}{\partial z}}_{\text{Mean gradient production}} \quad + \quad \underbrace{\beta g \overline{\theta'^2}}_{\text{Buoyant production}} \end{aligned} \quad (7.5)$$

The scaling parameters are: the surface convective velocity scale  $w_*$  and the convective temperature scale  $\theta_*$ , with:

$$w_* \triangleq (\beta g (\overline{\theta'w'})_s h_{ABL})^{1/3} \quad (7.6)$$

$$\theta_* \triangleq \frac{(\overline{\theta'w'})_s}{w_*} \quad (7.7)$$

The pressure covariance term can be modeled as (Crow (1968) [6], Moeng and Wyngaard (1986) [24]):

$$-\frac{1}{\rho_0} \overline{\theta' \frac{\partial p'}{\partial z}} = -a \beta g \overline{\theta'^2} - \frac{\overline{\theta' w'}}{\tau} \quad (7.8)$$

Where  $\tau$  is a relaxation-to-isotropy time scale. For isotropic turbulence:  $a = 1/3$  and for the ABL, Moeng and Wyngaard found  $a = 1/2$ . Above the ABL, the value of  $a$  depends on the stability and structure of the inversion layer. Finally with this approximation the sensible heat flux equation can be rewritten:

$$\frac{\partial \overline{\theta' w'}}{\partial t} = -\overline{w'^2} \frac{\partial \overline{\theta}}{\partial z} + (1 - 2a) \beta g \overline{\theta'^2} - 2 \frac{\overline{\theta' w'}}{\tau} + b \frac{(w_*)^2 \theta_*}{h_{ABL}} \quad (7.9)$$

In quasi-steady state (which is usually the case for scalar fluxes in the ABL), this gives the following relationship for the turbulent heat flux:

$$\frac{\overline{\theta' w'}}{\tau} \approx \underbrace{-\overline{w'^2} \frac{\partial \overline{\theta}}{\partial z}}_{\text{Diffusion term}} + \underbrace{b \frac{(w_*)^2 \theta_*}{h_{ABL}}}_{\text{Counter-gradient term}} \quad (7.10)$$

Assuming that:  $(1 - 2a) \beta g \overline{\theta'^2} \approx 0$  since  $a \approx 1/2$  in the modeling of the 24-hour evolution of the mean and turbulent structure of the boundary layer.

Hence equation (7.10), shows that the sensible heat flux in the convective ABL can be rewritten as the sum of a diffusion term and a counter-gradient term. Wyngaard and Weil (1991) showed that parameter  $b$  is proportional to the skewness of the vertical turbulent velocity:  $S = \frac{\overline{w'^3}}{(\overline{w'^2})^{3/2}}$ . In the convective ABL, the skewness is positive due to rapid convective rising updrafts and slow descending downdrafts.

Thus the counter-gradient and eddy-diffusivity terms of the sensible heat flux expression as presented by Deardorff (1966) [8] and (1972) [9] can be related to the different turbulence parameters:

$$\overline{\theta' w'} = -K_H \left( \frac{\partial \overline{\theta}}{\partial z} - \gamma_\theta \right) \quad (7.11)$$

with:

$$K_H = \overline{w'^2} \frac{\tau}{2} \quad (7.12)$$

$$\gamma_\theta = b \frac{(w_*)^2 \theta_*}{\overline{w'^2} h_{ABL}}. \quad (7.13)$$

Note that equation (7.10) is the theoretical basis of the justification of the K-theory and countergradient approach. In the near surface layer at quasi-steady state, the diffusion term is preponderant so that sensible heat flux can directly be expressed as function of the gradient of potential temperature. The similarity theory just assumes that the diffusion term and sensible heat flux are function of  $z/L_{MO}$  only, which is physically and mathematically correct. However, in non steady-state conditions, the problem is much different as the equation that should be considered is eq. (7.9) so that the diffusion term depends on both time  $t$  and  $z/L_{MO}$ . The time dependency is usually forgotten in most models and this approximation can be justified in unstable conditions as sensible heat flux in the convective boundary layer is almost always in quasi steady-state. However this result does not hold at night because of the small ABL height and small scale-intermittent turbulence, which tends to curve the profiles. The nighttime time dependency of the similarity theory is overlooked in almost all models and should be reconsidered.

Deardorff (1972) [9] obtained similar countergradient expression as (7.11) except that he neglected the turbulent transport term of the sensible heat flux turbulent equation and assumed that  $a = 0$ , so that the pressure covariance term reads  $-\overline{\theta'w'}/\tau_D$ . With these assumptions, the eddy-diffusivity coefficient and the counter-gradient terms were written:

$$K_H = \overline{w'^2} \frac{\tau_D}{2} \quad (7.14)$$



$$\gamma_\theta = \beta g \frac{\overline{\theta'^2}}{w'^2} \quad (7.15)$$

Therefore in these two approaches, the counter-gradient term displays very different interpretations: in Deardorff 1972 (D72), it corresponds to the production of sensible heat flux by buoyancy: this representation is physically reasonable as the generation of turbulence by shear effect is local and the effect of buoyancy is non-local in nature, whereas in the Holtslag and Moeng 1991 (HM91) approach, it corresponds to convective turbulent transport of sensible heat flux in the ABL. These two approaches might be valid but D72 is more appropriate to a highly stratified fluid and HM 91 to a highly convective process, it might be possible to mix these two phenomenon using either Monin-Obuhov length or Richardson number (for instance with a linear approximation between those two extreme values: free convection with little stratification and very stratified fluid). Such a mixed approach could be compared to more realistic second-order modeling such as Large-Eddy Simulations (LES).

As most parameterization are depending on the velocity variance, HM91 decided to parametrize this term so that it would fit the AMTEX observations and LES 96 simulations in the ABL ( $0 < z \leq h_{ABL}$ ) as plotted on Figure 7-1:

$$\left(\overline{w'^2}\right)^{3/2} = \left(1.6(u_*)^2 \left(1 - \frac{z}{h_{ABL}}\right)\right)^{3/2} + 1.2(w_*)^3 \frac{z}{h_{ABL}} \left(1 - 0.9 \frac{z}{z_i}\right)^{3/2} \quad (7.16)$$

And they consecutively modeled the eddy-diffusivity profile as:

$$\frac{K_H}{w_* h_{ABL}} = \left(\frac{z}{h_{ABL}}\right)^{4/3} \left(1 - \frac{z}{h_{ABL}}\right)^2 \left(1 + R_H \frac{z}{h_{ABL}}\right) \quad (7.17)$$

Where  $R_H$  was taken as 0.2 to fit the LES data.

The asymptotic behavior of (7.17) satisfies the free-convection limit in the vicinity of the surface:  $K_H \propto z^{4/3}$  as shown by Tennekes (1970) [32] or Panofsky and Dutton (1984) [25]. If we take into account the zero-displacement height in the ABL, this

equation should be:

$$\frac{K_H}{w_* h_{ABL}} = \left( \frac{z-d}{h_{ABL}} \right)^{4/3} \left( 1 - \frac{z-d}{h_{ABL}} \right)^2 \left( 1 + R_H \frac{z-d}{h_{ABL}} \right) \quad (7.18)$$

In real situation  $R_H$  could take different values between 0 and infinity.

The expression of  $K_H$  respects the free-convection asymptotic results, yet it should be improved to take into account the Monin-Obukhov similarity theory in the surface layer but the velocity variance does not respect any of them, therefore a more general formulation would be more suitable.

One problem of the original formulation is the fact that at  $z = 0$ , the eddy-diffusivity profile is null and similarly at  $z = h_{ABL}$ , yet this is not correct. One way to solve the bottom misformulation is to introduce a displacement height. On top of the ABL, in reality the heat flux only gradually approaches zero, and the proposed heat flux assumed that the entrainment zone is infinitely thin. To solve this issue: some physics should be added to the formulation either through radiative transfer (which is an important part of the entrainment zone enthalpy budget) as Newtonian cooling or with a compensating effect of large-scale advected air or using the effect of molecular diffusivity  $K_{molecular}$  instead of eddy diffusivity, even though this latter is usually small. With such kind of parameterization, the entire daily cycle of the ABL could be taken into account, thus improving the resolution of surface heat values and scalars.

### 7.3 Solving the Unstable/stable ABL

It is importance to introduce stability and instability in the ABL through for instance the use of Monin-Obukhov length. Indeed this instability/stability will control the development of the ABL throughout the day and in particular of its height. Yet in the case of the inclusion of instability/stability correction, the eddy-diffusivity term depends on this correction and becomes a non-linear coefficient of the PDE of potential temperature and specific humidity. The product of the eddy-diffusivity coefficient  $K_c$

with the scalar gradient  $\partial\bar{c}/\partial z$  will become a convolution in the Fourier domain. This renders the problem much more difficult to solve and avoids the possibility to obtain an analytical solution. Therefore the problem would have to be solved numerically, introducing a vertical sampling grid. The temporal spectral domain is also sampled using the natural representation of the Fast Fourier Transform of the incoming radiation at the land surface. Usually the time series of the forcing is given every 30 minutes, thus giving 48 temporal steps in the temporal domain and the corresponding number of FFT harmonics is:  $N_{FFT} = \mathbf{E}N_{steps}/2 + 1$ , where  $\mathbf{E}$  is the floor part and  $N_{steps}$  is the number of steps in the temporal domain, equals to 48 in this example. Here the number of harmonics  $N_{FFT} = 25$ . If the vertical grid size is  $N_z$ , the entire Fourier solution is given by the resolution of an  $N_z.N_{FFT}$  complex matrix (except that the coefficients of the first column should be real).

One possible algorithm to solve the problem of the Fourier transform of the unstable ABL could be the following:

- i) Analytically solve the neutral case (counter-gradient term is null in this case), with given input of incoming radiation. Then obtain the Fourier transform coefficients of the initial matrix:  $\tilde{\theta}_n(z)$  and  $\tilde{q}_n(z)$ . With those coefficients we can go back to the temporal profiles  $\theta(t, z)$  and  $q(z, t)$ .
- ii) From here on we can calculate the Monin-Obukhov length (local instability)  $L_{MO}(z, t)$  and the corresponding eddy-diffusion coefficient  $K_{cold}(t)$  and counter-gradient term  $\gamma_{cold}(t)$ . Finally we plug the Fourier transform of these terms into the Fourier ABL equation for scalar conservation:

$$j\omega\tilde{c}_n = \frac{d}{dz} \left[ \mathcal{F}(K_{cold}) * \frac{d\tilde{c}_n}{dz} + \mathcal{F}(\gamma_{cold}) \right]_n \quad (7.19)$$

And we simultaneously solve for the  $N_{FFT}$  complex scalar harmonics  $c_n$ . Notice that  $K_C$  needs to be corrected for instability. To do so, we use the former values of ABL height and instability coefficients.

- iii) Finally, iterates until convergence is reached for virtual potential temperature  $\theta_v$ , which is the best indicator of the stability/instability of the ABL. The criteria for

convergence could also include the ABL height, which in this case would be a diagnostic of the system. This height could be defined as either the inversion height  $z_i$ , where the sensible heat flux changes sign for the first time in the profile or it could be defined as the height of vanishing buoyancy flux  $\overline{w'\theta'_v} < \epsilon$ , where  $\epsilon$  is a convergence criteria because heat fluxes only asymptotically reaches zero. It should be noticed that this ABL height could be different (and usually higher) than ABL height defined either on vanishing sensible or latent heat flux. In particular, because of the decreasing humidity in the free troposphere, the height of vanishing latent heat flux is generally below the inversion level.

The interest of this approach is that with very little data: daily incoming radiation at the surface, mean daily potential temperature and specific humidity at any level (for instance anywhere in the free troposphere), the daily evolution of the profiles of  $\theta$  and  $q$  is obtained, with inclusion of instability/stability. We could use data assimilation of  $\theta$  or  $q$  profiles or surface measurements  $T_s$  to constrain the daily evolution of the profiles. Data assimilation could also be used to determine the value of the few parameters of the model.

This very simple approach could be used for any non-cloudy day, the strong periodicity constrain avoiding the need for specifying many boundary-conditions. Moreover after convergence we obtain the coefficients of the final Fourier ODE in the ABL and thus the phase and amplitude of the variables can still be studied as a function of the frequency of the forcing and as a function of height. The non linearity will introduce repercussion of one frequency forcing  $\omega_i$  on other frequencies  $\omega_j$  and can serve as an indicator of the strength of the non-linearity.

## 7.4 Radiative transfer

The modeling of radiative transfer in the ABL is usually very complex and will be difficult to use in a simplified coupled model. In particular the linearization would be rendered difficult, since the radiative transfer term is usually a strongly non-linear

function of  $\theta$  and  $q$ . With a numerical solution a simplified radiative scheme (e.g. André et al. 1978 [3]). However as already discussed in the first chapter, a way to simplify the problem is to use the fact that the sensible heat flux equation is insensitive to radiative transfer contrary to the mean potential temperature conservation equation. Therefore the radiative term would only appear in the mean potential temperature equation.

## 7.5 Free atmosphere

Above the inversion layer, the free atmosphere buoyancy is:  $b = g(\theta_v - \theta_{v0})/\theta_{v0}$  where  $\theta_{v0}$  is the reference value of  $\theta_v$ . In the free-atmosphere, we have:  $db/dz = N^2$ , where  $N$  is the Brunt-Vaisala (buoyancy) frequency as in Fedorovich (2004) [15]. Consequently the gradient of virtual potential temperature in the free troposphere is usually affine with a slope:  $\gamma_{\theta_v} = N^2$ . Because in this region the air is usually very dry we also have that:  $\gamma_{\theta} \approx \gamma_{\theta_v}$ . This term should be accounted for in improved studies, since this lapse rate controls the development of the diurnal ABL, as it corresponds to a subsidence term. In particular, this will be fundamental to study the effect of the ABL cloud formation.

## 7.6 Comparisons with coupled soil-LES: advantages/disadvantages

Only recently have researchers been able to couple Soil-Vegetation-Atmosphere-Transfer models with Large Eddy Simulations (LES) to theoretically comprehend the coupling between the land and the atmosphere at the daily time scale. To date, the main studies are the joint work of Albertson and Kustas (2001) [1] using observed infrared brightness temperature as a proxy for surface sensible and latent heat flux inferring, (2003) [21] with a fully coupled model; as well as the work of Patton et al. (2005) [26] with a fully coupled model. It remains difficult to couple both models because of several technical issue. The specification of the initial profiles in both the soil and

the atmosphere must be appropriate, since the simulation of an entire day with LES remains an issue, in particular because of the abrupt change in the structure of the ABL between nighttime and daytime. There does exist a strong horizontal variability of land-surface conditions, which leads to complication in the boundary conditions for LES. Yet near the ground because of the large scalar gradients, this parameterization will be of great importance for soil-atmosphere interactions as small scale changes will play an important role.

In the future, coupled SVAT-LES will certainly become an invaluable tool to further investigate the coupling between the soil and the atmosphere if those issues are further solved but at the time of this thesis, LES always fail to resolve the large-scale motions at the first few grid points. Therefore the restricted ability of LES to resolve very close to the ground raises some fundamental difference between LES and field data and will consequently remains the fundamental issue faced to obtain accurate representation and understanding of the coupling between the soil and the atmosphere.

## 7.7 Time-dependent ABL height

One of the necessary improvements to our study would be to take into account the time variations of the ABL height. In particular the nighttime collapse of the ABL will add more physical realism to the daily solution. In addition, the change in ABL height during daylight hours will modify the surface layer response and thus the changes in screen-level variables. The time variations of the ABL height might be fundamental to better understand the land-atmosphere coupling at the land surface, since it will modify the surface heat fluxes and thus the coupling. The effect of the ABL height changes and the non-linearities it induces still needs to be much further investigated.

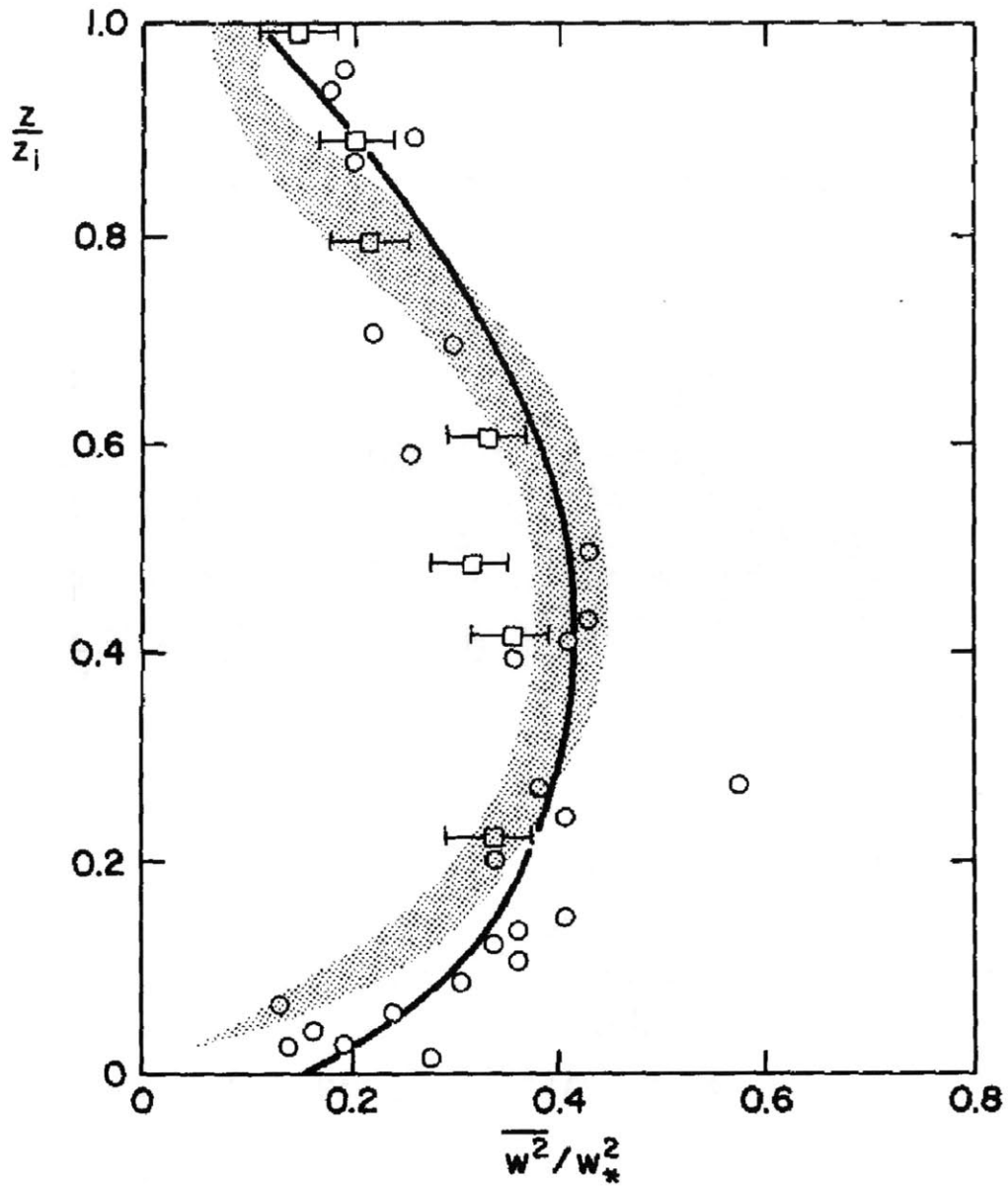


Figure 7-1: Non-dimensional vertical turbulent velocity variance, giving the eddy-diffusivity coefficient of the K-theory (from Holtslag and Moeng 1991). Solid curve is parameterized to fit the AMTEX data (circles) and 96 LES experiment (shaded region) and convection tanks (squares)

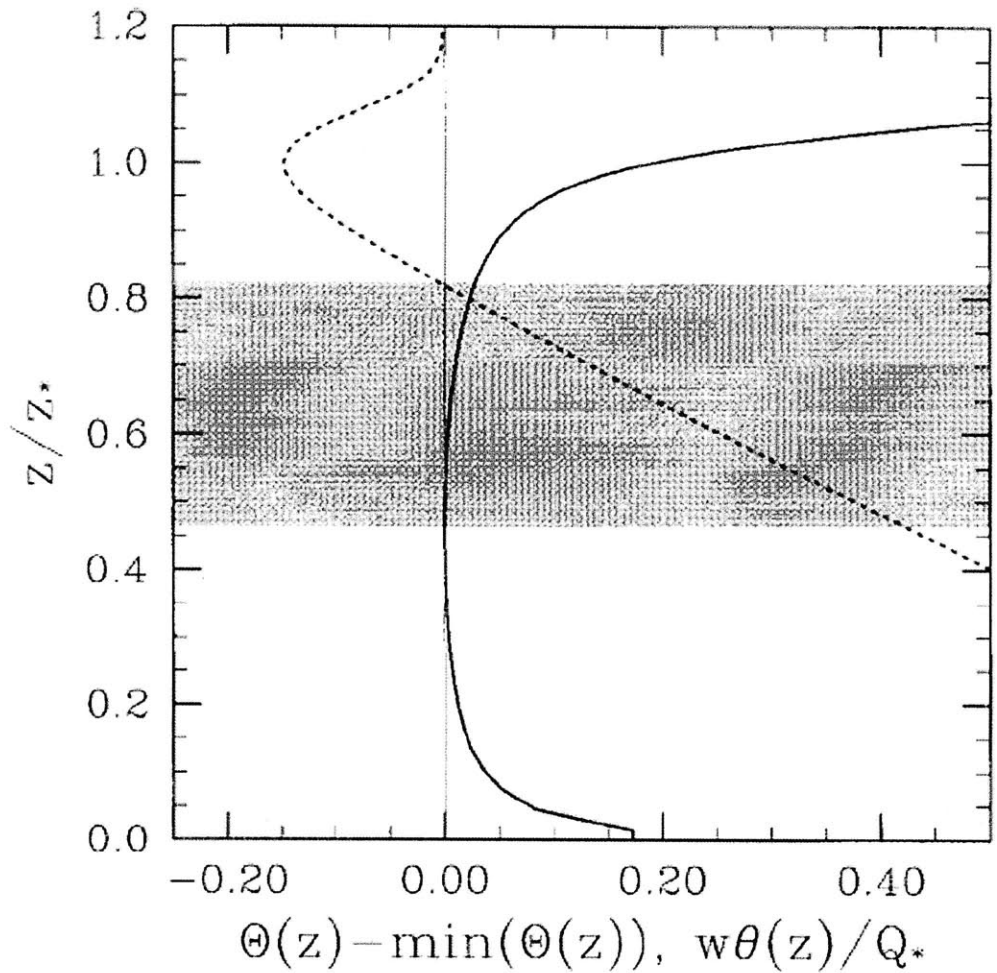


Figure 7-2: Profiles of the mean potential temperature (solid line) and sensible heat flux (dotted line) in steady state from Stevens (2000)



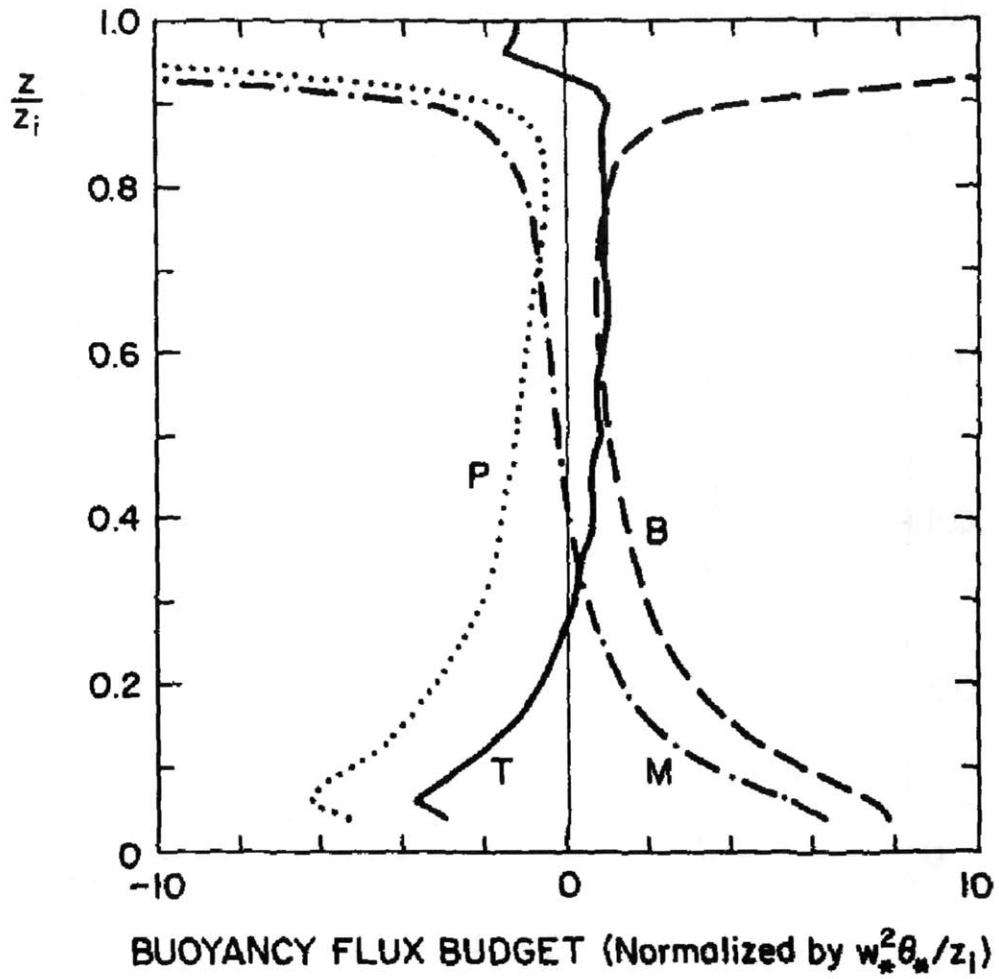


Figure 7-3: Normalized creation/destruction terms of turbulent sensible heat flux equation (7.5) as function of relative height (from Holtslag and Moeng 1991).

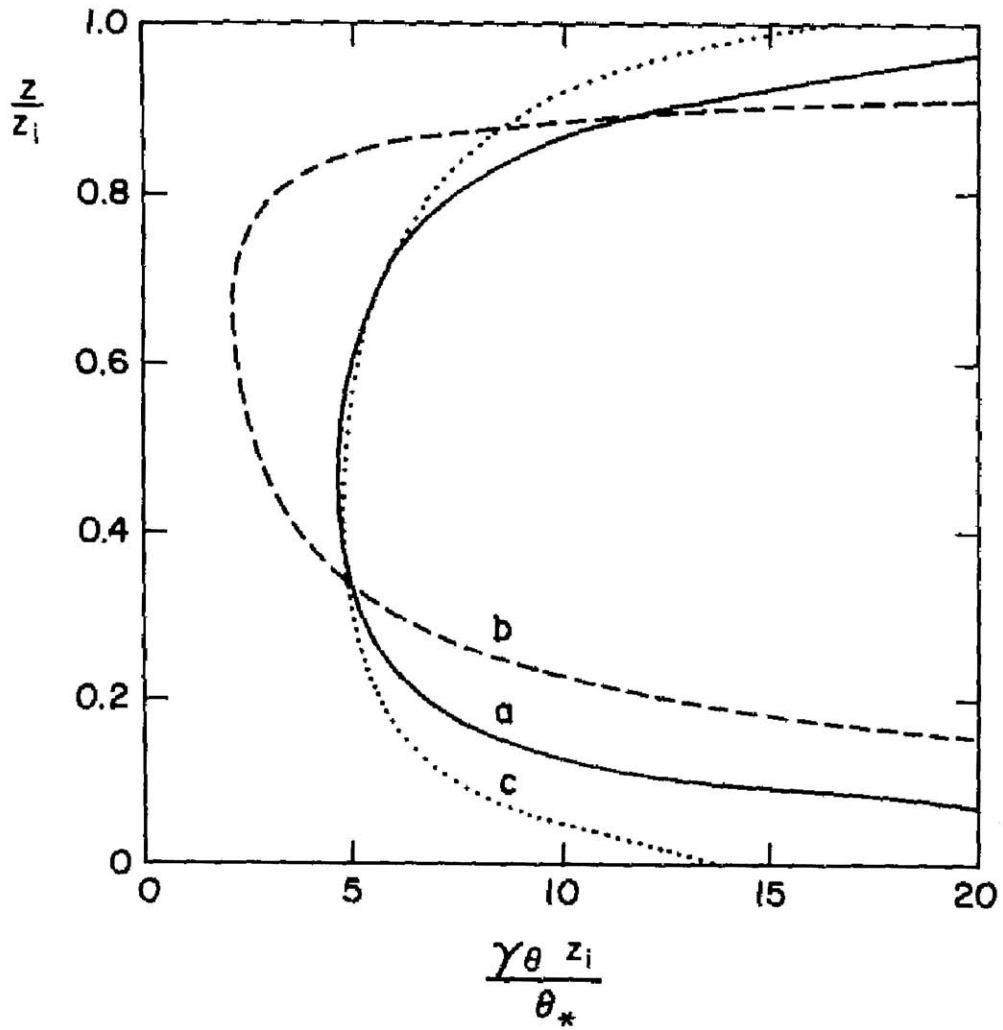


Figure 7-4: Non-dimensional counter-gradient term a)HM91 b)D72 c)HM91 with parametrized  $(\overline{w'^2})^{3/2}$  (from Holtslag and Moeng 1991).

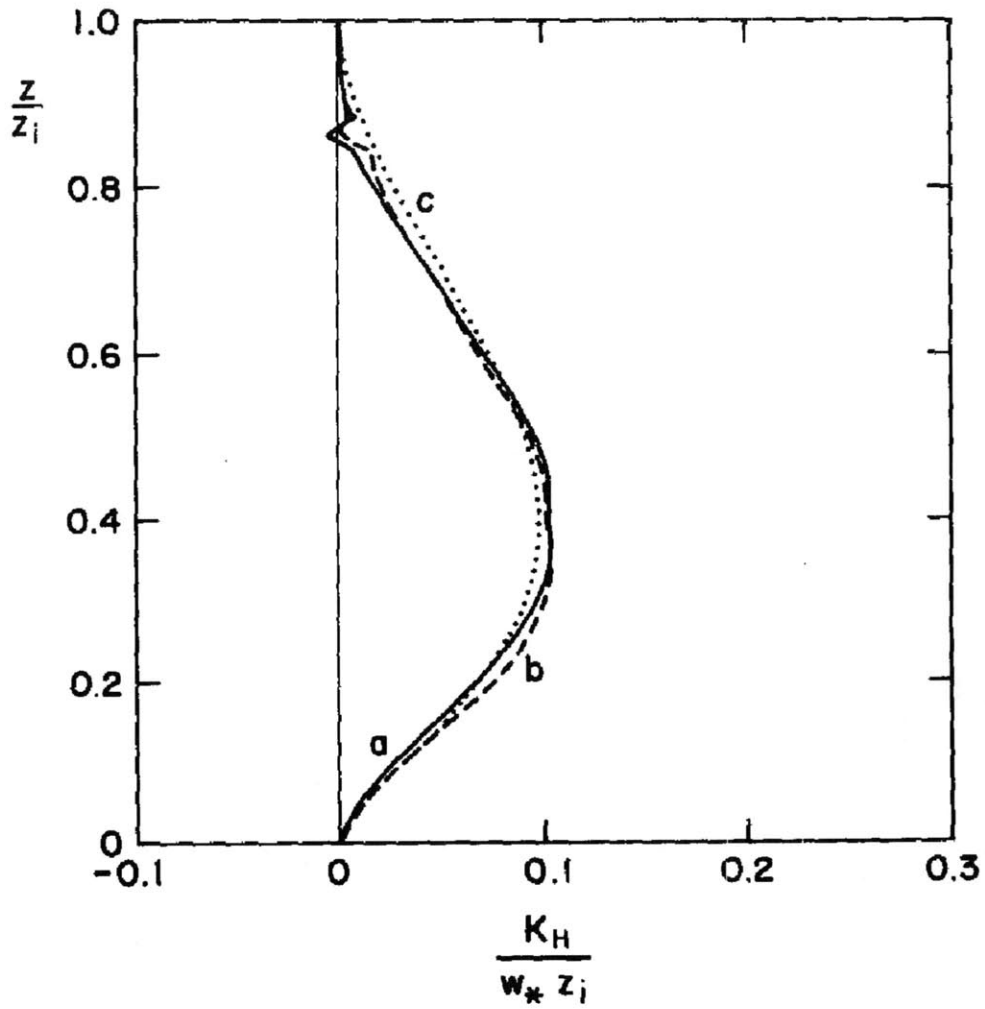


Figure 7-5: Non-dimensional eddy-diffusivity coefficient for heat a) HM91 with parameterized counter-gradient, b) HM91 with parameterized counter-gradient and velocity variance c) parameterized  $K_H$  (from Holtslag and Moeng 1991).



# Conclusions

In this PhD thesis, we have investigated the coupling of the land and the atmosphere at the daily timescale, using a linearized coupled land-atmosphere model responding to incoming radiation forcing at the land surface. This model couples the heat and water fluxes in the atmosphere and in the land through the energy budget at the and surface. Since the coupled model is linear it is solved in the (temporal) Fourier domain, yielding important new insights on the spectral behavior of the land-atmosphere coupling.

In a first deterministic study, ground heat flux was shown to act as a high-pass filter emphasizing the highest frequencies of the daily incoming forcing, thus explaining its high variability. Turbulent fluxes on the opposite side are low-pass filters of the incoming radiation since their response is limited by the slower response of land-surface temperature in response to radiative changes. In this first study the existence of the diurnal surface and mixed layers was theoretically confirmed with the existence of two distinctive scales for the scalars and fluxes. The response of these layers to surface forcing could be further highlighted emphasizing the role of the frequency of the incoming radiation forcing on the depth of these layers. Moreover the heat fluxes in the ABL were further confirmed to be in quasi steady state since the temporal delay of the land-surface temperature response limits the rapidity of the turbulent heat flux release. Indeed the propagation of the ABL fluxes in the ABL is nearly instantaneous compared to the changes in the land-surface temperature and thus of surface heat fluxes, which are controlled by the former. Finally, in a near-neutral ABL, friction velocity and vegetation height were shown to have a much stronger impact on the surface-layer height compared to the surface aerodynamic resistance

and evaporative fraction. In that case, the mixed-layer height is mainly controlled by friction velocity alone.

In a second study the linearized land-atmosphere model was further shown to well reproduce the daily course of land-surface and screen-level variables. Moreover the model was used to determine and derive the minimum asymptotical "plateau" value of the diurnal evaporative fraction. In addition evaporative fraction was shown to be a diurnal constant under very restrictive environmental conditions with a smooth, elevated solar incoming radiation forcing. Therefore the constant evaporative fraction assumption is mostly valid in fair-weather conditions experiencing elevated solar radiation.

In a last study, we investigated the response of the coupled model to surface energy balance noise: that is how does the daily energy balance noise translates onto land-surface and screen-level scalars and heat fluxes. Specific humidity was demonstrated to be influenced by surface energy budget errors contrary to land-surface and screen-level temperatures. L-band microwave brightness temperature was shown to be less influenced by radiation noise than infrared brightness temperature, thus emphasizing the usefulness of microwave satellites for the determination of the land-surface state (e.g. soil moisture). Finally, the synergy of air temperature and microwave brightness temperature was shown to be helpful to reduce the effect of incoming radiation noise on the land-surface state estimate within a data assimilation scheme.

The present PhD thesis has inherent limitations due to the strong assumptions used to yield an analytical solution of the coupling between the land and the atmosphere. A short list of possible improvements was presented:

- i) the introduction of stability/instability correction in the eddy-diffusion formulation.
- ii) The use of a countergradient formulation in the ABL.
- iii) Adding a varying ABL height, which could be a diagnostic of the system.
- iv) Inclusion of a lapse rate for the potential temperature and specific humidity gradients in the free troposphere.
- v) Addition of a radiation in the mean potential temperature equation.

# Appendix A

## Brownian Bridge

The Brownian Bridge could be expanded in series form using either the Karhunen-Loève or Fourier decomposition.

### A.1 Karhunen-Loève (K-L) expansion

A centered stochastic process with jointly continuous covariance function  $\text{Cov}_x(t, s)$  admits the following spectral decomposition:

$$\mathbf{W}_i = \int_0^T W_t \mathbf{e}_i(t) dt \quad (\text{A.1})$$

with  $\mathbf{W}_i$  being centered orthogonal random variables and (convergence in mean, uniform in  $t$ ):

$$W_t = \sum_{i=1}^{+\infty} \mathbf{e}_i(t) \mathbf{W}_i \quad (\text{A.2})$$

and

$$\text{Var}(\mathbf{W}_i) = \mathbb{E} \mathbf{W}_i^2 = \lambda_i \quad (\text{A.3})$$

is the eigenvalue corresponding to eigenvector  $\mathbf{e}_i(t)$ . In the case of Gaussian distribution: the r.v have joint Gaussian distribution and are jointly independent if the original process  $W_t$  is Gaussian. From [2], [11] and [12], the Brownian Bridge K-L

expansion is:

$$B_t = \sum_{i=1}^{+\infty} \mathbf{e}_i(t) \mathbf{W}_i \quad (\text{A.4})$$

In this case the convergence is pathwise and in  $L^2$  (square mean convergence). Note that the K-L expansion of the Bownian Bridge is  $2T$ -periodic and not  $T$ -periodic!

## A.2 Fourier expansion

From Kloeden and Platen [20] p198: the normalized Brownian Bridge can be extended in Fourier series with Gaussian coefficients and pairwise independent (the convergence is pathwise and in  $L^2$ ):

$$B_t = \frac{1}{2}a_0 + \sum_{k=1}^{+\infty} a_k \cos\left(\frac{2k\pi t}{T}\right) + b_k \sin\left(\frac{2k\pi t}{T}\right) \quad (\text{A.5})$$

And the coefficients, which are Gaussian r.v. (linear transformation of Gaussian process) are defined as:

$$\forall k > 1 \ a_k = \frac{2}{T} \int_0^T B_t \cos\left(\frac{2k\pi s}{T}\right) ds \quad (\text{A.6})$$

$$\forall k > 1 \ b_k = \frac{2}{T} \int_0^T B_t \sin\left(\frac{2k\pi s}{T}\right) ds \quad (\text{A.7})$$

These random variables are distributed as  $N(0, \sigma^2 T / 2\pi^2 k^2)$ , pairwise independent but correlated with  $a_0$ . Therefore as in the case of the Fast Fourier Transform in the deterministic case, a truncation of the series can be used to approximate the Brownian Bridge and it has differentiable sample paths.

Using complex series expansion we can use the simplified version of the Brownian Bridge in the complex Fourier domain:

$$B_t = \sum_{k=-\infty}^{+\infty} C_k e^{j\omega_k t} = C_0 + \sum_{k=1}^{+\infty} C_k e^{j\omega_k t} + C_k^* e^{-j\omega_k t} \quad (\text{A.8})$$

Where  $*$  denotes the complex conjugate. The  $C_k, k \neq 0$  are independent complex



Gaussian random variables, distributed as  $N(0, \sigma^2 T / \pi^2 k^2)$  and  $C_0$  is a real Gaussian random variable  $N(0, \sigma^2 T / 12)$ . The following relationships and correlations hold:

$$\forall (n_1, n_2), n_1 \neq n_2, n_1 \neq -n_2 : Cov(C_{n_1}, C_{n_2}) = \mathbb{E}(C_{n_1} C_{n_2}^*) = 0 \quad (\text{A.9})$$

i.e. the coefficient are pairwise uncorrelated Gaussian variables and are thus independent. Moreover:

$$Var(C_n) = \frac{\sigma^2 T}{n^2 \pi^2} \quad (\text{A.10})$$

and all coefficients are correlated with  $C_0$  as:

$$Cov(C_n, C_0) = \mathbb{E}(C_n C_0) = -\frac{1}{4} \frac{\sigma^2 T}{n^2 \pi^2} \quad (\text{A.11})$$

The Fourier extension has been chosen in our stochastic study because its T-periodicity makes it more convenient for projection on the natural T-periodic Fourier basis of the deterministic solution.



# Bibliography

- [1] JD Albertson, WP Kustas, and TM Scanlon. Large-eddy simulation over heterogeneous terrain with remotely sensed land surface conditions. *Water Resources Research*, 37(7):1939–1953, 2001.
- [2] TW Anderson and DA Darling. Asymptotic theory of certain "goodness of fit" criteria based on stochastic processes. *The Annals of Mathematical Statistics*, pages 193–212, 1952.
- [3] JC André, G De Moor, P Lacarrère, and R du Vachat. Modeling the 24-Hour Evolution of the Mean and Turbulent Structures of the Planetary Boundary Layer. *Journal of the Atmospheric Sciences*, 35(10):1861–1883, 1978.
- [4] RH Brooks and AT Corey. Hydraulic properties of porous media. 1964.
- [5] JA Businger, JC Wyngaard, Y. Izumi, and EF Bradley. Flux-profile relationships in the atmospheric surface layer. *Journal of the Atmospheric Sciences*, 28(2):181–189, 1971.
- [6] SC Crow. Viscoelastic properties of fine-grained incompressible turbulence. *Journal of Fluid Mechanics Digital Archive*, 33(01):1–20, 2006.
- [7] DA De Vries. Simultaneous transfer of heat and moisture in porous media. *Trans. Am. Geophys. Union*, 39(5):909–916, 1958.
- [8] JW Deardorff. The Counter-Gradient Heat Flux in the Lower Atmosphere and in the Laboratory. *Journal of the Atmospheric Sciences*, 23(5):503–506, 1966.

- [9] JW Deardorff. Theoretical expression for the countergradient vertical heat flux. *J. Geophys. Res*, 77(30):5900–5904, 1972.
- [10] JW Deardorff. Three-dimensional numerical study of turbulence in an entraining mixed layer. *Boundary-Layer Meteorology*, 7(2):199–226, 1974.
- [11] P Deheuvels. A Karhunen–Loève expansion for a mean-centered Brownian bridge. *Statistics and Probability Letters*, 77(12):1190–1200, 2007.
- [12] C Donati-Martin and M Yor. Fubini theorem for double Wiener integrals and the variance of the Brownian path. *Ann. Inst. Henri Poincaré*, 27:181–200, 1991.
- [13] AJ Dyer. A review of flux-profile relationships. *Boundary-Layer Meteorology*, 7(3):363–372, 1974.
- [14] H Ertel. Der vertikale Turbulenz-Wärmestrom in der Atmosphäre. *Meteor. Zeitung*, 59:250–253, 1942.
- [15] E Fedorovich, R Conzemius, and D Mironov. Convective entrainment into a shear-free, linearly stratified atmosphere: Bulk models reevaluated through large eddy simulations. *Journal of the Atmospheric Sciences*, 61(3):281–295, 2004.
- [16] P Gentine, D Entekhabi, A Chehbouni, G Boulet, and B Duchemin. Analysis of evaporative fraction diurnal behaviour. *Agricultural and Forest Meteorology*, 143(1-2):13–29, 2007.
- [17] SR Hanna. Summary of the third symposium on atmospheric turbulence, diffusion, and air quality. *Bulletin of American Meteorological Society*, 58:242–244, 1977.
- [18] AAM Holtslag, EIF De Bruijn, and HL Pan. A high resolution air mass transformation model for short-range weather forecasting. *Monthly Weather Review*, 118(8):1561–1575, 1990.

- [19] AAM Holtslag and CH Moeng. Eddy Diffusivity and Countergradient Transport in the Convective Atmospheric Boundary Layer. *Journal of the Atmospheric Sciences*, 48(14):1690–1698, 1991.
- [20] PE Kloeden and E Platen. *Numerical solution of stochastic differential equations*. Springer, 1992.
- [21] WP Kustas and JD Albertson. Effects of surface temperature contrast on land-atmosphere exchange: A case study from Monsoon 90. *Water Resources Research*, 39(6):1159, 2003.
- [22] H Lettau. Theory of surface temperature and heat-transfer oscillations near level ground surface. *EOS*, 32(2):189D200, 1951.
- [23] EN Lorenz. Deterministic nonperiodic flow. *Journal of the Atmospheric Sciences*, 20(2):130–141, 1963.
- [24] CH Moeng and JC Wyngaard. An analysis of closures for pressure-scalar covariances in the convective boundary layer. *Journal of the Atmospheric Sciences*, 43(21):2499–2513, 1986.
- [25] H.A. Panofsky and J.A. Dutton. *Atmospheric turbulence*. New York, 1984.
- [26] EG Patton, PP Sullivan, and CH Moeng. The influence of idealized heterogeneity on wet and dry planetary boundary layers coupled to the land surface. *Journal of the Atmospheric Sciences*, 62(7):2078–2097, 2005.
- [27] LA Richards. Capillary conduction of liquids through porous mediums: Physics, v. 1. 1931.
- [28] J Rotta. Statistische theorie nichthomogener turbulenz. *Zeitschrift für Physik A Hadrons and Nuclei*, 129(6):547–572, 1951.
- [29] T Sasamori. A linear harmonic analysis of atmospheric motion with radiative dissipation. *Atmospheric Radiation*, 1972.

- [30] FM Selten. An efficient description of the dynamics of barotropic flow. *Journal of the Atmospheric Sciences*, 52(7):915–936, 1995.
- [31] RB Stull. *An introduction to boundary layer meteorology*. Springer, 1988.
- [32] H Tennekes. Free convection in the turbulent Ekman layer of the atmosphere. *Journal of the Atmospheric Sciences*, 27(7), 1970.
- [33] AA Townsend. The effects of radiative transfer on turbulent flow of a stratified fluid. *Journal of Fluid Mechanics Digital Archive*, 4(04):361–375, 1958.
- [34] IB Troen and L Mahrt. A simple model of the atmospheric boundary layer; sensitivity to surface evaporation. *Boundary-Layer Meteorology*, 37(1):129–148, 1986.
- [35] T Yamada and G Mellor. A simulation of the Wangara atmospheric boundary layer data. *Journal of the Atmospheric Sciences*, 32(12):2309–2329, 1975.